

MULTICOMPONENT ION EXCHANGE ON SYNTHETIC ZEOLITES

A THESIS SUBMITTED TO
THE GRADUATE SCHOOL OF NATURAL AND APPLIED SCIENCES
OF
MIDDLE EAST TECHNICAL UNIVERSITY

BY

ELİF BEŞEL DÜZGÜN

IN PARTIAL FULFILLMENT OF THE REQUIREMENTS
FOR
THE DEGREE OF DOCTOR OF PHILOSOPHY
IN
CHEMICAL ENGINEERING

SEPTEMBER 2014

MULTICOMPONENT ION EXCHANGE ON SYNTHETIC ZEOLITES

submitted by **ELİF BEŞEL DÜZGÜN** in partial fulfillment of the requirements for the degree of **Doctor of Philosophy in Chemical Engineering Department, Middle East Technical University** by,

Prof. Dr. Canan Özgen
Dean, Graduate School of **Natural and Applied Sciences**

Prof. Dr. Halil Kalıpçılar
Head of Department, **Chemical Engineering**

Prof. Dr. Hayrettin Yücel
Supervisor, **Chemical Engineering Dept., METU**

Examining Committee Members:

Prof. Dr. Halil Kalıpçılar
Chemical Engineering Dept., METU

Prof. Dr. Hayrettin Yücel
Chemical Engineering Dept., METU

Prof. Dr. Zeki Aktaş
Chemical Engineering Dept., Ankara University

Prof Dr. Gürkan Karakaş
Chemical Engineering Dept., METU

Assoc. Prof. Naime Aslı Sezgi
Chemical Engineering Dept., METU

Date: September 26, 2014

I hereby declare that all information in this document has been obtained and presented in accordance with academic rules and ethical conduct. I also declare that, as required by these rules and conduct, I have fully cited and referenced all material and results that are not original to this work.

Name, Last Name: ELİF, BEŞEL DÜZGÜN

Signature :

ABSTRACT

MULTICOMPONENT ION EXCHANGE ON SYNTHETIC ZEOLITES

Beşel Düzgün, Elif

Ph.D., Department of Chemical Engineering

Supervisor: Prof. Dr. Hayrettin Yücel

September 2014, 244 pages

Zeolites are natural and synthetic microporous crystalline aluminosilicates with ion-exchange and molecular sieve properties. Zeolites consist of a three-dimensional framework of $(\text{SiO}_4)^{4-}$ and $(\text{AlO}_4)^{5-}$ tetrahedras, connected by a shared oxygen atom. The presence of aluminum in the aluminosilicate framework introduces a net negative charge. Zeolites are mostly used in ion exchange, adsorption processes and catalytic applications.

The objective of the study was to determine and model the multicomponent ion exchange behavior of Zeolite 13X for lead, cadmium and zinc ions. For this purpose, Pb^{2+} - Na^+ , Cd^{2+} - Na^+ and Zn^{2+} - Na^+ binary systems, Cd^{2+} - Pb^{2+} - Na^+ ternary systems and Cd^{2+} - Pb^{2+} - Zn^{2+} - Na^+ quaternary systems were investigated in batch and column operations. Breakthrough capacities and column efficiencies were determined at different concentrations, mesh ranges and flow rates. Optimum total

concentration were determined as 0.05 N, optimum flow rate as 10 mL/min, optimum particle size range as 0.6-0.7 mm (25/30 mesh ranges).

Ion exchange of Pb^{2+} , Cd^{2+} and Zn^{2+} on to NaX zeolite was modelled using the Langmuir, Freundlich, Tempkin, DR, Redlich Peterson, Sips and BET isotherms. Among all the isotherms tested, Redlich Peterson isotherm gave the best fit for all metals with the highest R^2 and lowest ARE values.

The Modified Langmuir Model, Jain and Snoeyink Model, SRS Model, Extended SIPS Model and IAST Model were used to fit the multicomponent ion exchange data; but only SRS Isotherm Model was observed to fit the experimental data with high linear coefficient of determination.

Pseudo-second order kinetic equation describe the batch system kinetics well. W&M model indicated that the intra-particle diffusion is not the only rate controlling step,

Finally possible mass transfer controlling mechanism in the column experiments was determined as solid diffusion. Solid-phase diffusion coefficients were evaluated as 4.3×10^{-6} cm²/min for Pb^{2+} - NaX exchange; 4.6×10^{-6} cm²/min for Cd^{2+} - NaX exchange and 2.2×10^{-6} cm²/min for Zn^{2+} - NaX exchange

Keywords: Ion exchange, Zeolite 13X, Zinc, Copper, Lead, Column

ÖZ

SENTETİK ZEOLİTLERLE ÇOK BİLEŞENLİ İYON DEĞİŞTİRME

Beşel Düzgün, Elif

Doktora, Department of Chemical Engineering

Tez Yöneticisi: Prof. Dr. Hayrettin Yücel

Eylül 2014, 244 sayfa

Zeolitler doğal ve sentetik mikro gözenekli iyon değiştirme ve moleküler elek özelliklerine sahip olan alüminosilikat kristallerdir. Zeolitler paylaşılan bir oksijen atomu ile birbirlerine bağlı $(\text{SiO}_4)^{4-}$ ve $(\text{AlO}_4)^{5-}$ dörtyüzlülerini içeren üç boyutlu bir çerçeveden oluşurlar. Alüminosilikat çerçevesinde bulunan alüminyum net negatif yük oluşturur. Zeolitler genellikle iyon değiştirme, adsorpsiyon ve kataliz uygulamalarında kullanılırlar.

Bu çalışmanın amacı, Zeolit 13X'in, kurşun, kadmiyum ve çinko iyonları için çok bileşenli iyon değiştirme davranışının belirlenmesi ve modellenmesidir. Bunun için, Pb^{2+} - Na^+ , Cd^{2+} - Na^+ ve Zn^{2+} - Na^+ ikili sistemleri, Cd^{2+} - Pb^{2+} - Na^+ üçlü sistemleri ve Cd^{2+} - Pb^{2+} - Zn^{2+} - Na^+ dörtlü sistemleri kesikli ve kolon operasyonlarıyla incelenmiştir. Değişik konsantrasyon, parça boyutları ve debi aralıklarında salıverme kapasiteleri ile kolon verimleri incelenmiştir. Optimum parça boyutu, 0.6-0.7 mm (25/30 standard mesh aralıkları), toplam konsantrasyon 0.05 N ve optimum akış hızı 10 ml/dak olarak belirlenmiştir.

Pb^{2+} , Cd^{2+} and Zn^{2+} NaX zeolite küresel parçacıkları üzerine iyon değişim davranışı Langmuir, Freundlich, Tempkin, DR, Redlich Peterson, Sips and BET isotermi kullanılarak incelenmiştir. İncelenen modellerden, DR isoterminin dışındaki tüm modeller deneysel verilerle uyum göstermiş ve en yüksek R^2 ve en düşük ARE değerleri ile en iyi uyumu Redlich Peterson modeli göstermiştir.

Çok komponentli iyon değişiminin modellenmesinde kullanılan Modified Langmuir Modeli, Jain ve Snoeyink, SRS, Extended SIPS modellerinden sadece SRS modeli deneysel verilerle iyi uyum göstermiştir.

Kütle aktarımını kontrol eden olası mekanizma katı difüzyonu olarak belirlenmiştir. Katı-faz difüzyon katsayıları Pb^{2+} - NaX ikili değişimi için 4.3×10^{-6} cm^2/dak , Cd^{2+} - NaX ikili değişimi için 4.6×10^{-6} cm^2/dak ve Zn^{2+} - NaX ikili değişimi için 2.2×10^{-6} cm^2/dak olarak hesaplanmıştır.

Anahtar kelimeler: İyon değişimi, Zeolite 13X, Çinko, Kadmiyum, Kurşun, kolon

To my family,

ACKNOWLEDGMENTS

I would like to express my sincere gratitude to my supervisor Professor Hayrettin Yücel for his help and guidance throughout this work. It was a great honor to work with him. Through his kindness, tolerance and encouragement, the study has been brought to a meaningful conclusion.

I would like to express my deepest appreciation to my the members of my thesis committee, Professor Zeki Aktaş and Professor Halil Kalıpçılar who always provided valuable feedback for the progress of this work.

Many thanks to all the technicians of the Chemical Engineering Department especially Kerime Güney for her friendship and help.

I would like to thank to my wonderful parents, Ayhan and Mustafa, for their endless emotional support, love and encouragement. I wouldn't able to succeed without them.

Special thanks to the love of my life, my husband Mehmet for his understanding, interest and patience especially in the last two years of this PhD-journey.

TABLE OF CONTENTS

ABSTRACT.....	v
ÖZ	vii
ACKNOWLEDGEMENTS	x
TABLE OF CONTENTS	xi
LIST OF TABLES	xvi
LIST OF FIGURES	xx
LIST OF SYMBOLS	xxvii
CHAPTERS	
1. INTRODUCTION	1
2. THEORETICAL BACKGROUND	5
2.1. Basic Principles of Ion Exchange	5
2.2. Ion Exchange Materials.....	6
2.2.1 Natural Inorganic Ion Exchangers	7
2.2.2 Natural Organic Ion Exchangers	7
2.2.2.1. Ion Exchange Coals	8
2.2.3.Synthetic Inorganic Ion Exchangers	8
2.2.4. Synthetic Organic Ion Exchangers.....	10
2.2.5.Ion-Exchange Membranes	10
2.3. Uses of Ion Exchangers.....	12
2.4. Zeolites.....	15
2.4.1 Zeolites X and Y	18
2.5. Ion Exchange Selectivity.....	19
2.6. Ion Exchange in Batch Systems.....	21
2.6.1. Adsorption Isotherm Models.....	22
2.6.1.1. Two Parameter Isotherms.....	22
2.6.1.1.1. Langmuir Isotherm.....	22
2.6.1.1.2. Freundlich Isotherm.....	24

2.6.1.1.3. Dubinin-Radushkevich Isotherm	25
2.6.1.1.4. Temkin Isotherm.....	26
2.6.1.2. Three Parameter Isotherms	27
2.6.1.2.1. Redlich-Peterson Isotherm	27
2.6.1.2.2. Sips Isotherm	28
2.6.1.3. Multilayer Physisorption Isotherms	29
2.6.1.3.1. Brunauer–Emmett–Teller (BET) Isotherm	29
2.6.1.3.2. Frenkel–Halsey–Hill (FHH) Isotherm.....	30
2.6.1.3.3. MacMillan–Teller (MET) Isotherm.....	30
2.6.1.4. Isotherms for multicomponent systems.....	31
2.6.1.4.1. The Extended Langmuir Model.....	31
2.6.1.4.2. The Modified Langmuir Model	31
2.6.1.4.3. Jain and Snoeyink Model	33
2.6.1.4.4. SRS Model.....	33
2.6.1.4.5. Extended SIPS Model.....	34
2.6.1.4.6. IAST (Ideal Adsorbed Solution Theory) Model	35
2.6.2. Kinetics.....	36
2.6.2.1. Pseudo-first order equation or Lagergren's kinetics equation	36
2.6.2.2. Pseudo second order kinetics equation.....	36
2.6.2.3. Intraparticle Diffusion Equation	37
2.6.2.4. Elovich Kinetic Model	36
2.6.2.5. Pore Diffusion Bangham’s Kinetic Model.....	38
2.6.2.6. Modified Freundlich Kinetic Model	39
2.6.2.7. External Mass Transfer Diffusion Model	39
2.6.3. Goodness of the experimental data	40
2.6.4. Thermodynamics Parameters	41
2.7. Ion Exchange in Columns	42
2.8. Modeling Multicomponent Ion Exchange in Column.....	46
2.8.1. Law of Mass Action Model	47
2.8.1.1. MAL for Equilibrium Systems	47
2.8.1.2. Nonequilibrium MAL.....	48

2.8.2. Adsorption Models.....	50
2.8.2.1. Intraparticle Transport Mechanisms ...	50
2.8.2.2. Extraparticle Transport and Dispersion Mechanisms.....	52
2.8.2.3. Combined Models.....	52
2.8.3. Simplified Diffusion Models	56
2.8.4. Surface Reaction (Thomas) Model.....	60
2.8.5. Yoon-Nelson Model.....	61
2.8.6. Adams-Bohart Model.....	62
3. THEORETICAL BACKGROUND	63
4. MATERIALS AND METHODS	69
4.1. Materials and Methods	69
4.2. Characterization of Zeolite 13X beads	70
4.3. BET analysis..	70
4.4. Chemicals.....	70
4.5. Batch Studies.....	71
4.5.1. Maximum Exchange Level (MEL) Experiments	71
4.5.2. Equilibrium Isotherms.....	71
4.5.3. Batch Kinetic Experiments.....	72
4.6. SEM/EDX Analysis.....	73
4.7. Column Studies.....	73
5. RESULTS AND DISCUSSIONS	77
5.1. TGA Results.....	77
5.2. BET analysis..	77
5.3. Batch Studies.....	78
5.3.1. Maximum Exchange Level (MEL) Experiments	78
5.3.2. Equilibrium Isotherms.....	78
5.3.2.1. Single component Ion Exchange Isotherm Studies.....	79
5.3.2.2. Multi component Ion Exchange Isotherm Studies	92
5.3.3. Batch Kinetic Experiments.....	99
5.3.3.1. Pseudo-first order equation or Lagergren's kinetics equation	100

5.3.3.2. Pseudo second order kinetics equation.....	101
5.3.3.3. Intraparticle Diffusion Equation	102
5.3.3.4. Elovich Kinetic Model	105
5.3.3.5. Pore Diffusion Bangham's Kinetic Model.....	106
5.3.3.6. Modified Freundlich Kinetic Model	107
5.3.3.7. External Mass Transfer Diffusion Model	108
5.3.4. Thermodynamic Calculations.....	109
5.4. SEM/EDX analysis	112
5.5. pH Results of the Batch Studies	115
5.6. Column Studies..	117
5.6.1. Binary Column Studies	118
5.6.1.1. pH Results	118
5.6.1.2. Pb ²⁺ -NaX binary column studies	119
5.6.1.3. Cd ²⁺ -NaX binary column studies	126
5.6.1.4. Zn ²⁺ -NaX binary column studies	134
5.6.2. Ternary Ion Exchange Experiments	140
5.6.3. Quaternary Ion Exchange Experiments.....	144
5.6.4. Mathematical Modeling	146
6. CONCLUSION	153
REFERENCES.....	157
APPENDICES.....	165
A. CALCULATION OF EXCHANGE CAPACITIES	165
B. MAXIMUM EXCHANGE LEVEL (MEL) DATA.....	167
C. SINGLE COMPONENT ION EXCHANGE ISOTHERM DATA	169
D. MULTI COMPONENT ION EXCHANGE ISOTHERM DATA	171
E. ION EXCHANGE BATCH KINETICS DATA	175
F. SEM and EDX RESULTS	179
G. DATA FOR BREAKTHROUGH CURVE	197
H. BET SPECIFIC SURFACE AREA DETERMINATION	211
I. MATERIAL BALANCES.....	217
J. CALCULATION OF MOLECULAR DISFFUSIVITY (D _m)	219

K. CALCULATION of the BREAKTHROUGH CAPACITY, TOTAL EXCHANGE CAPACITY and COLUMN EFFICIENCY from BREAKTHROUGH CURVES.....	221
L. BREAKTHROUGH MODELS FOR Pb ²⁺ -NaX EXCHANGE	225
M. BREAKTHROUGH MODELS FOR Cd ²⁺ -NaX EXCHANGE	227
N. BREAKTHROUGH MODELS FOR Zn ²⁺ -NaX EXCHANGE	229
O. PRELIMINARY BREAKTHROUGH DATA	231
P. EXPERIMENTAL COMPETITION COEFFICIENTS PRODUCT CALCULATION FOR THE SRS MULTICOMPONENT ISOTHERM MODEL	237
R. EFFICIENCY VALUES OF DIFFERENT COLUMNS	239
CURRICULUM VITAE	241

LIST OF TABLES

TABLES

Table 1.1 Uses of ion exchange materials.....	13
Table 2.2 Rate Equations for Mass Transfer in Spherical Ion Exchanger/ Sorbent Particles.....	54
Table 2.3 Rate Coefficient k and Driving Force Expressions	55
Table 5.1 Langmuir isotherm constants	81
Table 5.2 Equilibrium parameters for Langmuir isotherm	81
Table 5.3 Freundlich isotherm constants	83
Table 5.4 DR Isotherm constants	85
Table 5.5 Temkin Isotherm Constants	86
Table 5.6 Redlich-Peterson Isotherm Constants	88
Table 5.7 BET Isotherm Constants	89
Table 5.8 SIPS Isotherm Constants.....	90
Table 5.9 Isotherm Linear Coefficient of Determination (R^2) Values	91
Table 5.10 Isotherm ARE Values	91
Table 5.11 Competition coefficients a_{ij} for Pb^{2+} - NaX, Cd^{2+} - NaX and Zn^{2+} -NaX binary ion exchange on Zeolite 13X beads..	98
Table 5.12 Single (Freundlich) and multicomponent SRS Equations	99
Table 5.13 Pseudo first order and second order kinetic model constants	102
Table 5.14 Intraparticle Diffusion Model Constants.....	104
Table 5.15 Elovich Kinetic Model Constants	105
Table 5.16 Bangham Kinetic Model Constants	106
Table 5.17 Modified Freundlich kinetic Model Constants	107
Table 5.18 External Diffusion Model Constants.....	108
Table 5.19 Thermodynamic parameters for Pb^{2+} - NaX, Cd^{2+} - NaX and Zn^{2+} -NaX binary exchange on Zeolite13X beads	110

Table 5.20 Distribution coefficients K_0 (L/g), of the single and multi- component ion exchange of Pb^{2+} , Cd^{2+} and Zn^{2+} on Zeolite 13X.....	111
Table 5.21 Summary of the selected batch systems and EDX Results in Appendix F	114
Table 5.22 Thomas model parameters determined for breakthrough curve for Pb^{2+}	120
Table 5.23 Yoon-Nelson model parameters determined for breakthrough curve for Pb^{2+}	121
Table 5.24 Adams--Bohart model parameters determined for breakthrough curve for Pb^{2+}	122
Table 5.25 Thomas model parameters determined for breakthrough curve for Cd^{2+}	127
Table 5.26 Yoon-Nelson model parameters determined for breakthrough curve for Cd^{2+}	128
Table 5.27 Adams--Bohart model parameters determined for breakthrough curve for Cd^{2+}	129
Table 5.28 Thomas model parameters determined for breakthrough curve for Zn^{2+}	134
Table 5.29 Yoon-Nelson model parameters determined for breakthrough curve for Zn^{2+}	135
Table 5.30 Adams-Bohart model parameters determined for breakthrough curve for Zn^{2+}	136
Table 5.31 Results for binary ion experiments	140
Table 5.32 Results for Pb^{2+} - Cd^{2+} - NaX ternary ion exchange (particle size 25/30 Mesh and influent total concentration of 0.05 N, flow rate of 10 ml/min).....	141
Table 5.33 Results for Zn^{2+} - Cd^{2+} - NaX ternary ion exchange (particle size 25/30 Mesh and influent total concentration of 0.05 N, flow rate of 10 ml/min).....	143

Table 5.34 Results for Zn ²⁺ - Pb ²⁺ - NaX ternary ion exchange (particle size 25/30 Mesh and influent total concentration of 0.05 N, flow rate of 10 ml/min).....	144
Table 5.35 Results for Zn ²⁺ - Pb ²⁺ - Cd ²⁺ - NaX quaternary ion exchange (particle size 25/30 Mesh and influent total concentration of 0.05 N, flow rate of 10 ml/min).....	145
Table 5.36 Dimensionless Peclet and Stanton Numbers	150
Table B.1 Total exchange capacity results for Pb ²⁺ - NaX and Cd ²⁺ - NaX exchange on Zeolite13X beads at 0.1N total concentration	167
Table B.2 Total exchange capacity results for Pb ²⁺ - NaX and Cd ²⁺ - NaX exchange on Zeolite13X beads at 0.05N total concentration	168
Table B.3 Total exchange capacity results for Pb ²⁺ - NaX and Cd ²⁺ - NaX and Zn ²⁺ - NaX exchange Zeolite13X beads at 0.05N total concentration and 0.8 g sample weight.....	168
Table C.1 Pb ²⁺ - NaX binary exchange on zeolite 13X beads at 25 °C.....	169
Table C.2 Cd ²⁺ - NaX binary exchange on Zeolite 13X beads at 25 °C.....	170
Table C.3 Zn ²⁺ - NaX binary exchange on Zeolite 13X beads at 25 °C.....	170
Table D.1 Pb ²⁺ - Cd ²⁺ - NaX ternary exchange on Zeolite 13X beads at 25 °C	171
Table D.2 Pb ²⁺ - Zn ²⁺ - NaX ternary exchange on Zeolite 13X beads at 25 °C	172
Table D.3 Zn ²⁺ - Cd ²⁺ - NaX ternary exchange on Zeolite 13X beads at 25 °C	173
Table D.4 Pb ²⁺ - Zn ²⁺ - Cd ²⁺ - NaX quaternary exchange on zeolite 13X beads.	174
Table E.1 Kinetics for Pb ²⁺ -NaX binary exchange on Zeolite 13X beads at 0.05N	175
Table E.2 Kinetics for Cd ²⁺ -NaX binary exchange on Zeolite 13X beads at 0.05N	176
Table E.3 Kinetics for Zn ²⁺ -NaX binary exchange on Zeolite 13X beads at 0.05N	177
Table G.1 Pb ²⁺ -NaX binary ion exchange (particle size 25/30 Mesh and influent Pb ²⁺ concentration 0.05 N, flow rate of 10 ml/min).....	197
Table G.2 Cd ²⁺ -NaX binary ion exchange (particle size 25/30 Mesh and influent Cd ²⁺ concentration 0.05 N, flow rate of 10 ml/min).....	199

Table G.3 Zn ²⁺ -NaX binary ion exchange (particle size 25/30 Mesh and influent Zn ²⁺ concentration 0.05 N, flow rate of 10 ml/min).....	201
Table G.4 Pb ²⁺ -Cd ²⁺ -NaX ternary ion exchange (particle size 25/30 Mesh and influent total concentration 0.05 N, flow rate of 10 ml/min).....	203
Table G.5 Zn ²⁺ - Cd ²⁺ -NaX ternary ion exchange (particle size 25/30 Mesh and influent total concentration 0.05 N, flow rate of 10 ml/min).....	205
Table G.6 Zn ²⁺ - Pb ²⁺ - NaX ternary ion exchange (particle size 25/30 Mesh and influent total concentration 0.05 N, flow rate of 10 ml/min).....	207
Table G.7 Zn ²⁺ - Pb ²⁺ - Cd ²⁺ - NaX quaternary ion exchange (particle size 25/30 Mesh and influent total concentration 0.05 N, flow rate of 10 ml/min).....	209
Table H.1 BET isotherm values	213
Table H.2 Multipoint BET values	214
Table O1. Pb ²⁺ -NaX binary ion exchange (concentration 0.1 N, flow rate of 15 ml/min)	231
Table O2. Pb ²⁺ -NaX binary ion exchange (concentration 0.05 N, 25/30 mesh size)	234
Table R1. Efficiency values for different columns for Pb ²⁺ -NaX binary exchange (Mesh size: 20/25 (0.710-0.853 mm); Flow rate: 10 ml/min; packed height:5-6)	239

LIST OF FIGURES

FIGURES

Figure 2.1 Zeolite structure and primary building units in the structure.....	9
Figure 2.2 (a) Secondary building units and (b) polyhedral units in zeolite framework structures (Ruthven, 1984)	16
Figure 2.3 Structures of (a) Zeolite A, (b) zeolites X and Y	18
Figure 2.4 Ionic and hydrated radius of some ions	20
Figure 2.5 Three principal resistances to mass transfer in a composite pellet (Ruthven, 1984)	21
Figure 2.6 Three regions of an ion exchange column (Zagarodni, 2007)	43
Figure 2.7 Breakthrough curve (Zagarodni, 2007).....	45
Figure 2.8 Diffusion and mass transfer mechanisms in a fixed bed of porous adsorbent particles (Perry and Green, 2008).	50
Figure 2.9 The reactant pathway from bulk to active site including diffusion processes. (Cejka, Corma and Zones, 2010)	57
Figure 2.10 Typical C/C_0 against $N(T-1)$ curves for solid diffusion control (dotted line) and fluid film diffusion control ($La=0.2$) (Inglezakis, 2006)	60
Figure 4.1 NÜVE ST 402 shaking waterbath	72
Figure 4.2 Experimental setup	75
Figure 5.1 Langmuir equilibrium isotherm model for Pb^{2+} - NaX, Cd^{2+} - NaX and Zn^{2+} -NaX binary exchange on Zeolite13X beads..	80
Figure 5.2 Freundlich equilibrium isotherm model for Pb^{2+} - NaX, Cd^{2+} - NaX and Zn^{2+} -NaX binary exchange on Zeolite13X beads..	83
Figure 5.3 DR equilibrium isotherm model for Pb^{2+} - NaX, Cd^{2+} - NaX and Zn^{2+} -NaX binary exchange on Zeolite13X beads..	84
Figure 5.4 Temkin equilibrium isotherm model for Pb^{2+} - NaX, Cd^{2+} - NaX and Zn^{2+} -NaX binary exchange on Zeolite13X beads..	86

Figure 5.5 Redlich-Peterson equilibrium isotherm model for Pb^{2+} - NaX, Cd ²⁺ - NaX and Zn ²⁺ -NaX binary exchange on Zeolite13X beads..	87
Figure 5.6 BET equilibrium isotherm model for Pb^{2+} - NaX, Cd ²⁺ - NaX and Zn ²⁺ -NaX binary exchange on Zeolite13X beads..	89
Figure 5.7 SIPS equilibrium isotherm model for Pb^{2+} - NaX, Cd ²⁺ - NaX and Zn ²⁺ -NaX binary exchange on Zeolite13X beads..	90
Figure 5.8 Lead ion exchange isotherms in single and multicomponent systems	93
Figure 5.9 Cadmium ion exchange isotherms in single and multicomponent systems	93
Figure 5.10 Zinc ion exchange isotherms in single and multicomponent systems	94
Figure 5.11 Linear form of the SRS multicomponent isotherm, Pb^{2+} in the existence of Cd ²⁺	94
Figure 5.12 Linear form of the SRS multicomponent isotherm, Cd ²⁺ in the existence of Pb^{2+}	95
Figure 5.13 Linear form of the SRS multicomponent isotherm, Pb^{2+} in the existence of Zn ²⁺	95
Figure 5.14 Linear form of the SRS multicomponent isotherm, Zn ²⁺ in the existence of Pb^{2+}	96
Figure 5.15 Linear form of the SRS multicomponent isotherm, Zn ²⁺ in the existence of Cd ²⁺	96
Figure 5.16 Linear form of the SRS multicomponent isotherm, Cd ²⁺ in the existence of Zn ²⁺	97
Figure 5.17 Ion exchange kinetics of Pb^{2+} - NaX, Cd ²⁺ - NaX and Zn ²⁺ -NaX binary ion exchange on Zeolite 13X beads at 25°C	100
Figure 5.18 First order kinetic model	101
Figure 5.19 Pseudo second order kinetic model	102
Figure 5.20 W&M diffusion model	103
Figure 5.21 U&T Intraparticle diffusion model	104
Figure 5.22 Elovich kinetic model	105

Figure 5.23	Bangham kinetic model	106
Figure 5.24	Modified Freundlich Kinetic model	107
Figure 5.25	External Mass Transfer Diffusion Model	108
Figure 5.26	Plot of $\ln(q_e/C_e)$ versus q_e	109
Figure 5.27	(a) Example of a SEM Image of prepared Zeolite 13X beads (25-30 Mesh sizes), (b) Example of a SEM Image of zeolite crystals in the Zeolite 13X beads (Experiment Run No:I18 of Table D.2)	113
Figure 5.28	Influence of pH on the ion exchange of Cd^{2+} -NaX binary exchange and Cd^{2+} - Pb^{2+} -NaX ternary exchange onto Zeolite 13X beads	116
Figure 5.29	Influence of pH on the ion exchange of Zn^{2+} -NaX binary exchange and Cd^{2+} - Zn^{2+} -NaX ternary exchange onto Zeolite 13X beads	117
Figure 5.30	pH change of solution at the outlet of the column for Pb^{2+} -NaX exchange onto Zeolite 13X beads.....	119
Figure 5.31	Breakthrough curves- $C_{0,\text{Pb}}=50$ meq/L; $C_{0,\text{Na}}=0$ meq/L.....	120
Figure 5.32	Thomas model for breakthrough $C_{0,\text{Pb}}=50$ meq/L; $C_{0,\text{Na}}=0$ meq/L	119
Figure 5.33	Yoon-Nelson model for breakthrough $C_{0,\text{Pb}}=50$ meq/L; $C_{0,\text{Na}}=0$ meq/L.....	122
Figure 5.34	Adams-Bohart model for breakthrough $C_{0,\text{Pb}}=50$ meq/L; $C_{0,\text{Na}}=0$ meq/L	123
Figure 5.35	Simplified model for Pb^{2+} - NaX binary exchange on Zeolite 13X in fixed bed ($L_a=0.2$)	124
Figure 5.36	Simplified model for Pb^{2+} - NaX binary exchange on Zeolite 13X in fixed bed, estimated using batch method ($L_a=0.002$; $Q_M=5.4$ meq/g)	125
Figure 5.37	Simplified model for Pb^{2+} - NaX binary exchange on Zeolite 13X in fixed bed, estimated using column method ($Q_M=3.2$ meq/g).....	125

Figure 5.38 $N_s(T-1)$ versus $(T-1)$ graph for Pb^{2+} -NaX exchange ($La=0.002$; $Q_M=3.2$ meq/g).....	126
Figure 5.39 Breakthrough curves- $C_{0,Cd}=50$ meq/L; $C_{0,Na}=0$ meq/L.....	127
Figure 5.40 Thomas model for breakthrough $C_{0,Cd}=50$ meq/L; $C_{0,Na}=0$ meq/L.....	128
Figure 5.41 Yoon-Nelson model for breakthrough $C_{0,Cd}=50$ meq/L; $C_{0,Na}=0$ meq/L	129
Figure 5.42 Adams-Bohart model for breakthrough $C_{0,Cd}=50$ meq/L; $C_{0,Na}=0$ meq/L	130
Figure 5.43 Simplified model for Cd^{2+} - NaX binary exchange on Zeolite 13X in fixed bed ($La=0.2$).....	131
Figure 5.44 Simplified model for Cd^{2+} - NaX binary exchange on Zeolite 13X in fixed bed, estimated using batch method ($La=0.014$; $Q_M=4.2$ meq/g)	132
Figure 5.45 Simplified model for Cd^{2+} - NaX binary exchange on Zeolite 13X in fixed bed, estimated using column method ($Q_M=1.9$ meq/g).....	133
Figure 5.46 $N_s(T-1)$ versus $(T-1)$ graph for Cd^{2+} -NaX exchange ($La=1.52 \times 10^{-4}$; $Q_M=1.9$ meq/g)	133
Figure 5.47 Breakthrough curves- $C_{0,Zn}=50$ meq/L; $C_{0,Na}=0$ meq/L.....	134
Figure 5.48 Thomas model for breakthrough $C_{0,Zn}=50$ meq/L; $C_{0,Na}=0$ meq/L	135
Figure 5.49 Yoon-Nelson model for breakthrough $C_{0,Zn}=50$ meq/L; $C_{0,Na}=0$ meq/L	136
Figure 5.50 Adams-Bohart model for breakthrough $C_{0,Zn}=50$ meq/L; $C_{0,Na}=0$ meq/L	137
Figure 5.51 Simplified model for Zn^{2+} - NaX binary exchange on Zeolite 13X in fixed bed, estimated using batch method ($La=0.1$; $Q_M=3.5$ meq/g)	138
Figure 5.52 Simplified model for Zn^{2+} - NaX binary exchange on Zeolite 13X in fixed bed, estimated using column method ($Q_M=2.3$ meq/g).....	138

Figure 5.53 $N_s(T-1)$ versus $(T-1)$ graph for Zn^{2+} -NaX exchange ($L_a=0.034$; $Q_M=2.3$ meq/g).....	139
Figure 5.54 Breakthrough curves- $C_{0,Pb}=30$ meq/L; $C_{0,Cd}=30$ meq/L $C_{0,Na}=0$ meq/L	141
Figure 5.55 Breakthrough curves- $C_{0,Cd}=25$ meq/L; $C_{0,Zn}=25$ meq/L $C_{0,Na}=0$ meq/L	142
Figure 5.56 Breakthrough curves- $C_{0,Pb}=25$ meq/L; $C_{0,Zn}=25$ meq/L $C_{0,Na}=0$ meq/L	143
Figure 5.57 Breakthrough curves- $C_{0,Pb}=17$ meq/L; $C_{0,Cd}=17$ meq/L $C_{0,Zn}=16$ meq/L; $C_{0,Na}=0$ meq/L	145
Figure 5.58 Simulated breakthrough curve (C/C_0 versus t graph) $C_{0,Pb}=50$ meq/L $C_{0,Na}=0$ meq/L	151
Figure 5.59 Simulated 3D Breakthrough curve (C versus t versus x graph) $C_{0,Pb}=50$ meq/L $C_{0,Na}=0$ meq/L	152
Figure 5.60 Comparison between simulated and experimental breakthrough curves $C_{0,Pb}=50$ meq/L $C_{0,Na}=0$ meq/L	152
Figure A.1 TGA of commercial zeolite 13X beads	166
Figure F.1 (a) SEM Image of zeolite crystals in the Zeolite 13X beads (magnification: 10000x), (b) SEM Image of zeolite crystals in the Zeolite 13X beads (magnification: 50000x) for the Pb^{2+} - Cd^{2+} -NaX ternary ion exchange system.	179
Figure F.2 EDX analysis of Pb^{2+} - Cd^{2+} -NaX ternary ion exchange system	180
Figure F.3 (a) SEM Image of zeolite crystals in the Zeolite 13X beads (WD:9.4 mm), (b) SEM Image of zeolite crystals in the Zeolite 13X beads (WD:9.5 mm) for the Pb^{2+} - Cd^{2+} -NaX ternary ion exchange system.	181
Figure F.4 EDX analysis of Pb^{2+} - Cd^{2+} -NaX ternary ion exchange system	182
Figure F.5 (a) SEM Image of zeolite crystals in the Zeolite 13X beads (magnification: 10000x), (b) SEM Image of zeolite crystals in the Zeolite 13X beads (magnification: 50000x) for the Pb^{2+} - Zn^{2+} -NaX ternary ion exchange system.....	183

Figure F.6 EDX analysis of Pb^{2+} - Zn^{2+} -NaX ternary ion exchange system	184
Figure F.7 (a) SEM Image of zeolite crystals in the Zeolite 13X beads, (b) cross- section of the Zeolite 13X bead for the Pb^{2+} - Zn^{2+} -NaX ternary ion exchange system	185
Figure F.8 EDX analysis of Pb^{2+} - Zn^{2+} -NaX ternary ion exchange system	186
Figure F.9 (a) SEM Image of zeolite crystals in the Zeolite 13X beads (magnification: 10000x), (b) SEM Image of zeolite crystals in the Zeolite 13X beads (magnification: 50000x), for the Cd^{2+} - Zn^{2+} -NaX ternary ionexchange system.....	187
Figure F.10 EDX analysis of Cd^{2+} - Zn^{2+} -NaX ternary ion exchange system	188
Figure F.11 (a) SEM Image of zeolite crystals in the Zeolite 13X beads, (b) SEM Image of zeolite crystals in the Zeolite 13X beads for the Cd^{2+} - Zn^{2+} -NaX ternary ion exchange system from another region.....	189
Figure F.12 EDX analysis of Cd^{2+} - Zn^{2+} -NaX ternary ion exchange system	190
Figure F.13 (a) SEM Image of zeolite crystals in the Zeolite 13X beads (magnification: 10000x), (b) SEM Image of zeolite crystals in the Zeolite 13X beads (magnification: 50000x), for the Pb^{2+} - Cd^{2+} - Zn^{2+} -NaX quaternary ion exchange system.....	191
Figure F.14 EDX analysis of Pb^{2+} - Cd^{2+} - Zn^{2+} -NaX ternary ion exchange system	192
Figure F.15 (a) SEM Image of zeolite crystals in the Zeolite 13X beads, (b) cross- section of the Zeolite 13X bead for the Pb^{2+} - Cd^{2+} - Zn^{2+} -NaX quaternary ionexchange system	193
Figure F.16 EDX analysis of Pb^{2+} - Cd^{2+} - Zn^{2+} -NaX quaternary ion exchange system	194
Figure F.17 (a) SEM Image of zeolite crystals in the Zeolite 13X beads (magnification: 6000x), (b) SEM Image of zeolite crystals in the Zeolite 13X beads (magnification: 50000x), for the Pb^{2+} - Cd^{2+} - NaX ternary dynamic ion exchange system.....	195

Figure F.18 EDX analysis of Pb^{2+} - Cd^{2+} - Zn^{2+} -NaX quaternary dynamic ion exchange system	196
Figure H.1. BET Isotherm of Zeolite 13X	214
Figure H.2. Multipoint BET plot of Zeolite 13X	215
Figure K.1. Breakthrough curves- $C_{0,Pb}=50$ meq/L; $C_{0,Na}=0$ meq/L	222
Figure K.2. Representation of area under the curve A_u and breakthrough area A_{br}	223
Figure L.1. Linearization of Thomas Model Pb^{2+} -NaX Exchange	225
Figure L.2. Linearization of Yoon-Nelson Model Pb^{2+} -NaX Exchange	226
Figure L.3. Linearization of Adams-Bohart Model Pb^{2+} -NaX Exchange	226
Figure M.1. Linearization of Thomas Model Cd^{2+} -NaX Exchange	227
Figure M.2. Linearization of Yoon-Nelson Model Cd^{2+} -NaX Exchange	228
Figure M.3. Linearization of Adams-Bohart Model Cd^{2+} -NaX Exchange	228
Figure N.1. Linearization of Thomas Model Zn^{2+} -NaX Exchange	229
Figure N.2. Linearization of Yoon-Nelson Model Zn^{2+} -NaX Exchange	230
Figure N.3. Linearization of Adams-Bohart Model Zn^{2+} -NaX Exchange	230
Figure O1. Breakthrough curves at different mesh sizes-($C_{0,Pb}=50$ meq/L; $C_{0,Na}=0$ meq/L ; concentration 0.1 N, flow rate of 15 ml/min)	233
Figure O2. Breakthrough curves at different flow rates-($C_{0,Pb}=50$ meq/L; $C_{0,Na}=0$ meq/L ; concentration 0.05 N, 25/30 mesh size)	236

LIST OF SYMBOLS

a_e	: activity of metal ion in solution at equilibrium
a_s	: activity of metal ion in the zeolite phase
A	: initial rate (mg/gmin) in the Elovich Kinetic Model
ARE	: average of relative errors
b	: Langmuir constant (L/mg)
b_s	: Sips isotherm constant
b_i, b_j	: Langmuir constants of the adsorbates “i” and “j” in the multicomponent system
b_T	: Temkin constant related to the variation of adsorption energy (kJ/mol).
B	: Elovich Kinetic Model constant related to the surface coverage and the activation energy for chemisorptions (g/mg).
B_T	: Temkin constant related to the heat of adsorption (kJ/mol)
C_A	: equilibrium concentration of cation A in the solution phase (mg/L)
C_{BET}	: BET adsorption isotherm constant (L/mg)
C_e	: liquid-phase equilibrium concentration (mg/L)
C_{ei}, C_{ej}	: concentrations of the adsorbate “i” and “j” remaining in liquid at equilibrium
C_o	: initial concentration (mg/L)
C_{0A}	: initial concentration of A (mg/L)
CEC_{mz}	: cation exchange capacity of each dried zeolite mass
d	: Frenkel–Halsey–Hill (FHH) isotherm related to interlayer spacing
d_p	: the particle diameter
D_i	: diffusion coefficient in the solid.
E	: mean free energy of adsorption per mole of the adsorbate
H	: initial adsorption rate (mg g ⁻¹ h ⁻¹)
k	: MacMillan–Teller (MET) isotherm constant
k_0	: Pore Diffusion Bangham’s Kinetic Model constant [ml/(g/L)]
k_1	: pseudo-first order rate constant (L/min)

k_2	: pseudo second-order rate constant ($\text{gm g}^{-1} \text{ h}^{-1}$).
k_i	: the intraparticle diffusion rate constant ($\text{mg g}^{-1} \text{ min}^{0.5}$)
K_o	: thermodynamic distribution coefficient
K_F	: Freundlich isotherm constant (L/g)
K_{LF}	: Sips isotherm constant in the Langmuir-Freundlich form
K_{RP}	: Redlich-Peterson constant (L/g)
K_T	: equilibrium binding constant for Temkin isotherm (L/mg)
La	: equilibrium parameter for Langmuir isotherm
n	: Freundlich equation exponent
n_F	: FHH isotherm constant related to the inverse power of distance from the surface
q_d	: Dubinin–Radushkevich isotherm constant (mg/g)
q_e	: the zeolite phase concentration in equilibrium with the liquid-phase concentration C_e (mg/g)
$q_{e,i}$: equilibrium uptake of the adsorbate “i” in the multicomponent system
q_{max}	: solid-phase concentration in equilibrium with C_o
q_s	: column / theoretical isotherm saturation capacity (mg/g)
Q_{br}	: breakthrough capacity of the ion exchange column
Q_M	: Langmuir maximum adsorption capacity (meq/g)
Q_{Mi}	: Langmuir maximum adsorption capacity for the component i
R	: universal gas constant (8.314 J/mol.K)
t	: contact time (min).
T	: the absolute temperature (K)
V_{br}	: volume passed prior to the breakthrough moment
X_{AS}	: equivalent fraction of the same cation in solution
X_{AZ}	: equivalent fraction of the cation in the zeolite (solid) phase
Z_A, Z_B	: valences of arbitrary ions A and B
$1/n$: Sips isotherm exponent constant.
$1/n_{LF}$: Sips isotherm exponent constant in the Langmuir-Freundlich form

α	:	FHH isotherm constant (Jmr/mole)
α_B^A	:	separation factor
α_{ij}	:	the competition coefficient
α_{RP}	:	Redlich-Peterson constant (L/mmol)
β	:	constant related to the E
β	:	Redlich-Peterson constant
β_L	:	Liquid-solid mass transfer coefficient
γ_e	:	activity coefficient of metal ion in equilibrium solution
γ_s	:	activity coefficient of metal ion in the zeolite
ε	:	the Polanyi potential
R^2	:	linear coefficient of determination
X^2	:	non-linear Chi-square
ΔH^0	:	standard enthalpy change ($kJmol^{-1}$)
ΔG^0	:	standard Gibbs free energy ($kJmol^{-1}$)
ΔS^0	:	standard entropy change ($Jmol^{-1}K^{-1}$)

CHAPTER 1

INTRODUCTION

Cadmium is a very toxic metal that influences the activity of enzymes. It also decelerates photosynthesis, respiration, chlorosis and transpiration. Lead is not either as harmful or as available as cadmium but it is more omnipresent in the atmosphere and functions as an accruing contamination (Ahmed et al., 1998). Lead and cadmium are heavy metals and they are first concern harmful contaminants which usually intervene with the advantageous use of wastewater for flooding and industrial applications. Also at military and industrialized installments, they are common groundwater contaminants. (Mier et al, 2001).

Zinc is a adaptable metal and its molding and mechanical work are facilitated by its properties (Ostroski et al, 2009). Zinc is generally found in cereals and meat and it is necessary for growth and development. For providing corrosion resistance Zinc and its alloys are extensively used to electroplate steel, (Ostroski et al, 2012). The request for alkaline zinc manganese batteries, is higher than mercury batteries, and this causes difficulties if disposal of those batteries are not done in a proper way. In addition, the flooding of ore mines might be another source of the environment pollution (Ostroski et al, 2009).

Human wellbeing, living sources, and eco-friendly systems are affected badly by the rising amount of heavy metals in the atmosphere. Movable and dissolvable heavy metals are not environment-friendly and they cause numerous disorders and diseases by accumulating in living organisms. Wastewaters of many industries like mining

and metal plating are contaminated with heavy metals (Sprynsky et al. 2006). Pollution also exists in the soils which surround several military bases and becomes a danger of groundwater and surface water pollution. Considerable quantities of liquid and solidwaste consisting of various amounts of heavy metals are also produced by pulp, petroleum refining and few organic compounds industries (Trgo et al. 2006).

To remove dissolved heavy metals numerous processes can be used. These processes includes ion exchange, extraction, precipitation ultrafiltration and reverse osmosis. However a lot of them might be slightly economical or demanding to execute in countries which are developing. As a result, there is a simple, robust treatment strategy that also addresses local resources and constraints (Mier et al, 2001). If the separation process is selective enough the effective recovery of these metals is possible. To reduce the amount of metal wastes selective ion-exchangers can be used. They also can be used for purificating process liquids for re-use and for the treatment of final wastewaters (Pehlivan et al. 2007). Among the known ion exchangers, a special attention must be given to zeolites because of their high exchange capacity with reasonable costs (Barros et al., 2004).

Zeolites are crystalline alumino-silicate materials and they can contain an extensive diversity of positive ions, such as Cd^{2+} , Zn^{2+} , Pb^{2+} and others. These ions are not held tightly and in a contact solution they can easily be interchanged for others. Cavities and interconnected channels characterizes a very regular porous structure of zeolite. Some molecules can penetrate these channels while others are excluded. A small amount of binder palletizes the crystals. Therefore, for zeolites there are two distinct pores (macropores in the binder, micropores in the crystals) formation present (Gorka et al., 2008).

Among the various commercially available zeolites, binder free synthetic zeolites such as zeolite X, has steady and high ion exchange capacity which means their

exchangeable cations can easily be replaced and they can be utilized for extracting heavy metals from wastewaters (Barros et al., 2008).

Fixed-bed systems are used extensively for industrial separation processes especially in the petrochemical industry. These processes are progressively drawing attention in environmental engineering. Since the removal of secondary waste produced by ion exchange or sorption systems in industry requires additional costly treatment, precise modeling or simulation of the fixed bed processes in order to improve design parameters becomes crucial. Significant studies were done to model multicomponent ion exchange in the 1980s. The algebra needed for modeling ion exchange and sorption are basically identical unless ion exchange is rate limiting. For predicting results of different types of ion-exchange/sorption systems, various models have now been established. Unluckily, a common explanation for multicomponent ion exchange/sorption, that contains mass transfer, complex isotherms and hydrodynamic dispersion, is unavailable yet (Robinson et al., 1994).

In this thesis, the aim is to establish a useful mathematical representation of the binary and multicomponent ion exchange on synthetic zeolites in fixed-bed columns. Experimental results are recorded to verify this model and its numerical solution. This will involve:

- (1) obtaining multicomponent equilibrium data in batch systems,
- (2) obtaining experimental multicomponent breakthrough curves,
- (3) developing a model for binary and multicomponent ion exchange in fixed-bed columns,
- (4) developing a computer program to solve these equations,
- (5) comparing the simulated curves with the experimental ones.

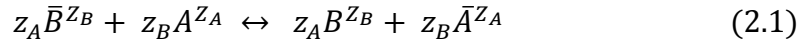
CHAPTER 2

THEORETICAL BACKGROUND

2.1. Basic Principles of Ion Exchange

Ion exchange is explained as the identical exchange of ions among two or more ionized species, settled in separate phases (i.e. liquid phase and solid phase) without the formation of other kinds of chemical bonds. Ion exchanger contains insoluble carrier (matrix) of electric charge. The matrix cannot move from the phase in which it is settled, that is because of dissolution. Ion-exchange capability exists in some natural materials, such as clays and zeolites, but synthetic materials are used in most of the industrial ion-exchange processes. They are prepared from organic polymers such as crosslinked polystyrene where ionizable functional groups are introduced. In solutions, the positive or negative charge of these fixed matrix sites is compensated for by ions of opposite charge, the supposed counterions. The latter are unobstructed for moving and different ions that bears the identical charge can take the place of them. Mobile ions that have the same sign charges with the matrix charge are referred to as co-ions.

Several different symbols have been used to present an exchange of counterions between solid (ion exchanger) and solution phases. One common way to present the binary exchange of $z_A z_B$ equivalents of two arbitrary ions A and B of valence z_A and z_B , respectively, in which overbars refer to counterions in the ion exchanger phase, is expressed as follows:



For such operations, the mathematical treatment of mass transfer is most generally done by analogy to adsorption through a formalism referred to as ion movement theory. This approach is established on the consideration that a solute (an ion in this case) within the packed section of an ion exchange column can be found in one of the following three locations: interstitial void space (between the particles), intraparticle voids (inside the particles) or adsorbed to the particles, thus imposing different velocities of movement for different ions depending on their physicochemical properties and on the type, capacity, and arrangement of ion-exchange particles. Furthermore, co-ions (ions with the identical charge as the functional groups fixed to the zeolite) generally are excluded and remain in the interstitial void space. Therefore, the movement of a target counterion is controlled by its ion-exchange isotherm and the ratio between zeolite ion exchange capacity and concentration of counterions in liquid phase. As a result, if the solution is dilute and the zeolite ion-exchange capacity is high, then counterions are expected to move more slowly. For the cases of ion-exchange beads or ion-exchange membranes, interdiffusion of counterions can be more simply described by phenomenological approaches. It has been so far most frequently described by the following Nernst–Planck equation without including a convection term in which the symbols used have their usual meanings:

$$\bar{J}_i = -\bar{D}_i \left(\text{grad} \bar{C}_i + z_i \bar{C}_i \frac{F}{RT} \text{grad} \varphi \right) \quad (2.2)$$

2.2. Ion Exchange Materials

Numerous natural organic and inorganic materials have ion exchange characteristics. At the end of the 1930s, the phenolic-type commodities were introduced then synthetic organic ion-exchange resins came to be accessible.

In the middle of 1940s styrenic resins became available, and about 20 years later acrylic resins appeared. From early to mid-1990s, the styrenic resins prevailed the ion-exchange market, however acrylic resins are becoming more and more valuable. Phenolic-based resins have nearly vanished.

There are other resin types which are accessible in the market but have not made an important effect. In several areas in which synthetic organic ion-exchange resins are not commonly utilized, inorganic materials remain important (Kirk-Othmer, 2010).

2.2.1. Natural Inorganic Ion Exchangers

Numerous natural inorganic minerals, like clays (i.e., kaolinite, montmorillonite and bentonite) and zeolites (i.e., chabazite, ferrierite and clinoptilolite) have capacity to exchange ions. Nevertheless, crystalline aluminosilicates are mainly the generally known natural minerals which has cation exchange characteristics (Hellferich, 1962). Other natural aluminosilicate materials, like green sand, are particularly used in waste-treatment operations (Inglezakis, 2006).

2.2.2. Natural Organic Ion Exchangers

Naturally occurring organic ion exchangers are listed below:

- proteins (casein, keratin, collagen and gelatin),
- polysaccharides (pectin, algic acid and cellulose),
- ion exchange coals (charcoals and lignitic coals).

Nevertheless, apart from ion exchange coals neither of them are used in industrial applications. Despite the fact that they are less effective than synthetic organic exchangers, they are an appealing choice because of their low cost.

2.2.2.1. Ion Exchange Coals

Ion exchange coals can be used as cation exchangers. Most of them swell excessively, are easily decomposed by alkali, and have a tendency to peptize. Therefore before using them, they must be “stabilized”.

Soft and hard lignitic coals can be stabilized by treatment with solutions of copper, chromium, or aluminum salts. Pitch and glance coals which are treated with sodium hydroxide or hydrochloric acid solutions are chemically more stable.

For converting most lignitic and bituminous coals and anthracites into strong-acid cation exchangers, they must be sulfonated with fuming sulfuric acid. In certain respects, sulfonated coals are similar to organic ion-exchange resins. They have fixed ionic groups and a gel structure. Nevertheless, their composition is less uniform and their mechanical and chemical stability, particularly their resistance to alkali, is inferior. The earlier Zeo-Karb ion exchangers, Zeolite H-53 and S-53 and Dusarit S are sulfonated coals (Helfferich, 1962).

2.2.3. Synthetic Inorganic Ion Exchangers

Synthetic zeolites (i.e., synthetic Zeolite X (synthetic Faujasite) and Zeolite A (no exact match in nature)) which are accessible in the form of powder, pellet, or bead, can be produced with a wide diversity of physicochemical characteristics and this is their advantage against natural zeolites. three dimensional representation is given in Figure 2.1.

Inorganic cation exchangers alternative to aluminosilicate frameworks have been synthesized. The oxides of zirconium and titanium which are stable to acids and bases are practically important. To remove metal ions especially uranium from water, titanium oxides are sufficiently used. To remove radioactive cesium ions transition metal hexacyanoferrates are used.

When compared with the organic ion exchanger resins, inorganic cation exchangers made from combination of group IV oxides with group V and VI (i.e., zirconium phosphates) are thermally more stable than and have higher exchange capacities and more resistant to radiation.

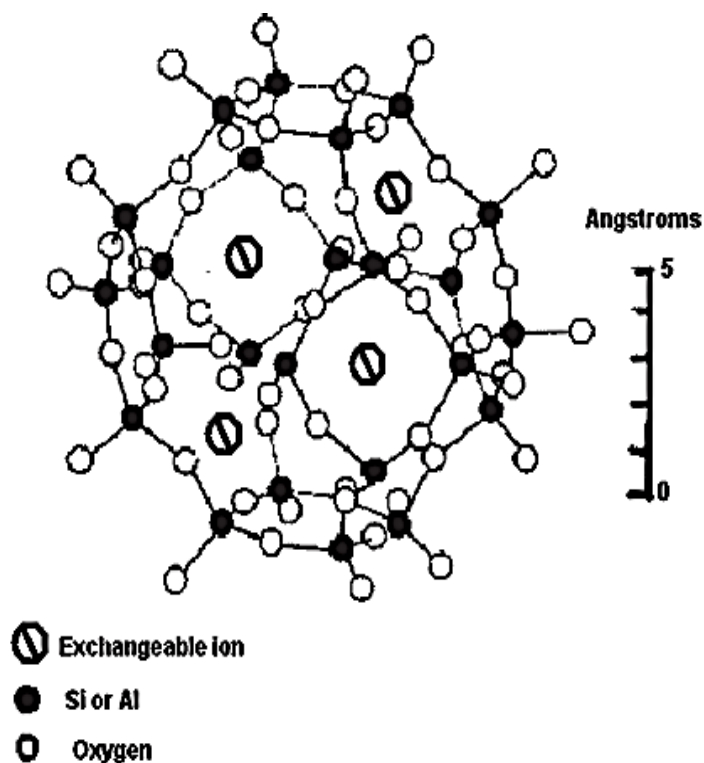


Figure 2.1. Zeolite structure and primary building units in the structure

2.2.4. Synthetic Organic Ion Exchangers

Synthetic organic resins are the largest group available among ion exchangers. Organic resins are synthesized by addition polymerization and condensation polymerization.

In cation exchangers, resin matrix framework consists of ionic groups such as SO_3^- , COO^- , PO_3^{2-} , AsO_3^{2-} , and in anion exchangers it consists of NH_3^+ , NH_2^+ , N^+ , S^+ . Hence, ion exchange resins are crosslinked polyelectrolytes (Helfferich, 1962).

The resins are made insoluble by crosslinks that adjoin hydrocarbon chains. This requires rupture of the carbon-carbon bonds. In this manner resins become insoluble and they are not damaged by any solvents. The matrix of the resins, unlike zeolites, is a flexible random network. The mesh width is not uniform and this a fact that is referred to as heteroporosity. Since the matrix is elastic and expandable the resins can swell by the introduction of the solvent (Helfferich, 1962).

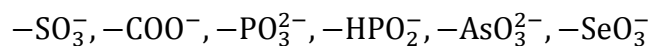
The swelling of the resin and the mobilities of the counter ions determines the range of crosslinking and the extent of crosslinking influences the chemical, thermal and mechanical stability of the resins. The nature and number of the fixed ionic groups affects selectivity and the ion exchange capacity of the resins (Helfferich, 1962).

2.2.5. Ion-Exchange Membranes

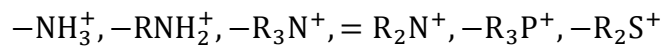
The characteristics and preparation procedures of ion exchange resins and ion exchange membranes are alike. Ion exchange membranes are mainly utilized in electrodialysis, membrane electrolysis, batteries, and fuel cells. Mostly, the matrix of an ion-exchange membrane contains a hydrophobic polymer like polystyrene, polyethylene, or polysulfone.

The type and the concentration of fixed ionic groups affect the selectivity and the electrical resistance and additionally influence mechanical properties of the membrane mainly by controlling the degree of swelling.

The following functional groups are most commonly utilized as fixed ionic groups in cation exchange membranes:



In anion exchange membranes fixed ionic groups can be some of the following:



Special types of ion exchange membranes (eg, monovalent ion selective, bipolar, and perfluorinated proton-conductive membranes) also have been developed for particular applications.

Bipolar membranes recently have achieved expanding consideration as an effective instrument in order to produce acids and bases from their equivalent salts by electrically enforced accelerated water separation (Nagarale et al, 2006).

Monovalent cation and anion selective ion-exchange membranes have been utilized in Japan for producing sodium chloride (edible salt) by electro-dialytic concentration of seawater (Kirk-Othmer, 2010).

The perfluorinated proton-conductive membranes, such as Nafion (sulfonated tetrafluoroethylene based fluoropolymer-copolymer which has a molecular formula of $\text{C}_7\text{HF}_{13}\text{O}_5\text{S}$. C_2F_4 , discovered in 1960 by DuPont), are important elements of fuel cells.

These membranes provide high stability and great conductivity because of the hydrophilicity of the sulfonic acid side chain groups and hydrophobicity of the fluorinated polymer matrix.

2.3. Uses of Ion Exchangers

Possibly, the initial broad investments in the advancement of ion exchangers and ion exchange processes were carried out by considering the possible utilization for isotope separation in nuclear industry. Nevertheless, the maximum quantity of ion exchange materials commercially available present day is used for applications in water treatment. Water is consumed mostly by the nuclear and electronics industries (Zagarodni, 2007).

Ion exchange resins are commonly used in food industry and pharmaceuticals because however they are chemically active and very stable, they do not contaminate the product.

The extensive utilization of ion exchange resins in pharmaceuticals and in food industry is described by another benefit of these materials. Although they are chemically active and very stable, they cause no contamination in the product (Zagarodni, 2007).

A wide ranging utilization of chelate forming ion exchangers in hydrometallurgy is that it is possible to develop very selective separation systems for few ions. Removal of uranium or noble metals can be cited as most generally known examples.

Many of the utilizations in biochemistry and biotechnology capitalize on separate particular phenomena in addition normally applied ion exchange interactions.

These phenomena let to design of extraordinary methods and technologies for obtaining beneficial products and side products from complex biochemical mixtures.

Utilizations of ion exchangers in pharmaceutical are under thorough improvement. A controlled drug release is one of the most apperant prospects. Certain ion exchange materials can be included in the pharmaceutical recipes for delaying consumption of the drug by a patient's body. Because of their high chemical stability, polymers like these are not harmful when, for instance, they are taken as pills.

Utilizations in chemical analysis are expansive and by some means dissimilar from industrial utilizations. The explanation is in the substially particular aim of the treatment: acquiring or enhancement of the analytical signal rather than a chemical product. Precision like this influences the methods of materials' using, as long as all processes are established by the identical physico-chemical principles (Zagarodni, 2007).

Some of the uses of ion exchange materials are listed in Table 1.1

Table 1.1. Uses of ion exchange materials.

Water preparation ■ pure and ultrapure deionised water ■ water softening,	Isotope separation: ■ Eu^{3+} isotopes, ■ lithium, boron, nitrogen isotopes,
Removal of specific constitutes: ■ removal toxic ions like chromium from drinking water, ■ organic matter removal, ■ iron and manganese removal, ■ nitrate removal ■ ammonia removal	Purification of sugars and polyhydric alcohols: ■ purification of cane, corn, and beet sugars, ■ purification of fructose, ■ separation of monosaccharides, ■ purification of glycerine
Nuclear industry: ■ separation of uranium isotopes, ■ waste decontamination	Pulp and paper industry: ■ removal of inorganic salts from liquid.

Table 1.1. (cont'd) Uses of ion exchange materials.

<p>Recovery of waste streams:</p> <ul style="list-style-type: none"> ■ removal of heavy metal ions, ■ removal of radioactive substances, ■ recycling of industrial water. 	<p>Food industry:</p> <ul style="list-style-type: none"> ■ removing off odors, ■ recovery of glutamic-acid, ■ deacidification of fruit juice.
<p>Separation of biological molecules:</p> <ul style="list-style-type: none"> ■ amino acids, ■ proteins, ■ enzymes, ■ DNA 	<p>Winery:</p> <ul style="list-style-type: none"> ■ sorption of wine proteins ■ stabilisation ■ ethylbenzene synthesis ■ catalytic reduction of nitrogen oxides
<p>Biotechnology:</p> <ul style="list-style-type: none"> ■ separation of lactic acid ■ production of l-glutamine and ■ production of citric acid ■ production of organic acids 	<p>Separation in hydrometallurgy</p> <ul style="list-style-type: none"> ■ uranium, thorium, tungsten ■ rare earth metals like yttrium, scandium ■ transition metals like silver and gold.
<p>Soil science and technology:</p> <ul style="list-style-type: none"> ■ artificial soils ■ remediation of contaminated soils ■ evaluation of soil properties 	<p>Pharmaceutics and medicine:</p> <ul style="list-style-type: none"> ■ antibiotics ■ vitamins ■ active ingredients ■ controlled and sustained drug release ■ immobilisation of drugs
<p>Analysis:</p> <ul style="list-style-type: none"> ■ chromatography, ■ sample preparation: separation, concentrating, purification, 	<p>Drying of different media:</p> <ul style="list-style-type: none"> ■ Desiccation of solvents with zeolites, ■ Gas drying with polymeric exchangers and zeolites.
<p>Catalysis:</p> <ul style="list-style-type: none"> ■ petroleum refining with zeolites. 	

2.4. Zeolites

Zeolites are absorbent crystalline aluminosilicates. The zeolite structure involves an assembly of SiO_4 and AlO_4 tetrahedra, attached together in miscellaneous regular arrangements though shared oxygen atoms, to develop an open crystal lattice includes pores of molecular dimensions into which target molecules can diffuse.

Considering the micropore framework is verified by the crystal lattice it is strictly uniform without distribution of pore size. This characteristic distinguishes the zeolites from the other microporous adsorbents.

Approximately 38 different zeolite framework structures have been identified, including both natural and synthetic forms.

In analyzing zeolite framework it is appropriate to view the structures as developed from assemblages of secondary building units. These units are polyhedra which consists of various SiO_4 and AlO_4 tetrahedra. The secondary building units and some of the generally occurring polyhedral units in zeolite framework structures are schematically represented in Figure 2.2. In the diagrams each vertex depicts the location of a Si or Al atom and the lines depict, approximately, the diameters of the oxygen atoms or ions. These ions are quite bigger than the tetrahedral Si or Al atoms.

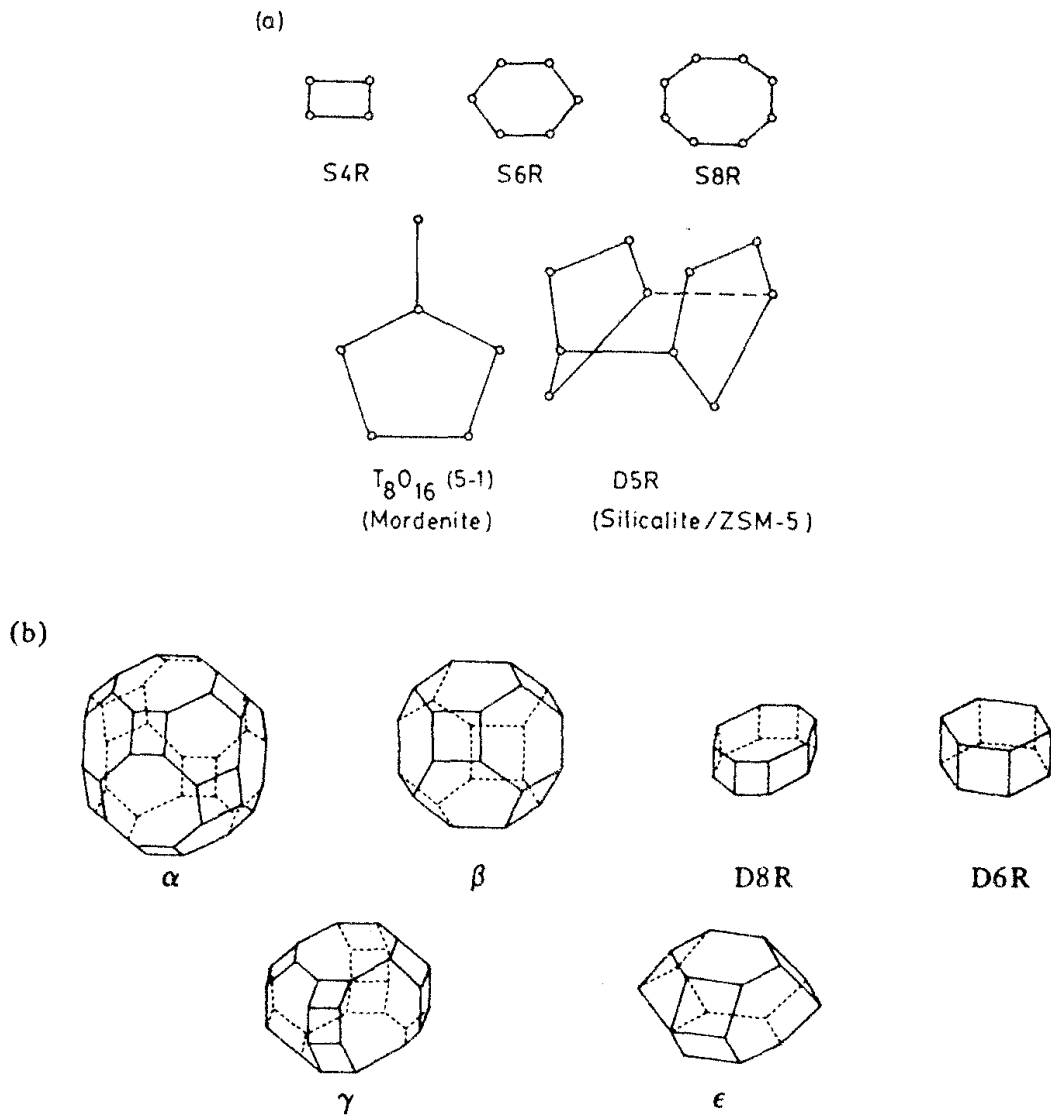


Figure 2.2. (a) Secondary building units and (b) polyhedral units in zeolite framework structures (Ruthven, 1984).

Every aluminum atom adds one negative charge on the framework that have to be adjusted by an interchangeable cation.

The form of zeolite A is shown schematically in Figure 2.3.a. The pseudo cell made up of eight β cages (or sodalite cages) settled at the corners of a cube and attached through a four-membered oxygen rings (S4R).

This composition produces a big polyhedral α cage of free diameter about 11.4 Å accessible through eight-membered oxygen windows. If these units are piled in a cubic lattice, a three-dimensional isotropic channel structure forms. This structure is restrained by eight-membered oxygen rings.

Each pseudo cell contains 24 tetrahedral (AlO_2 or SiO_2) units and as the Si/Al ratio in zeolite A is always close to 1.0 there are 12 univalent interchangeable cations per cell. Three different cation sites have been identified; near the centers of the six-rings in the eight corners of the central cavity (type I), in the eight-rings (type II), and on the cage wall in close proximity to a four-ring (type II), and on the cage wall in close proximity to a four-ring (type III). With most cations the type I sites are occupied as a choice, followed by the type II sites, and the type III sites are filled only after all sites of type I and II have been occupied. In the sodium form (4A) there are 12 cations for each cage. These are held in the eight type I sites and the three type II sites (six eight-rings are each shared between two cages) with one cation in a type III site. All windows are therefore partially obstructed by a sodium cation and the efficient aperture of the sieve is therefore reduced from about 4.4 to 3.8 Å. If the Na^+ cations are exchanged for Ca^{2+} or Mg^{2+} the number of cations for each cell decreases. At 67% exchange there are only eight cations for each cell and all these can be held in the type I sites. Therefore in Ca^{2+} or Mg^{2+} form (5A) the effective aperture is increased and somewhat larger molecules can penetrate.

Considering the diameter of the potassium ion is greater than that of sodium, a sieve with a smaller effective aperture (3A sieve) is obtained by potassium exchange. The 3A sieve is widely used for drying reactive hydrocarbons such as olefins because the small pore size prevents penetration of the lattice and thus possibility of reaction.

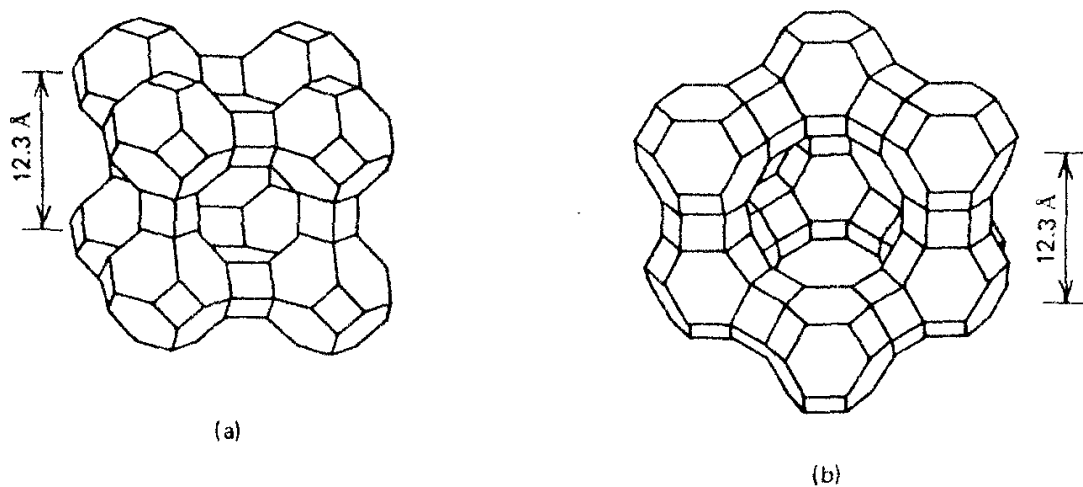


Figure 2.3. Structures of (a) Zeolite A, (b) Zeolite X and Zeolite Y.

2.4.1. Zeolites X and Y

The synthetic zeolites X and Y and the natural zeolite faujasite all have the same structure which can be seen in Figure 2.3b. The crystallographic unit cell made up of an array eight cages including overall 192 AlO_2 and SiO_2 tetrahedral units. The structure can be thought of as a tetrahedral lattice of sodalite units joined by six-membered oxygen bridges, or likewise as a tetrahedral form of double six-ring units. The final channel structure is vastly open with each cage joined by four other cages through twelve-membered oxygen rings of free diameter $\sim 7.4 \text{ \AA}$. Huge molecules such as neopentene and tertiary butyl amine can penetrate these pores.

The difference between the X and Y sieves lies in the Si/Al ratio which is within the range 1-1.5 for X and 1.5-3.0 for Y. There is a corresponding difference in the number of exchangeable univalent cations, which changes from about 10-12 per cage for X to a low as 6 for high silica Y.

2.5. Ion Exchange Selectivity

As far as the ion exchange reaction between two counterions which is given in Equation (2.1) is considered, the distribution of counter-ions between phases is not equal at equilibrium. In this manner for a specific exchanger one ion is for the most part preferred over the other and the exchanger is said to show selectivity.

Selectivity exhibited by an exchanger (zeolite) can be represented by the separation factor α_B^A that is determined by:

$$\alpha_B^A = \frac{X_{AZ} X_{BS}}{X_{BZ} X_{AS}} \quad (2.3)$$

where X_{AS} and X_{BS} are the equilibrium fractions of cations A and B in the solution phase; X_{AZ} and X_{BZ} are the equilibrium fractions of cations A and B and in the zeolite phase.

Equilibrium fractions of cations in the solution phase and zeolite phase can be defined by Equation (2.4).

$$X_{AS} = \frac{C_A}{C_{0A}} \quad \text{and} \quad X_{AZ} = \frac{(C_{0A} - C_A)}{CEC_{mz}} \quad (2.4)$$

where C_A represents the equilibrium concentration of cation A in the solution phase; C_{0A} represents the initial concentration of A and CEC_{mz} is the cation exchange capacity of each dried zeolite mass.

The separation factor α_B^A value greater than one means that cation A is preferred by the zeolite (ion exchanger) for a given point on the exchange isotherm. Thus $\alpha_B^A > 1$ means favourable and $\alpha_B^A < 1$ means unfavourable equilibrium isotherm behavior for cation A.

Water content of the zeolite, total exchange capacity, size, hydrated radius and charge of the counter ions and nature of the fixed ions effects selectivity of the zeolite to particular cations. The higher the exchange capacity the lower the separation factor (Harland, 1994).

Hydration of ions is determined as the electrostatic interaction of ions with water molecules. As interaction of water molecules with ions rely on ionic density of charge, smaller ions (and therefore ions of better ionic potential) hold more water dipole molecules. The consequence is tha the hydrated Radius is inversely related to non-hydrated radius which is demonstrated in Figure 2.4.

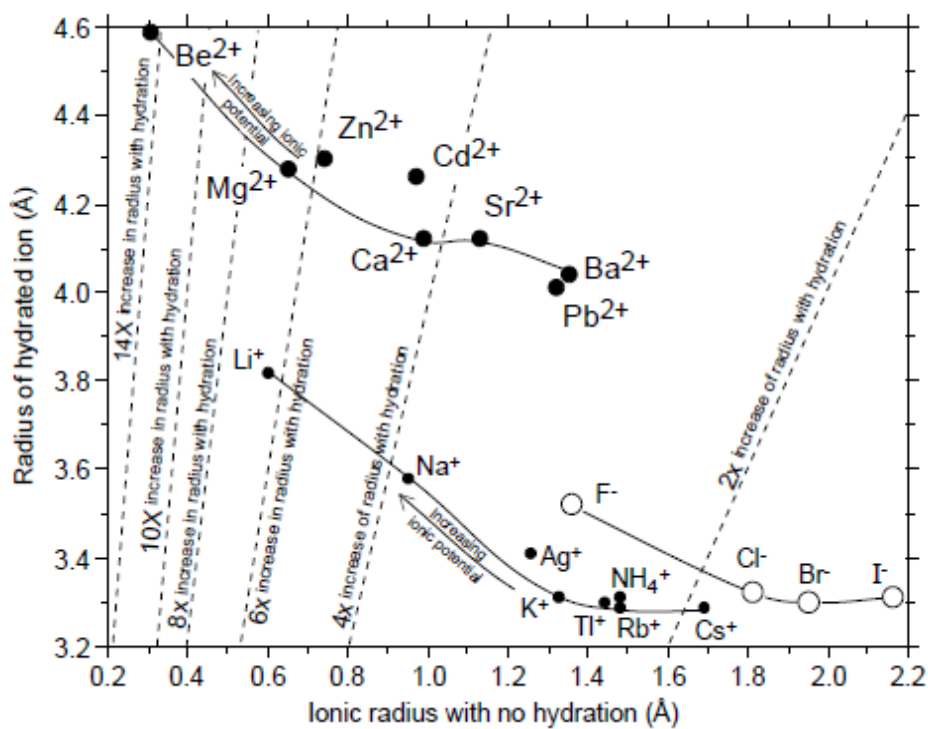


Figure 2.4. Ionic and hydrated radius of some ions.

2.6. Ion Exchange in Batch Systems

The ion-exchange/sorption processes for zeolites can be much more complex than the same processes for organic ion exchange resins. The ion exchanger/ zeolite made up of small crystals. These crystals have sizes in the range of approximately 1 - 10 μm , and wrapped with a small amount of binder. Therefore, for zeolites there are two different kind of pore structures. These structures are micropores in the crystals and macropores in the binder. Three principal mass transfer resistances governs the kinetics in these heterogeneous particles (Figure 2.5): film diffusion from the bulk liquid to the pellet surface, diffusion through the macropores of the pellet, and diffusion inside the micropores of the zeolite crystals. The materials involved and the particular operating conditions determine the comparative importance of the resistances. Ion-sieve, steric, and electrostatic forces inside the zeolite pores can also complicate zeolite ion exchange (Robinson, et al., 1994).

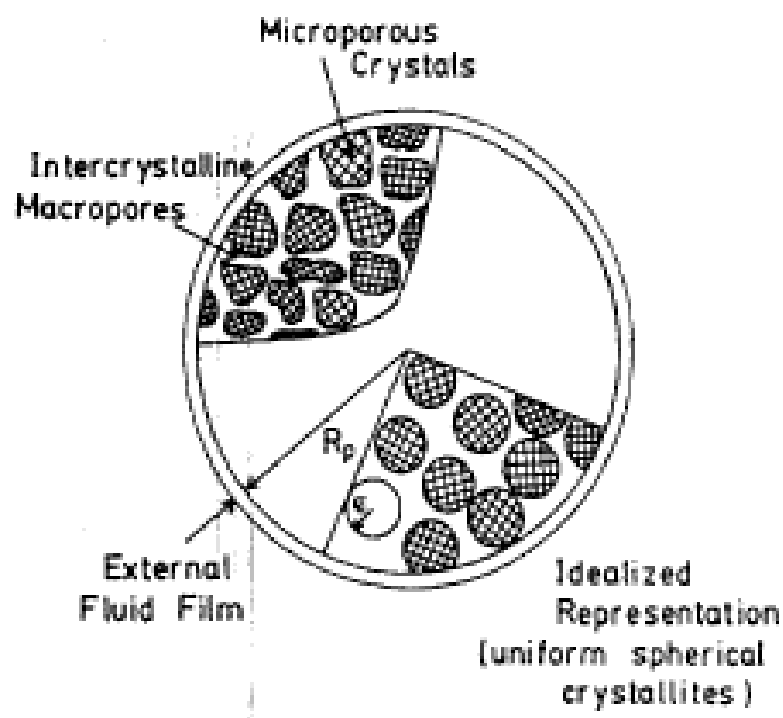


Figure 2.5. Three principal resistances to mass transfer in a composite pellet (Ruthven, 1984)

2.6.1. Adsorption Isotherms Models

Adsorption isotherms are algebraic models which explain the phenomenon controlling the ability of a diffusing material to move from liquid phase to sorbate/zeolite phase at fixed temperature. While a zeolite/sorbate phase has been in connection with the sorbent for an adequate time, adsorption and desorption rates become equal and adsorption equilibrium is established. That means, the zeolite/sorbate concentration in the bulk solution is in a dynamic balance with the interface concentration (Hameed and Foo, 2010).

2.6.1.1. Two Parameter Isotherms

2.6.1.1.1 Langmuir isotherm

This model assumes monolayer sorption/ion exchange of metal ions on a homogeneous surface. No interaction between sorbed ions occurs, that is to say, sorption can only happen at a fixed number of distinct localized sites, which are alike and similar. The Langmuir isotherm equation is determined as:

$$q_e = \frac{Q_M b C_e}{1 + b C_e} \quad (2.5)$$

in which q_e is the zeolite phase concentration in equilibrium with the liquid-phase concentration C_e , Q_M is the maximum sorption/ion exchange capacity (meq/g), and b is an equilibrium constant (L/mg).

Linear form of the Langmuir isotherm equation is given as:

$$\frac{C_e}{q_e} = \frac{1}{Q_M b} + \frac{C_e}{Q_M} \quad (2.6)$$

Applying the same equation for $C_e = C_o$,

$$\frac{q_{max}}{Q_M} = \frac{bC_o}{1 + bC_o} \quad (2.7)$$

in which q_{max} is the solid-phase concentration in equilibrium with C_o . When Equation (2.5) is divided by Equation (2.7) giving:

$$\frac{q_e}{q_{max}} = \frac{C_e}{C_o} \frac{1 + bC_o}{1 + bC_e} \quad (2.8)$$

Inserting the equilibrium parameter La as

$$La = \frac{1}{1 + bC_o} \quad (2.9)$$

the Langmuir equation in dimensionless form is given as:

$$Y = \frac{X}{La + (1 - La)X} \quad (2.10)$$

where

$$X = C/C_o \text{ and } Y = q/q_{max}$$

La can be expressed from the dimensionless equilibrium relationship as follows,

$$La = \frac{X(1 - Y)}{Y(1 - X)} \quad (2.11)$$

2.6.1.1.2. Freundlich isotherm

Freundlich isotherm explains the non-ideal and reversible adsorption and is applicable to both monolayer and multilayer adsorption.

The amount adsorbed onto the heterogeneous surface of an adsorbent, is the sum of adsorption on every site with the stronger binding sites are inhabited first, just before adsorption energy are rapidly declined at the time of the conclusion of adsorption process. The Freundlich isotherm model is described as:

$$q_e = K_F C_e^{1/n} \quad (2.12)$$

Linear form of Equation (2.12) is represented by:

$$\ln q_e = \ln K_F + \frac{1}{n} \ln C_e \quad (2.13)$$

in which C_e (mg/L) is the equilibrium concentration in the liquid phase and q_e (mg/g) is the equilibrium concentration in the zeolite/sorbent phase. K_F (L/g) is the Freundlich constant which indicates the relative ion exchange/sorption capacity of the zeolite/sorbent. n is the Freundlich exponent which indicates the heterogeneity of the zeolite/sorption surface and adsorption intensity of the adsorbent onto the adsorbent surface.

The Freundlich exponent, n , may have values ranging from 1 to 10 which is classified as good sorption/ion exchange (Shahmohammadi-Kalalagh et al., 2011). A value of n closer to 1, points to linear adsorption, a value less than 1 indicates monolayer adsorption (chemisorption) whereas a value greater than 1, implies multilayer adsorption (physisorption).

2.6.1.1.3. Dubinin–Radushkevich (DR) isotherm

Dubinin–Radushkevich isotherm, is a semi-empirical model which assumes that the sorption/ion exchange has a multilayer character. It is based on the sorption theory of Polanyi potential and micropore volume filling (Boporai et al., 2011).

The DR isotherm model is shown as:

$$q_e = (q_d)\exp(-\beta\varepsilon^2) \quad (2.14)$$

where q_d is the DR isotherm constant (mg/g), β is the constant in relation with E , mean free energy of adsorption for each mole of the adsorbate while it moves to the surface of the zeolite/sorbent from infinite distance in the solution (Igwe and Abia, 2007).

$$E = \left[\frac{1}{\sqrt{2\beta}} \right] \quad (2.15)$$

The linear form of DR isotherm model is represented by:

$$\ln q_e = \ln q_d - \beta\varepsilon^2 \quad (2.16)$$

where ε is the Polanyi potential that can be correlated as:

$$\varepsilon = RT \ln \left[1 + \frac{1}{C_e} \right] \quad (2.17)$$

in which R , T and C_e corresponds to the gas constant (8.314 J/mol K), absolute temperature (K) and the equilibrium concentration in the liquid phase (mg/L), correspondingly.

2.6.1.1.4. Temkin isotherm

Temkin isotherm includes a component which definitely considers sorbent–sorbate interactions. The model estimates that heat of sorption (function of temperature) of all molecules in the layer would reduce linearly instead of logarithmic with coverage by disregarding the extremely low and large value of concentrations.

When q_e versus $\ln C_e$ is plotted, the uniform distribution of binding energies (until some maximum binding energy) and the constants were found out from the slope and intercept (Dada et al., 2012). The Temkin isotherm is represented by:

$$q_e = \frac{RT}{b_T} \ln(K_T C_e) \quad (2.18)$$

in which, T is the absolute temperature (K), R is the universal gas constant (8.314 J/mol.K), K_T is the equilibrium binding constant (L/mg), and b_T is the change of sorption energy (kJ/mol).

Linear form of Equation (2.18) is given as:

$$q_e = \frac{RT}{b_T} \ln K_T + \frac{RT}{b_T} \ln C_e \quad (2.19)$$

in which,

$$B_T = \frac{RT}{b} \quad (2.20)$$

$$q_e = B_T \ln K_T + B_T \ln C_e \quad (2.21)$$

B_T is Temkin constant related to the heat of sorption (kJ/mol)

2.6.1.2. Three Parameter Isotherms

2.6.1.2.1. Redlich–Peterson isotherm

Redlich–Peterson isotherm model which is a combination of both Langmuir and Freundlich isotherm models, can be used for both homogeneous and heterogeneous systems because of its versatility.

Redlich–Peterson model is represented by:

$$q_e = \frac{K_{RP} C_e}{1 + \alpha_{RP} C_e^\beta} \quad (2.22)$$

where K_{RP} (L/g), α_{RP} (L/mmol) and β are Redlich-Peterson constants. The value of β varies between 0 and 1. In the high concentration limit, while the exponent β tends to zero, it approaches Freundlich isotherm model. In the low concentration limit, when the β values are all close to one, it appeals to ideal Langmuir condition.

Linear form of Equation (2.22) is written as:

$$\frac{C_e}{q_e} = \frac{1}{K_{RP}} + \frac{\alpha_{RP}}{K_{RP}} C_e^\beta \quad (2.23)$$

or

$$\ln\left(K_{RP} \frac{C_e}{q_e} - 1\right) = \beta \ln(C_e) + \ln(\alpha_{RP}) \quad (2.24)$$

2.6.1.2.2. Sips isotherm

The Sips isotherm model which is a hybrid isotherm of Langmuir and Freundlich isotherm models, represented by following equation:

$$q_e = \frac{q_s(b_s C_e)^{1/n}}{1 + (b_s C_e)^{1/n}} \quad (2.25)$$

where q_s is the column saturation capacity, b_s is the isotherm constant and $1/n$ is the exponent constant.

In the Langmuir-Freundlich form, it can be written as:

$$q_e = \frac{K_{LF}(C_e)^{1/n_{LF}}}{1 + b_{LF}(C_e)^{1/n_{LF}}} \quad (2.26)$$

The linear form of this Equation (2.26) is as follows:

$$\left(\frac{1}{n_{LF}}\right) \ln C_e = -\ln\left(\frac{K_{LF}}{q_e}\right) + \ln(b_{LF}) \quad (2.27)$$

This equation simplifies to Freundlich isotherm at low adsorbate concentrations, as it estimates monolayer adsorption capacity characteristics of the Langmuir isotherm at high concentrations (Hameed and Foo, 2010).

2.6.1.3. Multilayer Physisorption Isotherms

2.6.1.3.1. Brunauer–Emmett–Teller (BET) Isotherm

BET theory was published by Stephen Brunauer, Paul Emmett and Edward Teller in 1938. The BET theory is an expansion of the Langmuir theory and is a theory for multi-layer physisorption and is of profound significance in the development of this field. It is most generally used in the gas–solid equilibrium systems. Its extended model applied to liquid–solid interface is as follows:

$$q_e = \frac{q_s C_{BET} C_e}{(C_o - C_e)[1 + (C_{BET} - 1)(C_e/C_o)]} \quad (2.28)$$

where C_{BET} , C_o , q_s and q_e are the BET adsorption isotherm constant (L/mg), initial concentration (mg/L), theoretical isotherm saturation capacity (mg/g) and equilibrium concentration (mg/g), correspondingly.

The linear form of Equation (2.28) as follows:

$$\frac{C_e}{q_e(C_o - C_e)} = \frac{1}{q_s C_{BET}} + \frac{(C_{BET} - 1) C_e}{q_s C_{BET} C_o} \quad (2.29)$$

As C_{BET} and $C_{BET} (C_o/C_s)$ are much higher than 1, the Equation (2.29) is reduced to:

$$q_e = \frac{q_s}{1 - (C_o/C_s)} \quad (2.30)$$

2.6.1.3.2. Frenkel–Halsey–Hill (FHH) isotherm

Frenkel–Halsey–Hill (FHH) isotherm is an another multilayer adsorption theory and may be written as:

$$\ln\left(\frac{C_e}{C_s}\right) = -\frac{\alpha}{RT}\left(\frac{q_s}{q_e d}\right)^{n_F} \quad (2.30)$$

in which d , α and n_F are the sign of the interlayer spacing (m), isotherm constant (Jm²/mole) and inverse power of distance from the surface correspondingly.

2.6.1.3.3. MacMillan–Teller (MET) isotherm

MacMillan–Teller (MET) isotherm is an extension of BET isotherm adsorption model in which surface tension effects are included and it is written as:

$$q_e = q_s \left(\frac{k}{\ln(C_s/C_e)} \right)^{1/3} \quad (2.31)$$

where k is an isotherm constant.

When C_s/C_e approaches to 1, the logarithmic term is reduced to:

$$q_e = q_s \left(\frac{k}{C_s - C_e} \right)^{1/3} \quad (2.32)$$

2.6.1.4. Isotherms For Multicomponent Systems

2.6.1.4.1. The Extended Langmuir Model

The adsorption of a multi-component mixture can be easily explained by the Extended Langmuir model with the same assumptions made by modeling the single component systems. The model can be represented by:

$$q_{e,i} = Q_{M,i} \frac{b_i C_{ei}}{1 + \sum_{j=1}^n b_j C_{ej}} \quad (2.33)$$

where C_{ei} and C_{ej} are the equilibrium concentrations of the components “i” and “j” in the liquid phase, $q_{e,i}$ and $q_{e,j}$ are the equilibrium concentrations of the components “i” and “j” in the zeolite phase of multicomponent system. b_i and b_j are the Langmuir constants of the components “i” and “j” in the multicomponent system and Q_{Mi} is the Langmuir maximum exchange/sorption capacity.

This model is thermodynamically consistent only if the adsorbent saturation capacities of all the components are the same $Q_{M,1} = Q_{M,2}$. However, such an assumption is unrealistic for physical adsorption of molecules of widely different sizes (Besedova and Bobok, 2005).

2.6.1.4.2. The Modified Langmuir Model

The Modified Langmuir Model is simple development of the single component Langmuir isotherms to explain multicomponent systems. It is assumed that every component sorbs onto the surface in accordance with ideal solute behaviour under homogeneous conditions without any competition among molecules occurs (Ho and McKay, 2000).

The modified Langmuir isotherm which is useful while every single component follows Langmuir behaviour in a mono-component system, which can be written as:

The Modified Langmuir Model is straightforward advancement of the single-part Langmuir isotherms to record for multicomponent systems. It is accepted that every segment sorbs onto the surface as indicated by perfect solute conduct under homogeneous conditions with no cooperation or rivalry between particles occurring

$$q_{e,i} = \frac{Q_{M,i}b_iC_{ei}}{1 + \sum_{j=1}^n b_jC_{ej}} \quad (2.34)$$

The modified Langmuir isotherms for a binary system can be represented by:

$$q_{e,1} = \frac{Q_{M,1}b_1C_{e1}}{1 + b_1C_{e1} + b_2C_{e2}} \quad (2.35)$$

$$q_{e,2} = \frac{Q_{M,2}b_2C_{e2}}{1 + b_1C_{e1} + b_2C_{e2}} \quad (2.36)$$

where $q_{e,1}$ and $q_{e,2}$ are the equilibrium zeolite phase concentrations of component 1 and 2 in units of (meq/g). C_{e1} and C_{e2} are the equilibrium solution phase concentrations of component 1 and 2 in units of (mg/L). $Q_{M,1}$ and $Q_{M,2}$ are the maximum exchange/sorption capacities of component 1 and 2, correspondingly. These are found out from single-component systems and, thus, correlate to a monolayer coverage of the exchanger/sorbent. b_1 and b_2 are the Langmuir constants and are a function of the energy of sorption of components 1 and 2, correspondingly. They can also be found out from single-component systems.

2.6.1.4.3. Jain and Snoeyink Model

Jain and Snoeyink Model which is based on partial competition in multicomponent adsorption (Baig et al., 2009), can be written as follows for two component systems:

$$q_{e,1} = \frac{(Q_{M,1}-Q_{M,2})b_1C_{e1}}{1 + b_1C_{e1}} + \frac{Q_{M,1}b_1C_{e2}}{1 + b_1C_{e1} + b_2C_{e2}} \quad (2.37)$$

$$q_{e,2} = \frac{Q_{M,2}b_2C_{e2}}{1 + b_1C_{e1} + b_2C_{e2}} \quad (2.38)$$

The additional initial term of the right-hand side of Equation (2.37) which is proportional to, $(Q_{M,1}-Q_{M,2})$, gives reason for the amount of component 1 that sorbed without competition and the second term, which is related to the original Modified Langmuir Isotherm, represents the quantity of component 1 sorbed under competition with component 2. Equation (2.38) can be used to calculate the quantity of component 2 adsorbed while competing with component 1 (Baig et al., 2009).

2.6.1.4.4. SRS Model

Sheindorf, Rebhun and Sheintuch (1981) developed a Freundlich type multicomponent adsorption isotherm called SRS Model (the letters signify the each authors' surname) which is established from the hypothesis that an exponential distribution of adsorption energies exists for each component.

$$q_i = K_{Fi}C_i \left(\sum_{j=1}^k a_{ij} C_j \right)^{m_i-1} \quad (2.39)$$

If both concentrations change during the experiment the isotherm for a binary system can be represented by:

$$\frac{C_1}{C_2} = \frac{1}{C_2} \beta_1 - a_{12} \quad (2.40)$$

$$\frac{C_2}{C_1} = \frac{1}{C_1} \beta_2 - a_{21} \quad (2.41)$$

where

$$\beta_i = \left(\frac{q_i}{K_{Fi} C_i} \right)^{1/m_i - 1} \quad (2.42)$$

a_{ij} is the competition coefficient

$$a_{ij} = \frac{1}{a_{ji}} \quad (2.43)$$

The Freundlich constants K_{Fi} and m_i ($m_i = 1/n_i$ in the Freundlich model for a single-component system) are of the single-component system while q_i and C_i are the equilibrium concentrations in the solid and liquid phases of the component “i” in the multicomponent system, subsequently.

2.6.1.4.5. Extended SIPS Model

The Sips model which is a Freundlich-Langmuir type model can be enhanced to characterize the multicomponent systems. The Sips multicomponent adsorption isotherm model is given as:

$$q_i = \frac{q_{si} b_i C_i (\sum_{j=1}^k b_j C_j)^{1/n_i - 1}}{1 + (\sum_{j=1}^k b_j C_j)^{1/n_i}} \quad (2.44)$$

where q_{si} , n_i and b_i are the single component Sips constants.

It is crucial to mention that although single component isotherm experimental data are effectively characterized by the Sips model, Equation. (2.26), this does not certainly indicate that Equation (2.44) will perform a favorable description of the multicomponent ion exchange/sorption experimental data.

2.6.1.4.6. IAST (Ideal Adsorbed Solution Theory) Model

The Ideal Adsorption Solution Theory (IAST) Model; which is established from the hypothesis that the solution is ideal, that is, unless there is adsorbed-adsorbent interaction; is a clarification of the multicomponent Freundlich isotherm and can be successfully utilized to estimate the multicomponent adsorption isotherms utilizing single component equilibrium data described by the Freundlich isotherm (Al-Asheh et al., 2000). The model is given as:

$$C_i = \frac{q_i}{\sum_{j=1}^N q_j} \left[\frac{\sum_{j=1}^k n_j q_j}{n_i K_i} \right]^{n_i} \quad (2.45)$$

in which N is the number of components in the system and n and K are the single-component Freundlich constants.

For a binary system, the model can be represented by:

$$C_1 = \frac{q_1}{q_1 + q_2} \left[\frac{n_1 q_1 + n_2 q_2}{n_1 K_1} \right]^{n_1} \quad (2.46)$$

$$C_2 = \frac{q_2}{q_1 + q_2} \left[\frac{n_1 q_1 + n_2 q_2}{n_2 K_2} \right]^{n_2} \quad (2.47)$$

where C_1 and C_2 are the concentrations of components 1 and 2 remaining in the solution at the equilibrium, and q_1 and q_2 are the equilibrium zeolite/sorbent concentrations in the multicomponent system. K_1 , K_2 , n_1 and n_2 are the Freundlich constants of the components 1 and 2 in the mono-component systems.

2.6.2. Kinetics

2.6.2.1. Pseudo-first order equation or Lagergren's kinetics equation (Lagergren, 1898)

It is generally utilized for the ion adsorption of an adsorbate from an aqueous solution. It can also be utilized to determine the kinetics of ion exchange on zeolites.

$$\frac{dq_t}{dt} = k_1(q_e - q_t) \quad (2.48)$$

The linear form of pseudo first order model is given by:

$$\log(q_e - q_t) = \log q_e - \frac{k_1}{2.303} t \quad (2.49)$$

where q_t is the amount of cation exchanged for each unit of zeolite (mg/g) at time t , k_1 is the pseudo-first order rate constant (L/min), and t is the contact time (min). The pseudo-first order rate constant (k_1) were computed from the plot of $\log(q_e - q_t)$ against t .

2.6.2.2. Pseudo second order kinetics equation

Ho and McKay, (1999) introduced the pseudo-second order kinetic as:

$$\frac{dq_t}{dt} = k_2(q_e - q_t)^2 \quad (2.50)$$

in which k_2 is the pseudo second-order rate constant ($\text{gmg}^{-1} \text{h}^{-1}$).

Equation (2.50) is linearly shown as:

$$\frac{t}{q_t} = \frac{1}{k_2 q_e^2} + \frac{1}{q_e} t \quad (2.51)$$

where $k_2 q_e^2$ or h ($\text{mg g}^{-1} \text{h}^{-1}$) is the initial sorption rate. The h , q_e and k_2 can be determined from the linear plot of t/q_t versus t .

2.6.2.3. Intraparticle Diffusion Equation

The most generally implemented intraparticle diffusion equation is determined by Weber and Morris (1963) as follows:

$$q_t = k_i t^{0.5} + C \quad (2.52)$$

in which k_i is the intraparticle diffusion rate constant ($\text{mg g}^{-1} \text{min}^{0.5}$) and C is the intercept.

Urano and Tachikawa, 1991 (U&T) Model which assumes that external mass transfer resistance is negligible is written as Urano, K., Tachikawa, H:

$$f\left(\frac{q}{q_m}\right) = -\left[\log\left(1 - \left(\frac{q}{q_m}\right)^2\right)\right] = \frac{4\pi^2 D_i t}{2.3 d_p^2} \quad (2.53)$$

where q and q_m are the concentrations in the zeolite phase at t and $t \rightarrow \infty$, d_p the particle diameter and D_i the diffusion coefficient.

2.6.2.4. Elovich Kinetic Model

The Elovich Kinetic Model is given as:

$$\frac{dq_t}{dt} = \alpha e^{\beta q_t} \quad (2.54)$$

in which α is the initial rate (mg/gmin) and β is related to the surface coverage and the activation energy for chemisorptions (g/mg).

Linear form of the Elovich Model is given as:

$$q_t = \frac{1}{\beta} \ln(\alpha \beta) + \frac{1}{\beta} \ln t \quad (2.55)$$

2.6.2.5. Pore Diffusion Bangham's Kinetic Model

This model can be utilized to investigate if the pore diffusion mechanism is the rate controlling mechanism or not. It is represented by:

$$\log \log \left(\frac{C_0}{C_0 - q_t m} \right) = \log \left(\frac{k_0 m}{2.303V} \right) + \alpha \log t \quad (2.56)$$

in which C_0 is the initial cation concentration in liquid phase (mg/L) q_t , is the cation concentration in the zeolite phase, V is the volume of solution (ml), m is the weight of the zeolite (g/L), k_0 is the constant [ml/(g/L)].

The value of the constant α is always less than 1.

2.6.2.6. Modified Freundlich Kinetic Model

The Modified Freundlich Kinetic Model is expressed as:

$$q_t = k_F C_0 t^{1/m} \quad (2.57)$$

where k_F is the Freundlich constant (l/gmin) and C_0 is the initial concentration.

The linear form of this model is shown as:

$$\ln q_t = \ln k_F + \frac{1}{m} \ln t \quad (2.58)$$

2.6.2.7. External Mass Transfer Diffusion Model

External Mass Transfer Diffusion Model is given as:

$$\frac{dC}{dt} = -\beta_L S (C - C_s) \quad (2.59)$$

in which β_L is the liquid – solid mass transfer coefficient, C is the concentration in the liquid phase at time t , and $C = C_0$ at $t = 0$; C_s the concentration at the particle surface; and S the specific surface area for mass transfer.

Under the assumption of surface concentration C_s is negligible at $t = 0$ consequently intraparticle diffusion is negligible, Equation (2.59) is simplified to:

$$\left[\frac{d(C/C_0)}{dt} \right]_{t \rightarrow 0} = -\beta_L S \quad (2.60)$$

2.6.3. Goodness of the experimental data

The most suitable among the kinetic models is determined by the linear coefficient of determination (R^2), non-linear Chi-square (X^2) and the ARE (average of relative errors).

The linear coefficient of determination can be represented by:

$$R^2 = \frac{(q_{e,exp} - q_{e,cal})^2}{\sum(q_{e,exp} - q_{e,cal})^2 + (q_{e,exp} - q_{e,cal})^2} \quad (2.61)$$

where $q_{e,exp}$ is experimental equilibrium capacity data and $q_{e,cal}$ is the equilibrium capacity from a model.

The Nonlinear Chi-square test calculates the difference between the experimental and model data. The mathematical form of this test statistic can be written as:

$$X^2 = \sum \frac{(q_{e,exp} - q_{e,cal})^2}{q_{e,exp}} \quad (2.62)$$

Small X^2 value indicates that the data from the model similarities between the model and the experimental data while larger X^2 value represents the difference between the model and the experimental data.

Average Relative Error (ARE) model that lessens the fractional error distribution over the entire studied concentration range is given as follows:

$$ARE = \frac{1}{N} \sum \frac{(q_{e,exp} - q_{e,cal})}{q_{e,exp}} \quad (2.63)$$

The linear coefficient of determination (R^2) gives the fit between experimental data and isotherm equations and at the same time the average percentage errors (ARE) indicates the fitting between the experimental and predicted values of ion exchange capacity used for plotting isotherm curves (Hamdaouia and Naffrechoux., 2007)

2.6.4. Thermodynamics Parameters

The thermodynamic parameters can be found out from the thermodynamic equilibrium constant which is called thermodynamic distribution coefficient K_o . The standard Gibbs free energy $\Delta G^o(kJmol^{-1})$, standard enthalpy change $\Delta H^o(kJmol^{-1})$, standard entropy change $\Delta S^o(Jmol^{-1}K^{-1})$ can be determined by the equations listed below.

$$\Delta G^o = -RT \ln K_o \quad (2.64)$$

$$\ln K_o = \frac{\Delta S^o}{R} - \frac{\Delta H^o}{RT} \quad (2.65)$$

K_o can be defined as:

$$K_o = \frac{a_s}{a_e} = \frac{\gamma_s q_e}{\gamma_e C_e} \quad (2.66)$$

where a_s is the activity of cation in the zeolite phase, a_e is the activity of cation in liquid phase at equilibrium, γ_s is the activity coefficient of cation in the zeolite, γ_e the activity coefficient of cation in liquid phase at equilibrium ion, q_e is the cation exchanged on zeolite surface ($mmol\ g^{-1}$), and C_e is the cation concentration in liquid phase at equilibrium ($mmol/mL$).

The expression of K_o can be reduced using the assumption that the concentration in the liquid phase approximate to zero following in $q_e \rightarrow 0$ and $C_e \rightarrow 0$ and the activity coefficients approximate to one at these very low concentrations (Bopari et al., 2011).

Consequently Equation (2.66) can be represented by:

$$q_e \xrightarrow{\text{lim } 0} \frac{q_e}{C_e} = \frac{a_s}{a_e} = K_0 \quad (2.67)$$

2.7. Ion Exchange in Columns

Most of the commercial and laboratory applications of ion exchange involve operations where the solution to be treated (feed or influent) is passed downflow through a fixed bed (column) of ion exchanger contained within a cylindrical vessel. The apparent difference between a stirred reactor (batch) contact of exchanger with the solution and a column process is that the former situation may be defined by a 'static' or true equilibrium. This is not the case with column operations considering the position of equilibrium is always changing because:

1. The composition of a volume element of solution changes just as it progresses down the column.
2. A given volume of element of the column feed is always contacting unequilibrated resin just as it passes down the column.
3. The displacement of the ionic products of the forward exchange reaction forces the exchange equilibrium to the right resulting in the course of time in complete conversion (exhaustion) of the exchanger commencing at the top of the column.
4. The linear or specific flowrate (mh^{-1}) and the kinetics controlling the rate of exchange influences the extent of deviation from rapid attainment of local equilibrium within zeolite layers greatly.

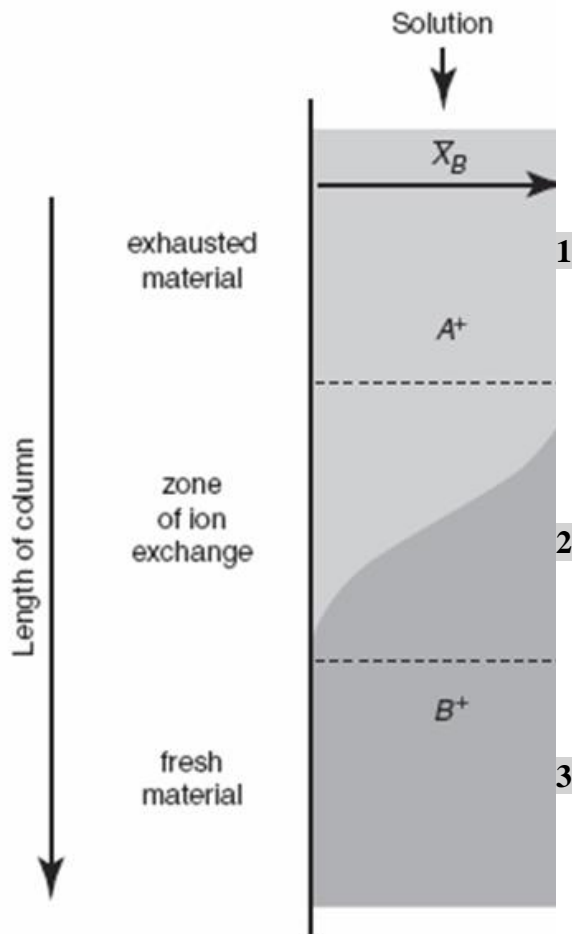


Figure 2.6. Three regions of an ion exchange column (Zagarodni, 2007)

Ion exchange column anytime can be split into three zones: 1-exhausted material zone, 2-ion exchange reaction zone and 3-fresh material zone (Figure 2.6).

At the same time the solution is first pumped towards the column, it will exchange every B^+ ions to A^+ ions in the region 1 of Figure 2.6. At this moment the solution which includes only A^+ passes to the below part (region 2) of the column with no additional change in the composition. While the solution is carried on, region 1 of the bed are continually exposed to the fresh solution. Finally, region 1 is entirely converted to B^+ and become exhausted. The region of the column in which the ion exchange occurs is hence displaced downstream (region 2). Eventually, this region

reaches the bottom of the column (region 3) . This is the “breakthrough” of B^+ the point where ions B^+ first appear in the effluent. The operation is stopped at or shortly before the breakthrough and the column is regenerated. Continuation beyond breakthrough leads to complete displacement of A^+ by B^+ . Consequently the column is in equilibrium with the feed solution. Until pumping of the solution is discontinued, no additional changes in the phase composition happen (Helfferich, 1962).

Breakthrough Curve

At the same time a solution is treated with the zeolite/ion exchanger solution composition changes. Primary interest is the changes in concentration at the outlet of the column since the process is dynamic (Zagarodni, 2007).

Plots of,

$$C_i = f(t) \text{ or } C_i = f(V) \quad (2.68)$$

which are called breakthrough curves, show concentration of component i at the outlet of the column. t represents time spent from the start of the process and V is the total volume of solution pumped.

In general the relation between the two expressions of (2.68) is linear, if the pump rate is constant. If the relation is not linear when volume is the essential measure which demonstrates the capacity of the column to gather targeted ions. This is usually achieved when distinct volumes of the solution are pumped with inconstant rate (Zagarodni, 2007).

The x-axis in Figure 2.7 represent both V and t . $V_{br}(t_{br})$ is the breakthrough time; $V_{eq}(t_{eq})$ is the time when C gets to be equivalent to C_0 . $V_{lim}(t_{lim})$ is the time when the ion exchange method could be stopped for practical concern.

Figure 2.7. shows dependency regarding the pumping is carried on following breakthrough. Plots like this are broadly utilized to display the efficiency of ion exchange columns (Zagarodni, 2007).

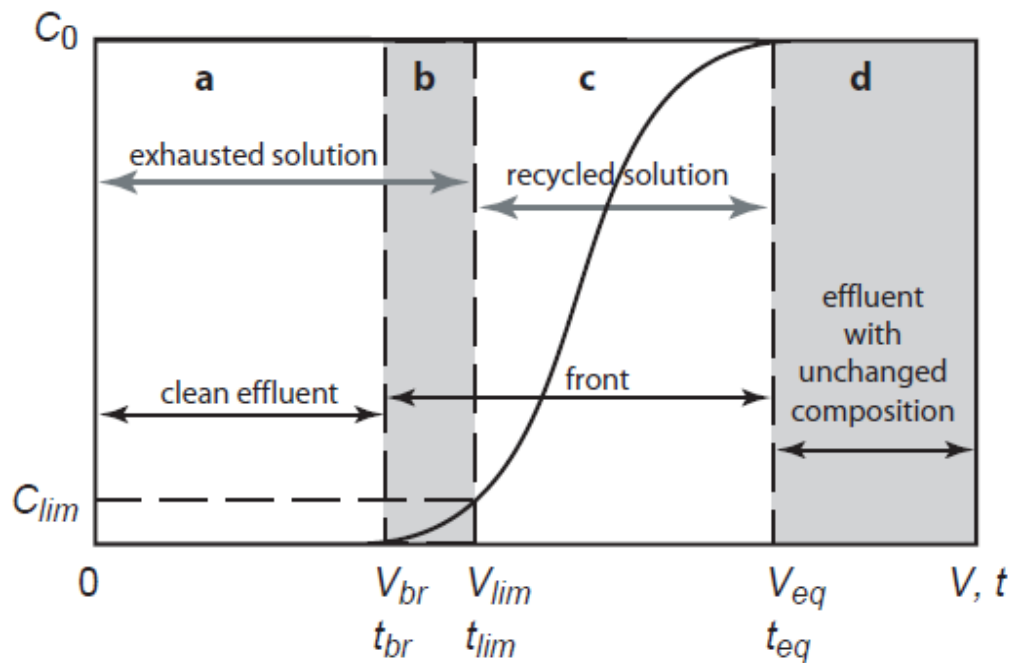


Figure 2.7. Breakthrough curve (Zagarodni, 2007).

Breakthrough capacity of the ion exchange column which is shown by part (a) in Figure 2.7 is the amount of ions that can be extracted from the solution by the column before the breakthrough. Breakthrough capacity is given as:

$$Q_{br} = \int_0^{V_{br}} (C_0 - C) dV \quad (2.69)$$

in which C_0 is the cation concentration in the beginning, C is the effluent ion concentration in the liquid phase and V_{br} is the volume of the solution passed preceding breakthrough time.

Breakthrough capacity of the column is smaller than *Total Exchange Capacity* of the column since the bottom regions (region 3) are not entirely exchanged to B^+ form. Column efficiency is described as the ratio of the breakthrough to total exchange capacities.

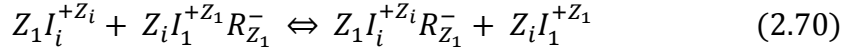
2.8. Modeling Multicomponent Ion Exchange in Column

For predicting results for different ion-exchange systems various models have now been developed. Unluckily, a common solution for multicomponent ion exchange that contains hydrodynamic dispersion, mass-transfer effects, interference effects, and nonlinear complex isotherms, is unavailable yet. The mathematical models established up to now have utilized various degrees of complexity for describing multicomponent ion exchange processes. Because of the complexity and nonlinearity of some of the models, analytical solutions are not possible. Numerical solutions of stiff partial differential equations are generally necessary.

For predicting ion exchange equilibrium, three models are utilized: the first model depends on the law of mass action; in the second model ion exchange is considered as an adsorption process and in the third model, which is the combination of the first and the second model, the zeolite phase is known to contain sites for both ion exchange and adsorption (Gorká et al. 2008).

2.8.1. Law of Mass Action Model

Mass Action Law (MAL) for binary ion exchange of component i with component 1 is written as:



in which I depicts an exchanging cations, R depicts an anion site of the ion exchanger, and Z is the valence.

Considering, for a N_c component system, there are $N_c - 1$ independent equations, component 1 is chosen as the reference counterion.

Even though Equation (2.70), is composed for cation-exchange reactions, the mathematical statements to take after are relevant to both anion and cation exchange systems.

2.8.1.1 MAL for Equilibrium Systems

The mass action equilibrium constant for binary exchange is written as:

$$K_{i,1} = \left(\frac{\bar{C}_i}{C_i} \right)^{Z_1} \left(\frac{C_1}{\bar{C}_1} \right)^{Z_i} \quad (2.71)$$

where

$$C_i = \text{the equiv/l of solution}, \quad (2.71a)$$

$$\bar{C}_i = \text{the equiv/l of zeolite}, \quad (2.71b)$$

$$Z_i = \text{valence} \quad (2.71c)$$

In an accurate sense, Equation (2.71) could be expressed with regard to activities contrary to concentrations. Nevertheless, in case that it is estimated that solution and zeolite phases display ideal behavior, then activity coefficients can be neglected.

Because the number of fixed sites on the zeolite is limited and electroneutrality must be conserved, the whole zeolite phase concentration must be constant. This restraint is presented by a zeolite phase site balance equation:

$$\bar{C}_T = \sum_{i=1}^{N_c} \bar{C}_i \quad (2.72)$$

with C_T as the total zeolite phase capacity for each solid volume with all the concentrations in eq/L of solid volume.

2.8.1.2 Nonequilibrium MAL

For nonequilibrium systems, when the exchange kinetics are slow, the reaction rate equation for components 2 through N_c is shown by:

$$\left. \frac{d\bar{C}_i}{dt} \right|_{i>1} = I_{+,i} C_i^{Z_1} \bar{C}_1^{Z_i} - I_{-,i} \bar{C}_i^{Z_1} \quad (2.73)$$

where $I_{+,i}$ and $I_{-,i}$ are the forward (adsorption) and reverse (desorption) reaction rate constants, respectively. There are $N_c - 1$ of these equations.

Equation (2.69) is differentiated with respect to time and giving net ion-exchange rate:

$$\frac{d\bar{C}_1}{dt} = - \sum_{i=2}^{N_c} \frac{d\bar{C}_i}{dt} \quad (2.74)$$

Equation 2.74 is not a rate-limiting step in most of the ion exchange systems. The rate-limiting step in ion exchange systems is determined from mass transfer processes such as pore or surface diffusion. Verifying Equation 2.74 directly is hard to do and has not been reported up until now. Equation 2.74, nevertheless, is suggested here for the reasons below:

- (1) Nonequilibrium systems can be simulated by Equation (2.74).
- (2) At ion exchange equilibrium Equation (2.74) reduces to Equation (2.72).
- (3) For considering surface diffusion effects, the zeolite phase concentrations and solution phase concentrations must be solved at the same time.

In addition, in the case of surface diffusion solving Equation 2.72 may necessitate significant changes in the solution algorithm. When surface diffusion effects are not important, Equation 2.74 can still be utilized for equilibrium ion-exchange systems without changes in solution algorithm when adequately large $I_{+,i}$ and $I_{-,i}$ are utilized in the simulation while keeping mass action equilibrium constant as:

$$K_{i,1} = \frac{I_{+,i}}{I_{-,i}} \quad (2.75)$$

In binary equilibrium systems, Equation 2.71 is usually simplified by using the dimensionless groups below:

$$x_i = \frac{C_i}{C_T} \quad (2.76a)$$

$$y_i = \frac{\bar{C}_i}{\bar{C}_T} \quad (2.76b)$$

where C_T and \bar{C}_T are the total solution phase concentration and the total exchange capacity, correspondingly. In this case, mass action equilibrium constant is defined as:

$$\underline{K_{i,1}} = K_{i,1} \left(\frac{\bar{C}_T}{C_T} \right)^{z_i - z_1} \quad (2.77)$$

$$\underline{K_{i,1}} = K_{i,1} \left(\frac{y_i}{x_i} \right)^{z_1} \left(\frac{x_1}{y_1} \right)^{z_i} \quad (2.78)$$

2.8.2. Adsorption Models

Figure 2.8 shows porous adsorbent particles in a fixed bed and the nature and location of individual transport and diffusion mechanisms. These mechanisms include a different driving force and mostly generates a different form of mathematical result.

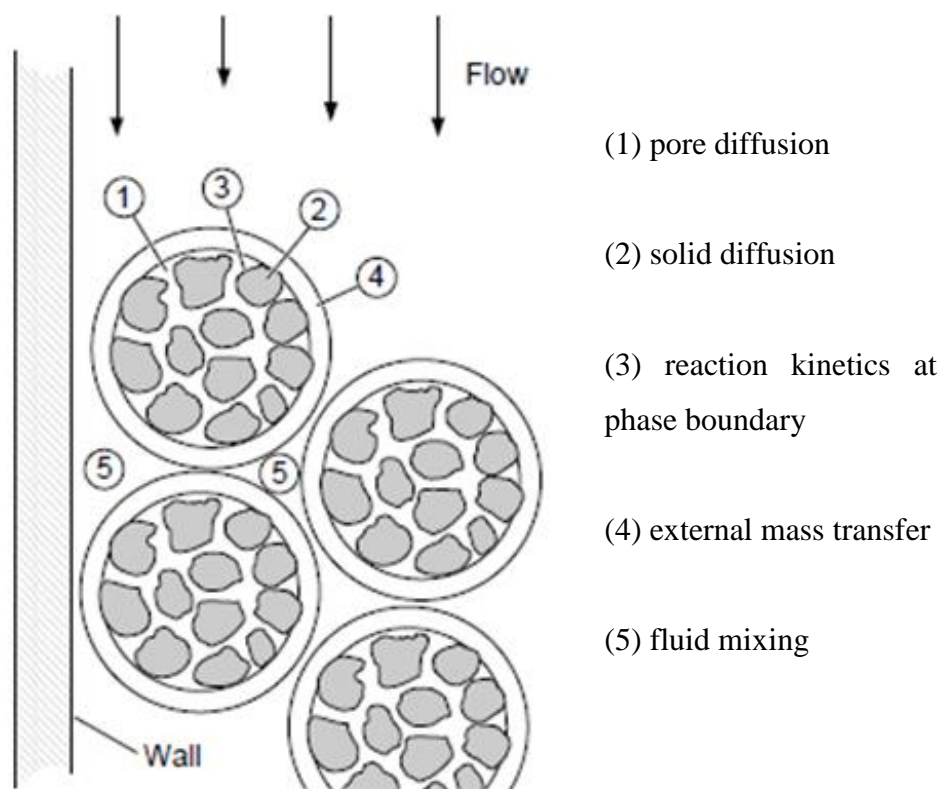


Figure 2.8. Diffusion and mass transfer mechanisms in a fixed bed of porous adsorbent particles (Perry and Green, 2008).

2.8.2.1. Intraparticle Transport Mechanisms

Intraparticle transport mechanisms are pore diffusion, solid diffusion, reaction kinetics at phase boundary or combinations of two or more.

Pore or macropore diffusion: If the diameter of the pores are large (macropores) then the diffusing molecules getaway from the force field of the zeolite/adsorbent surface. This type of diffusion is also called as *macropore diffusion* since the interactions between zeolite and the diffusing molecules happen on molecular scale. The driving force for this diffusion is the variation in mole fraction or concentration of the diffusing molecules within the pores.

If the zeolite or sorbent has huge and well-associated pores intraparticle diffusion will occur in fixed beds. Since the bulk flow over the pores of the sorbent is just a few portion of the total flow, intraparticle diffusion can influence the transport of very slowly diffusing macromolecules. In that case, the driving force is the pressure drop facing every single particle which is caused by the frictional resistance to flow encountered by the fluid as this flows through the packed bed.

Solid or micropore diffusion: When the pore diameter is adequately small and it becomes comparable to the size of the molecules then the diffusing molecules never getaway from the force field of the zeolite/adsorbent surface which means that interaction between the molecules with the pore walls become important. This mechanism is often called *micropore diffusion in zeolites*. The driving force for the process can thus be evaluated by the concentration gradient of the diffusion molecules in its adsorbed state.

Reaction kinetics at phase boundary: Mass transfer within the pore structure generally controls the rates of adsorption and desorption in porous sorbents instead the kinetics of sorption at the surface. Affinity-adsorption systems used for biological separations and chemisorption where the kinetics of bond formation can be very slow are the inconsistencies.

2.8.2.2.Extraparticle Mass Transfer Mechanisms

External mass transfer: The driving force in the external mass transfer or interparticle diffusion is the concentration difference between the external surfaces of the zeolite/sorbent particles and over the boundary layer surrounding each particle.

At the point when fluid flows through zeolite beads/sorbent particles there exists regions near the surface of the zeolite beads/sorbent particles called boundary layer where fluid velocity is very low. In such regions around the external surface of the zeolite beads/sorbent particles a near stagnant fluid film is present through which the adsorbate needs to be transported.

Mixing: Mixing or axial dispersion may happen through the presence of a velocity distribution or dead zones in a fixed bed or through ineffective mixing in an agitated reactor.

There are two diffusional resistances for controlling the mass transfer kinetics: external film diffusion and the micropore diffusion in the zeolite crystals. At low solution concentration external mass transfer was the controlling mechanism when in fact zeolite phase diffusion was the controlling mechanism at higher concentration.

2.8.2.3. Combined Models

Linear Driving Force (LDF) Model

Though solid diffusion and pore diffusion act in parallel, the efficient diffusion rate is the sum of these two rates. When solid diffusion is the controlling mechanism then mass transfer can be simply expressed in relation to the LDF approximation (Perry and Green 2008).

Linear Driving Force Model can be utilized for explanation of ion exchange/sorption concerning both intraparticle and extraparticle mass transfer. Rate equation, rate coefficient k and driving force expressions are presented in Table 2.2 and Table 2.3.

Table 2.2. Rate Equations for Mass Transfer in Spherical Ion Exchanger/Sorbent Particles

Mechanism	Flux equation	Rate equation
A. Pore diffusion	$J_t = -\epsilon_p D_{ps} \frac{\partial c_{ps}}{\partial r}$	$\epsilon_p \frac{\partial c_{ps}}{\partial t} + \rho_p \frac{\partial n_t}{\partial t} = \frac{1}{r^2} \frac{\partial}{\partial r} \left(\epsilon_p D_{ps} r^2 \frac{\partial c_{ps}}{\partial r} \right)$ $(\partial c_{ps} / \partial r)_{r=0} = 0, (\epsilon_p D_{ps} \partial c_{ps} / \partial r)_{r=r_p} = k_f (c_t - c_{ps,r})$ or $(c_{ps})_{r=r_p} = c_t$ for no external resistance
B. Solid diffusion	$J_t = -\rho_p D_s \frac{\partial n_t}{\partial r}$	$\frac{\partial n_t}{\partial t} = \frac{1}{r^2} \frac{\partial}{\partial r} \left(D_s r^2 \frac{\partial n_t}{\partial r} \right)$ $(\partial n_t / \partial r)_{r=0} = 0, (\rho_p D_s \partial n_t / \partial r)_{r=r_p} = k_f (c_t - c_t^*)$ or $(n_t)_{r=r_p} = n_t^*(c_t)$ for no external resistance
C. Parallel pore and solid diffusion (local equilibrium between pore and adsorbed phase)	$J_t = -D_{eff}(c_{ps}) \frac{\partial c_{ps}}{\partial r}$	$\left(\epsilon_p + \rho_p \frac{dn_t^*}{dc_t} \right) \frac{\partial c_{ps}}{\partial t} = \frac{1}{r^2} \frac{\partial}{\partial r} \left[r^2 \left(\epsilon_p D_{ps} + \rho_p D_s \frac{dn_t^*}{dc_t} \right) \frac{\partial c_{ps}}{\partial r} \right]$ $(\partial c_{ps} / \partial r)_{r=0} = 0, [(\epsilon_p D_{ps} + \rho_p D_s \frac{dn_t^*}{dc_t}) \partial c_{ps} / \partial r]_{r=r_p} = k_f (c_t - c_{ps,r})$ or $(c_{ps})_{r=r_p} = c_t$ for no external resistance
D. Diffusion in bidispersed particles (no external resistance)	$J_t = -\epsilon_p D_{ps} \frac{\partial c_{ps}}{\partial r}$ $J_t = -\rho_p D_s \frac{\partial n_t}{\partial r}$	$\frac{\partial n_t}{\partial t} = \frac{1}{\rho^2} \frac{\partial}{\partial \rho} \left(D_s \rho^2 \frac{\partial n_t}{\partial \rho} \right), (\partial n_t / \partial \rho)_{\rho=0} = 0, (n_t)_{\rho=r_c} = n_t^*(c_{ps})$ $\bar{n}_t(r,t) = \frac{3}{r_c^3} \int_0^r \rho^2 n_t d\rho$ $\epsilon_p \frac{\partial c_{ps}}{\partial t} + \rho_p \frac{\partial \bar{n}_t}{\partial t} = \frac{1}{r^2} \frac{\partial}{\partial r} \left(\epsilon_p D_{ps} r^2 \frac{\partial c_{ps}}{\partial r} \right), (\partial c_{ps} / \partial r)_{r=0} = 0, (c_{ps})_{r=r_p} = c_t$

Table 2.3. Rate Coefficient k and Driving Force Expressions

Mechanism	1. External film	2. Solid diffusion	3. Pore diffusion
Expression for rate coefficient, k	$k_c = \frac{k_f a}{\rho_b} = \frac{3(1-\epsilon)k_f}{\rho_b r_p}$	$k_s = \frac{15\psi_s D_s}{r_p^2}$	$k_p = \frac{15\psi_p(1-\epsilon)\epsilon_p D_{pt}}{\Lambda r_p^2}$
A. Linear driving force (LDF)	$c - c_i^*$	$n_i^* - \bar{n}_i$	$n_i^* - \bar{n}_i$
LDF for constant R	$c_i - \frac{Rc^{mf}\bar{n}_i/n^{mf}}{1 - (R-1)\bar{n}_i/n^{mf}}$	$\frac{n^{mf}c_i/c^{mf}}{R + (R-1)c_i/c^{mf}} - \bar{n}_i$	$\frac{n^{mf}c_i/c^{mf}}{R + (R-1)c_i/c^{mf}} - \bar{n}_i$
Correction factors ψ for constant R	—	$\frac{0.894}{1 - 0.106R^{0.5}}$	$\frac{0.775}{1 - 0.225R^{0.5}}$
B. Alternate driving force for constant R	—	$\frac{n_i^{*2} - \bar{n}_i^2}{2\bar{n}_i}$	$\frac{n_i^* - \bar{n}_i}{[1 - (R-1)\bar{n}_i/n^{mf}]^{0.5}}$
Correction factors ψ for alternate driving force	—	$\frac{0.590}{1 - 0.410R^{0.5}}$	$\frac{0.548}{1 - 0.452R^{0.5}}$
C. Reaction kinetics for constant R	—	—	—

2.8.3. Simplified Diffusion Models

Determination of the controlling mechanism of the ion exchange in fixed bed is a complex phenomenon. Controlling mechanism depends mainly on fluid linear velocity. However fluid-film diffusion may be the controlling mechanism at low velocities, in general, particle diffusion inside the solid matrix is the controlling mechanism. In the case of ion exchange zeolites which are made from both macro pore and micropore structure both controlling mechanism may be significant.

The pores can be divided into three groups:

- macropores, for diameters above 50 nm,
- mesopores, for diameters in the range 2–50 nm,
- micropores, for diameters below 2 nm.

Most of the particles used in ion exchange are porous that display large surface areas. Pore radius of a particle must be known, considering the pore radius allows or does not allow a molecule to move through the pores according to its size. As a consequence, certain part of the surface area may not be available to the species that diffuse. The individual pores of the porous solid may differ considerably in both size and shape and between one and another.

The reactant pathway from bulk to active site including diffusion processes in a fixed bed was shown in Figure 2.9. External resistances are film layers around the particles that can introduce mass transfer limitations. In addition, macropores in the pelleted particles and meso- and micropores in the small particles or crystals can cause internal (diffusional) mass transport limitations.

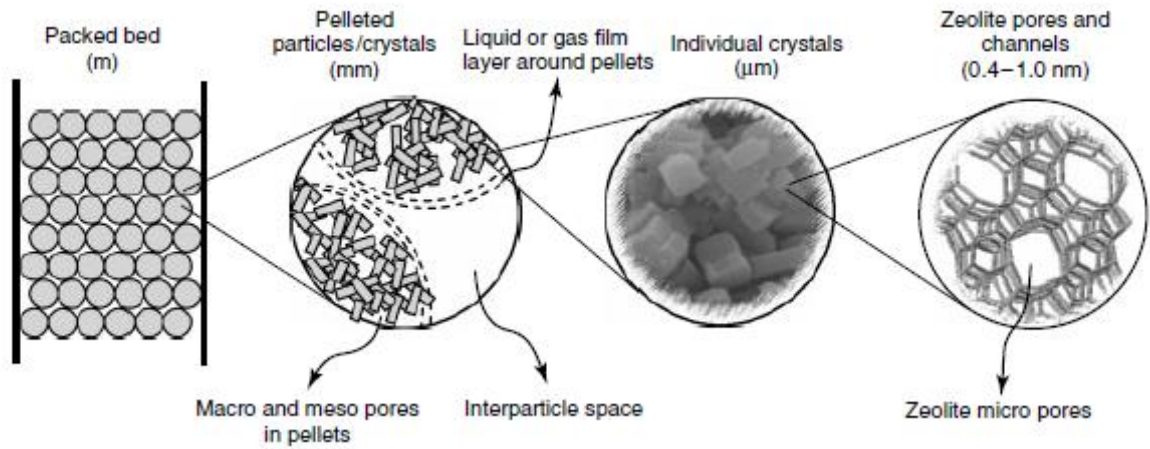


Figure 2.9 The reactant pathway from bulk to active site including diffusion processes. (Cejka, Corma and Zones, 2010)

Plug flow and constant pattern assumptions can be used to evaluate the controlling mechanism in the mass transfer.

1. Plug flow: This assumption is valid provided that the axial Peclet number of the bed (Pe_L) is higher than about 100. For porous particles of irregular shape, like zeolites and 0.5 mm particle size, a bed of 50-cm height is adequate, for superficial velocities greater than about 0.2 cm/s. Nevertheless, by the use upflow operation, this value can be lowered easily. In most cases, if upflow mode is used, the quality of the flow is much better, particularly at low velocities (Inglezakis, 2006).

In the assumption of plug flow by neglecting the initial term of Equation (I.4), Equation (I.4) reduces to:

$$u \frac{\partial C}{\partial z} = \varepsilon_p \frac{\partial C}{\partial t} + \rho_b \frac{\partial q}{\partial t} \quad (2.79)$$

2. Constant pattern condition: This assumption is valid if the equilibrium is favorable ($0 < La < 1$; in connection with Langmuir isotherm) and at high residence times. Nevertheless, the constant pattern assumption is poor if very slow kinetics were exhibited by the system. This assumption simplifies the mass balance Equation (I.4) into: $C/C_0 = \bar{q}/q_{max}$.

$$u \frac{\partial X}{\partial z} = \varepsilon_p \frac{\partial X}{\partial t} + \frac{\rho_b q_{max}}{C_0} \frac{\partial Y}{\partial t} \quad (2.80)$$

Multiplying both sides with $\frac{\partial t}{\partial x}$

$$\frac{\partial z}{\partial t} = - \frac{u}{\varepsilon_p + \frac{\rho_b q_{max}}{C_0} \frac{\partial Y}{\partial t}} \quad (2.81)$$

where

$$\frac{\partial z}{\partial t} < 0$$

This could only happen when

$$\frac{\partial Y}{\partial x} = const. \Rightarrow Y = c_1 X + c_2 \Rightarrow Y = X \quad (2.82)$$

In the case of the constant pattern and plug-flow assumptions, dimensionless terms which are listed below can be used.

$$\Lambda = \frac{\rho_b q_{max}}{C_0} \quad (2.83)$$

$$T = \frac{t - \left(\frac{V_0 \varepsilon}{Q}\right)}{\left(\frac{\Lambda V_0}{Q}\right)} \quad (2.84)$$

$$N_{f=} = \frac{k_f a_u V_0}{Q} \quad (2.85)$$

$$N_{p=} = \frac{15D_p (1 - \varepsilon)V_0}{Q} \quad (2.86)$$

$$N_{s=} = \frac{15D_s \Lambda V_0}{r_0^2 Q} \quad (2.87)$$

In the case of the constant pattern and plug-flow assumptions for the favorable Langmuir isotherm, Equations (2.88), (2.89) and (2.90) yield the approximate solutions for the fixed bed columns.

$$N_f(T - 1) = \frac{\ln(X) - La \ln(1 - X)}{1 - La} + 1 \quad (2.88)$$

$$N_s(T - 1) = \frac{1}{\Psi_s} \left[\frac{La \ln(X) - \ln(1 - X)}{1 - La} - 1 \right] \quad (2.89)$$

where

$$\Psi_s = \frac{0.894}{1 - 0.106La^{0.5}} \quad (2.90)$$

Experimental methods to determine the controlling mass transfer mechanism in fixed bed columns:

To evaluate the controlling mass transfer mechanism in fixed bed columns, the subsequent approach can be utilized (Inglezakis, 2006). Solely the dynamic data and particularly, data of outlet concentrations and the corresponding elapsed times are needed in this approximate method. When $(T - 1)$ against C/C_0 is plotted, C is the outlet concentration, C_0 is the initial concentration, and T is the dimensionless time constant.

When $N(T - 1)$ against C/C_0 is plotted, C/C_0 at which $N(T - 1)$ and consequently $(T - 1) = 0$ is termed the stoichiometric point and is independent of the volumetric

flow rate. At this point the quantity of cation that has leaked past the reference point in the bed exactly equals to the residual unfilled capacity of the zeolite/sorbent contained before that point (Inglezakis, 2006). The typical C/C_0 against $N(T-1)$ curves is demonstrated in Figure 2.10.

This point is ever less than about $C/C_0 = 0.7$, despite the controlling mechanism (fluid film, pore, or solid diffusion or a combination of them), for Langmuir and Freundlich isotherms. Moreover, the values of $(C/C_0)_{stoch}$ for solid diffusion control are in the range of 0.51 to 0.70 and the more favorable equilibrium leads to greater values of $(C/C_0)_{stoch}$. The values of $(C/C_0)_{stoch}$ for fluid-film control are in the range of 0.31 to 0.5 (Inglezakis, 2006).

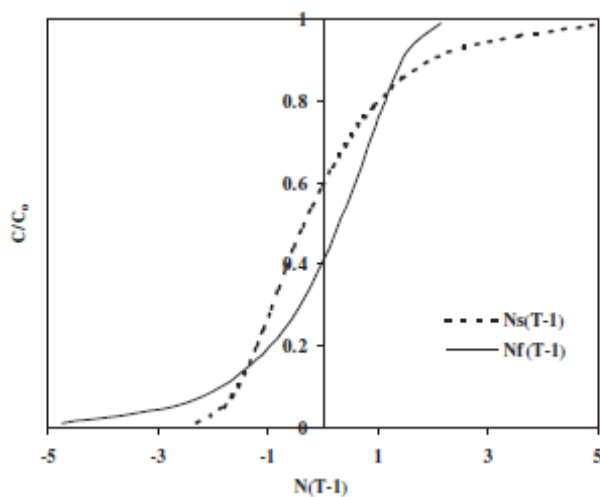


Figure 2.10 Typical C/C_0 against $N(T-1)$ plots for solid diffusion control (dotted line) and fluid film diffusion control ($La=0.2$) (Inglezakis, 2006).

2.8.4. Surface Reaction (Thomas) Model

Thomas model is a constant pattern model which neglects both the intraparticle (solid) and the external (fluid-film) mass transfer resistances.

This model compete with the Langmuir isotherm and the second-order reversible reaction kinetics (Farajpourlar et al, 2013). The model which is useful for the design of ion exchange column is given as:

$$\frac{C}{C_0} = \frac{1}{1 + \exp \left[\left(\frac{k_{Th} q_{max} m}{Q} \right) - k_{Th} C_0 t \right]} \quad (2.91)$$

where q_{max} is the maximum exchange capacity (meq/g), k_{Th} is the Thomas model constant (L/g.min), Q is the volumetric flow rate (ml/min).

The linear form of Thomas model is expressed as:

$$\ln \left(\frac{C_0}{C} - 1 \right) = \frac{k_{Th} q_{max} m}{Q} - k_{Th} C_0 t \quad (2.92)$$

2.8.5. Yoon - Nelson Model

The model which was established by Yoon and Nelson, 1984 for a single component system can be written as:

$$\frac{C}{C_0 - C} = \exp(k_{YN} t - \tau k_{YN}) \quad (2.93)$$

where k_{YN} is the rate constant in min^{-1} and τ (min) is the time required for 50% breakthrough. The linear form of Yoon and Nelson model is expressed as:

$$\ln \left(\frac{C}{C_0 - C} \right) = k_{YN} t - \tau k_{YN} \quad (2.94)$$

2.8.6. Adams-Bohart Model

The model which was developed by Bohart and Adams, 1920, can only be utilized for describing the initial part of the breakthrough curve and is represented by:

$$\frac{C}{C_0} = \exp(k_{AB}C_0t - k_{AB}N_0\frac{z}{U_0}) \quad (2.95)$$

where k_{AB} is the rate constant in L/min.mg, z is the bed height in cm, N_0 is the maximum ion exchange capacity per unit volume of the column in mg/L and U_0 is the linear velocity in cm/min. The linear form of the Adams-Bohart model is expressed as:

$$\ln\left(\frac{C}{C_0}\right) = k_{AB}C_0t - k_{AB}N_0\frac{z}{U_0} \quad (2.96)$$

CHAPTER 3

THEORETICAL BACKGROUND

Franklin and Townsend (1985) showed that if a recently derived thermodynamic model can also be used although partial exchange inhibits the evaluation of the standard free energies, it is attainable to estimate ternary equilibrium data well for zeolites.

Shetata et al. (2000) successfully modeled the behavior of ternary ion exchange equilibrium by using the binary batch experiment data. The model was established on equilibrium constants for the ion-exchange reactions written in relation to liquid and zeolite phase activities. By using the Debye and Huckel model, liquid phase activity coefficients were determined. Zeolite phase activity coefficients were determined from the Wilson equation.

Mumford et al., (2008) used a currently created temperature dependent semiempirical thermodynamic ion-exchange model for predicting ion-exchange equilibrium behaviors of binary and ternary systems upon a natural zeolite. The ion exchange system contains ammonium, potassium, and calcium, at chloride cation concentrations changing within the limits of 0.005 to 0.25 M. System temperature is variable within the limits of 4.0 to 40.0 °C ± 0.2 °C. The ion-exchange behavior is well described by this model.

Barros et al., (2006) researched the dynamic ion exchange of Cr³⁺, Ca²⁺, Mg²⁺ and K⁺ cations onto NaX and NaY in ternary systems of Cr/Ca/K, Cr/Ca/Mg and Cr/Mg/K at

30°C. The balance selectivity was acquired as $\text{Cr}^{3+} > \text{Mg}^{2+} > \text{Ca}^{2+} \approx \text{K}^+$ for zeolite NaY and $\text{Ca}^{2+} \gg \text{Cr}^{3+} > \text{Mg}^{2+} \approx \text{K}^+$ for zeolite NaX. Sequential ion exchange where chromium ions can take the place of the competing cations were shown in the breakthrough curves. Some mass transfer parameters, like length of unused bed and overall mass transfer coefficient, were examined. Chromium retention was examined too by a mass balance. They concluded that a greater similarity towards Cr^{3+} was shown in NaY for both equilibrium and dynamic systems and its sites were more effectively utilized in the ion exchange. Chromium was less retained in NaX because it showed great selectiveness for calcium ions.

Barros et al., (2003) used breakthrough curves for studying the ion exchange of Na for Cr/K, Cr/Mg and Cr/Ca in Y and X zeolites. They noticed that few competing ions that had been interchanged before at the zeolitic sites could be removed by Cr^{3+} ions and this process produces a ion exchange which occurs in an order. They also studied some mass transfer parameters like length of unused bed, overall mass transfer coefficient and practical ratio. The ion in the NaX zeolite columns which competes, influenced the chromium uptake much more. Cr/K solution generated a higher axial dispersion than the Cr/Mg and Cr/Ca systems, possibly as a result of some interaction between Cr^{3+} and K^+ ions was indicated by the dimensionless variance. The cation uptake provided that the order of dynamic selectivity, was $\text{Cr}^{3+} > \text{Ca}^{2+}$, $\text{Cr}^{3+} > \text{Mg}^{2+}$ and $\text{Cr}^{3+} > \text{K}^+$ for NaY zeolite and $\text{Ca}^{2+} \approx \text{Cr}^{3+}$, $\text{Mg}^{2+} > \text{Cr}^{3+}$ and $\text{Cr}^{3+} > \text{K}^+$ for NaX zeolite. Because of the more appropriate mass transfer parameters and greater affinity for Cr^{3+} , it was deduced that NaY zeolite was more effective at chromium exchange in competing systems.

Trgo et al. (2006) investigated the kinetics of zinc and lead ions extraction by altered clinoptilolite. The rate of the ion exchange process for lead ions is quicker than for zinc ions, and also the time which is necessary to attain the equilibrium. The ion exchange capacity of zinc ions is twice lower than that of lead ions Diffusion models

in accordance with the Vermeulen's approximation, the parabolic and the homogeneous diffusion models have been examined with the experimental data of ion exchange for zinc and lead. The Vermeulen's approximation and the homogeneous diffusion model with $t \rightarrow t_{\infty}$ show the best fit of the models suggested with the experimental data for both systems examined

Inglezakis et al., (2003) investigated the ion exchange of Pb^{2+} , Cu^{2+} , Fe^{3+} , and Cr^{3+} on natural clinoptilolite in relation to selectivity toward the above heavy metals in single and multicomponent batch systems. At total concentration 0.01 N and acidity 2 in both single and multicomponent system selectivity followed the order $\text{Pb}^{2+} > \text{Fe}^{3+} > \text{Cr}^{3+} > \text{Cu}^{2+}$. They reached the conclusion that this order was fixed after the first days of equilibration and nevertheless, Cu^{2+} showed important differences in selectivity and mainly its uptake and selectivity were rising by time. However, the selectivity in single metal solutions in which acidity is not modified followed the order $\text{Pb}^{2+} > \text{Cr}^{3+} > \text{Fe}^{3+} \cong \text{Cu}^{2+}$.

Valverde et al., (1999) examined in contrast two models which are used in predicting multicomponent ion exchange equilibria. In the first model, a heterogeneous model, established according to the law of mass action where ideal behavior for both the solution and the zeolite phase and the heterogeneity of ion exchange sites has been estimated; and the other a homogeneous model, established according to the same mass action law where nonideal behavior for both the solution and the zeolite phase has been estimated. The way that the distribution of functional groups impacts the estimation of the binary equilibria, in which counterions with different valences are included, has been researched. The most excellent fit was reached while the energy distribution was almost symmetric.

Robinson et al., (1994) researched Na-Ca-Mg-Cs-Sr ion exchange from an aqueous solution by utilizing a chabazite zeolite. They figured out the mass-transfer from experimental batch-reactor data for binary and multicomponent systems. The

experimental data indicated that diffusion through the microporous zeolite crystals was the fundamental diffusional resistance and macropore diffusion greatly contributed to the mass-transfer resistance too. Different mass transfer models were examined in contrast with the experimental data for determining values for intraparticle diffusivities. Efficient diffusivities acquired precisely estimate experimental data by utilizing different models. Only the model justifying micropore and macropore diffusion in series precisely predict multicomponent data by utilizing diffusivities from the binary system. Macropore diffusion was improved by liquid and surface diffusion. Surface and micropore diffusivities were concentration-dependent for the system of interest.

Angélica et al., (2008) researched the ion exchange isotherms of Cr^{3+} , Mg^{2+} , Ca^{2+} and K^+ in ternary mixtures (Cr/Mg/Ca, Cr/Ca/K, Cr/Mg/K) by utilizing NaX zeolite at 30 °C, 45 °C and 60°C and noted the selectivity order as follows: $\text{Cr}^{3+} > \text{Ca}^{2+} > \text{Mg}^{2+}$ at 30 °C, $\text{Ca}^{2+} > \text{Cr}^{3+} > \text{Mg}^{2+}$ at 45 °C and $\text{Ca}^{2+} > \text{Mg}^{2+} > \text{Cr}^{3+}$ at 60 °C for Cr/Ca/Mg–NaX isotherms. For the Cr/Ca/K–NaX isotherms the sequence was $\text{Cr}^{3+} > \text{Ca}^{2+} > \text{K}^+$ over the whole temperature spectrum and lately for the Cr/Mg/K–NaX isotherms, $\text{Cr}^{3+} > \text{Mg}^{2+} > \text{K}^+$ at 30 and 45 °C and $\text{Mg}^{2+} > \text{K}^+ > \text{Cr}^{3+}$ at 60 °C.

Barros et al. (2002) demonstrated that NaA and NaX zeolites have very much alike appropriate exchange isotherms and close affinities for chromium ions in batch equilibrium systems at 30°C; regarding the dynamic experiments, the optimal flow rate for NaA and NaX beds could be deemed as 11 and 9 mL/min, correspondingly, because of the superior performance of the column and appropriate values of the mass transfer parameters; NaX turn out to be more effective for chromium uptake than NaA due to the zeolite framework and principally supercage apertures have a noticeable impact in the dynamic performance.

Borba et al. (2012) investigated the ion exchange dynamics of Cu^{2+} – Zn^{2+} – Na^+ a ternary ion exchange system using Amberlite IR120 resin. The ternary ion exchange

in the fixed bed was studied with regard to Mass Action Law. When modeling, the external and internal mass transfer limitations and thermodynamic equilibrium on the liquid–solid interface were taken into account.

Ternary ion exchange system in fixed bed was modeled by Aniceto et al. (2013). They suggested that modeling -ternary ion exchange isotherms with artificial neural networks (ANN) are really advantageous when the resulting model is constantly complicated and urges researchers for selecting empirical expressions which in most cases don't have any predictive ability.

Shebil et al. (2007) studied the uptake of Ca^{2+} by Amberlite IR120 by utilizing the Langmuir isotherm for describing the equilibrium and the internal and external mass transfer limitations were taken into account.

Lee et al. (2008) studied the $\text{Cu}^{2+}/\text{H}^+$, $\text{Zn}^{2+}/\text{H}^+$, and $\text{Cd}^{2+}/\text{H}^+$ systems by utilizing Amberlite IR-120 and self-sharpening and constant-pattern wave models were used to predict the column dynamics. The self-sharpening wave model assumes local ion exchange equilibrium might supply a clear and fast prediction for the breakthrough volume, yet the estimated breakthrough curves did not fit the experimental data exactly. Contrastingly, they showed that the constant-pattern wave model which uses a fixed driving force model for finite ion-exchange rate supplied a superior fit for the experimental data.

CHAPTER 4

MATERIALS AND METHODS

4.1. Materials and Methods

Synthetic Zeolite 13X beads was used for investigating the ion exchange of Pb^{2+} - Na^+ and Cd^{2+} - Na^+ binary systems, Cd^{2+} - Pb^{2+} - Na^+ ternary systems and Cd^{2+} - Pb^{2+} - Zn^{2+} - Na^+ quaternary systems in this study.

The commercial Zeolite 13X which were in the form of beads procured from Acros Organics and Zeochem in different mesh sizes. Pure Zeolite 13X crystals is known to have an ideal chemical formula $\text{Na}_{86}[(\text{AlO}_2)_{86}(\text{SiO}_2)_{106}] \cdot n\text{H}_2\text{O}$ although Si/Al may vary within certain extent. However it is also known that bead or pellets of zeolites usually contain a clay type binder material of about 20 %. The pore diameter of Zeolite 13X is 10 Å.

To determine the most suitable particle size preliminary column experiments were done with 8/12 mesh sizes which lead to lower ion exchange capacities. Samples which were in the size range of 20/40 mesh range were sieved and fractionated to have a narrower size range of 25/30 mesh which corresponds to a size range of 0.599-0.710 mm. Zeolite 13X beads were kept in a desiccator containing saturated NaCl solution for several days to maintain constant moisture content. Samples thus prepared were used in characterization and ion exchange experiments.

4.2.Characterization of Zeolite 13X beads

Several characterization techniques are used to characterize original Zeolite 13X samples. Samples of Zeolite 13X beads (15-20 mg) were used and heated from 25 °C to 1000 °C at constant rate. The weight loss and water content of the commercial Zeolite 13X beads was determined by Thermogravimetric Analysis (TGA) and thermal stability of Zeolite 13X beads was determined by Differential Thermal Analysis (DTA). Since the ion exchange capacity of a zeolite relies upon chemical composition, ion exchange capacity of Zeolite 13X beads can be calculated from the chemical composition determined from TGA. TGA instrument used was Shimadzu DTG 60-H at METU Chemical Engineering Department.

4.3.BET analysis

BET analysis was done to calculate the specific surface area of Zeolite 13X beads utilizing N₂ gas as adsorbent. BET instrument used was “Quantachrome Autosorb-6B Surface Area and Pore Size Analyzer” at METU Central Laboratory

4.4.Chemicals

The metal salts utilized in this study were analytical grade reagents retrieved from Merck. Pb(NO₃)₂, Zn(NO₃)₂ and Cd(NO₃)₂ salts were utilized as cation source for Pb²⁺, Cd²⁺ and Zn²⁺. The aqueous solutions of Pb²⁺, Cd²⁺ and Zn²⁺ will be made by dissolving Pb(NO₃)₂, Zn(NO₃)₂ and Cd(NO₃)₂ in highly deionized water obtained from Millipore Ultrapure Water System.

4.5. Batch Studies

4.5.1. Maximum Exchange Level (MEL) Experiments

MEL experiments were carried out as by mixing measured quantities of Zeolite 13X beads (samples of 25/30 mesh sizes and 0.2-1.0 grams) with constant concentrations of metal salt solutions (0.05/0.1N) in pyrex bottles. Total volume of the mixtures were 50 mL.

Mixtures were agitated in NÜVE ST 402 shaking waterbath for 4 days at 25°C. After the equilibrium was reached, the solution parts of the mixtures were analyzed for Pb^{2+} , Zn^{2+} and Cd^{2+} ions by using Shimadzu AA-6300 atomic absorption spectrophotometry at METU Chemical Engineering Department. Flame photometer (Jenway) at Chemical Engineering Department was used to determine the Na^+ ions. Maximum ion exchange capacities were calculated from the measured final equilibrium concentrations.

4.5.2. Equilibrium Isotherms

In order to obtain the equilibrium isotherm data for Pb^{2+} - NaX, Cd^{2+} - NaX and Zn^{2+} - NaX binary exchange systems; Pb^{2+} - Cd^{2+} - NaX, Pb^{2+} - Zn^{2+} - NaX and Zn^{2+} - Cd^{2+} - NaX ternary exchange systems and Pb^{2+} - Zn^{2+} - Cd^{2+} - NaX quaternary exchange systems, batch experiments were performed like the following:

A measured quantity of Zeolite 13X (0.8 g) was added to pyrex bottles that include 50 ml metal nitrate salts ($Pb(NO_3)_2$, $Zn(NO_3)_2$ and $Cd(NO_3)_2$) at different initial concentrations (0.01-0.1 N). The temperature was kept at constant 25 °C. The samples were agitated in NÜVE ST 402 shaking waterbath, until the equilibrium was reached (Figure 4.1).

The zeolite phase was separated by filtration and the solution phase was examined for all the exchanging ions by atomic absorption spectrophotometer. The final pH of metal salt solutions was measured by pH meter.

Measuring the initial and final equilibrium concentrations in the solution phase and considering mass balance, the zeolite phase concentrations were determined from Equation (4.1):

$$q_e = \frac{(C_o - C_e)V}{m} \quad (4.1)$$

where C_o and C_e are the initial and equilibrium concentrations in the solution phase (meq/l), respectively, q_e is the zeolite phase concentrations (meq/g), m is the mass of the zeolite (g) and V is the volume of solution (l).



Figure 4.1. NÜVE ST 402 shaking waterbath

4.5.3. Batch Kinetic Experiments

For investigating the kinetic parameters for Pb^{2+} - NaX, Cd^{2+} - NaX and Zn^{2+} - NaX binary exchange systems batch experiments were carried out using erlenmeyer polypropylene flasks. 0.8 g of Zeolite 13X

A measured quantity of Zeolite 13X (0.8 g) was added to erlenmeyer polypropylene flasks containing 250 ml metal nitrate salts ($\text{Pb}(\text{NO}_3)_2$, $\text{Zn}(\text{NO}_3)_2$ and $\text{Cd}(\text{NO}_3)_2$) at constant initial concentrations (0.05 N). The temperature was maintained constant 25 °C. The samples were agitated in NÜVE ST 402 shaking waterbath and 5.0 mL of samples were removed at constant time intervals and the solution phase was analysed for the exchanging ions by atomic absorption spectrophotometer. The zeolite phase concentrations were determined from Equation (4.1).

4.6. SEM/EDX analysis

The external and internal texture surface Zeolite 13X beads were done by Scanning Electron Microscope (QUANTA 400F in METU Central Laboratory). Samples of the Zeolite 13X beads were placed onto adhesive carbon tape supported on a stud. The elemental composition of Zeolite 13X beads were also determined after ion exchange by randomly selecting areas on the zeolite surfaces and analyzing by Energy Dispersive X-ray (EDX) in connection with SEM.

4.7. Column Studies

Preliminary experiments were done to determine the optimum conditions. (size and height of the column (1.0/2.0/3.2 cm inside diameter; 20 cm height), weight of the zeolite (15-80 g), mesh size the zeolite beads (8-12, 20-25, 25-30) initial concentration of the metal ions (0.05/0.1 N).

The single component and multicomponent ion exchange studies were performed utilizing a column of 2.0 cm in diameter (\emptyset) and 5.0-7.0 cm in height (hc). The column was filled with 15 g of synthetic zeolite beads with 0.599-0.710 mm particle sizes. The column and the zeolite bed specifications are given below.

Equipment Specifications

Inside Column Diameter: 2.0 cm

Weight of Zeolite: 15 grams

Packed Height : 5.8 cm

Particle Size : 25/30

Operating Conditions

Feed Concentration: 0.05 N

Flow Rate : 10 mL/min

pH : 5-6

Experiment setup is given in Figure 4.2.

The metal salt solutions (pH:5-6) were pumped from a tank to the zeolite loaded column in an upflow mode at different flow rates (10, 15, 20 ml/min) , using a peristaltic pump (ColeParmer Masterflex L/S). Effluent samples (pH:5-6) from the column were collected at fixed time intervals for determining the cation concentrations in the effluent as a function of time or volume.

For a single component feed solution, the process was halted while the ion concentration in the outflow equals to the initial concentration in the influent. Collected samples were investigated to determine of Pb^{2+} , Cd^{2+} or Zn^{2+} concentrations and the breakthrough curves were demonstrated. Attention should be given to that in the breakthrough analysis, the breakthrough point concentration was taken as 5% of the feed concentration.

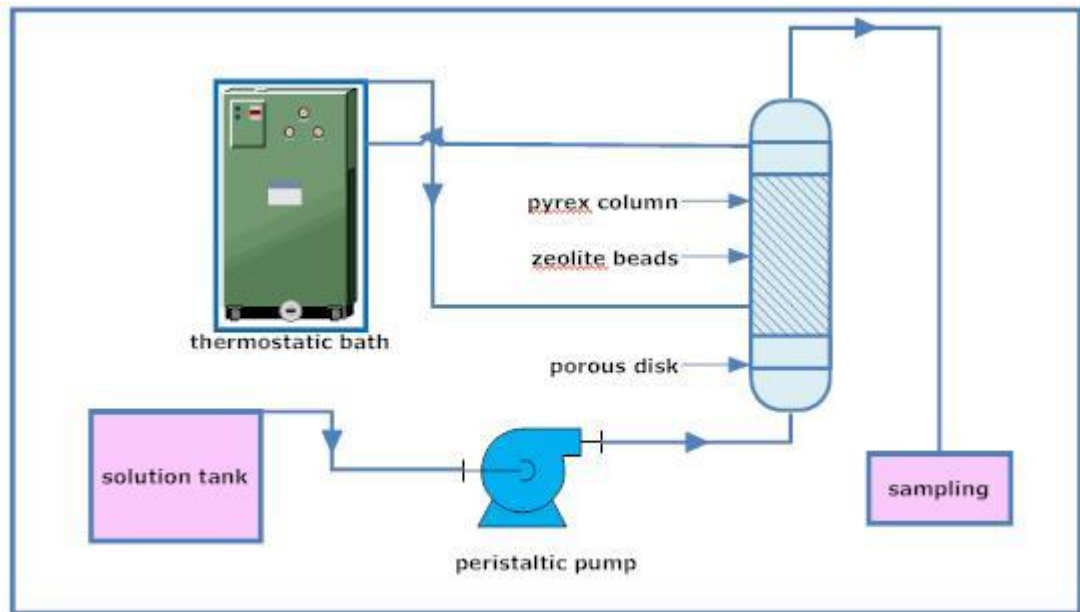


Figure 4.2. Experiment setup

CHAPTER 5

RESULTS AND DISCUSSION

5.1. TGA Results

TGA results indicated that nearly all of the water was lost at 400°C. Total weight loss content of the commercial Zeolite 13X beads was found as 22.035 wt % from TGA analysis and the amount of water molecules for each unit cell of Zeolite 13X was calculated as 210. Then the ion exchange capacity of Zeolite 13X was determined as 5.00 meq/g in hydrous base and 6.40 meq/g in anhydrous base.

The calculation of exchange capacities are given in Figure A.1.

5.2. BET analysis

The specific surface area of Zeolite 13X beads (mesh range of 25/30) was calculated as 690.20 (m²/g) from the BET Isotherm of Zeolite 13X (Figure H.2) and using Equations (C.2) and (C.3). The value calculated was in the range (600-700 m²/g) reported for Zeolite 13X (Perry and Green, 2008).

5.3. Batch Studies

5.3.1. Maximum Exchange Level (MEL) Experiments

Total exchange capacities of Zeolite 13X were calculated as 5.0-7.7 meq/g for Pb^{2+} – Na^+ binary ion systems and 3.5-8.9 meq/g for Cd^{2+} - Na^+ binary ion systems at 0.1 N total solution concentration at different zeolite weights (Table B.1).

Total exchange capacities of Zeolite 13X were calculated as 2.5-9.4 meq/g for Pb^{2+} – Na^+ binary ion systems and 2.5-5.7 meq/g for Cd^{2+} - Na^+ binary ion systems at 0.05 N total solution concentration at different zeolite weights (Table B.2).

Total exchange capacities of Zeolite 13X were calculated as 6.2 meq/g for both Pb^{2+} – Na^+ and Cd^{2+} - Na^+ binary ion systems; 5.7 meq/g for Zn^{2+} - Na^+ binary ion systems at 0.05 N total solution concentration and 0.8 g zeolite weight. (Table B.3).

5.3.2. Equilibrium Isotherms

Both batch and column systems can be used to determine ion exchange equilibrium isotherms. Although ion exchange columns don't function at local equilibrium, when the flow rate is very low, ion exchange rate is huge and the particle size of the ion exchanger is little, local equilibrium assumption can be used. The use of this assumption in zeolite loaded columns will be not correct since the ion exchange rate is slow.

Consequently, in this study batch method was used to determine ion exchange equilibrium isotherms.

5.3.2.1. Single component Ion Exchange Isotherm Studies

The experimental data were evaluated using seven adsorption isotherm models; Langmuir, Freundlich, Tempkin, DR, Redlich Peterson, Sips and BET. Mono component ion exchange isotherm data are shown at Tables C.3, C.4 and C.5.

Langmuir Isotherm

Langmuir isotherm parameters, Q_M and b , for Pb^{2+} - NaX, Cd^{2+} - NaX and Zn^{2+} - NaX binary exchange at constant temperature were computed from the slope and the intercept of (C_e/q_e) against (C_e) plots (Figure 5.1). The linear coefficient of determinations ($R^2 \geq 0.914$) which were presented in Table 5.1 showed that Langmuir isotherm model parameters were in good agreement with the observed behavior. Maximum adsorption capacities Q_M on the Zeolite13X beads at room temperature (297 K) were calculated as 555.55 mg/g (5.4 meq/g) for Pb^{2+} , 238.09 mg/g (4.2 meq/g) Cd^{2+} and 114.94 mg/g (3.5 meq/g) for Zn^{2+} (Table 5.1). The equilibrium constant, b which is based on the apparent energy of sorption for Pb^{2+} (0.0870 L/mg) was higher than that of Cd^{2+} (0.0250 L/mg) and Zn^{2+} (0.0047 L/mg).

As far as ionic radius of the cations ($Pb^{2+} = 1.30A^\circ$; $Cd^{2+} = 0.97 A^\circ$; $Zn^{2+} = 0.70A$) were concerned, the cation with lower ionic radius will face the exchange sites more rapidly than that of higher ionic radius. Beyond, the data in Table 5.1 showed that the selectivity sequence for Zeolite13X beads against the studied cations was $Pb^{2+} > Cd^{2+} > Zn^{2+}$.

Furthermore, a dimensionless constant called equilibrium parameter La , which was defined by Equation (2.9) could be used to explain the effectiveness of the three metals on Zeolite 13X. If the value of La is zero, Langmuir isotherm is irreversible; If the value of La is greater than 1 Langmuir isotherm is unfavorable.

Values between 0 and 1 indicate favorable ion exchange. Equilibrium parameter for Langmuir isotherm La and separation factor is related as follows:

$$\alpha_B^A = \frac{1}{La} \quad (5.1)$$

The La values Pb^{2+} - NaX, Cd^{2+} - NaX and Zn^{2+} -NaX binary exchange on Zeolite 13X beads at different concentrations, which were presented in Table 5.2, were less than unity. This indicated that Zeolite 13X was a convenient ion exchanger for the Pb^{2+} , Zn^{2+} and Cd^{2+} cations. The smallest La value which is an implication of an a highly favorable ion exchange is attained by Pb^{2+} at all concentrations. Thus, Pb^{2+} will compete for exchange sites on Zeolite 13X more rapidly than Zn^{2+} and Cd^{2+} since La value of $Zn^{2+} > Cd^{2+} > Pb^{2+}$.

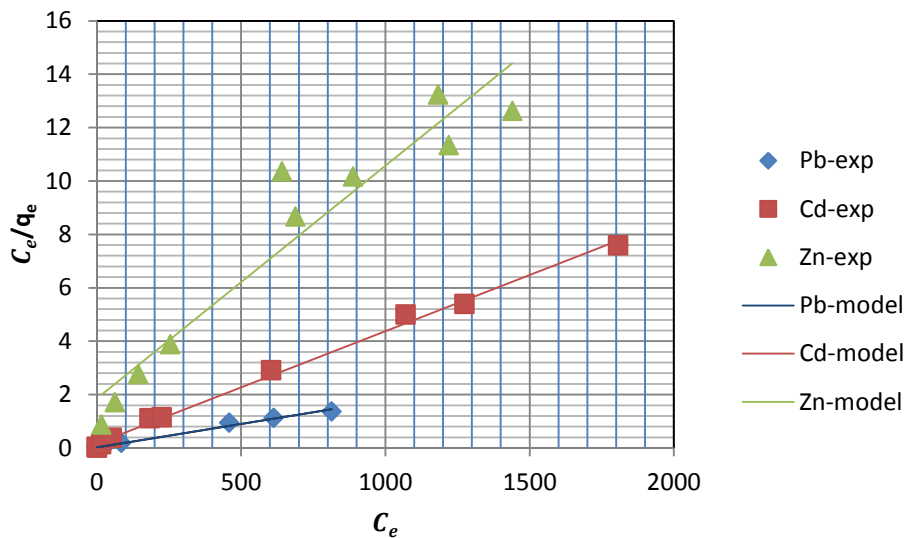


Figure 5.1. Langmuir equilibrium isotherm model for Pb^{2+} - NaX, Cd^{2+} - NaX and Zn^{2+} -NaX binary exchange on Zeolite 13X beads.

Table 5.1. Langmuir isotherm constants

Metal ions	Q_M (mg/g)	Q_M (meq/g)	b (L/mg)	R^2
Pb ²⁺	555.55	5.4	0.0870	0.991
Cd ²⁺	238.09	4.2	0.0250	0.996
Zn ²⁺	114.94	3.5	0.0047	0.916

Table 5.2. Equilibrium parameters for Langmuir isotherm

Metal ions	Equilibrium parameter, La		
	$C_o=300$ mg/L	$C_o=5000$ mg/L	$C_o=10000$ mg/L
Pb ²⁺	3.7×10^{-2}	2.3×10^{-3}	1.1×10^{-3}
Cd ²⁺	1.2×10^{-1}	7.8×10^{-3}	3.9×10^{-3}
Zn ²⁺	4.1×10^{-1}	4.1×10^{-2}	2.1×10^{-2}

Freundlich Isotherm

Freundlich isotherm which gives sufficient information of ion exchange data over a limited range of concentrations is also appropriate for a highly heterogeneous surface (Juang et al. 1996). The Freundlich isotherm constants K_F and $(1/n)$ are found out from the intercept and slope of a plot of $\ln q_e$ versus $\ln C_e$ (Figure 5.2). Steepness and curvature of the isotherm can be determined from the values of K_F and $(1/n)$.

The linear coefficient of determinations ($R^2 \geq 0.946$) which are presented in Table 5.3 showed that this model also gave adequate definition of the ion exchange in the range of concentration investigated in all three metal systems, with the cadmium and zinc isotherms seeming to fit the experimental data more favorable than lead.

The Freundlich isotherm constants for Pb^{2+} -NaX, Cd^{2+} -NaX and Zn^{2+} -NaX binary exchange on Zeolite13X were listed in Table 5.3. The ultimate ion exchange capacity/sorption K_F , could be utilized to predict the ion exchange/sorption intensity of the three metal ions on the Zeolite 13X surface. If the value of K_F , is higher, than the adsorption intensity is greater. The K_F value of Pb^{2+} (235.56 mg/g) is greater than that of Cd^{2+} (63.12 mg/g) and Zn^{2+} (7.94 mg/g), confirms that adsorption tendency of Pb^{2+} towards the Zeolite13X was greater than that of the other two metals. This significant difference is may be because of the difference between the hydrated radius of these metals (hydrated radius of Pb^{2+} , Cd^{2+} and Zn^{2+} are about 4.0, 4.2, and 4.30 Å, respectively). If the hydrated radius is smaller than the affinity for adsorption onto the Zeolite13X is higher.

The values of Freundlich isotherm constant ($1/n$) less than unity were obtained for Zeolite 13X which is an indication of monolayer adsorption (chemisorption). That means considerable sorption occurs at low concentration yet the increase in the quantity adsorbed with concentration turns out less considerable at higher concentrations and vice versa. Hence, the high $1/n$ value of Zn^{2+} (0.36) in relation to Pb^{2+} (0.13) and Cd^{2+} (0.19) indicates the ability of the Zeolite13X to extract zinc ions from solution better than other two metals even at high concentrations. Furthermore, n values for both metals changes between one and ten signifies a beneficial sorption process.

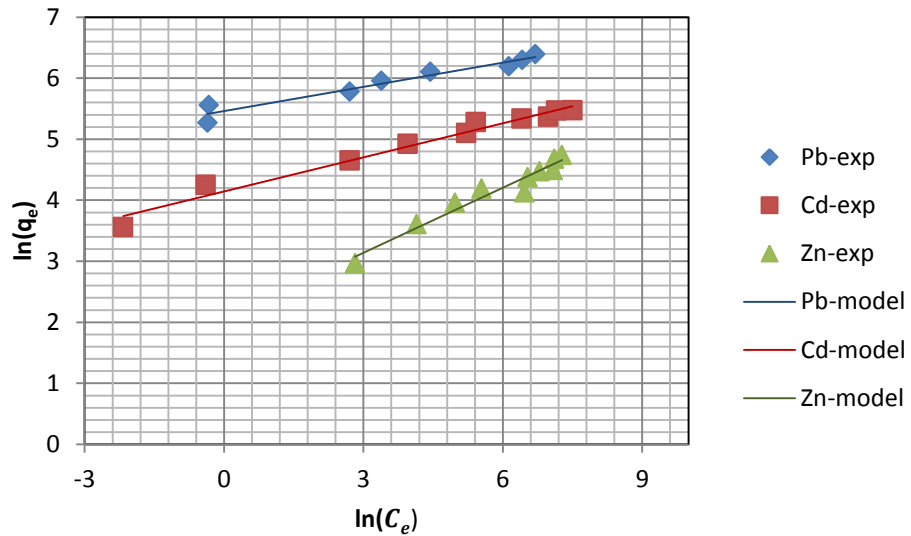


Figure 5.2. Freundlich equilibrium isotherm model for the Pb^{2+} - NaX, Cd^{2+} - NaX and Zn^{2+} -NaX binary exchange on Zeolite13X beads.

Table 5.3. Freundlich isotherm constants

Metal ions	K_F (mg/g)	1/n	R^2
Pb^{2+}	235.56	0.13	0.946
Cd^{2+}	63.12	0.19	0.973
Zn^{2+}	7.94	0.36	0.950

Dubinin–Radushkevich (DR) isotherm

The slope and intercept of plots of $\ln q_e$ versus ϵ^2 were utilized to compute the DR isotherm parameters (Figure 5.3). From the linear coefficient of determination R^2 values which are in the range from 0.65 to 0.79 (Table 5.4), it was possible to decide that the DR model was not good for explaining Pb^{2+} - NaX, Cd^{2+} - NaX and Zn^{2+} -NaX binary exchange on Zeolite 13X beads.

The mean free energy of adsorption (E) and the Dubinin-Radushkevich isotherm constants could be seen on Table 5.4. The DR constant q_D value of Pb^{2+} (388.80 mg/g) was higher than that of Cd^{2+} (169.88 mg/g) and Zn^{2+} (74.68 mg/g) indicated high sorption capacity of lead on Zeolite 13X. The q_D values were also accordant with the Q_M values that were already deduced for the Langmuir isotherm.

The mean free energy of adsorption (E) can be used for estimating the type of adsorption. The (E) value which was smaller than 8 kJ/mol is an indication of physisorption dominates chemisorption which occurs because of weak Van der Waals forces among sorbates and sorbents (Itodo et al., 2010). The values of E computed by utilizing Equation (2.15) were 4.472, 4.472 and 0.120 kJ/mol for lead, cadmium and zinc correspondingly. These values depict physisorption process.

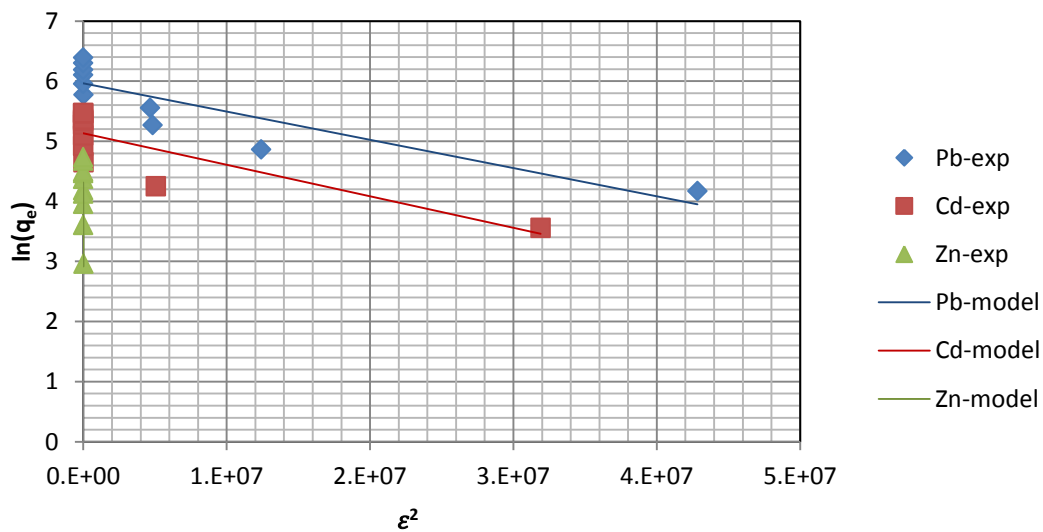


Figure 5.3. DR equilibrium isotherm model for the Pb^{2+} - NaX, Cd^{2+} - NaX and Zn^{2+} -NaX binary exchange on Zeolite13X beads.

Table 5.4. DR Isotherm constants

Metal ions	q_D (mg/g)	β (mol ² /J ²)	E (kJ/mol)	R ²
Pb ²⁺	388.80	5×10^{-8}	4.472	0.786
Cd ²⁺	169.88	5×10^{-8}	4.472	0.712
Zn ²⁺	74.68	7×10^{-5}	0.120	0.657

Temkin isotherm

Linear plots for Temkin adsorption isotherm (Figure 5.4), fitted with the experimental data quite better than DR isotherm with correlation coefficients ≥ 0.88 shown in Table 5.5 provided a more favorable choose for describing sorption energies.

The equilibrium binding constant, K_T of Zeolite 13X for Pb²⁺ - NaX, Cd²⁺ - NaX and Zn²⁺-NaX binary exchange on Zeolite13X beads were 60.64 (L/g), 27.42 (L/g) and 0.118 (L/g) respectively. This indicated a greater adsorption potential of Zeolite 13X for Pb²⁺ than that of Cd²⁺ and Zn²⁺. The Temkin constant, B_T related to heat of sorption for Pb²⁺ - NaX, Cd²⁺ - NaX and Zn²⁺-NaX binary exchange on Zeolite13X beads were 51.71 J/mol, 21.16 J/mol and 19.12 J/mol respectively. The sorption process was found to be mostly a physisorption process since the heat of sorption values were smaller than 8 kJ/mol (Ho et al., 2002).

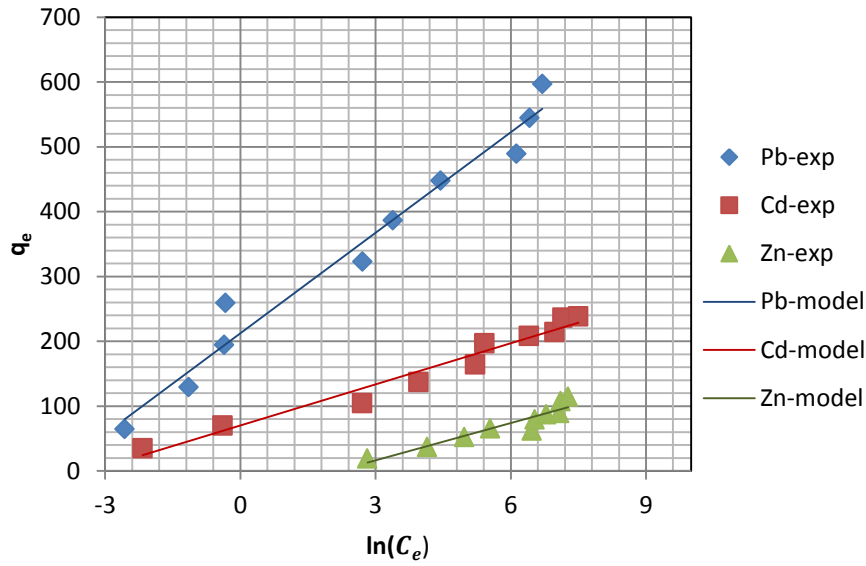


Figure 5.4. Temkin equilibrium isotherm model for Pb^{2+} - NaX, Cd^{2+} - NaX and Zn^{2+} -NaX binary exchange on Zeolite13X beads.

Table 5.5. Temkin Isotherm Constants

Metal ions	K_T (L/g)	B_T (J/mol)	R^2
Pb^{2+}	60.64	51.71	0.970
Cd^{2+}	27.42	21.16	0.962
Zn^{2+}	0.118	19.12	0.885

Redlich-Peterson Isotherm

By using the plot between C_e/q_e versus C_e^β and using Equation (2.22) the Redlich–Peterson isotherm constants could be estimated.

To predict three unknown isotherm parameters α_{RP} , K_{RP} and β , a method is used to expand the linear coefficient of determination R^2 and minimize the variance between q_e estimated from the linear form of Redlich–Peterson equation and experimentally

calculated q_e values. The Redlich–Peterson isotherm parameters predicted are given in Table 5.6. Examination of the Figure 5.5 demonstrated that the Redlich-Peterson isotherm correctly explained Pb^{2+} - NaX, Cd^{2+} - NaX and Zn^{2+} -NaX binary exchange on Zeolite13X beads over the concentration ranges studied.

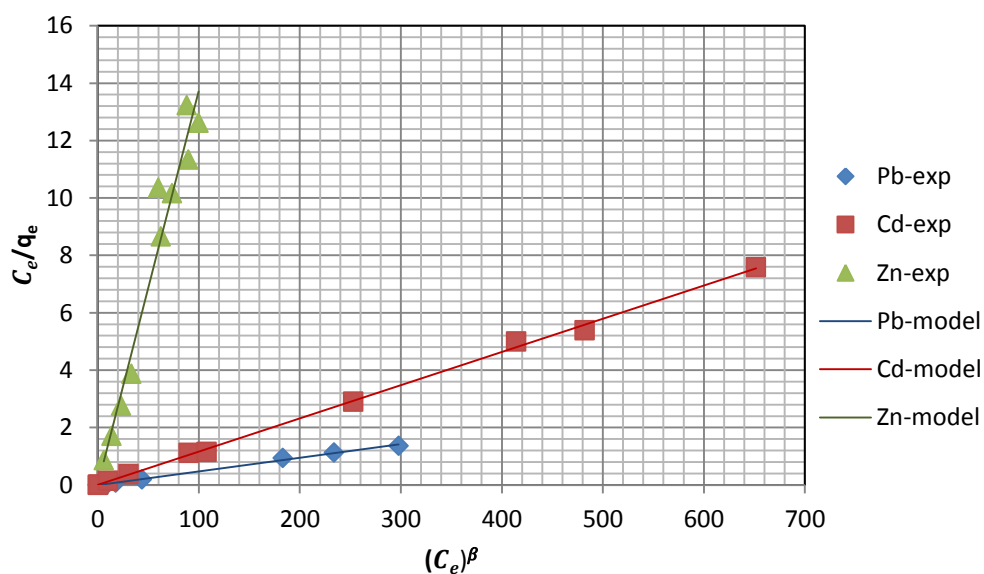


Figure 5.5. Redlich-Peterson equilibrium isotherm model for Pb^{2+} - NaX, Cd^{2+} - NaX and Zn^{2+} -NaX binary exchange on Zeolite13X beads.

Because the linear coefficient of determination values were maximized in the method used to develop the Redlich-Peterson isotherm parameters, it was not unexpected that the Redlich-Peterson isotherms presented very high R^2 values showing, that it generated a significantly superior fit in contrast with the preceding parameter isotherms.

Table 5.6. Redlich-Peterson Isotherm Constants

Metal ions	K_{RP} (L/g)	α_{RP} (L/mmol)	β	R^2
Pb ²⁺	1000.00	4.70	0.850	0.9997
Cd ²⁺	555.55	6.55	0.864	0.9986
Zn ²⁺	208.33	28.58	0.633	0.9569

BET Isotherm

Equation (2.29) which is the linear form of BET isotherm equation was used for the determination of BET isotherm constants. From the linear plots of $C_e/(q_e(C_o - C_e))$ versus C_e/C_o shown in Figure 5.6, BET isotherm constants were calculated and given in Table 5.7.

BET isotherm constant, C_{BET} , characterizes the binding of a molecule to the surface. It has exactly the same meaning as the constant Q_M in Langmuir's equation.

Table 5.7 shows that C_{BET} values were greater than 500 for Pb²⁺, Cd²⁺ indicating that ion exchange is the mechanism, C_{BET} value less than 20 for Zn²⁺ indicating physisorption. Linear coefficient of determination R^2 values more than 0.9092 showing that BET isotherm model also competent with the experimental values.

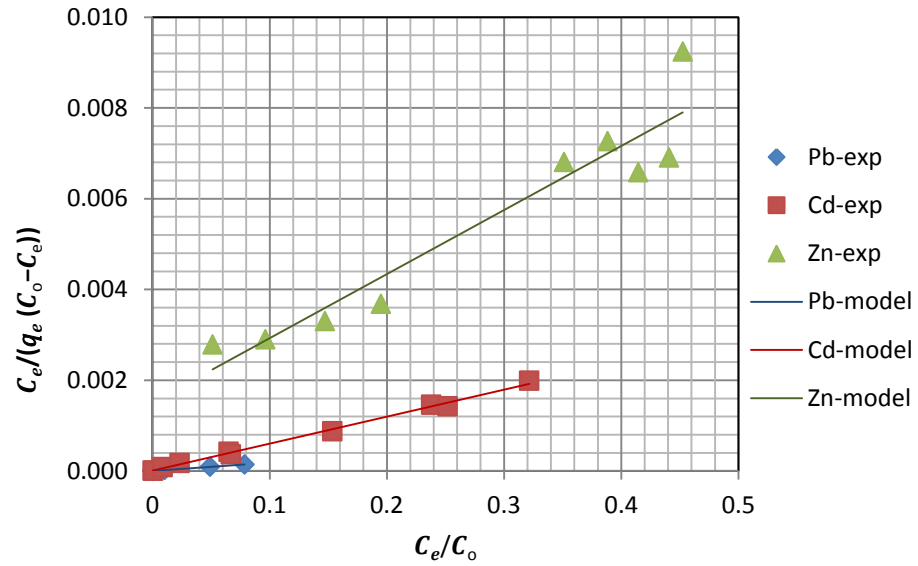


Figure 5.6. BET equilibrium isotherm model for Pb^{2+} - NaX, Cd^{2+} - NaX and Zn^{2+} - NaX binary exchange on Zeolite13X beads.

Table 5.7. BET Isotherm Constants

Metal ions	Q_s	C_{BET}	R^2
Pb^{2+}	555.25	1801	0.9995
Cd^{2+}	166.48	858.10	0.9959
Zn^{2+}	64.10	10.40	0.9092

SIPS Isotherm

From the linear plots of $\ln(K_{LF}/q_e)$ against $\ln C_e$ shown in Figure 5.7, SIPS isotherm constants are calculated.

The Sips model was also found to be well adapted to explain the Pb^{2+} - NaX, Cd^{2+} - NaX and Zn^{2+} -NaX binary exchange on Zeolite13X beads because of high linear coefficient of determination R^2 values (Table 5.8).

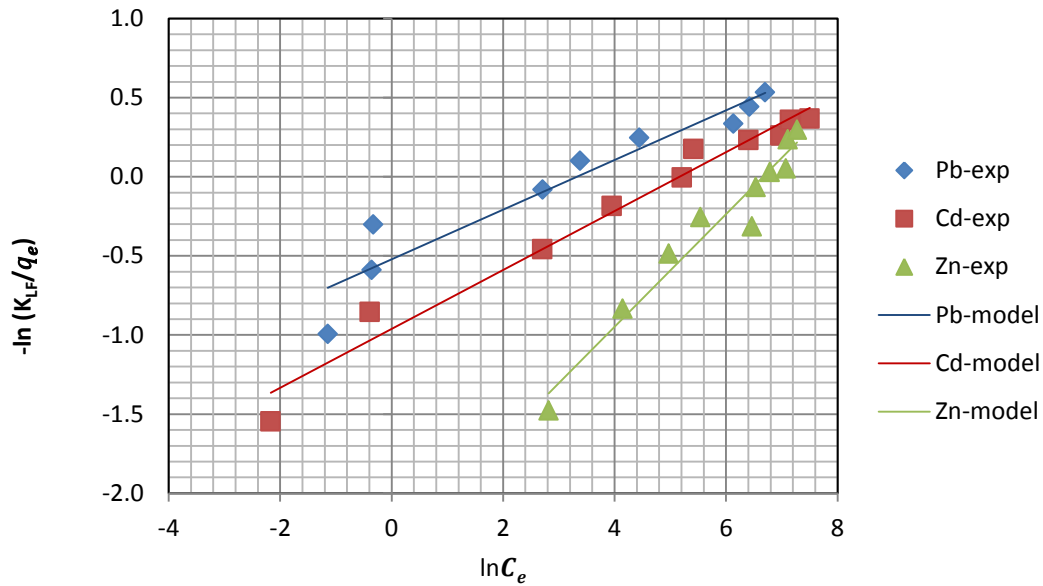


Figure 5.7. SIPS equilibrium isotherm model Pb^{2+} - NaX, Cd^{2+} - NaX and Zn^{2+} -NaX binary exchange on Zeolite13X beads.

Table 5.8. SIPS Isotherm Constants

Metal ions	K_{LF} (L/g)	b_{LF} (L/mmol)	$1/n$	R^2
Pb^{2+}	350	1.69	0.157	0.9106
Cd^{2+}	167	2.64	0.186	0.9731
Zn^{2+}	85	10.70	0.336	0.9500

Pb^{2+} - NaX, Cd^{2+} - NaX and Zn^{2+} -NaX binary ion exchange on to Zeolite 13X beads was modelled by utilizing the Langmuir, Freundlich, Langmuir, Temkin, Dubinin–Radushkevich (DR), Redlich Peterson, BET and SIPS isotherms with the quality of the fit determined utilizing the linear coefficient of determination (R^2). (R^2) data for the seven models which were presented in Table 5.9 demonstrates that all the models, except DR, were appropriate in explaining the experimental data ($R^2 > 0.90$) with the Redlich Peterson being more suitable.

Redlich Peterson model produced the lowest average relative error (ARE) whereas SIPS model produced the highest ARE value for all metals (Table 5.10). For the cadmium ion Freundlich model produced the lowest ARE value.

Table 5.9. Isotherm Linear Coefficient of Determination (R^2) Values

Isotherms	Metal ions		
	Pb ²⁺	Cd ²⁺	Zn ²⁺
Langmuir	0.956	0.914	0.958
Freundlich	0.946	0.973	0.950
DR	0.786	0.712	0.657
Temkin	0.970	0.962	0.885
Redlich Peterson	0.9997	0.9986	0.9569
BET	0.9995	0.9959	0.9092
SIPS	0.9106	0.9731	0.9500

Table 5.10. Isotherm ARE Values

Isotherms	Metal ions		
	Pb ²⁺	Cd ²⁺	Zn ²⁺
Langmuir	0.189	0.270	0.140
Freundlich	0.272	0.062	0.105
DR	0.235	0.354	0.269
Temkin	0.193	0.105	0.113
Redlich Peterson	0.121	0.065	0.096
BET	0.178	0.135	0.143
SIPS	0.530	0.596	0.595

5.3.2.2. Multi component Ion Exchange Isotherm Studies

The Modified Langmuir Model, Jain and Snoeyink Model, SRS Model, Extended SIPS Model and IAST Model were utilized to match up to the experimental data; but only SRS Isotherm Model was observed to match up to the experimental data with high linear coefficient of determination values ($R^2 > 0.96$).

The single component ion exchange isotherms, that can be explained with the Freundlich model, were of the L-curve type (Figures 5.8, 5.9 and 5.10) which signifies comparatively great resemblance of Zeolite 13X at low cation concentrations. While the surface coverage with the Zeolite 13X increases affinity decreases (Antoniadis and Tsadilas, 2007). Lead isotherms were of the L-curve type both in binary and ternary systems, indicating that sorption/ion exchange mechanism did not change under competition (Figure 5.8). There were insignificant dissimilarities among mono component and competitive ion exchange at low lead ion concentration, however at high concentrations, decrease in metal ion exchange was observed. Cadmium and zinc isotherms were not L-curve type in ternary systems, resulting that the ion exchange/sorption mechanism changed under competition (Figures 5.9 and 5.10). Decrease in metal sorption was observed as a result of competition at low cadmium and zinc ion concentrations. At high metal concentrations, no significant differences between mono component and competitive ion exchange was observed.

The multicomponent SRS isotherm model coefficients can be found out from the single component isotherm apart from the ion exchange/sorption competition coefficients, a_{ij} , which must be found out empirically. The competition coefficients a_{ij} explain the hindrance to the sorption of component i by component j.

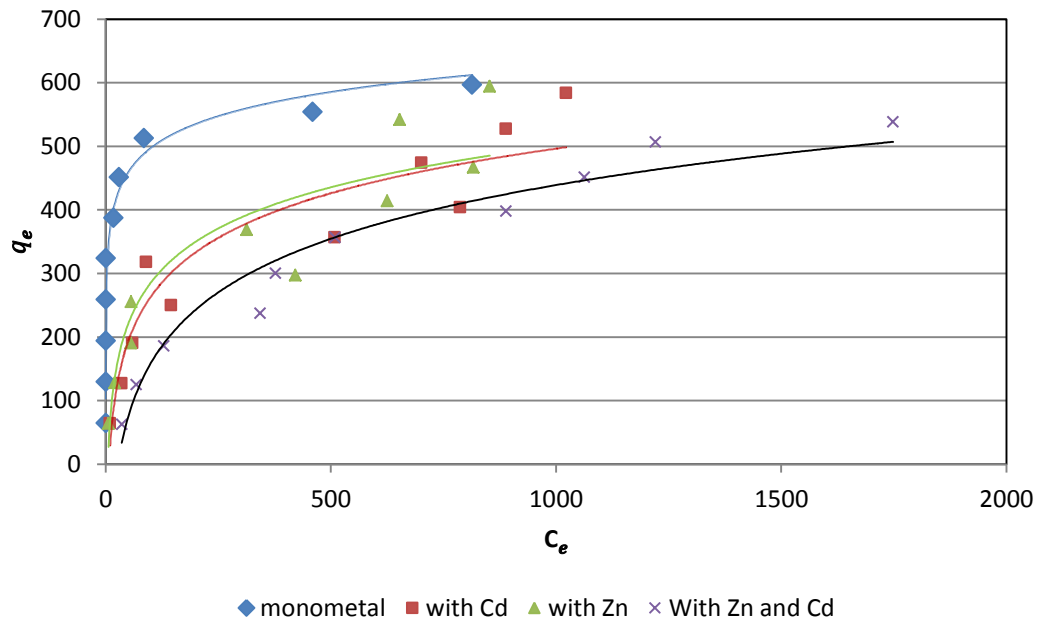


Figure 5.8. Lead ion exchange isotherms in single and multicomponent systems.

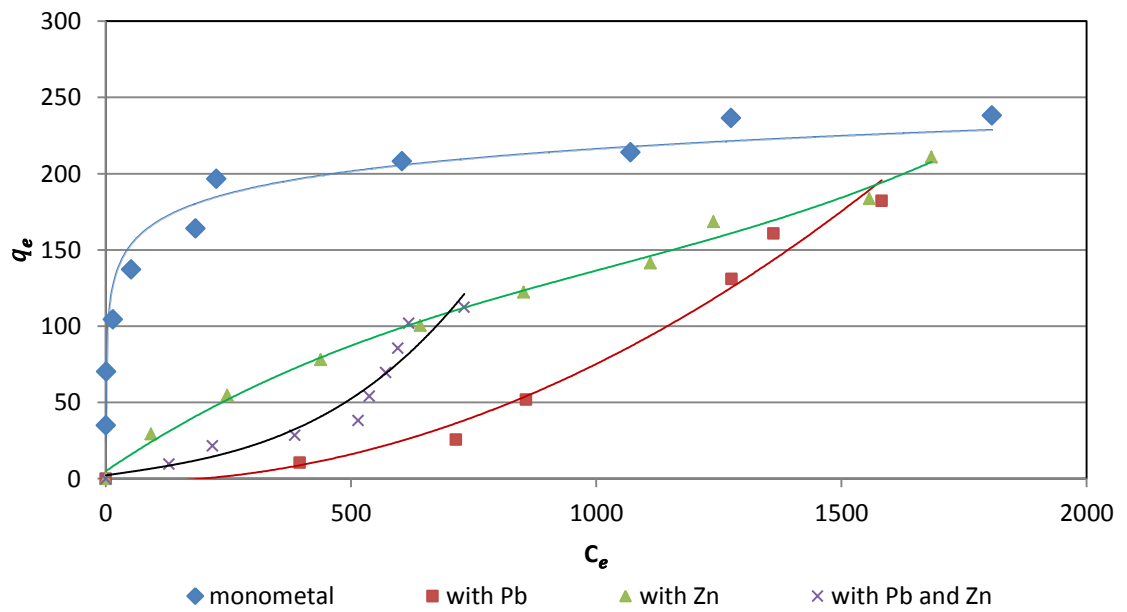


Figure 5.9. Cadmium ion exchange isotherms in single and multicomponent systems.

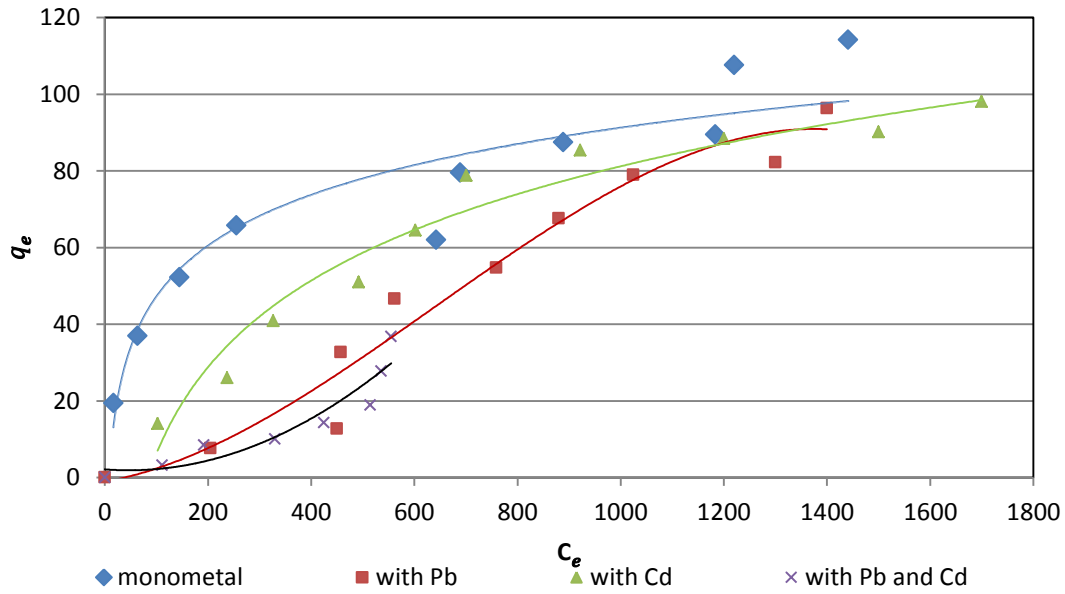


Figure 5.10. Zinc ion exchange isotherms in single and multicomponent systems.

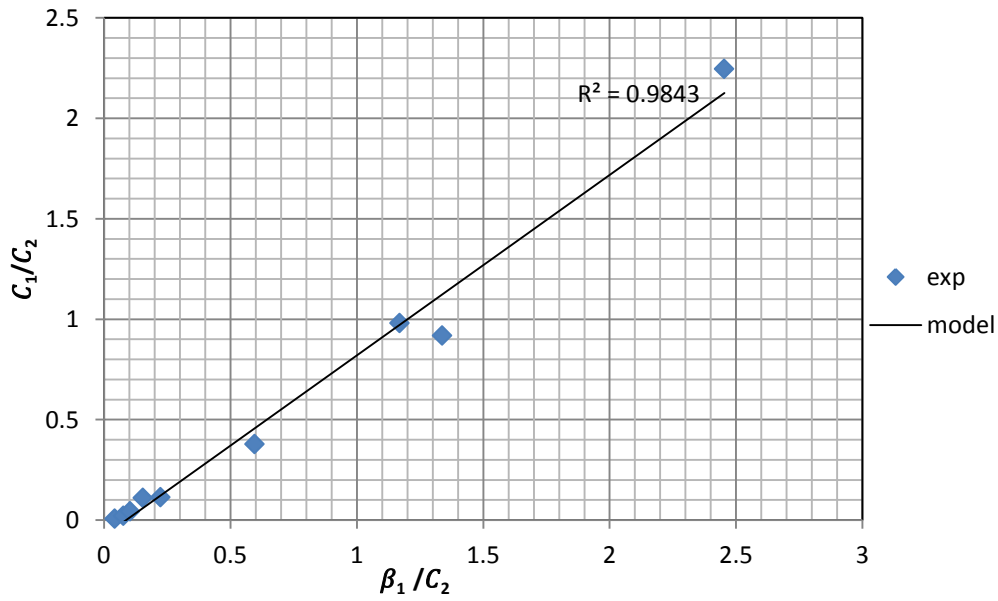


Figure 5.11. Linear form of the SRS multicomponent isotherm, Pb^{2+} in the existence of Cd^{2+}

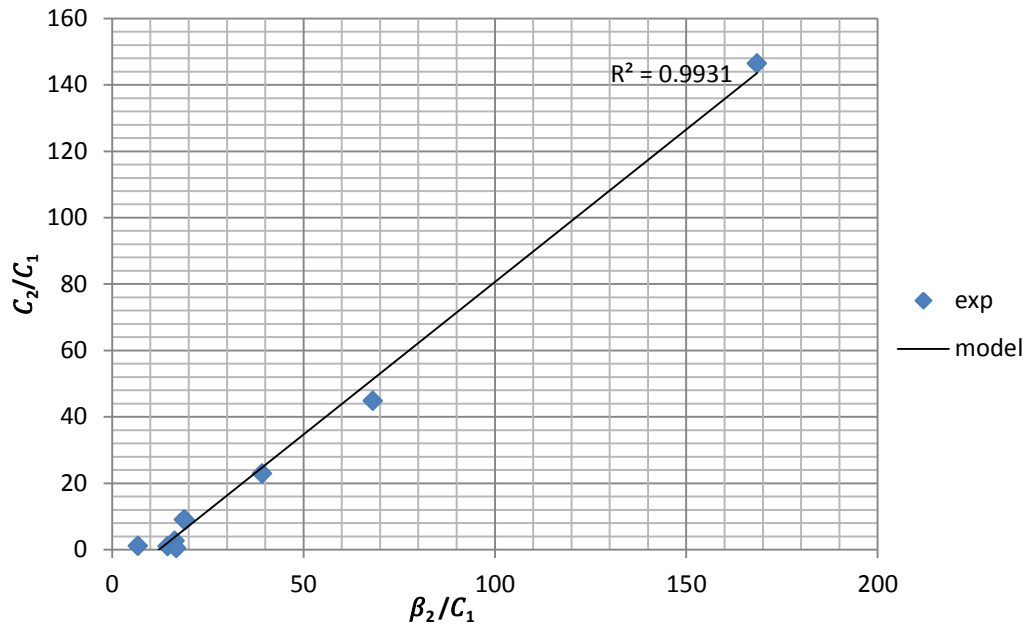


Figure 5.12. Linear form of the SRS multicomponent isotherm, Cd^{2+} in the existence of Pb^{2+}

The slopes of Figure 5.11 and Figure 5.12 are close to unit and the competition coefficients were $a_{12} = 0.0789$ and $a_{21} = 11.243$ (compared to $1/a_{12} = 12.674$)

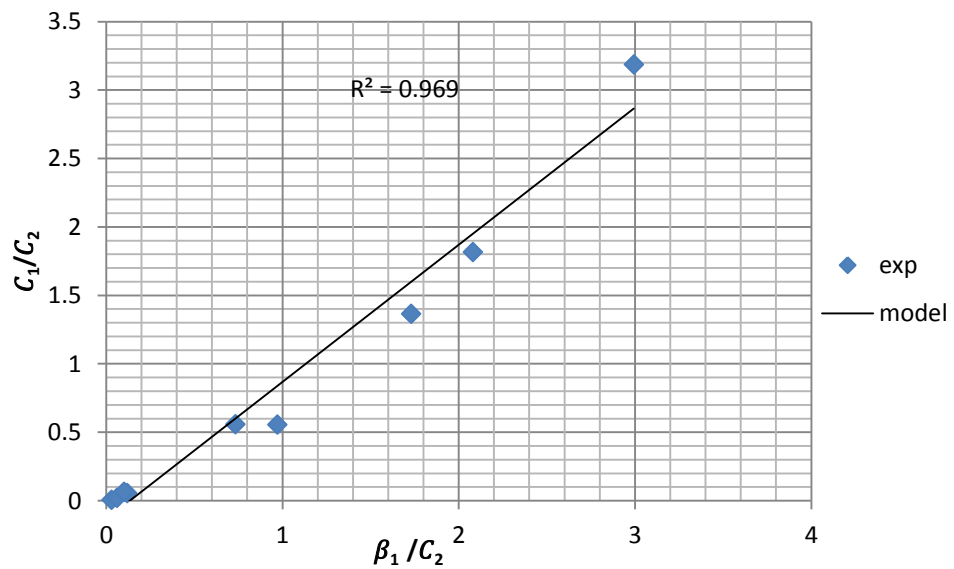


Figure 5.13. Linear form of the SRS multicomponent isotherm, Pb^{2+} in the existence of Zn^{2+} .

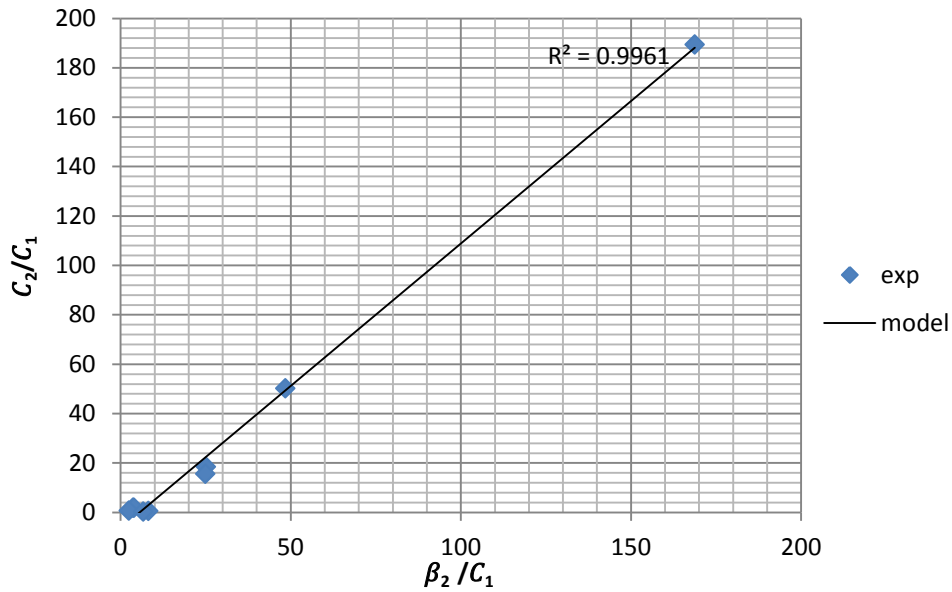


Figure 5.14. Linear form of the SRS multicomponent isotherm, Zn^{2+} in the existence of Pb^{2+} .

The slopes of Figure 5.13 and Figure 5.14 are close to unit and the competition coefficients were $a_{13} = 0.135$ and $a_{31} = 7.39$ (compared to $1/a_{13} = 7.5$)

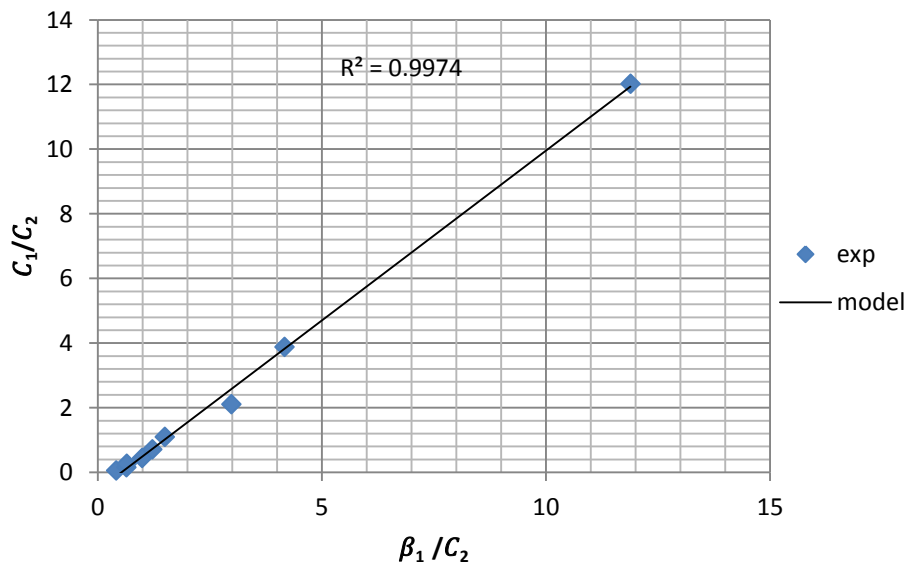


Figure 5.15. Linear form of the SRS multicomponent isotherm, Zn^{2+} in the existence of Cd^{2+} .

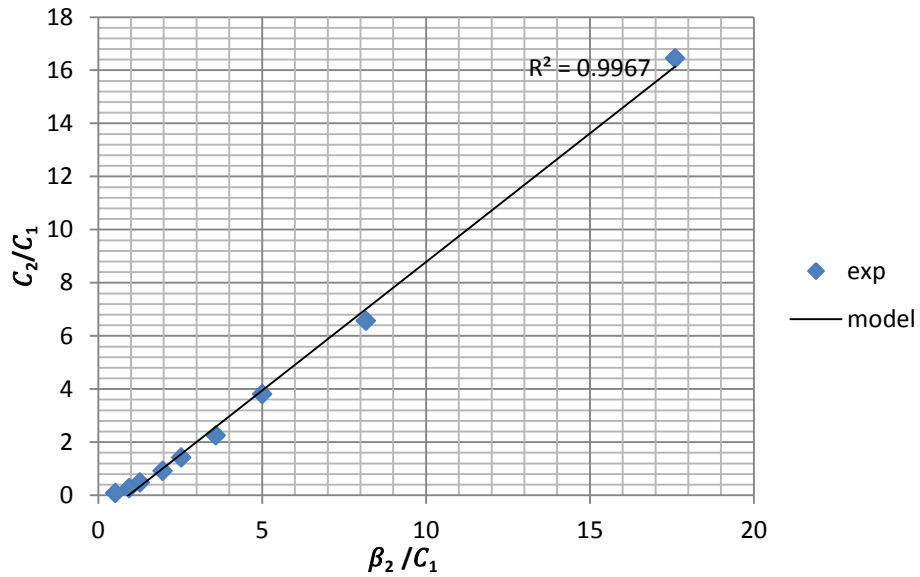


Figure 5.16. Linear form of the SRS multicomponent isotherm, Cd^{2+} in the existence of Zn^{2+} .

The slopes of Figure 5.15 and Figure 5.16 are close to unit and the competition coefficients were $a_{23} = 0.55$ and $a_{32} = 1.81$

Competition coefficients for binary systems were given in Table. 5.11. Lead a_{ij} values were less than 0.2, indicating that it was very moderately influenced by the metal competition. Cadmium a_{ij} value was in all cases greater than one, confirming that a significant decline in sorption while it competed with lead or zinc. Zinc a_{ij} was less than one while it competed with cadmium, signifying that it was moderately influenced by competitive action in the existence of cadmium. Zinc a_{ij} was greater than one when in competition with lead. It showed a powerful decline in sorption while it competed with lead.

Table 5.11 Competition coefficients a_{ij} for Pb^{2+} - NaX, Cd^{2+} - NaX and Zn^{2+} -NaX binary ion exchange on to Zeolite 13X beads.

Metal ion	In the Existence of Pb^{2+}	In the Existence of Cd^{2+}	In the Existence of Zn^{2+}
Pb^{2+}	---	0.079	0.135
Cd^{2+}	11.20	---	1.80
Zn^{2+}	7.40	0.55	---

In accordance with the SRS Model

$$a_{12} \times a_{23} \times a_{31} = 1$$

and the product of experimental competition coefficients was calculated as 1.052 (Appendix P).

There was great consensus of the experimental data with the proposed isotherm since the product of the competition coefficients was close to unity for Pb^{2+} - Cd^{2+} - Zn^{2+} -NaX exchange on Zeolite13X beads. Each cation ion exchange on Zeolite 13X beads in this ternary system was presented like the following:

$$q_{Pb} = 235.56C_{Pb}(C_{Pb} + 0.079C_{Cd} + 0.135C_{Zn})^{-0.87}$$

$$q_{Cd} = 63.12C_{Cd}(C_{Cd} + 11.2C_{Pb} + 1.8C_{Zn})^{-0.81}$$

$$q_{Zn} = 7.94C_{Zn}(C_{Zn} + 7.4C_{Pb} + 0.55C_{Cd})^{-0.64}$$

The summary of monometal and multicomponent SRS Equations are given in Table 5.12. The multicomponent SRS equation predicted adequately the competing ion exchange behavior of all three metals at the concentration range studied.

Table 5.12. Single (Freundlich) and multicomponent SRS Equations

System	SRS Equations
Pb	$q_{Pb} = 235.6C_{Pb}^{0.13}$
Cd	$q_{Cd} = 63.1C_{Cd}^{0.19}$
Zn	$q_{Zn} = 7.9C_{Zn}^{0.36}$
Pb in the existence of Cd	$q_{Pb} = 235.6C_{Pb}(C_{Pb} + 0.079C_{Cd})^{-0.87}$
Pb in the existence of Zn	$q_{Pb} = 235.6C_{Pb}(C_{Pb} + 0.135C_{Zn})^{-0.87}$
Cd in the existence of Pb	$q_{Cd} = 63.1C_{Cd}(11.2C_{Pb} + C_{Cd})^{-0.81}$
Cd in the existence of Zn	$q_{Cd} = 63.1C_{Cd}(1.8C_{Zn} + C_{Cd})^{-0.81}$
Zn in the existence of Pb	$q_{Zn} = 7.9C_{Zn}(7.4C_{Pb} + C_{Zn})^{-0.64}$
Zn in the existence of Cd	$q_{Zn} = 7.9C_{Zn}(C_{Zn} + 0.55C_{Cd})^{-0.64}$
Pb in the existence of Cd&Zn	$q_{Pb} = 235.6C_{Pb}(C_{Pb} + 0.079C_{Cd} + 0.15C_{Zn})^{-0.87}$
Cd in the existence of Pb&Zn	$q_{Cd} = 63.1C_{Cd}(11.2C_{Pb} + C_{Cd} + 1.8C_{Zn})^{-0.81}$
Zn in the existence of Pb&Cd	$q_{Zn} = 7.9C_{Zn}(7.4C_{Pb} + C_{Zn} + 0.55C_{Cd})^{-0.64}$

5.3.3. Batch Kinetic Experiments

Figure 5.17 showed that Pb^{2+} -NaX, Cd^{2+} -NaX and Zn^{2+} -NaX binary ion exchange on Zeolite 13X beads rate raises with time and it remains fixed at 500 min. For examining the rate limiting step like mass transfer and chemical reaction ion exchange process, an appropriate model is required to evaluate experimental data. Numerous models have been implemented to batch systems for expressing the diffusion of metals within the zeolites. The fit among experimentally calculated and estimated values was described by non-linear Chi-square test (X^2) and linear coefficient of determination (R^2).

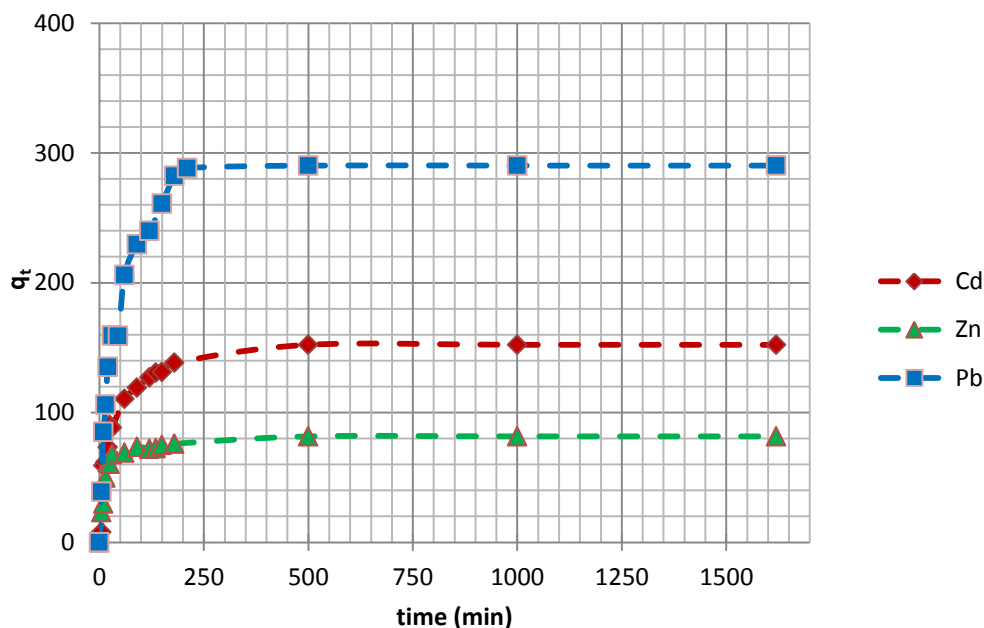


Figure 5.17. Ion exchange kinetics of Pb^{2+} - NaX, Cd^{2+} - NaX and Zn^{2+} -NaX binary ion exchange on Zeolite 13X beads at 25°C

5.3.3.1. Pseudo-first order equation or Lagergren's kinetics equation

Lagergren first order kinetic model can be used to describe the batch system kinetics. Linear form of this model was shown on Figure 5.18 for Pb^{2+} -NaX, Cd^{2+} -NaX and Zn^{2+} -NaX binary ion exchange on Zeolite 13X beads. The pseudo first order constants k_1 and q_e are found out from the slope and intercept of $\log(q_e - q_t)$ versus t plot. According to R^2 and X^2 values which were given in Table 5.13, Lagergren first order kinetic model provided good fitting to the experiments for Pb^{2+} -NaX, Cd^{2+} -NaX binary exchange but not for Zn^{2+} -NaX binary exchange.

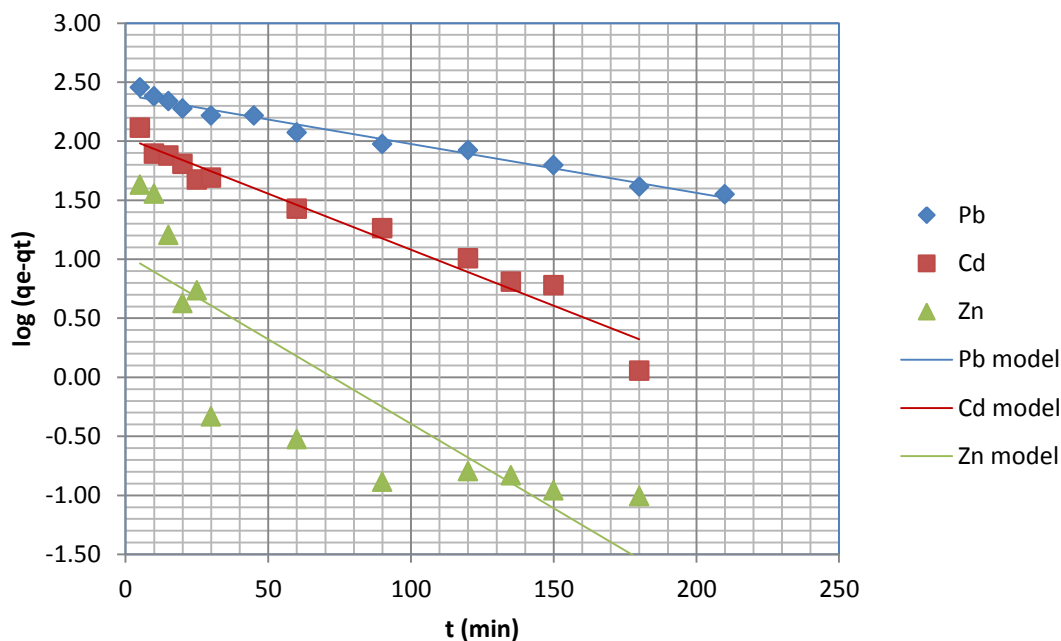


Figure 5.18. First order kinetic model

5.3.3.2. Pseudo second order kinetics equation

The pseudo second order rate constants k_2 and q_e were found out from the slope and intercept of (t/q_t) versus t (Figure 5.19). R^2 and X^2 values are given in Table 5.13. R^2 values obtained were higher than 0.998 for all metals. X^2 values obtained were smaller than 4.32 indicating that q_e values determined from this model fit adequately with the experimental values. When in comparison with pseudo first order kinetic model, pseudo second order kinetic model describes the kinetic data more fitting than the pseudo first order model.

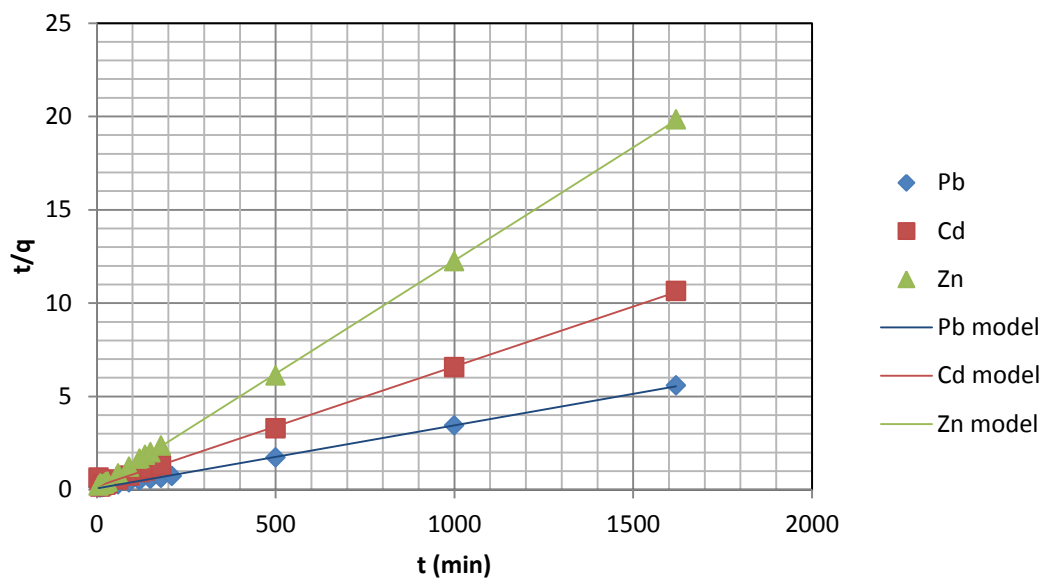


Figure 5.19. Pseudo second order kinetic model

Table 5.13. Pseudo first order and second order kinetic model constants

Metal	Pseudo-first order					Pseudo second order			
	$q_{e,exp}$	$k_1 \times 10^3$	$q_{e,cal}$	R^2	X^2	$k_2 \times 10^4$	$q_{e,cal}$	R^2	X^2
Pb ²⁺	323.7	9.4	245.5	0.98	18.8	1.5	294.1	0.99	2.70
Cd ²⁺	137.3	21.9	107.1	0.96	6.6	2.2	156.2	0.99	2.63
Zn ²⁺	65.8	3.3	107.1	0.73	45.8	10.1	82.6	0.99	4.32

5.3.3.3. Intraparticle diffusion equation

Plot of q_t versus $t^{0.5}$ presented multilinearity, revealing that two or more steps occurs (Figure 5.20). The first straight sharper region indicated external surface or boundary layer diffusion (macropore diffusion). The second region indicated intraparticle or micropore diffusion. The third region was the final equilibrium region.

According to W&M Model, the second region of Figure 5.20 were found to be linear with a slope k_i and intercept C which confirmed that the ion exchange kinetics took after the intra-particle diffusion process. The second portion of Figure 5.20 did not pass through origin. If the intra-particle diffusion process was the rate limiting step, then plots should have passed through origin. In addition, it is known that the values of C indicates the dimension of the boundary layer; boundary layer effect is directly proportional to the intercept value (Rajoriya et al, 2007). These additionally showed that the intra-particle diffusion was not the sole rate controlling mechanism, yet different kinetic models might have control the rate too. The values of intraparticle diffusion rate parameters were shown in Table 5.14.

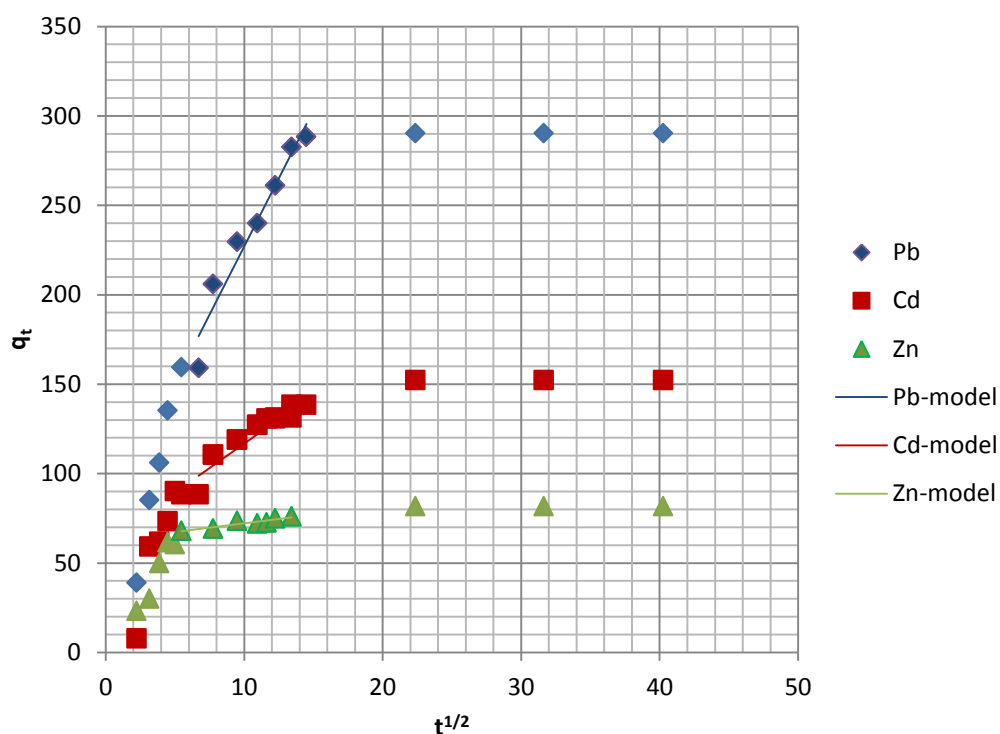


Figure 5.20. W&M diffusion model

In accordance with the U&T equation, the slope of a plots of $f(q/q_m)$ versus t gives the diffusion coefficient D_i for all metals.

U&T model was distinguished by an inadequate match up to experimental results compared with W&M Model especially in the case of lead and cadmium ion exchange on Zeolite 13X (Table 5.14). Considering the U&T model does not acknowledge external mass transfer resistance, it seems insufficient for the process.

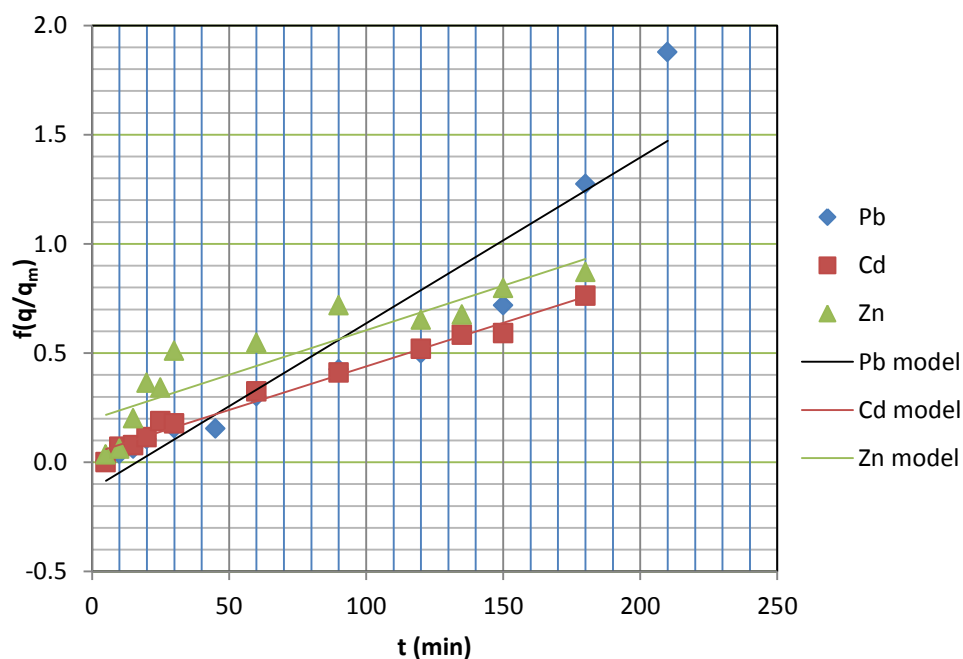


Figure 5.21. U&T Intraparticle diffusion model

Table 5.14. Intraparticle Diffusion Model Constants

Metal Ions	W&M Model			U&T Model	
	$k_i \times 10^3$ ($mg/g \cdot min^{-0.5}$)	C (mg/g)	R^2	$D_i \times 10^3$ (min^{-1})	R^2
Pb ²⁺	15.26	74.5	0.9465	7.6	0.8921
Cd ²⁺	6.04	59.6	0.9688	4.0	0.9838
Zn ²⁺	0.98	62.4	0.8626	4.1	0.8921

5.3.3.4. Elovich Kinetic Model

According to Equation (2.55) and Figure 5.22 Elovich Kinetic Model constants were calculated and given in Table 5.15. α constants for Pb^{2+} -NaX, Cd^{2+} -NaX and Zn^{2+} -NaX binary ion exchange on Zeolite 13X beads were 0.015, 0.031 and 0.073 (mg/gmin) respectively. β constants for Pb^{2+} -NaX, Cd^{2+} -NaX and Zn^{2+} -NaX binary exchange were 3.6, 71.5 and 28.42 (g/mg) respectively.

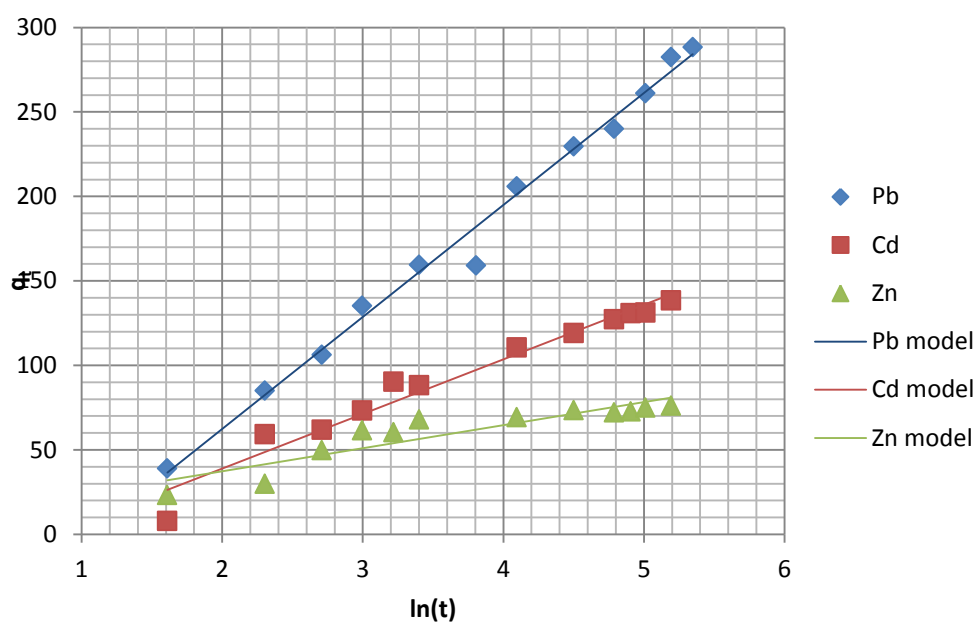


Figure 5.22. Elovich kinetic model

Table 5.15. Elovich Kinetic Model Constants

Metal Ions	β $\left(\frac{g}{mg} \cdot min\right)$	α $\left(\frac{g}{mg}\right)$	R^2
Pb^{2+}	0.015	3.6	0.98
Cd^{2+}	0.031	71.5	0.96
Zn^{2+}	0.073	28.42	0.83

5.3.3.5. Pore Diffusion Bangham's Kinetic Model

Plots of $\log \log \left(\frac{C_0}{C_0 - q_t m} \right)$ versus $\log t$ ($R^2 = 0.85$ to 0.99) gave straight lines for at 25°C (Figure 5.23) which confirms that Pb^{2+} -NaX, Cd^{2+} -NaX and Zn^{2+} -NaX binary exchange is pore-diffusion controlled.

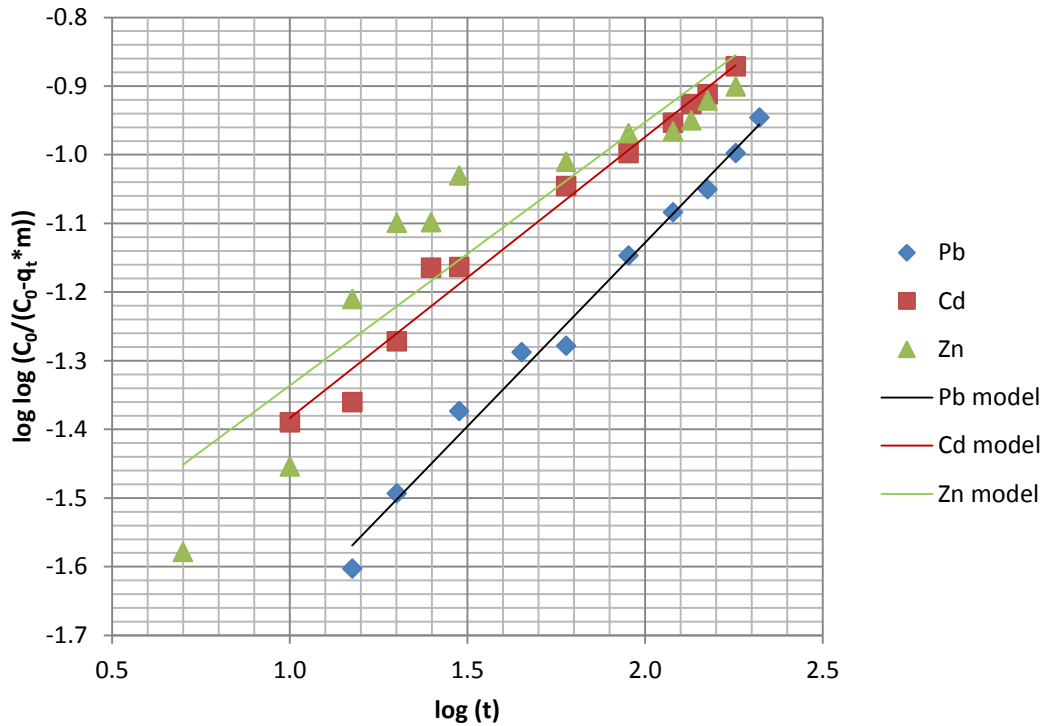


Figure 5.23 Bangham kinetic model

Table 5.16. Bangham Kinetic Model Constants

Metal Ions	$k_0 \left(\frac{ml}{g/L} \right)$	α (min^{-1})	R^2
Pb^{2+}	1.14	0.54	0.9896
Cd^{2+}	2.90	0.41	0.9797
Zn^{2+}	3.43	0.38	0.8450

5.3.3.6. Modified Freundlich Kinetic Model

According to Equation (2.58) and Figure 5.24 Freundlich constants were calculated and given in Table 5.17. This model fits the experimental data favorably for Pb^{2+} -NaX, Cd^{2+} -NaX binary exchange but not for Zn^{2+} -NaX binary exchange.

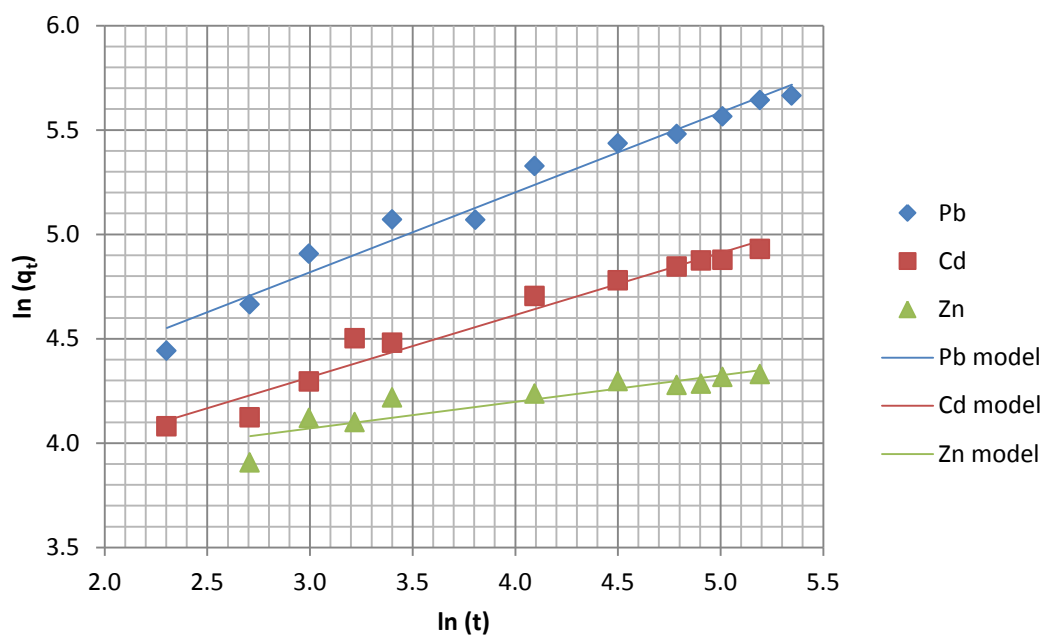


Figure 5.24. Modified Freundlich Kinetic Model

Table 5.17. Modified Freundlich Kinetic Model Constants

Metal Ions	$k_F \left(\frac{L}{g \cdot min} \right)$	$1/m$	R^2
Pb^{2+}	39.25	0.38	0.9896
Cd^{2+}	30.63	0.30	0.9797
Zn^{2+}	40.03	0.13	0.8450

5.3.3.7. External Mass Transfer Diffusion Model

External Mass Transfer Diffusion Model was described by an inadequate match up to experimental results for Cd^{2+} - NaX and Zn^{2+} - NaX binary exchange with β_L values of 1.6×10^{-6} and 1.2×10^{-6} $((g/cm^2)min^{-1})$ respectively (Table 5.18). External mass transfer diffusion model fitted well to the Pb^{2+} - NaX binary exchange experimental data and external film mass transfer coefficient was found as 1.3×10^{-6} $((g/cm^2)min^{-1})$.

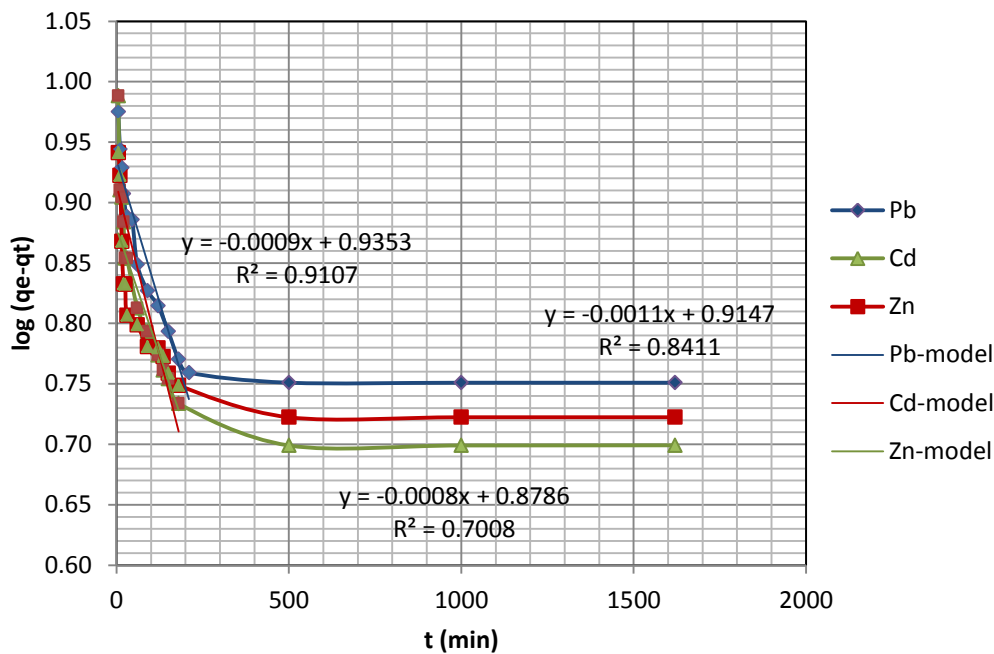


Figure 5.25 External Mass Transfer Diffusion Model

Table 5.18. External Diffusion Model Constants

Metal Ions	$\beta_L S \times 10^4$ (min^{-1})	$\beta_L \times 10^6$ ($\frac{g}{cm^2} \cdot min^{-1}$)	R^2
Pb^{2+}	9	1.3	0.9107
Cd^{2+}	11	1.6	0.8410
Zn^{2+}	8	1.2	0.7008

5.3.4. Thermodynamic Calculations

The distribution coefficient K_0 at constant temperature was determined by plotting $\ln(q_e/C_e)$ against q_e (Figure 5.26) and extrapolating q_e to zero.

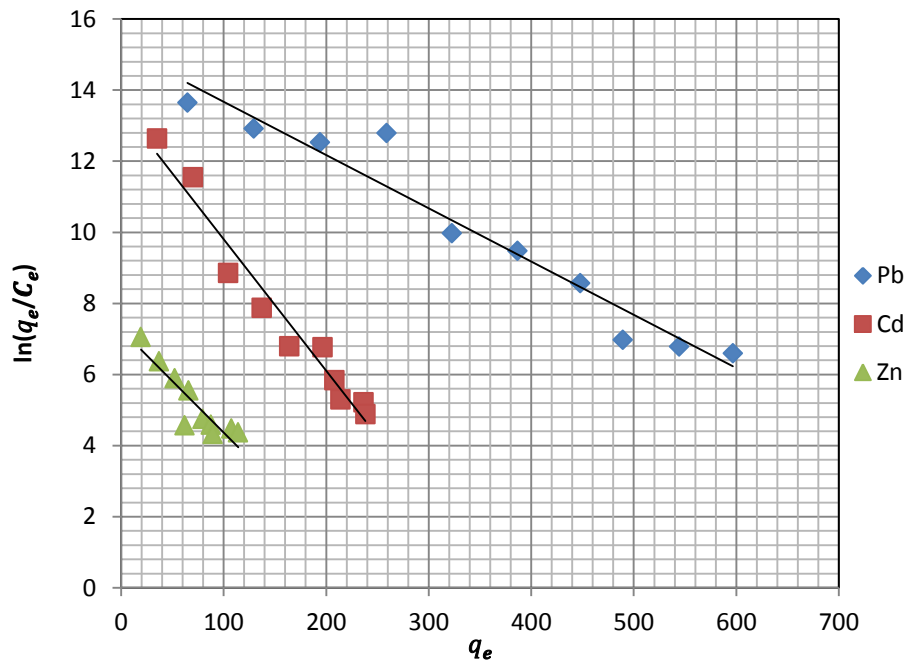


Figure 5.26. Plot of $\ln(q_e/C_e)$ versus q_e

The distribution coefficient, K_0 , decreased in the order: $\text{Pb}^{2+} > \text{Cd}^{2+} > \text{Zn}^{2+}$ (Table 5.19). This order signifies the higher inclination of Zn^{2+} for remaining in solution when compared with the other two metals. In case of ionic radius of the metals are concerned, metals of lower ionic radius would occupy the exchange sites more rapidly and this would cause that the selectivity for ion exchange decreased in the order: $\text{Zn}^{2+} = 0.70\text{\AA} > \text{Cd}^{2+} = 0.97\text{\AA} > \text{Pb}^{2+} = 1.30\text{\AA}$. This also indicates that ion exchange was not completely electrostatic. Metals which are able to form hydroxy bonds with zeolite surfaces may be particularly sorbed. If the pK value of the metal hydrolysis reaction ($M^{2+} + H_2O = MOH^+ + H$) is lower then the metal specific sorption would be stronger (Grzybowski, 2006). If specific metal sorption was prevalent, the ion exchange sequence, would be: $\text{Pb}^{2+} > \text{Zn}^{2+} > \text{Cd}^{2+}$, in

consideration of the pK values of the first hydrolysis products at 25°C which are Pb²⁺ (8.0), Zn²⁺ (9.0) and Cd²⁺ (10.1).

The standard Gibbs free energy ΔG (kJ/mol) determined from Equation (2.6.4) was given in Table 5.19. As expected, ΔG values calculated were negative for Pb²⁺ - NaX, Cd²⁺ - NaX and Zn²⁺ - NaX binary exchange on Zeolite 13X beads.

Table 5.19. Thermodynamic parameters for Pb²⁺ - NaX, Cd²⁺ - NaX and Zn²⁺ - NaX binary exchange on Zeolite 13X beads

Metal ion	K ₀ (L/g)	ΔG (kJ/mol)
Pb ²⁺	15.2	-6.742
Cd ²⁺	13.5	-6.455
Zn ²⁺	7.3	-4.916

K₀ values were smaller in the multicomponent systems in comparison to the single component systems (Table 5.20). K₀ decrease was much more evident in the quaternary systems which signify that competition between cations increase when accessible ion exchange sites lessen (because the amount of components increase). Nevertheless, decrease in the ion exchange rate for every cation was different. Competition influences Pb²⁺, the most powerfully ion exchanged cation, lower than it influences Cd²⁺ and Zn²⁺. This may be made clear considering the fact that the Zeolite 13X beads retained Pb²⁺ powerfully and in this manner Pb²⁺ competed efficiently with the inadequately retained Cd²⁺ and Zn²⁺.

There may also be different reason for the strong retention of Pb²⁺ by Zeolite 13X beads. This may be related with the reason that Pb, besides being specifically sorbed, may further be influenced by other uneasily reversible retention mechanisms more than Cd²⁺ and Zn²⁺. Pb²⁺ cations may diffuse into zeolite crystals in the Zeolite 13X

beads and produce insoluble compounds (e.g., $\text{Pb}(\text{OH})_2$, which is the second hydrolysis product of Pb^{2+}). These processes are almost irrevocable in the period of the experiment, and can hence generate a considerable amount of the Pb^{2+} to be unaccessible for ion exchange. Hence Zn^{2+} seems to be less influenced by competition than Cd^{2+} that is inadequately exchanged.

Consequently, in this study the distribution coefficient of Pb^{2+} decreased less than Cd^{2+} and Zn^{2+} in multicomponent systems. On the contrary, Zn^{2+} , which was the most inadequately sorbed metal in comparison with Cd^{2+} and Pb^{2+} , as determined by the single component systems, was influenced by competitive action less than Cd^{2+} . Cd^{2+} greatly effected by competitive action. Its K_0 value was decreased by nearly a factor of 2.75 in the quaternary exchange systems in contrast with the binary exchange systems.

Table 5.20. Distribution coefficients K_0 (L/g), of the single and multi component ion exchange of Pb^{2+} , Cd^{2+} and Zn^{2+} on Zeolite 13X.

Metal ion	Monometal system	In the Presence of Zn^{2+}	In the Presence of Cd^{2+}	In the Presence of Pb^{2+}	Quaternary systems
Zn^{2+}	7.3	---	5.1	4.4	3.9
Cd^{2+}	13.5	5.7	---	4.8	4.9
Pb^{2+}	15.2	9.3	8.9	---	7.8

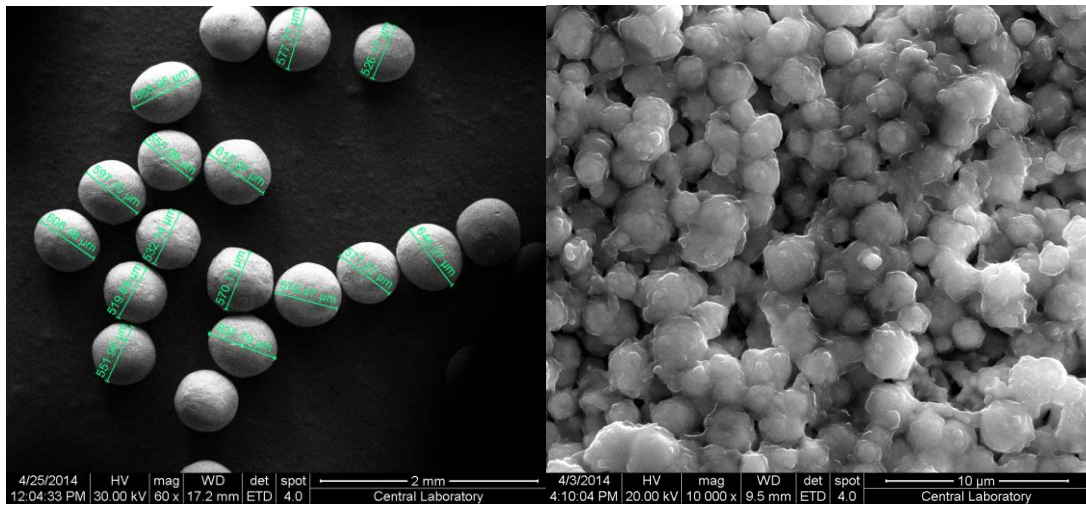
5.4.SEM/EDX analysis

Samples of eight batch systems with different compositions and one dynamic system are selected for SEM image and EDX analysis. The elemental composition of Zeolite 13X beads after metal ion exchange was established by choosing areas on the 13X crystals surfaces and analyzing by Energy Dispersive X-ray (EDX) in combination with SEM (Results are given in Appendix F). EDX results in Appendix F are analyzed in Tables 5.21

SEM images of Zeolite 13X beads indicate that zeolite 13X beads have sizes ranging from 570 to 711 μm (Figure 5.27). These beads consist of 13X crystals having an approximate size range of 2-4 μm . This small Zeolite crystals provides the main capacity for ion exchange. EDX analysis was performed to investigate the ion exchange of Pb^{2+} - Cd^{2+} -NaX; Pb^{2+} - Zn^{2+} -NaX; Zn^{2+} - Cd^{2+} -NaX ternary exchange and Pb^{2+} - Cd^{2+} - Zn^{2+} -NaX quaternary exchange on Zeolite 13X beads.

The EDX spectrum for Zeolite 13X beads implied the existence of Al and Si in the framework structure. Average Si/Al ratio is calculated as 1.3 which is equal to Si/Al ratio reported for Zeolite 13X (Payne and Abdel-Fattah, 2004). The EDX spectrum supplies the characteristic peaks for Pb at 2.0-3.0 and 9.0-12.0 keV; For Cd at 3.0-4.0 keV; for Zn 8.0-10.0 keV which verifies the binding of the metal ions to the zeolite crystals in the Zeolite 13X beads.

Pb^{2+} - Cd^{2+} -NaX dynamic system EDX result indicates that ion exchange capacity of lead on Zeolite 13X higher than that of cadmium (Figure F.18).



(a)

(b)

Figure 5.27. (a) Example of a SEM Image of prepared Zeolite 13X beads (25-30 Mesh sizes), (b) Example of a SEM Image of zeolite crystals in the Zeolite 13X beads (Experiment Run No:MI18 of Tables D.2 and 5.21)

Table 5.21 Summary of the selected batch and dynamic systems and EDX Results in Appendix F

Batch System Run No	[Pb/Cd] _{exp} (g/g) *	[Pb/Cd] _{EDX} (g/g) **	[Pb/Zn] _{exp} (g/g) **	[Pb/Zn] _{EDX} (g/g) *	[Zn/Cd] _{exp} (g/g) **	[Zn/Cd] _{EDX} (g/g) *	[Si/Al] (atomic ratio)
MI2	0.67	0.34	-	-	-	-	1.40
MI8	18.30	18.98	-	-	-	-	1.23
MI12	-	-	37.43	29.70	-	-	-
MI18	-	-	1.30	1.80	-	-	1.21
MI22	-	-	-	-	0.14	0.23	1.16
MI28	-	-	-	-	1.89	1.60	1.45
MI32	1.23	0.5	2.8	1.4	0.44	0.98	1.47
MI38	20.98	16.00	53.44	36.00	0.39	0.45	1.26
Pb ²⁺ -Cd ²⁺ -NaX Dynamic System		14.47	-	-	-	-	1.30

* Calculated from solution composition

** Solid analysis by EDX

5.5. pH Results of the Batch Studies

The presence of such a mixture of strong, weak, and very weak acid groups can take a significant part in the general performance of ion exchange process.

The equilibrium of ion exchange in a batch system is unlike of that in a fixed bed system. In a fixed bed system, ions exchanged by the zeolite are continuously extracted from the system. The equilibrium in the liquid phase corresponding to the initial concentration and the solution pH is inaccurate all along the experiment.

In batch systems the ions exchanged by the zeolite are preserved in solution. Additions of acid and/or basic solutions may be essential to preserve the pH constant. Later, the ionic strength of the liquid phase, and also the interactions between the liquid phase and the zeolite phase can be altered. In this study no acid and/or base solutions were introduced to the system since these additions can destroy some exchange sites, causing ion exchange capacity loss.

The additions of cation nitrate solutions into the Zeolite 13X beads led to complicated pH alterations and the alterations in the initial pH (in the range of 5.0 to 6.0) and equilibrium pH of zeolite/cation salt solutions can be associated with the first and second hydrolysis products and hydrogen uptake by the Zeolite 13X beads.

Figure 5.28 showed the pH values of Cd^{2+} -NaX binary exchange and Cd^{2+} - Pb^{2+} -NaX ternary exchange onto Zeolite 13X beads. The pH value of Cd^{2+} -NaX binary exchange suddenly increased from 5.0-6.0, which was the initial pH value, to 8.0 at low equilibrium liquid concentration, than equilibrium pH value (pH=6.0) is reached. Since pK value for Cd^{2+} (10.1) is higher than pH=8.0, The sudden increase in pH may be due to hydrolysis of metal ions and concurrent sorption of hydrogen ions by Zeolite 13X beads. The pH values of Cd^{2+} - Pb^{2+} -NaX ternary exchange onto Zeolite 13X beads was not changed significantly, and an equilibrium pH value was attained at 5-6.

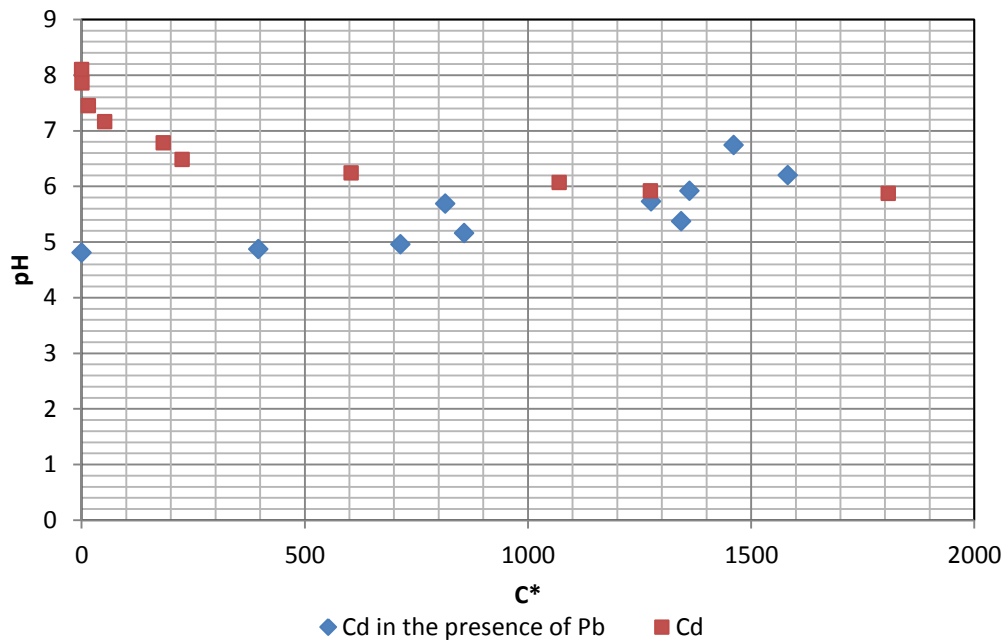


Figure 5.28. Influence of pH on Cd^{2+} -NaX binary exchange and Cd^{2+} - Pb^{2+} -NaX ternary exchange onto Zeolite 13X beads.

Figure 5.29 showed the pH values Zn^{2+} -NaX binary exchange and Zn^{2+} - Pb^{2+} -NaX ternary exchange onto Zeolite 13X beads. The pH value of Zn^{2+} -NaX binary exchange suddenly increased from 4.0-5.0, which was the initial pH value, to 7.0 and equilibrium was reached at this pH value (pH=7.0). This increase in pH value throughout the experiments was because of the concurrent sorption of hydrogen ions by zeolite samples and hydrolysis of metal ions. The pH values of Zn^{2+} - Pb^{2+} -NaX ternary exchange onto Zeolite 13X beads was not changed significantly, and an equilibrium pH value was attained at 5-6.

The solution pH does not affect the ion exchange isotherms since pH values are lower than pK values of all metals.

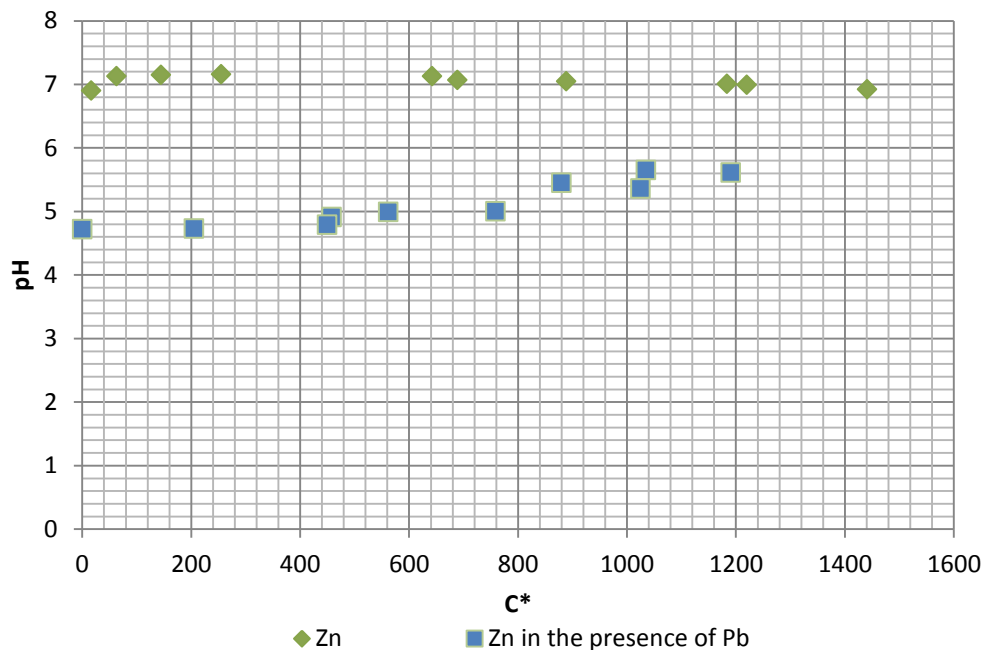


Figure 5.29. Influence of pH on Zn²⁺-NaX binary exchange and Zn²⁺- Pb²⁺-NaX ternary exchange onto Zeolite 13X beads

5.6.Column Studies

In preliminary studies, columns of different sizes (inside diameters (\varnothing) 1.0 / 2.0 /3.2 cm) were tested for binary ion exchange experiments especially for lead and the best efficiency result was obtained with the one which has an inside diameter of 2.0 cm (Table R.1). Thus this column was used in all experiments.

Selection of suitable particle size is an important parameter for ion exchange studies in fixed bed column systems. 8/12 mesh sizes were used for determining the most appropriate particle size in the preliminary study which lead to lower ion exchange capacities. It is known that tiny particle sizes leads to high flow resistance inside the fixed bed. Also, channeling and high pressure drops may take place in fixed bed systems. On the other hand, smaller particle sizes causes greater ion exchange performance. Therefore 20/40 mesh sizes were used in this study. Zeolite 13X samples (25/40 mesh sizes) were sieved again to 20/25, 25/30, 30/35 and 35/40 mesh sizes.

25/30 mesh sizes were used in this study since breakthrough curves obtained were better than the larger bead sizes. (Table O.1, Figure O.1).

In preliminary studies different flow rates were studied (10-30 ml/min). Breakthrough curve obtained with the lowest flow rate was the best ((Table O.2, Figure O.2).

Zeolite 13X beads were stored in a desiccator which contains saturated NaCl solution for several days for ensuring constant moisture content, available for additional use.

5.6.1. Binary Column Studies

The column of 2.0 cm in diameter (\varnothing) was packed with 15.0 g, 25/30 mesh sizes commercial zeolite 13X was used in all binary column experiments. The packed bed height was approximately 5.8 cm. The metal nitrate solutions were introduced at a constant volumetric flow rate of 10 ml/min and concentration of 0.05 N by utilizing a peristaltic pump in up-flow mode.

5.6.1.1 pH Results

The pH change of the solution at the outlet of the column was shown in Figure 5.30. The experimental pH observed varied from 5.6 to 6.4 with an average value of 5.3. Since the feed solution pH was 5.5 and the fluctuations in the pH during the ion exchange experiments were small, it was assumed that the presence of the H⁺ ions in the ion exchange process was insignificant.

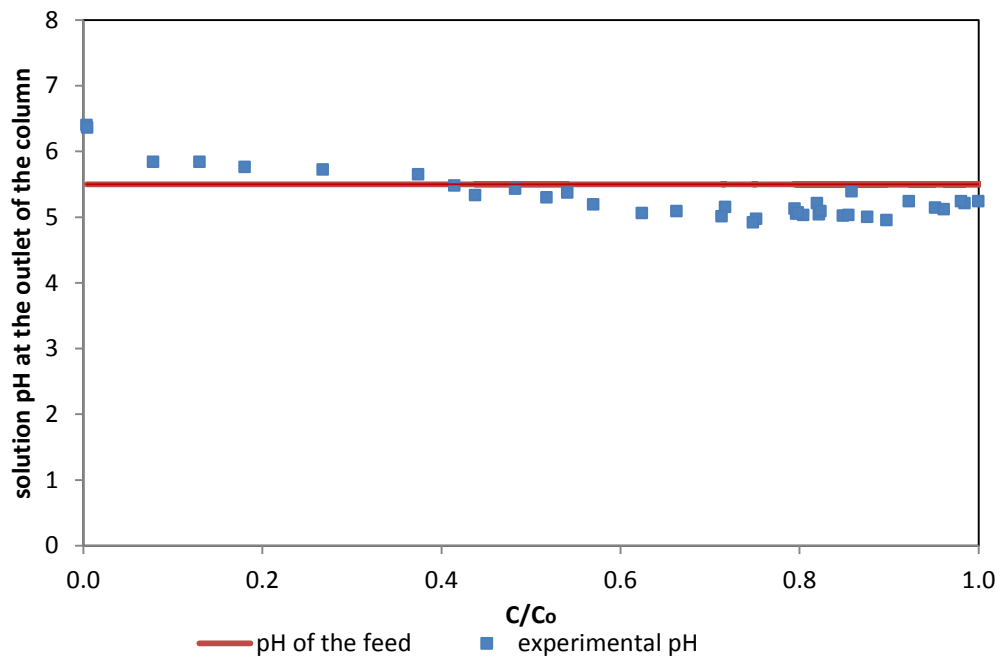


Figure 5.30. pH change of solution at the outlet of the column for Pb^{2+} -NaX binary exchange onto Zeolite 13X beads.

5.6.1.2 Pb^{2+} -NaX binary column studies

From breakthrough analysis of Pb^{2+} -NaX binary exchange system which was shown in Figure 5.31, total exchange capacity and breakthrough capacity were determined as 3.20 meq/g and 1.02 meq/g respectively. Column efficiency was calculated as 0.32.

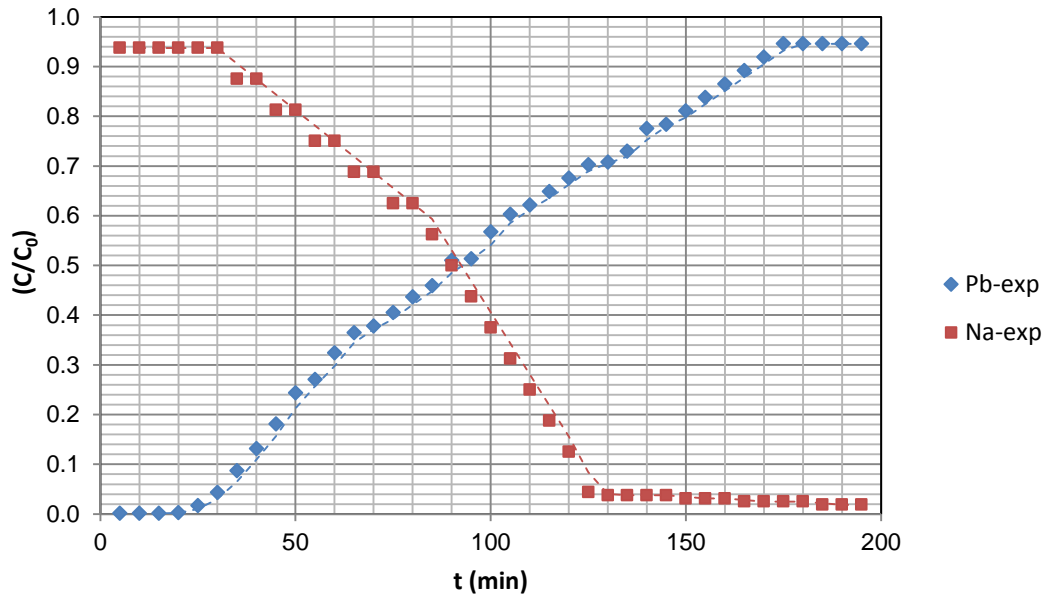


Figure 5.31 Breakthrough curves- $C_{0,Pb}=50$ meq/L; $C_{0,Na}=0$ meq/L

In this study, The Thomas model, Yoon-Nelson model and Adams-Bohart model were utilized for predicting the behaviour of the ion-exchange system.

According to Equation (2.92) and Figure 5.32, Thomas model constant K_{Th} and the total exchange capacity q_0 were calculated as 6.68×10^{-4} (L/min.meq) and 3.25 (meq/g) respectively (Table 5.22). The calculated value of the q_0 is very close to the experimental value ($X^2 = 0.1$).

Table 5.22 Thomas model parameters determined for breakthrough curve for Pb^{2+}

C_0 (meq/L)	Q (mL/min)	$K_{Th} \times 10^4$ (L/min.meq)	$q_{0, exp}$ (meq/g)	$q_{0, cal}$ (meq/g)	X^2	R^2
50	10	6.68	3.20	3.25	7.8×10^{-4}	0.9

Figure 5.32 shows the comparison of the calculated curve of the Thomas Model with the experimental curve. Since Thomas model showed a favorable fit with the experimental results, this model can be used in simulations of the breakthrough of Pb^{2+} at a flow rate 10 ml/min, initial concentration of 50 meq/L.

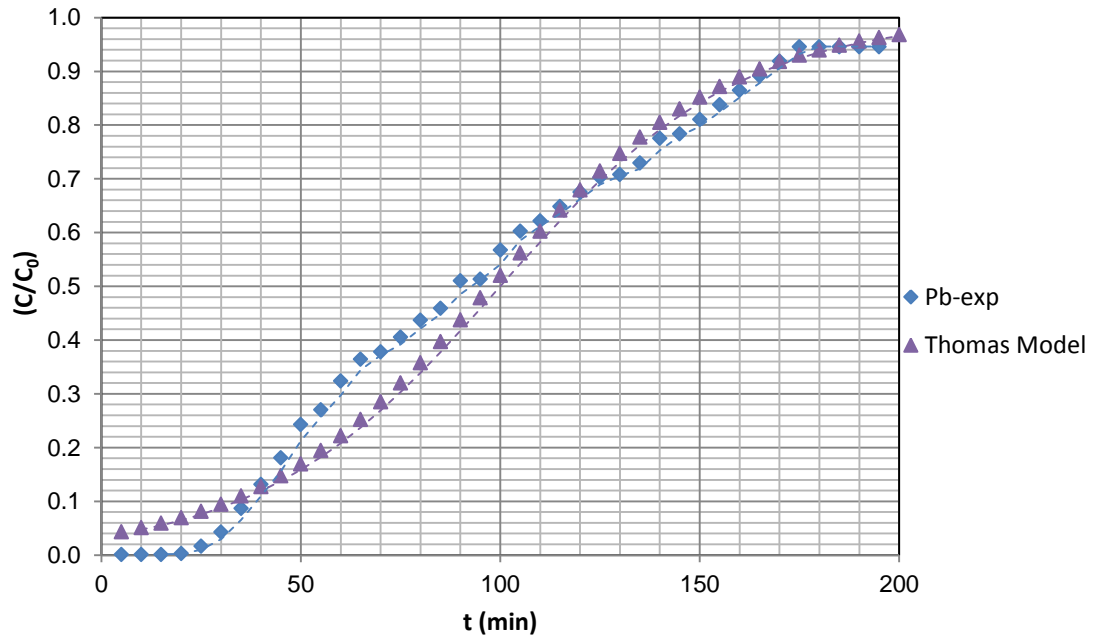


Figure 5.32 Thomas model for breakthrough $C_{0,Pb}=50$ meq/L; $C_{0,Na}=0$ meq/L

According to Equation (2.94) and Figure 5.33, Yoon-Nelson model rate constant K_{YN} and the time necessitate for 50% breakthrough τ were determined as 4.6×10^{-2} (1/min) and 104 (min) respectively (Table 5.23). The data in Table 5.23 and Figure 5.33 implied that the τ values as estimated from the model were fitted with the experimental results. Furthermore this model was not as good as Thomas model for the simulations of breakthrough of Pb^{2+} at a flow rate 10 ml/min, initial concentration of 50 meq/L.

Table 5.23 Yoon Nelson model parameters determined for breakthrough curve for Pb^{2+}

C_0 (meq/L)	Q (mL/min)	$K_{YN} \times 10^2$ (1/min)	τ_{exp} (min)	τ_{cal} (min)	X^2	R^2
50	10	4.6	90	104	2.2	0.8

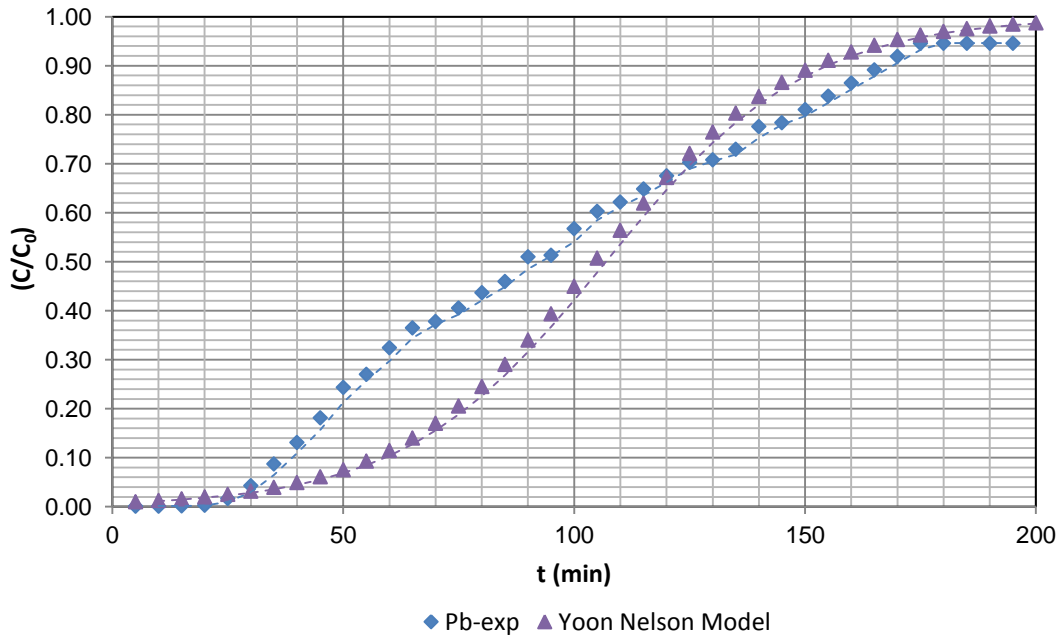


Figure 5.33 Yoon-Nelson model for breakthrough $C_{0,Pb}=50$ meq/L; $C_{0,Na}=0$ meq/L

For the determination of the fit in the Adams-Bohart model with the experimental data the, linear form of Equation (2.95) was used. The kinetic coefficients of mass transfer K_{AB} and the total exchange capacity (N_0) calculated from this Equation were shown on Table 5.24. Since there is good fit between experimental N_0 value and the theoretical one, the lower R^2 values relative to the other models can be interpreted that this model is an inappropriate model for breakthrough curve of Pb^{2+} .

Table 5.24 Adams-Bohart model parameters determined for breakthrough curve for Pb^{2+}

C_0 (meq/L)	h (cm)	U_0 (cm/min)	$K_{AB} \times 10^4$ (L/min.mg)	$N_{0,exp}$ (meq/g)	$N_{0,cal}$ (meq/g)	X^2	R^2
50	6.5	3.18	6.3	3.20	3.13	1.5×10^{-3}	0.65

As seen from Figure 5.34, the Adams-Bohart model was only appropriate for the simulation of the initial part of the breakthrough analysis.

When other models were considered, Adams-Bohart model indicated poor performance for the determination of dynamic Pb^{2+} -NaX binary exchange on Zeolite 13X beads.

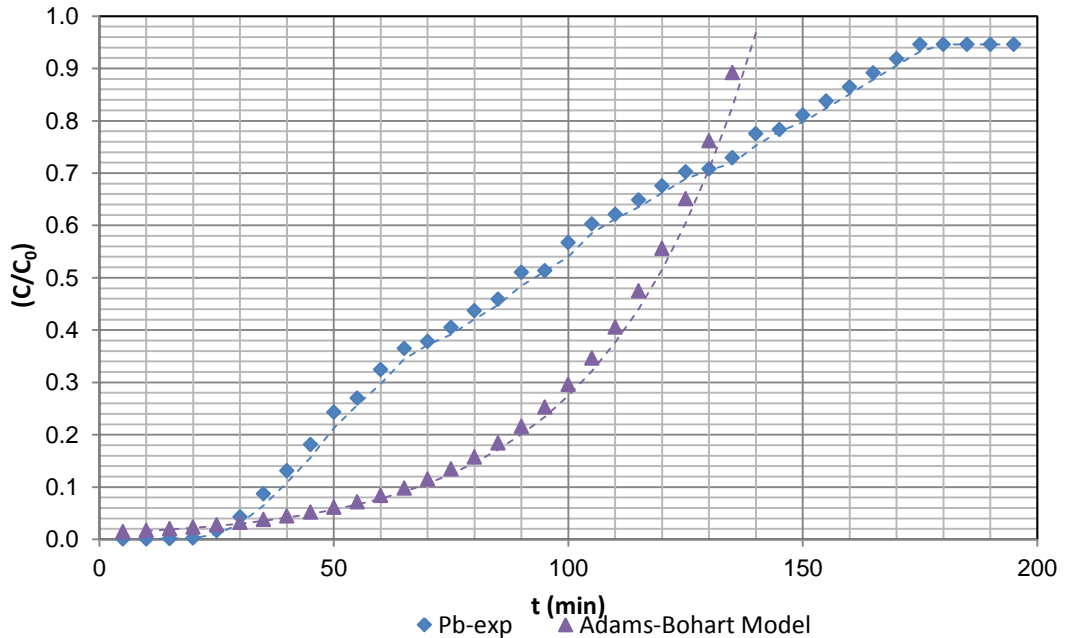


Figure 5.34 Adams-Bohart model for breakthrough $C_{0,\text{Pb}}=50 \text{ meq/L}$; $C_{0,\text{Na}}=0 \text{ meq/L}$

For the evaluation of the controlling mechanism in fixed beds simplified model (under assumption of the constant pattern and plug-flow for the favorable Langmuir isotherm) was used to determine, L_a and $N(T-1)$ values using Equations (2.88), (2.89) and (2.90).

In Figure 5.35, the simplified model results for Pb^{2+} - NaX binary exchange on Zeolite 13X in fixed bed at $L_a=0.20$ were presented. From Figure 5.35, it was seen that with regard to liquid-film control, the curve has a tail in the beginning, while with regard to solid diffusion control, the tail is at the end.

$(C/C_0)_{stoich}$ values for solid diffusion control is 0.70 which is the most favorable equilibrium that can be achieved. The values of $(C/C_0)_{stoich}$ for fluid-film diffusion control is 0.50 which is the least favorable equilibrium that can be achieved.

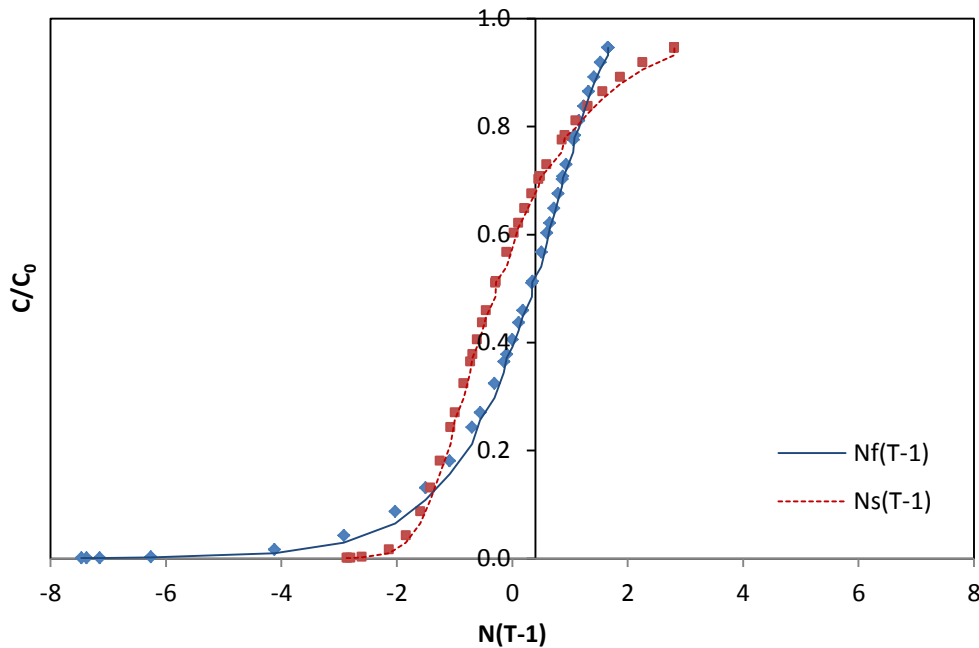


Figure 5.35 Simplified model for Pb^{2+} - NaX binary exchange on Zeolite 13X in fixed bed ($\text{La}=0.2$)

Langmuir isotherm for Pb^{2+} -NaX binary exchange on Zeolite 13X in batch system, was applied to the simplified model. In Figure 5.36, the simplified model results for Pb^{2+} -NaX binary exchange on Zeolite 13X beads at $\text{La}=0.002$ are presented.

Figure 5.36 demonstrates that $(C/C_0)_{stoich}$ value was slightly higher than 0.7 indicated that the batch estimated model did not perform acceptable results.

The use of column-estimated (Q_M) value gave good results since $(C/C_0)_{stoich}$ value was about 0.7 (Figure 5.37). $(C/C_0)_{stoich}$ value was about 0.7 indicated that the possible controlling mechanism was solid diffusion.

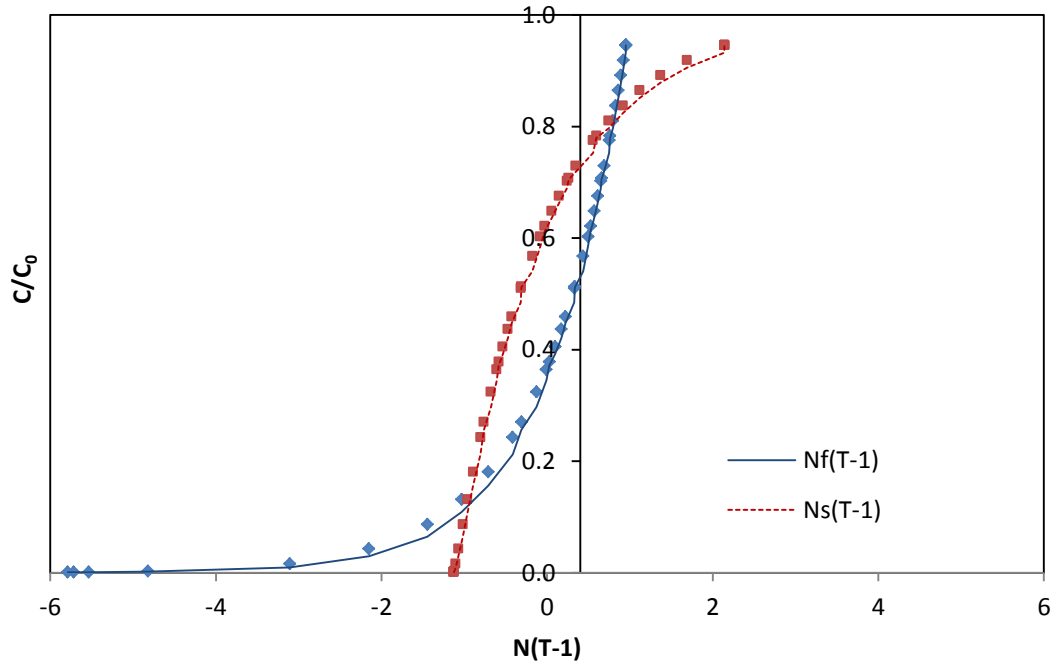


Figure 5.36 Simplified model for Pb^{2+} - NaX binary exchange on Zeolite 13X in fixed bed, estimated using batch method ($L_a=0.002$; $Q_M=5.4$ meq/g)

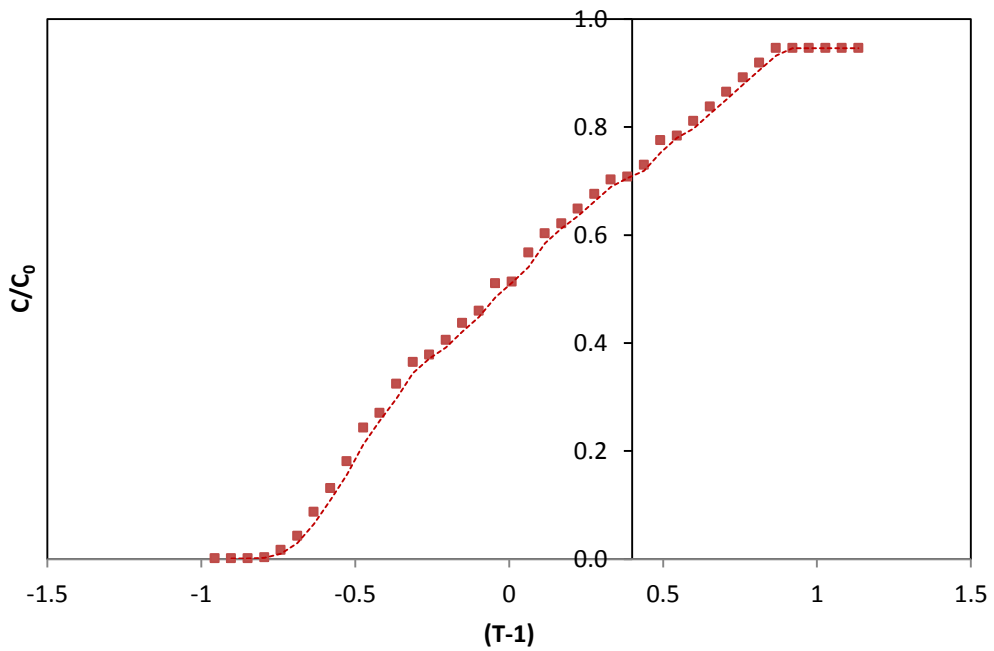


Figure 5.37 Simplified model for Pb^{2+} - NaX binary exchange on Zeolite 13X in fixed bed, estimated using column method ($Q_M=3.2$ meq/g)

Plotting $N_s(T-1)$ versus $(T-1)$ graph gives straight line with slope equal to N_s . Then, D_s can be determined using Equation 2.87. From Figure 5.38, N_s was determined as 1.4 and D_s was determined as $4.3 \times 10^{-6} \text{ cm}^2/\text{min}$.

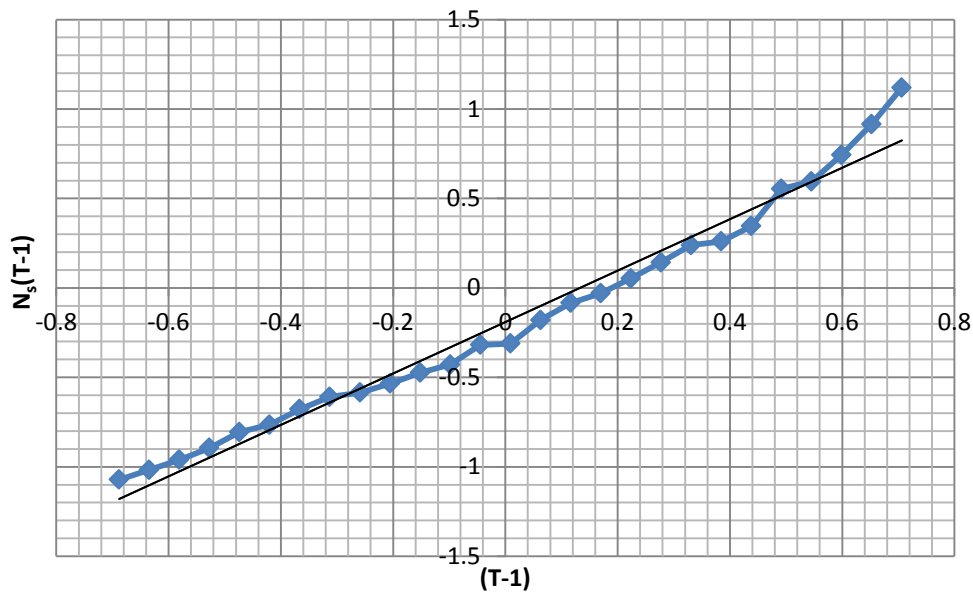


Figure 5.38 $N_s(T-1)$ versus $(T-1)$ graph for Pb^{2+} -NaX binary exchange ($L_a=0.002$; $Q_M=3.2 \text{ meq/g}$)

5.6.1.3 Cd^{2+} -NaX binary column studies

From breakthrough analysis of Cd^{2+} -NaX binary exchange system on Zeolite 13X which was presented in Figure 5.39, total exchange capacity and breakthrough capacity were determined as 1.91 meq/g and 0.43 meq/g respectively. Column efficiency was calculated as 0.22.

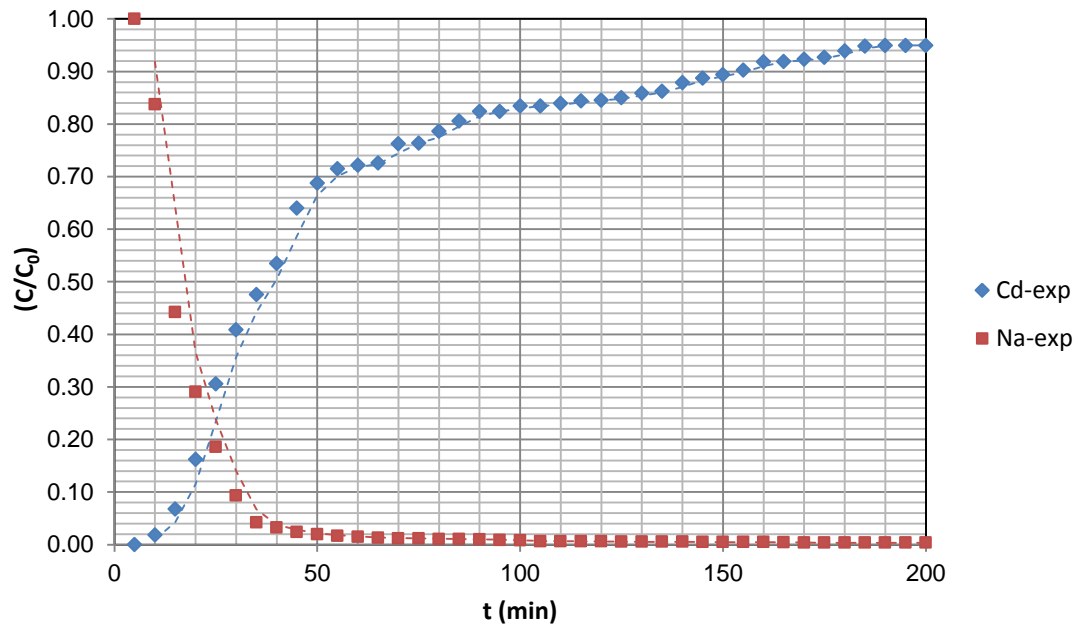


Figure 5.39 Breakthrough curves- $C_{0,Cd}=50$ meq/L; $C_{0,Na}=0$ meq/L

According to Equation (2.92) and Figure 5.40, Thomas model constant K_{Th} and the total exchange capacity q_0 were calculated and the calculated values were shown on Table 5.25. The calculated value of the q_0 is close to the experimental value ($X^2 = 0.02$).

Table 5.25 Thomas model parameters determined for breakthrough curve for Cd^{2+}

C_0 (meq/L)	Q (mL/min)	$K_{Th} \times 10^4$ (L/min.meq)	$q_{0 \text{ exp}}$ (meq/g)	$q_{0 \text{ cal}}$ (meq/g)	X^2	R^2
50	10	4.92	1.91	1.71	0.02	0.8

Figure 5.40 shows the comparison of the calculated curve of the Thomas Model with the experimental curve. Since Thomas model showed a good fit with the experimental results for the determination of the final part of the breakthrough, this model can be used in simulations of the final part of breakthrough of Cd^{2+} at a flow rate 10 ml/min, initial concentration of 50 meq/L.

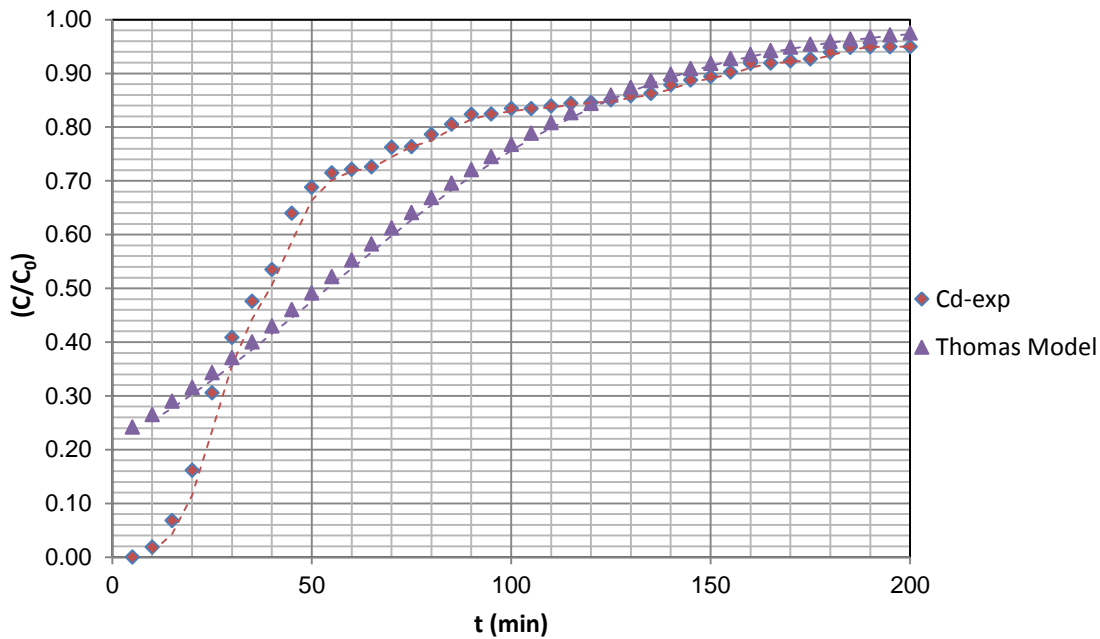


Figure 5.40 Thomas model for breakthrough, $C_{0,Cd}=50$ meq/L; $C_{0,Na}=0$ meq/L

According to Equation (2.94) and Figure 5.33, Yoon-Nelson model rate constant K_{YN} and the time necessitate for 50% breakthrough τ were calculated as 2.7×10^{-2} (1/min) and 90 (min) respectively (Table 5.26). The data in Table 5.26 and Figure 5.41 implied that the τ values as estimated from this model were poorly fitted with the experimental results.

Table 5.26 Yoon-Nelson model parameters determined for breakthrough curve for Cd^{2+}

C_0 (meq/L)	Q (mL/min)	$K_{YN} \times 10^2$ (1/min)	τ_{exp} (min)	τ_{cal} (min)	X^2	R^2
50	10	2.7	40	90	62	0.91

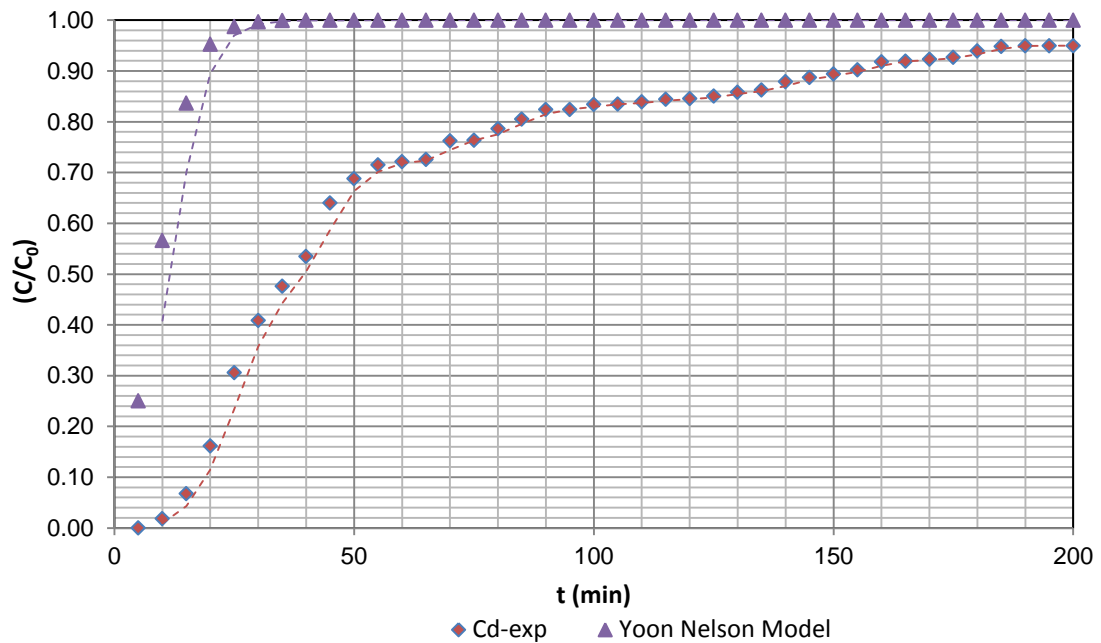


Figure 5.41 Yoon Nelson model for breakthrough, $C_{0,Cd}=50$ meq/L; $C_{0,Na}=0$ meq/L

For the determination of the fit in the Adams-Bohart model with the experimental data the, linear form of Equation (2.95) was used. The kinetic coefficients of mass transfer K_{AB} and the total exchange capacity (N_0) calculated from this Equation were shown on Table 5.27. Since there is good fit between experimental N_0 value and the theoretical one, the lower R^2 values relative to the other models can be interpreted that this model is an inappropriate model for breakthrough curve of Cd^{2+} .

Table 5.27 Adams-Bohart model parameters determined for breakthrough curve for Cd^{2+}

C_0 (meq/L)	h (cm)	U_0 (cm/min)	$K_{AB} \times 10^4$ (L/min.mg)	$N_{0,exp}$ (meq/g)	$N_{0,cal}$ (meq/g)	X^2	R^2
50	6.5	3.18	21	1.91	0.93	0.5	0.86

As seen from Figure 5.42, the Adams-Bohart model was only appropriate for the description of the initial part of the breakthrough curve. When other models were considered, Adams-Bohart model indicated poor performance for the characterization of Cd^{2+} -NaX binary ion exchange on Zeolite 13X beads.

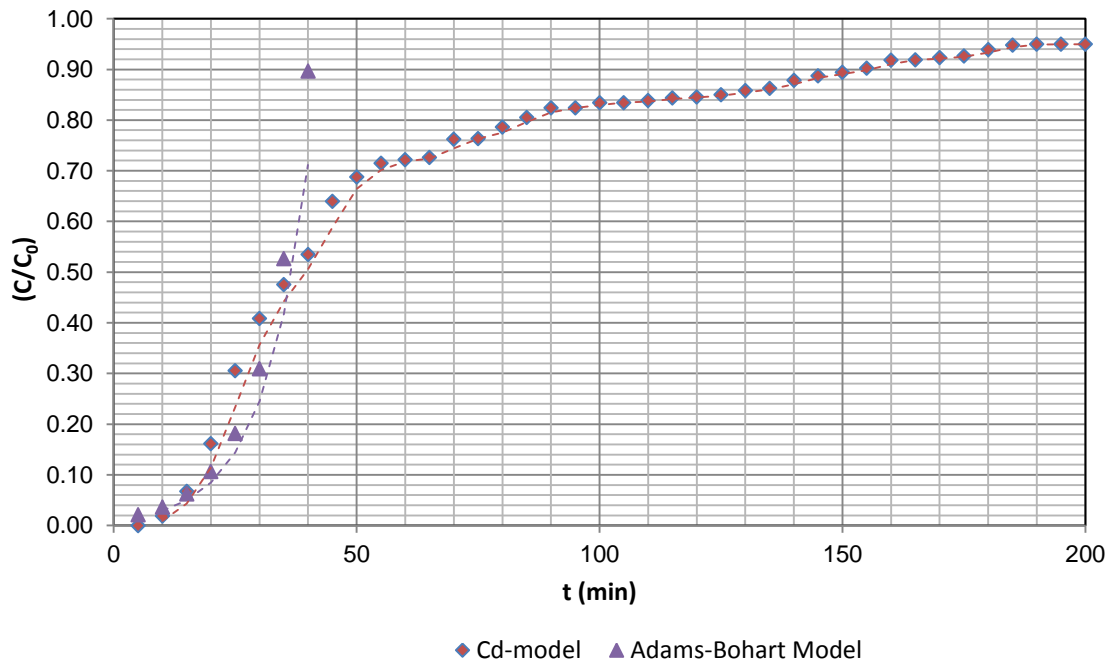


Figure 5.42 Adams-Bohart model for breakthrough, $C_{0,\text{Cd}}=50$ meq/L; $C_{0,\text{Na}}=0$ meq/L

In Figure 5.43, the simplified model results for Cd^{2+} - NaX binary exchange on Zeolite 13X in fixed bed at $L_a=0.20$ were presented. From Figure 5.43, it was seen that $(C/C_0)_{stoich}$ values for solid diffusion control is 0.70 which is the most favorable equilibrium that can be achieved. The values of $(C/C_0)_{stoich}$ for fluid-film diffusion control is 0.50 which is the least favorable equilibrium that can be achieved.

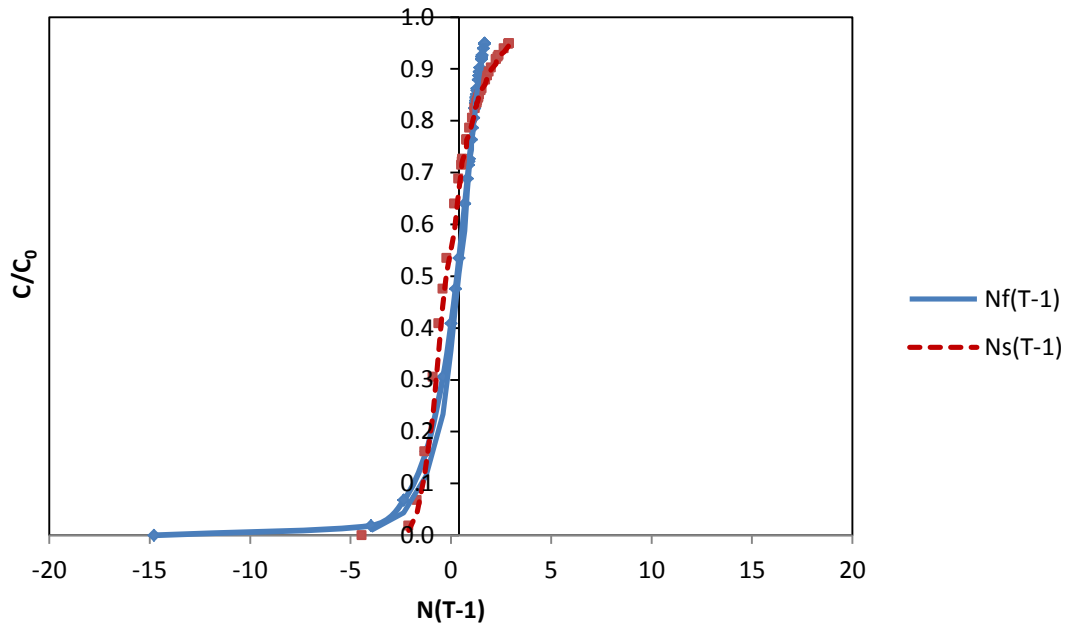


Figure 5.43 Simplified model for Cd^{2+} -NaX binary exchange on Zeolite 13X in fixed bed ($\text{La}=0.2$)

Langmuir isotherm for Cd^{2+} -NaX binary exchange on Zeolite 13X in batch system, was applied to the simplified model. In Figure 5.44, the simplified model results for Pb^{2+} -NaX binary exchange on Zeolite 13X beads at $\text{La}=0.014$ are presented.

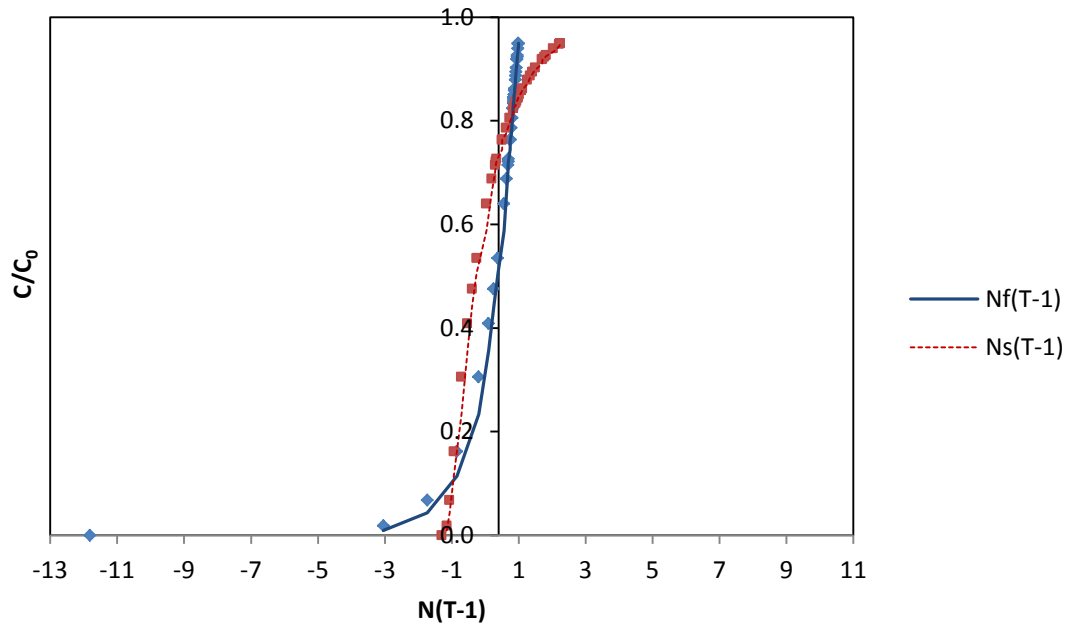


Figure 5.44 Simplified model for Cd^{2+} - NaX binary exchange on Zeolite 13X in fixed bed, estimated using batch method ($La=0.014$; $Q_M=4.2$ meq/g)

Figure 5.44 demonstrates that $(C/C_0)_{stoich}$ value was slightly lower than 0.8 indicated that the batch estimated model was not successful in representing the experimental results.

On the contrary, the use of column-estimated (Q_M) value gave good results since $(C/C_0)_{stoich}$ value was about 0.7 (Figure 5.45). $(C/C_0)_{stoich}$ value was about 0.7 indicated that the possible controlling mechanism was solid diffusion.

From Figure 5.46, N_s was determined as 0.9 and D_s was determined as $4.7 \times 10^{-6} \text{ cm}^2/\text{min}$

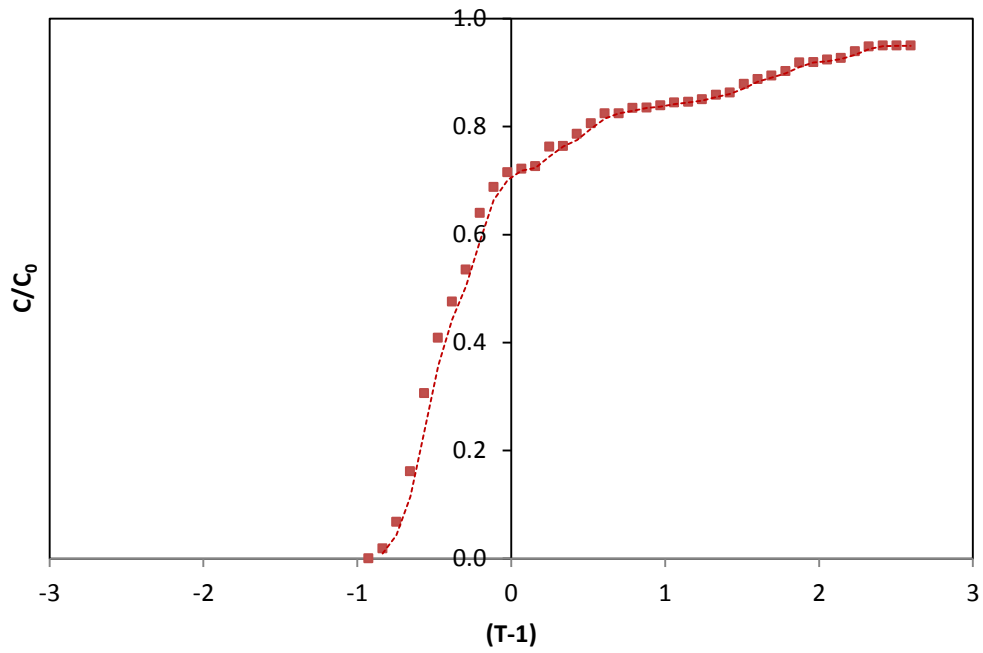


Figure 5.45 Simplified model for Cd^{2+} -NaX binary exchange on Zeolite 13X in fixed bed, estimated using column method ($Q_M=1.9$ meq/g)

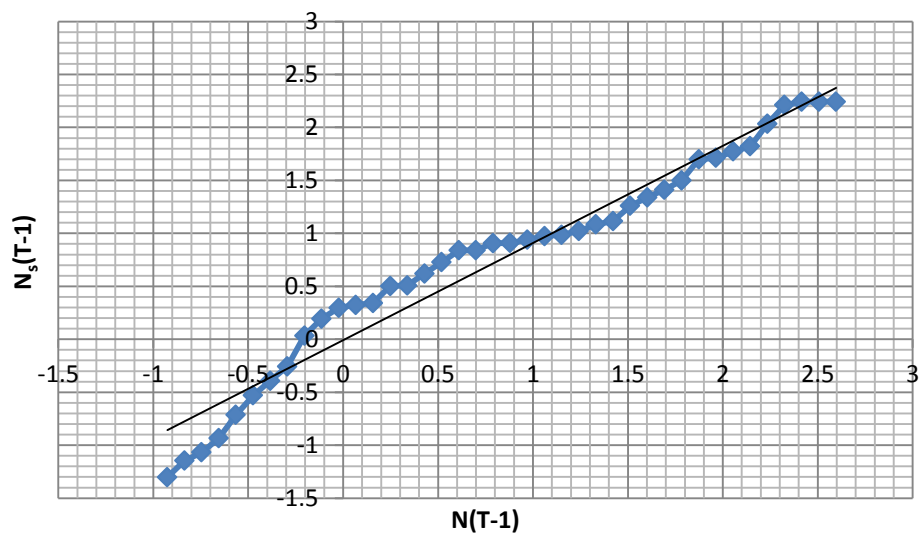


Figure 5.46 $N_s(T-1)$ versus $(T-1)$ graph for Cd^{2+} -NaX binary exchange ($La=1.52 \times 10^{-4}$; $Q_M=1.9$ meq/g)

5.6.1.4 Zn²⁺-NaX binary column studies

From breakthrough analysis of Cd²⁺-NaX binary exchange system on Zeolite 13X which was presented in Figure 5.47, total exchange capacity and breakthrough capacity were determined as 2.36 meq/g and 0.52 meq/g respectively. Column efficiency was calculated as 0.22.

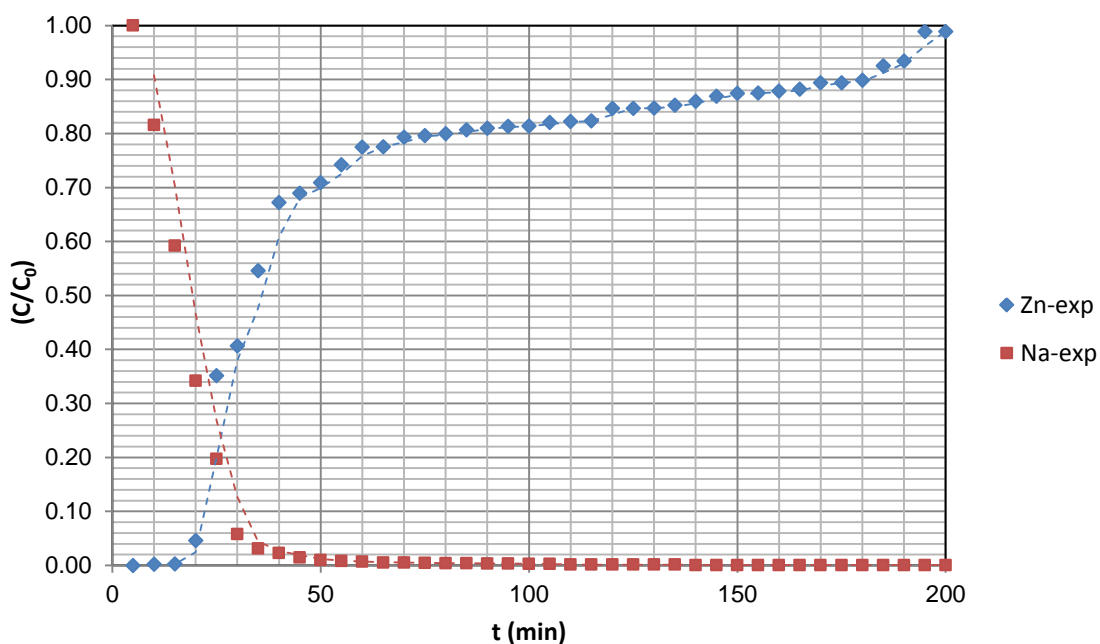


Figure 5.47 Breakthrough curves- $C_{0,Zn} = 50$ meq/L; $C_{0,Na} = 0$ meq/L

According to Equation (2.92) and Figure 5.48, Thomas model constant K_{Th} and the total exchange capacity q_0 were calculated and the calculated values were shown on Table 5.28. The calculated value of the q_0 is very close to the experimental value ($X^2 = 0.026$).

Table 5.28 Thomas model parameters determined for breakthrough curve for Zn²⁺

C_0 (meq/L)	Q (mL/min)	$K_{Th} \times 10^4$ (L/min.meq)	$q_{0, exp}$ (meq/g)	$q_{0, cal}$ (meq/g)	X^2	R^2
50	10	3.85	2.36	2.11	0.026	0.6

Figure 5.48 shows the comparison of the calculated curve of the Thomas Model with the experimental curve. Because Thomas model showed a favorable fit with the experimental results, this model can be used in simulations of the breakthrough of Zn^{2+} at a flow rate 10 ml/min, initial concentration of 50 meq/L.

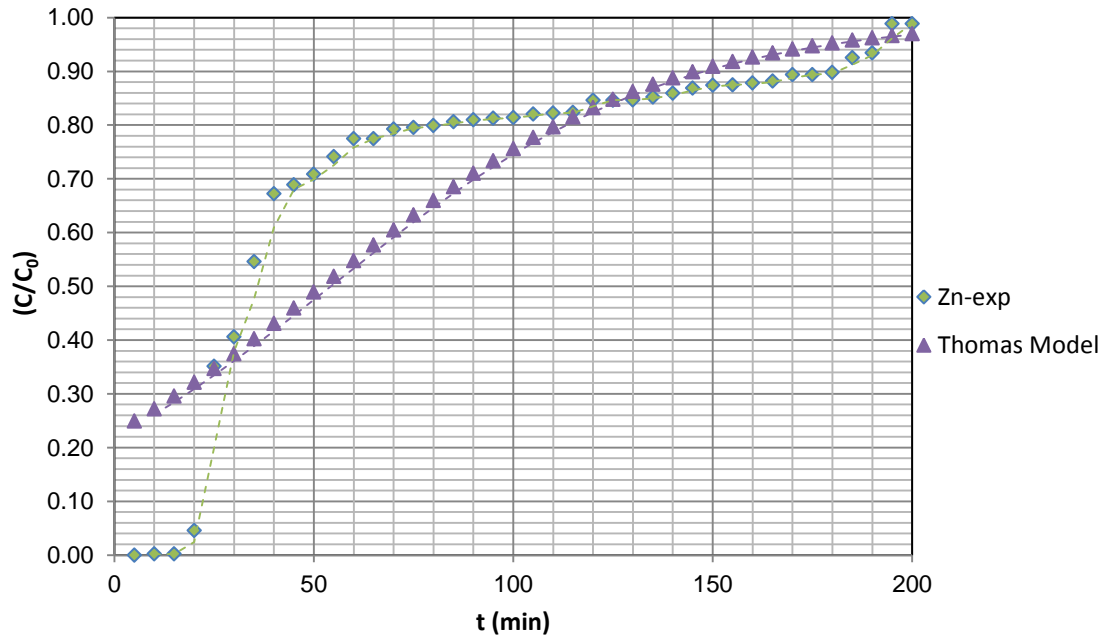


Figure 5.48 Thomas model for breakthrough, $C_{0,Zn} = 50$ meq/L; $C_{0,Na} = 0$ meq/L

According to Equation (2.94) and Figure 5.49, Yoon-Nelson model rate constant K_{YN} and the time necessitate for 50% breakthrough τ were calculated as 2.3×10^{-2} (1/min) and 72 (min) respectively (Table 5.29). The data in Table 5.29 and Figure 5.49 implied that the τ values as estimated from the Yoon-Nelson model were poorly fitted to the experimental results.

Table 5.29 Yoon-Nelson model parameters determined for breakthrough curve for Zn^{2+}

C_0 (meq/L)	Q (mL/min)	$K_{YN} \times 10^2$ (1/min)	τ_{exp} (min)	τ_{cal} (min)	X^2	R^2
50	10	2.3	35	72	39	0.98

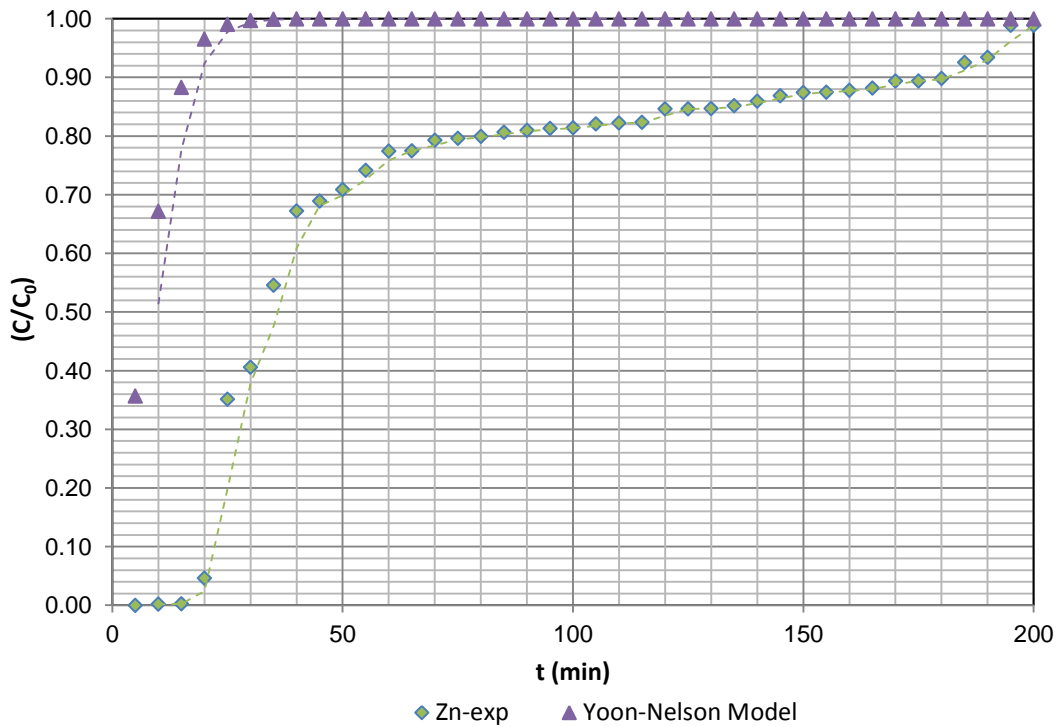


Figure 5.49 Yoon-Nelson model for breakthrough, $C_{0,Zn} = 50 \text{ meq/L}$; $C_{0,Na} = 0 \text{ meq/L}$

For the determination of the fit in the Adams-Bohart model with the experimental data the, linear form of Equation (2.95) was used. The kinetic coefficients of mass transfer K_{AB} and the total exchange capacity (N_0) calculated from this Equation were shown on Table 5.30. Since there is no good fit between experimental N_0 value and the theoretical one, the Adams-Bohart model is an unsuitable model for the breakthrough curve of Zn^{2+} .

Table 5.30 Adams-Bohart model parameters determined for breakthrough curve for Zn^{2+}

C_0 (meq/L)	h (cm)	U_0 (cm/min)	$K_{AB} \times 10^4$ (L/min.mg)	$N_{0,exp}$ (meq/g)	$N_{0,cal}$ (meq/g)	X^2	R^2
50	6.5	3.18	62	2.36	0.80	1.0	0.86

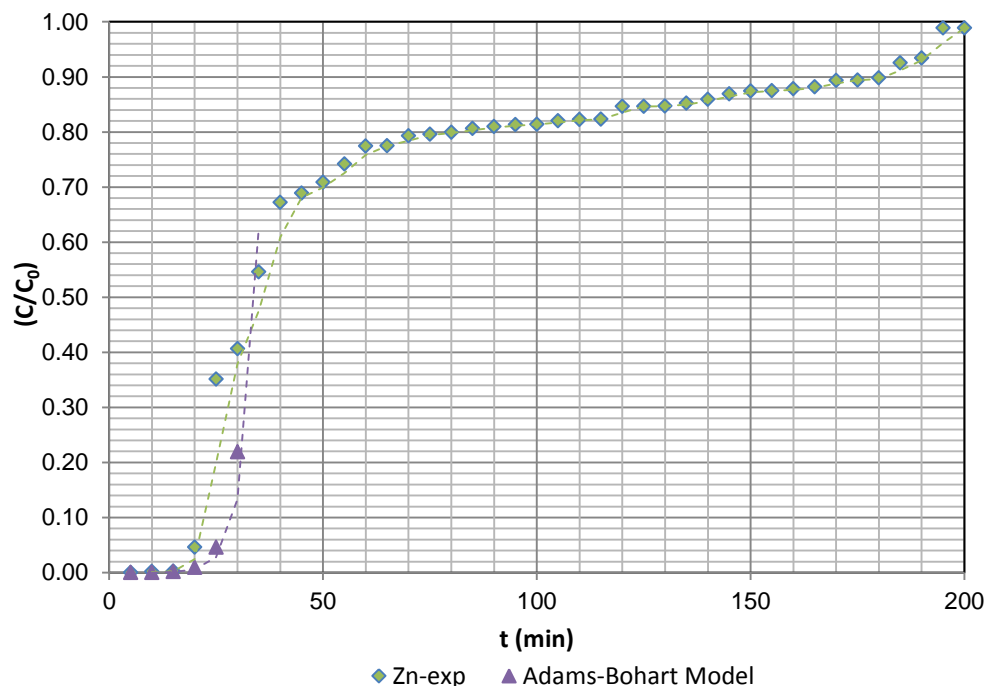


Figure 5.50 Adams-Bohart model for breakthrough, $C_{0,Zn}=50$ meq/L; $C_{0,Na}=0$ meq/L

As seen from Figure 5.50, the Adams-Bohart model was only appropriate for the description of the initial part of the breakthrough curve. When other models were considered, Adams-Bohart model indicated poor performance for describing Zn^{2+} -NaX binary ion exchange on Zeolite 13X beads.

Langmuir isotherm for Zn^{2+} -NaX binary exchange on Zeolite 13X in batch system, was applied to the simplified model. In Figure 5.51, the simplified model results for Zn^{2+} - NaX binary exchange on Zeolite 13X in fixed bed at $La=0.10$ were presented.

The use of batch method estimated (Q_M) value failed to determine the experimental results because $(C/C_0)_{stoich}$ value was about 0.8 (Figure 5.51). On the other hand, the use of column-estimated (Q_M) value also gave poor results since $(C/C_0)_{stoich}$ value was slightly lower than 0.8 (Figure 5.52). This may be due to higher experimental error. From another point of view assuming that the possible controlling mechanism was solid diffusion.

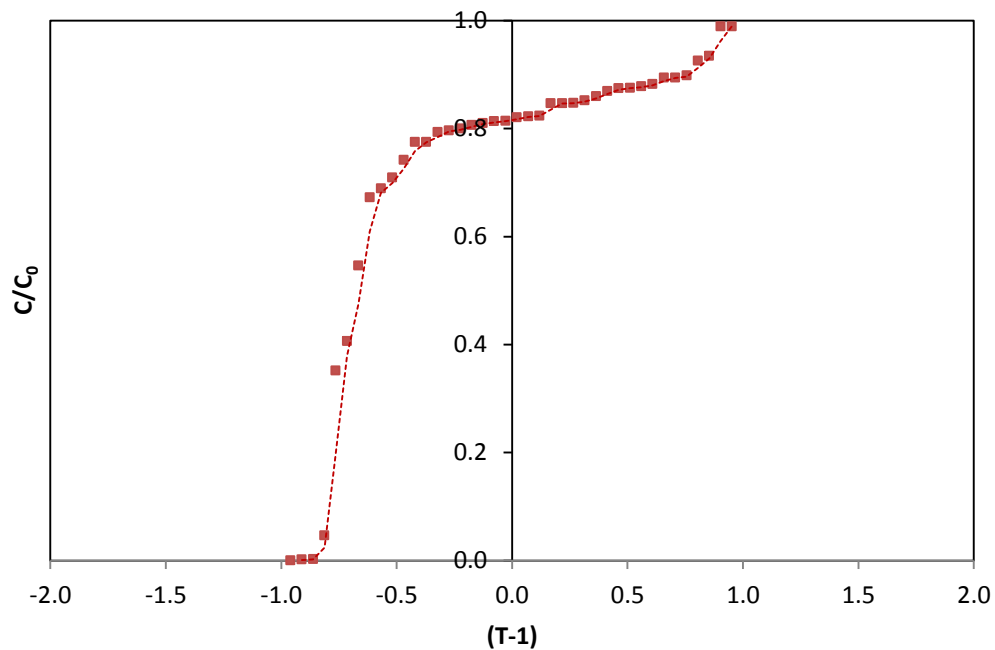


Figure 5.51 Simplified model for Zn^{2+} - NaX binary exchange on Zeolite 13X in fixed bed, estimated using batch method ($La=0.1$; $Q_M=3.5$ meq/g)

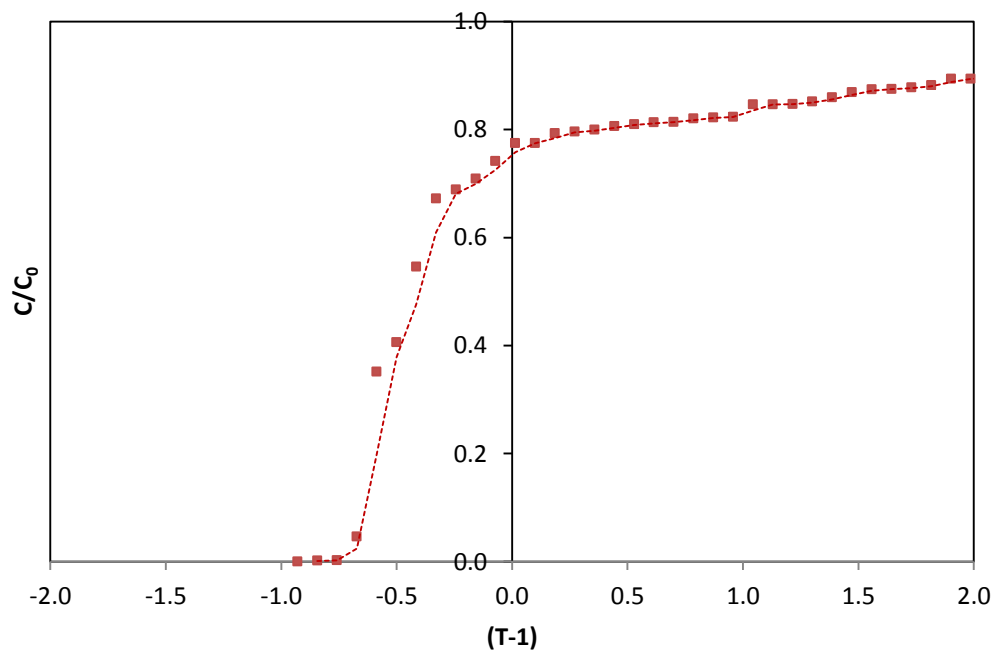


Figure 5.52 Simplified model for Zn^{2+} - NaX binary exchange on Zeolite 13X in fixed bed, estimated using column method ($Q_M=2.3$ meq/g)

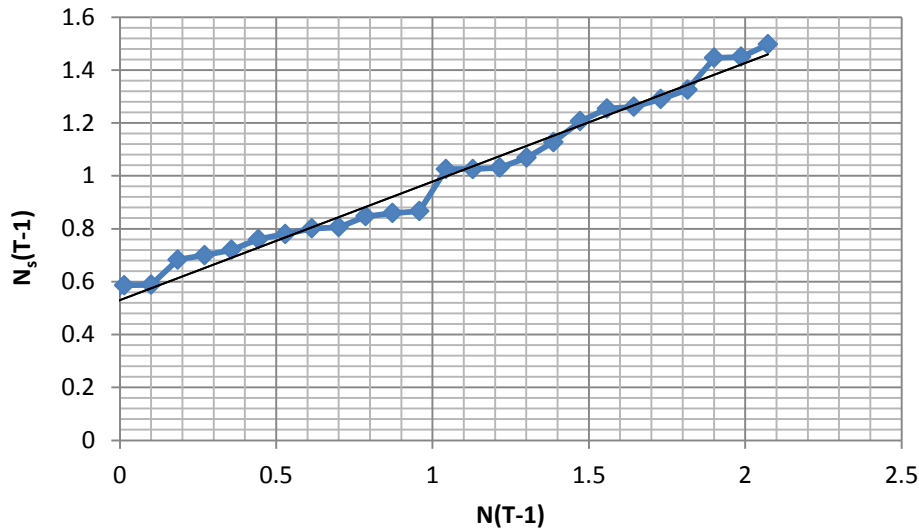


Figure 5.53 $N_s(T-1)$ versus $(T-1)$ graph for Cd^{2+} -NaX binary exchange ($La=0.1$;
 $Q_M=2.3$ meq/g)

From Figure 5.53, N_s was determined as 0.49 and D_s was determined as $2.4 \times 10^{-6} \text{ cm}^2/\text{min}$.

When the breakthrough capacities for Pb^{2+} -NaX, Cd^{2+} - NaX and Zn^{2+} - NaX binary exchange systems on Zeolite 13X were compared, it was seen that the breakthrough capacities of Pb^{2+} -NaX binary exchange was greater than that of Cd^{2+} - NaX and Zn^{2+} - NaX binary exchange systems on Zeolite 13X. In addition, the total exchange capacity shows the same behavior. When height of exchange zones was compared, the breakthrough curve for Pb^{2+} -NaX binary exchange was more similar to the ideal curve with insignificant mass-transfer resistance (Table 5.31).

Therefore, the cations selectivity sequence for Zeolite 13X in accordance with their affinity was found as: $Pb^{2+} > Zn^{2+} > Cd^{2+} > Na^+$

Table 5.31 Results of binary ion experiments.

System	Breakthrough capacity (meq/g)	Total exchange capacity (meq/g)	Efficiency	H _{UNB}
Pb ²⁺ -Na	1.02	3.20	0.32	3.17
Cd ²⁺ -Na	0.43	1.91	0.22	4.34
Zn ²⁺ -Na	0.52	2.36	0.22	4.61

5.6.2. Ternary Ion Exchange Experiments

The lead and cadmium nitrate solution (0.025 N each) was pumped in up flow mode at a fixed volumetric flow rate of 10 ml/min and total concentration of 0.05 N. From Figure 5.54, the total exchange capacity for lead was determined as 1.93 meq/g and for cadmium as 1.09 meq/g. Breakthrough capacity was determined as 0.53 for lead and 0.34 for cadmium. Column efficiency was calculated as 0.27 for lead and 0.32 for cadmium. Mass transfer zone (H_{UNB}) was calculated as 4.1 (Table 5.32).

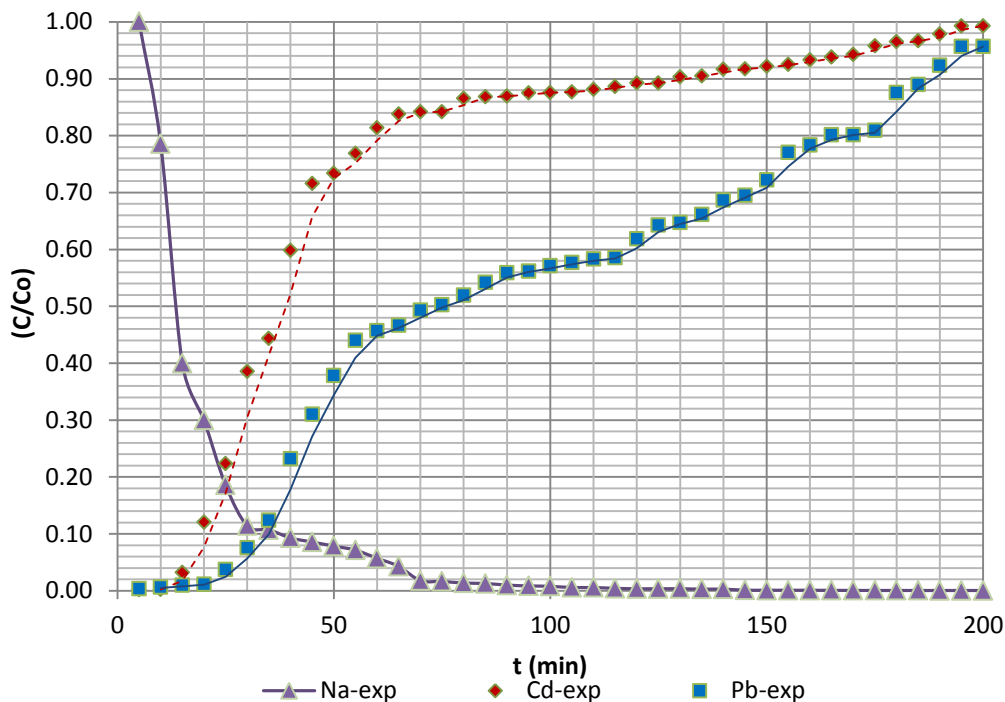


Figure 5.54 Breakthrough curves- $C_{0,Pb}=30$ meq/L; $C_{0,Cd}=30$ meq/L $C_{0,Na}=0$ meq/L

Table 5.32 Results for $Pb^{2+} - Cd^{2+} - NaX$ ternary ion exchange (particle size 25/30 Mesh and influent total concentration of 0.05 N, flow rate of 10 ml/min)

	Pb	Cd	Na
Total Exchange Capacity (mg/L)	1.93	1.09	5.98
Breakthrough capacity (mg/L)	0.53	0.34	
Column efficiency	0.27	0.32	
H_{UNB} (cm)	4.1	4.1	

By comparing the breakthrough capacities for $Pb^{2+}-Cd^{2+}-Na^+$ ternary systems, it was observed that the breakthrough capacity and total exchange capacity of lead was higher than that of cadmium. (Table 5.32). This result is compatible with the results found in binary column experiments.

The zinc and cadmium nitrate solution was added at a constant volumetric flow rate of 10 ml/min and total concentration of 0.05 N in up flow mode. Total exchange capacity for zinc was 1.34 meq/g and for cadmium was 1.38 meq/g. Breakthrough capacity was 0.41 for zinc and 0.24 for cadmium. Column efficiency was 0.30 for zinc and 0.17 for cadmium (Figure 5.55).

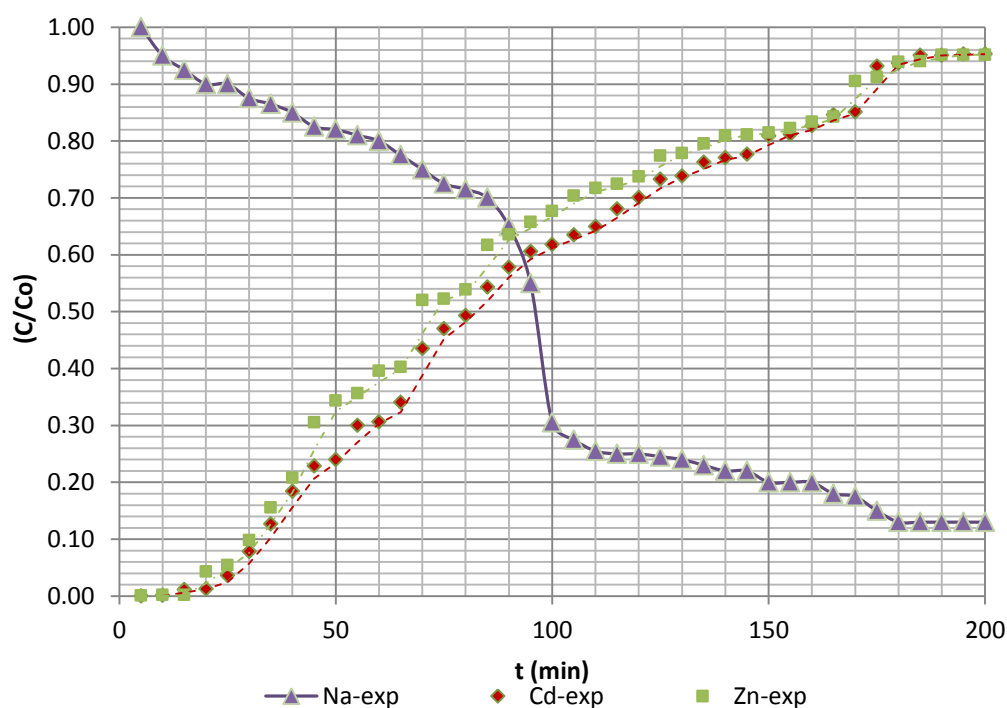


Figure 5.55 Breakthrough curves- $C_{0,Cd}=25$ meq/L; $C_{0,Zn}=25$ meq/L $C_{0,Na}=0$ meq/L

By comparing the breakthrough capacities for Zn^{2+} - Cd^{2+} - NaX ternary exchange systems on Zeolite 13X, it was seen that the breakthrough capacity of zinc was greater than that of cadmium while the total exchange capacity of zinc and cadmium were approximately the same. When height of exchange zones are compared, the breakthrough curve for zinc was more close to an ideal step (Table 5.33). This result is also compatible with the results found in binary column experiments.

Table 5.33 Results for Zn²⁺ - Cd²⁺ - NaX ternary ion exchange (particle size 25/30 Mesh and influent total concentration of 0.05 N, flow rate of 10 ml/min)

	Zn	Cd	Na
Total Exchange Capacity (mg/L)	1.34	1.38	5.52
Breakthrough capacity (mg/L)	0.41	0.24	
Column efficiency	0.30	0.17	
H _{UNB} (cm)	3.96	4.85	

The zinc and lead nitrate solution was added at a constant volumetric flow rate of 10 ml/min and total concentration of 0.05 N in up-flow mode.

From Figure 5.56, the total exchange capacity for zinc was determined as 1.14 meq/g and for lead as 1.80 meq/g. Breakthrough capacity was determined as 0.34 for zinc and 0.74 for lead. Column efficiency was calculated as 0.30 for zinc and 0.41 for lead. Mass transfer zone (H_{UNB}) was calculated as 4.09 for zinc and 2.97 for lead respectively (Table 5.34).

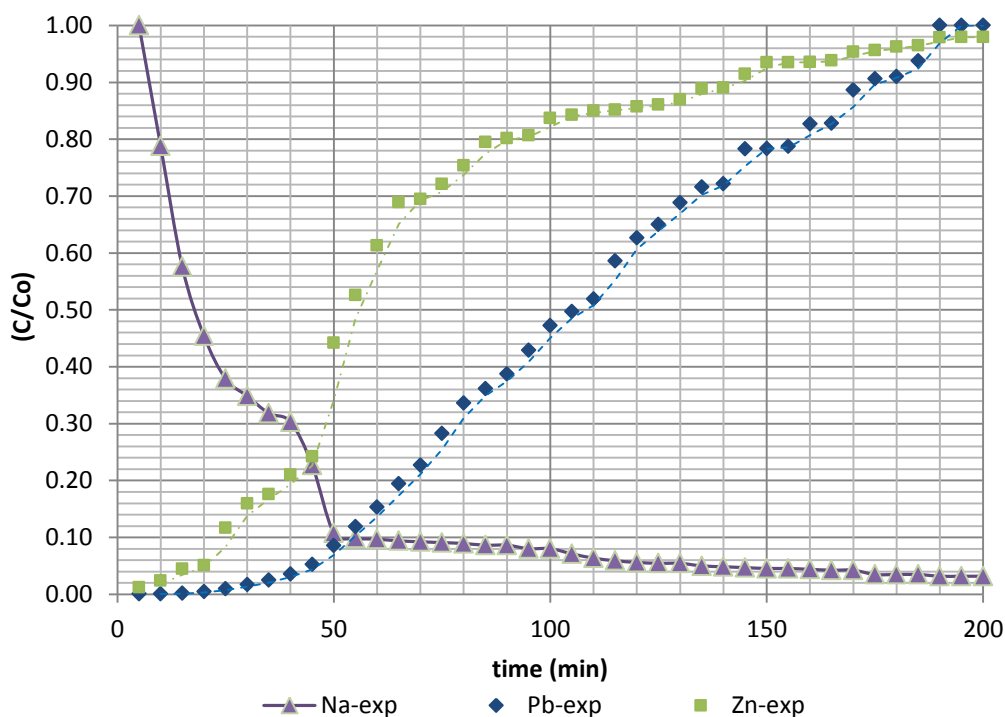


Figure 5.56 Breakthrough curves- $C_{0,Pb}=25$ meq/L; $C_{0,Zn}=25$ meq/L $C_{0,Na}=0$ meq/L

By comparing the breakthrough capacities for Zn^{2+} - Pb^{2+} - Na^+ ternary systems, it was observed that the breakthrough capacity and total exchange capacity of lead were greater than that of zinc. When height of exchange zones are compared, the breakthrough curve for lead is more close to an ideal step (Table 5.34). This result is also compatible with the results found in binary column experiments.

Table 5.34. Results for Zn^{2+} - Pb^{2+} - NaX ternary ion exchange (particle size 25/30 Mesh and influent total concentration of 0.05 N, flow rate of 10 ml/min)

	Zn	Pb	Na
Total Exchange Capacity (mg/L)	1.14	1.80	5.52
Breakthrough capacity (mg/L)	0.34	0.74	
Column efficiency	0.30	0.41	
H_{UNB} (cm)	4.09	2.97	

5.6.3. Quaternary Ion Exchange Experiments

The zinc, cadmium and lead nitrate solution were added at a fixed volumetric flow rate of 10 ml/min and total concentration of 0.05 N by utilizing a peristaltic pump in up-flow mode. Total exchange capacity for zinc was 1.63 meq/g, for lead is 1.16 and for cadmium was 0.60 meq/g. Breakthrough capacity was 0.34 for zinc, 0.47 for lead and 0.15 for cadmium. Column efficiency was 0.24 for zinc, 0.40 for lead and 0.23 for cadmium (Figure 5.57).

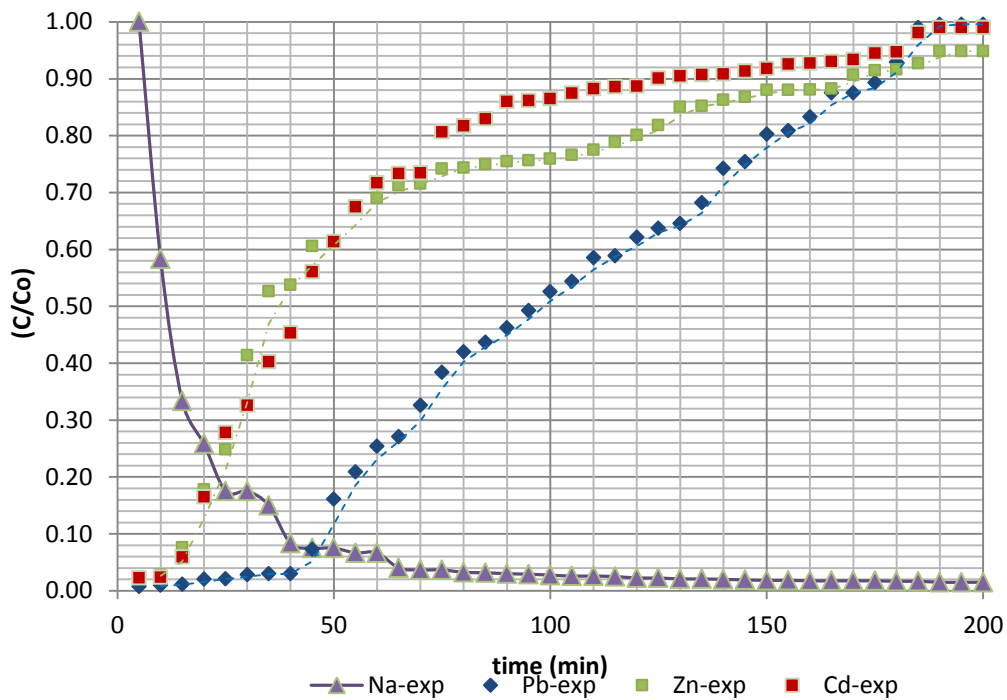


Figure 5.57 Breakthrough curves- $C_{0,Pb} = 17$ meq/L; $C_{0,Cd} = 17$ meq/L; $C_{0,Zn} = 16$ meq/L
 $C_{0,Na} = 0$ meq/L

By comparing the breakthrough capacities for $Pb^{2+}Zn^{2+}-Cd^{2+}-Na^{+}$ quaternary systems, it was seen that the breakthrough capacity of lead was greater than that of cadmium and zinc. But total exchange capacity of zinc was greater than lead. (Table 5.35). This result is not compatible with the results found in binary column experiments.

Table 5.35 Results for $Zn^{2+} - Pb^{2+} - Cd^{2+} - NaX$ quaternary ion exchange (particle size 25/30 Mesh and influent total concentration of 0.05 N, flow rate of 10 ml/min)

	Zn	Pb	Cd	Na
Total Exchange Capacity (mg/L)	1.63	1.16	0.60	5.52
Breakthrough capacity (mg/L)	0.34	0.47	0.15	
Column efficiency	0.24	0.40	0.23	
H_{UNB} (cm)	4.57	3.56	4.88	

5.6.4. Mathematical Modeling

Despite the fact that dynamic method is the most generally utilized method for ion exchange, modeling ion exchange in fixed bed is very complicated. “Equilibrium (isotherm and capacity), kinetic (diffusion and convective coefficients) and hydraulic (liquid holdup, geometric analogies and maldistribution)” are known to be the important parameters which effects fixed bed operation (Inglezakis, 2006). Therefore, a predictive modeling of fixed-bed systems necessitates comprehensive experimental data and complicated mathematical tools. Subsequently, the complete modeling of the multicomponent ion exchange process is very complex

Ion exchange in the fixed bed was modeled using the assumptions listed below:

- constant physical properties of the zeolite
- isothermal and isobaric process
- negligible radial dispersion within the fixed bed.
- homogeneously distributed sites available for exchange
- sorption of H⁺ ions by Zeolite 13X is negligible.
- concentration profile within the pores determined by LDF Method.

Concentrations of lead, cadmium and zinc in the zeolite phase at equilibrium with the liquid phase were computed from breakthrough curves by utilizing Equation (5.2). The liquid phase mass balance for component j (Pb²⁺-Cd²⁺-Zn²⁺-Na⁺) is:

$$\frac{\partial C_j}{\partial t} + \frac{\rho_L}{\varepsilon} \frac{\partial q_j}{\partial t} = -u_0 \frac{\partial C_j}{\partial z} + D_{axj} \frac{\partial^2 C_j}{\partial z^2} \quad (5.2)$$

C_j: concentration of component j in liquid phase (meq/L),

q_j: concentration of component j in the zeolite phase (meq/g),

ρ_L: bed density (g/L)

u_0 : interstitial velocity of the solution (cm/ min),
 $D_{ax,j}$: axial dispersion mass transfer coefficient (cm²/min),
 ε : total bed porosity,
 t : time (min) and
 z : spatial coordinate in the axial direction (cm).

Dimensionless variables:

$$\begin{aligned}
 Pe_b &= \text{Peclet number for bed} = \frac{Lu}{D_{ax}} \\
 St_D &= \text{Stanton number for bed} = \frac{K_f u}{L} \\
 \tau &= \text{dimensionless time coordinate} = \frac{tu}{L} \\
 \xi &= \text{dimensionless axial coordinate} = \frac{z}{L}
 \end{aligned}$$

Using dimensionless variables determined above Equation (5.2) becomes:

$$\frac{\partial C_j}{\partial \tau} + \frac{\rho_L}{\varepsilon} \frac{\partial q_j}{\partial \tau} = - \frac{\partial C_j}{\partial \xi} + \frac{1}{Pe_b} \frac{\partial^2 C_j}{\partial \xi^2} \quad (5.3)$$

Rearranging Equation (5.3)

$$\frac{\partial C_j}{\partial \tau} = - \frac{\partial C_j}{\partial \xi} + \frac{1}{Pe_b} \frac{\partial^2 C_j}{\partial \xi^2} - \frac{\rho_L}{\varepsilon} \frac{\partial q_j}{\partial \tau} \quad (5.4)$$

$$C_j = C_j(\xi, t) \quad (5.5)$$

$$\frac{\partial q_j}{\partial \tau} = St_D (q_j^* - q_j) \quad (5.6)$$

q_j^* : equilibrium concentration of component j in the zeolite phase.

$$q_j^* = \frac{q_{max} b_j C_j^*}{1 + \sum_{i=1}^4 b_i C_i^*} \quad (5.7)$$

C_j^* : equilibrium concentration of component j in the liquid phase.

The initial concentration of each component in the liquid phase is given by Equation (5.8)

$$C_j(\xi, 0) = 0 \quad (5.8)$$

The initial concentrations of Zn^{2+} , Pb^{2+} and Cd^{2+} in the zeolite phase are given by Equation (5.9) and initial concentration of Na^+ is given by Equation (5.10).

$$q_j(\xi, 0) = 0 \quad (5.9)$$

$$q_{Na}(\xi, 0) = CTC \quad (5.10)$$

The boundary conditions which were proposed by Danckwerts were used for all cations.

$$\frac{\partial C_j}{\partial \xi} = Pe_b (C_j(0, \tau) - C_j^F) \quad \text{at} \quad \xi = 0 \quad (5.11)$$

$$\frac{\partial C_j}{\partial \xi} = 0 \quad \text{at} \quad \xi = 1 \quad (5.12)$$

$$D_1 = D_2 = D_3 = D_4 = D$$

$$St_{D1} = St_{D2} = St_{D3} = St_{D4} = St_D$$

The equilibrium Na^+ concentration in the zeolite phase was computed by utilizing Equation (5.14). Equation (5.13) was acquired by mass balance in the column. Equation (5.14) was acquired regarding the electroneutrality principle in the zeolite.

$$q_j^* = \frac{C_j^F \dot{Q}}{m} \int_0^{t_{sat}} \left(1 - C_j|_{z=L} / C_j^F \right) dt - \frac{V \epsilon C_j^F}{m} \quad (5.13)$$

where

$$q_{Na}^* = CTC - q_{Pb}^* - q_{Cd}^* - q_{Zn}^* \quad (5.14)$$

where

- q_j^* : equilibrium concentration of component j in the zeolite phase (meq/g),
- $C_j|_{z=L}$: outlet concentration of component j (meq/L),
- C_j^F : concentration of component j in the feed (meq/L),
- \dot{Q} : volumetric flow rate (cm³/L),
- t : time (min),
- t_{sat} : time necessitated to saturate the bed (min),
- V : bed volume (L),
- m : weight of zeolite (g),
- ε : bed porosity
- CTC** : total cation exchange capacity of Zeolite 13X (meq/g).

The system of ordinary differential equations (Equations (5.4)-(5.7) with the boundary and initial conditions (5.8)-(5.12) were solved by MATLAB.

The mass transfer coefficient for the zeolite (K_{sj}), is acquired from the experimentally derived breakthrough curves of Pb²⁺-NaX Cd²⁺-NaX and Zn²⁺-NaX binary exchange on Zeolite 13X beads.

The axial dispersion coefficient was predicted by utilizing Equation (5.15).

$$\frac{D_{axj}}{u_0 d_p} = \frac{20}{\varepsilon} \left(\frac{D_{mj}}{u_0 d_p} \right) + \frac{1}{2} \quad (5.15)$$

where d_p is the average particle diameter of the zeolite and D_{mj} is the molecular diffusion of component j in water.

D_{axj} was calculated as 2.3×10^{-3} (cm²/s) for Pb²⁺-NaX and as 2.2×10^{-3} (cm²/s) for both Cd²⁺-NaX and Zn²⁺-NaX binary exchange on Zeolite 13X.

Using Equations (5.16)-(5.19) which were suggested by Wilson and Geankoplis, the external mass transfer coefficient (K_{fj}) was computed.

$$J_D = \frac{1.09}{\varepsilon} (Re)^{-2/3} \quad (5.16)$$

where

$$J_D = \frac{k_{fj}}{u_0} (Sc)^{2/3} \quad (5.17)$$

$$K_{fj} = a_e k_{fj} \quad (5.18)$$

$$a_e = \frac{6(1 - \varepsilon)}{d_p} \quad (5.19)$$

where J_D is the Chilton–Colburn factor, k_{fj} is the liquid film mass transfer coefficient, Sc is the Schmidt number, K_{fj} is the volumetric mass transfer coefficient in the liquid film and a_e is the particle specific area.

a_e was calculated as 46 cm^{-1} and K_{fj} was calculated as $60 \text{ (g/cm}^3\text{)min}^{-1}$ for Pb^{2+} -NaX, $74 \text{ (g/cm}^3\text{)min}^{-1}$ Cd^{2+} -NaX and $55 \text{ (g/cm}^3\text{)min}^{-1}$ for Zn^{2+} -NaX binary exchange.

Dimensionless Peclet and Stanton Numbers calculated for all metals were given in Table 5.36. $Pe_b < 400$ also indicated that ion exchange was diffusion controlled.

Table 5.36 Dimensionless Peclet and Stanton Numbers

Ion Exchange System	Pe_b	St_D
Pb^{2+} -NaX	134.2	32.9
Cd^{2+} -NaX	138.9	40.5
Zn^{2+} -NaX	139.3	30.4

Simulated breakthrough curves and the comparison between simulated and experimental breakthrough curves were given in Figures 5.57 – 5.59. Since the simulated breakthrough curves did not fit well with the experimental values, only the one for the Pb^{2+} –NaX binary exchange was given in this study.

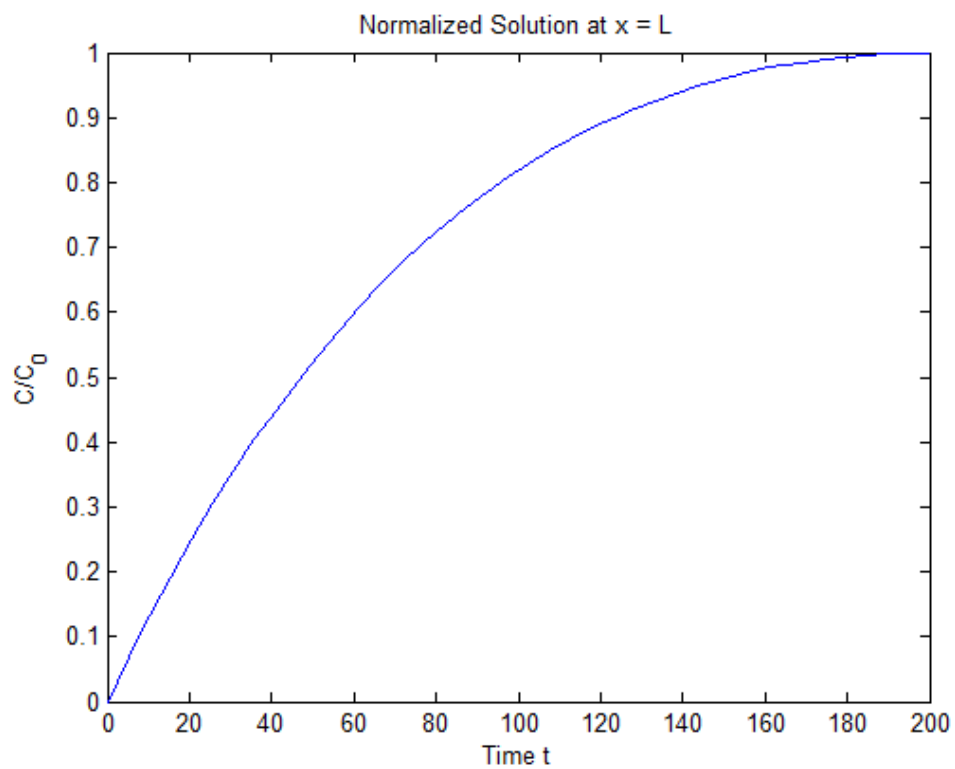


Figure 5.58 Simulated breakthrough curve (C/ C_0 versus t graph) - $C_{0,\text{Pb}}=50$ meq/L;
 $C_{0,\text{Na}}=0$ meq/L

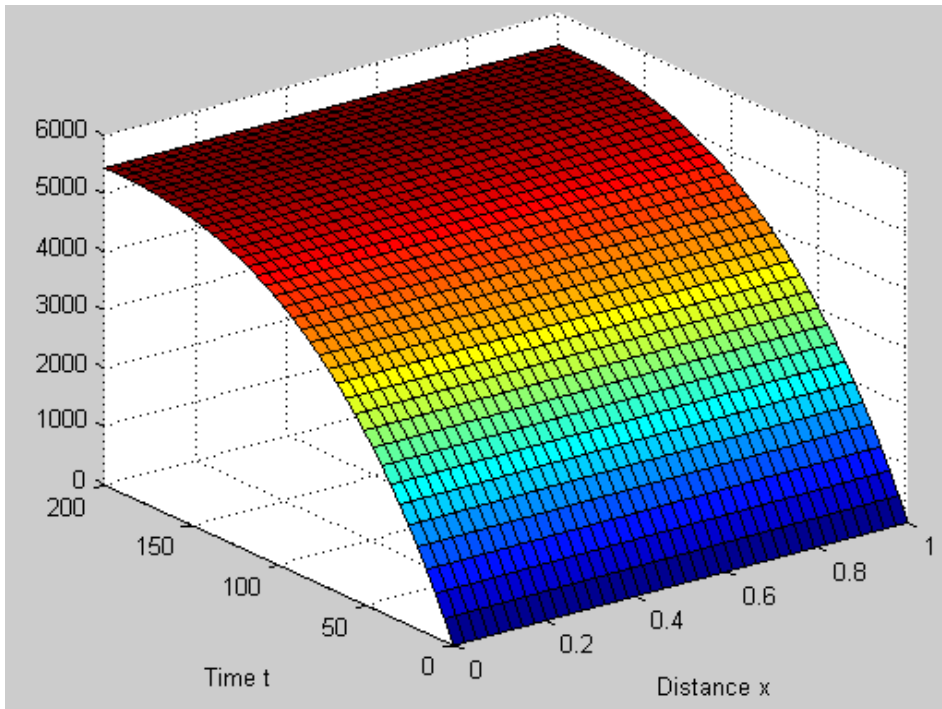


Figure 5.59 Simulated 3D Breakthrough curve (C versus t versus x graph) - $C_{0,Pb} = 50$ meq/L; $C_{0,Na} = 0$ meq/L

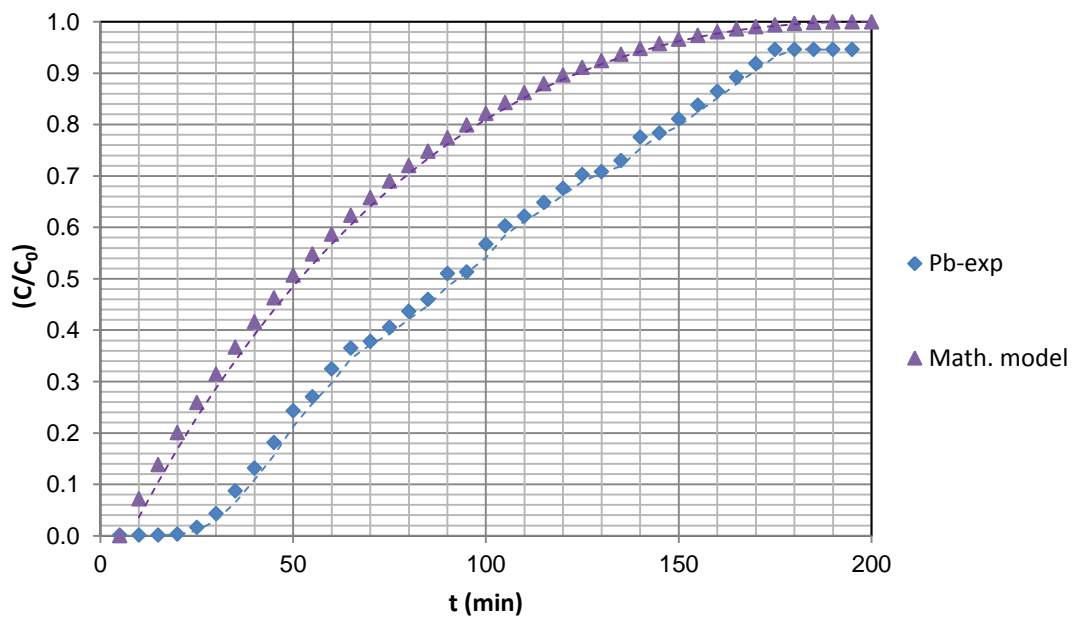


Figure 5.60 Comparison between simulated and experimental breakthrough curves - $C_{0,Pb} = 50$ meq/L; $C_{0,Na} = 0$ meq/L

CHAPTER 6

CONCLUSION

This study confirmed that synthetic Zeolite 13X in the form of beads can be used effectively in the process that removes lead, cadmium and zinc ions from solutions separately or at the same time by using ion exchange specifically at low initial concentrations and low flow rates.

Ion exchange of Pb^{2+} , Cd^{2+} and Zn^{2+} on to NaX zeolite was modelled by utilizing the Langmuir, Freundlich, Tempkin, DR, Redlich Peterson, Sips and BET isotherms. Among all the isotherms tested, Redlich Peterson isotherm gave the best fit for all metals with the highest R^2 and lowest ARE values.

The Modified Langmuir Model, Jain and Snoeyink Model, SRS Model, Extended SIPS Model and IAST Isotherm Models were used to model multicomponent ion exchange in Zeolite 13X beads; but only SRS Isotherm Model was observed to fit the batch data with highest linear coefficient of determination.

Pseudo-second order kinetic equation describes the batch system kinetics well. W&M model indicated that the intra particle diffusion was not the only rate limiting step. Intraparticle diffusion coefficients were determined as $15.26 \times 10^{-3} (mg/g.min^{-0.5})$ for Pb^{2+} -NaX binary exchange; $6.04 \times 10^{-3} (mg/g.min^{-0.5})$ for Cd^{2+} -NaX binary exchange and $6.04 \times 10^{-3} (mg/g.min^{-0.5})$ for Zn^{2+} -NaX binary exchange on Zeolite

13X beads. Pb^{2+} -NaX; Cd^{2+} -NaX and Zn^{2+} -NaX binary exchange pore diffusion coefficients were 1.14, 2.90 and 3.43 $\left(\frac{ml}{g/L}\right)$ respectively.

External mass transfer diffusion model fitted well to the Pb^{2+} - NaX binary exchange experimental data and external film mass transfer coefficient was determined as $1.2 \times 10^{-6} ((g/cm^2)min^{-1})$.

The standard free energy (ΔG) values were found to be -6.7 (kJ/mol) for Pb^{2+} -NaX; -6.4 (kJ/mol) for Cd^{2+} -NaX and -4.9 (kJ/mol) for Zn^{2+} -NaX which implied that ion exchange of Pb^{2+} , Zn^{2+} and Cd^{2+} onto Zeolite 13X beads was spontaneous.

The maximum exchange capacity for Pb^{2+} -NaX binary exchange on Zeolite 13X was calculated as 3.2 meq/g in column studies.

By comparing dynamic exchange in binary and systems, it was noticed that breakthrough capacities per cadmium and lead ions were bigger in binary column experiments than those values acquired in ternary column experiments. The cause for this was pointed out as the competitive action that happens in ternary studies among lead and cadmium ions for diffusing into the exchange channels inside the zeolite structure.

In ternary studies, it was concluded that a competition between Pb^{2+} and Cd^{2+} or Zn^{2+} ions for the exchange sites on Zeolite 13X was in favor of lead ions. It was also concluded that a competitive action between Zn^{2+} and Cd^{2+} ions for the exchange sites on Zeolite 13X was favorable for zinc ions.

Both binary and ternary column experiments revealed that the Zeolite 13X had more affinity for Pb^{2+} ions than that for Cd^{2+} or Zn^{2+} . Thus, it was deduced that the selectivity sequence for Zeolite 13X against the analyzed cations were as: $Pb^{2+} > Zn^{2+} > Cd^{2+} > Na^+$.

Possible mass transfer controlling mechanism in the column experiments was determined as solid diffusion using simplified diffusion models. Solid-phase diffusion coefficients were evaluated as 4.3×10^{-6} cm²/min for Pb²⁺- NaX binary exchange; 4.6×10^{-6} cm²/min for Cd²⁺- NaX binary exchange and 2.2×10^{-6} cm²/min for Zn²⁺- NaX binary exchange on Zeolite 13X beads.

Thomas model showed a good fit with the experimental results. Therefore it can be used in simulations of the breakthrough of Pb²⁺- NaX binary exchange at a flow rate 10 ml/min, initial concentration of 50 meq/L.

The simulated breakthrough curves given were not fitted well with the experimental data. This may be due to the external mass transfer resistances were not taken into account and Langmuir isotherm model was used in order to express the dynamic equilibrium data. Moreover, in the mathematical modeling the system was considered as single component and the effect of cations released by the zeolite beads were neglected.

REFERENCES

- Ahmed, S., Chughtai, Keane., M.A. The Removal of Cadmium and Lead from Aqueous Solution by ion exchange with Na-Y zeolite, *Separation and Purification Technology*, Vol. 13, 57-64, 1998.
- Al-Asheh, S., Banat, F., Al-Omari, R., Duvnjak, Z., Predictions of binary sorption isotherms for the sorption of heavy metals by pine bark using single isotherm data. *Chemosphere*, Vol. 41, 659-665, 2000.
- Angélica, M., Barros, S.D., Arroyo, P.A., Sousa-Aguiar, E.F., Tavares, Célia R.G. Multicomponent ion exchange isotherms in NaX zeolite: evaluation of Cr/Ca/Mg, Cr/Ca/K and Cr/Mg/K systems. *Journal of Chemical Technology and Biotechnology*., Vol. 83, 983–990, 2008.
- Aniceto, J.P.S, Fernandes, D.L.A, Silva, C.M., Modeling ion exchange equilibrium of ternary systems using neural networks, *Desalination*, Vol. 309, 267–274, 2013.
- Antoniadis, V., Tsadilas, C.D., Sorption of cadmium, nickel, and zinc in mono-and multimetal systems, *Applied Chemistry*, Vol. 22, 2375-2380, 2007.
- Baig, K.S., Doan, H.D., Wu, J., Multicomponent isotherms for biosorption of Ni²⁺ and Zn²⁺, *Desalination*, Vol. 249, 429–439, 2009.
- Barros, M.A.S.D., Zola, A.S., Arroya, P.A., Sousa-Aguiar, E.F., Tavares, C.R.G., Equilibrium and dynamic ion exchange studies of Cr³⁺ on zeolites NaA and NaX, *Acta Scientiarum, Maringá*, Vol. 24 (6), 1619-1625, 2002.

Barros, M.A.S.D., Zola, A.S., Arroyo, P.A., Sousa-Aguiar, E.F., Tavares, C.R.G., Binary ion exchange of metal ions in y and x zeolites, *Brazilian Journal of Chemical Engineering*. 20(4), 413 – 421, 2003.

Barros, M.A.S.D., Silva, E.A., Arroyo, P.A., Tavares, C.R.G., Schneider, R.M., Suszek, M., Sousa-Aguiar, E.F., Removal of Cr (III) in the fixed bed colyaumn and batch reactors using as adsorbent zeolite NaX., *Chemical Engineering Science*, Vol. 59, 5959-5966, 2004.

Barros, M.A.S.D., Zola, A.S., Arroyo, P.A., Tavares, C. R. G., Sousa-Aguiar, E. F. Chromium uptake from tricomponent solution in zeolite fixed bed, *Adsorption*, Vol. 12, 239-248, 2006.

Barros, M.A.S.D., Arroyo, P.A., Sousa-Aguiar, E.F., Tavares, Célia R.G. Multicomponent ion exchange isotherms in NaX zeolite: evaluation of Cr/Ca/Mg, Cr/Ca/K and Cr/Mg/K systems, *Journal of Chemical Technology and Biotechnology*., Vol. 83, 983–990, 2008.

Besedova, E., Bobok, D., Single-Component and Binary Adsorption Equilibrium of 1,2-Dichloroethane and 1,2-Dichloropropane on Activated Carbon, *Petroleum & Coal*, Vol. 47, 2, 47-54, 2005.

Bohart, G.S., Adams, E.Q., Some aspects of the behavior of charcoal with respect to chlorine, *Journal of the American Chemical Society*, Vol. 42, 523-544, 1920.

Boparai, H.K., Joseph, M., O'Carroll, D.M., Kinetics and thermodynamics of cadmium ion removal by adsorption onto nano zerovalent iron particles, *Journal of Hazardous Materials*, Vol. 186, 458–465, 2011.

Borba, C.E., Santos, G.H.F., Silva E.A., Mathematical modeling of a ternary Cu-Zn-Na ion exchange system in a fixed bed column using Amberlite IR 120, *Chemical Engineering Journal*, Vol. 189-190, 49-56, 2012.

Cejka, J., Corma, A., and Zones, S., *Zeolites and Catalysis: Synthesis, Reactions and Applications*, 2010.

Dada A.O., Olalekan, A.P., Olatunya, A.M., Dada, O., Langmuir, Freundlich, Temkin and Dubinin-Radushkevich Isotherms Studies of Equilibrium Sorption of Zn^{2+} Unto Phosphoric Acid Modified Rice Husk, *IOSR Journal of Applied Chemistry*, Vol. 3, Issue 1, 2278-5736, 2012.

Dean, J.A., 1999., *Lange's Handbook of Chemistry*, Mc Graw Hill, New York,

Farajpourlar, M., Rao, R.M., Rao, V.V.B., Studies on Fixed and Fluidized Bed Ion Exchange Column to Treat Wastewater, *IOSR Journal of Environmental Science, Toxicology and Food Technology*, Vol. 6, Issue 1, 1-6, 2013

Franklin, K.R., Townsend, R., Multicomponent Ion Exchange in Zeolites Part 2 .- Prediction of Exchange Equilibria over a Range of Solution Concentrations, *Journal of the Chemical Society, Faraday Transactions I: Physical Chemistry in Condensed Phases*, Vol. 81(12), 3127-3141, 1985.

Gorká, A., Bochenek, R., Warchoń, J., Kaczmarski, K., Antos, D., Ion exchange kinetics in removal of small ions. Effect of salt concentration on inter- and intraparticle diffusion, *Chemical Engineering Science*, Vol. 63, 637-650, 2008.

Grzybkowski, W., Nature and Properties of Metal Cations in Aqueous Solutions, *Polish Journal of Environ. Stud.*, Vol. 15, No.4, 655-663, 2006.

Harland, C.E., *Ion Exchange: Theory and Practice*, Royal Society of Chemistry Paperbacks, UK, 1994.

Hamdaoui, O., Naffrechoux, E., Modeling of adsorption isotherms of phenol and chlorophenols onto granular activated carbon Part II. Models with more than two parameters. *Journal of Hazardous Materials*, Vol. 147, 401-411, 2007.

Hameed, B.H., Foo, K.Y., Insights into the modeling of adsorption isotherm systems, *Chemical Engineering Journal*, Vol. 156, 2–10, 2010.

Helfferich, 1962, F.G., *Ion Exchange*, Mc Graw Hill, New York, 1962.

Ho, Y.S., McKay, G., Correlative biosorption equilibria model for a binary batch system, *Chemical Engineering Science*, Vol. 55, 817-825, 2000.

Ho, Y.S., Porter, J.F., McKay, G., Equilibrium isotherm studies for the sorption of divalent metal ions onto peat: copper, nickel and lead single component systems, *Water, Air and Soil Pollution*, Vol. 141: 1-33, 2002.

Igwe, J.C., Abia, A.A., Equilibrium sorption isotherm studies of Cd(II), Pb(II) and Zn(II) ions detoxification from waste water using unmodified and EDTA-modified maize husk, *Electronic Journal of Biotechnology*, Vol.10 No.4, 536-548, 2007.

Inglezakis, V.J., Loizidou, M.D., Grigoropoulou, H.P., Ion exchange of Pb^{2+} , Cu^{2+} , Fe^{3+} , and Cr^{3+} on natural clinoptilolite: selectivity determination and influence of acidity on metal uptake, *Journal of Colloid and Interface Science*, Vol. 261, 49–54, 2003.

Inglezakis, V.J., Pouloupoulos, *Adsorption, ion exchange, and catalysis: Design of operations and environmental applications*, 2006, Elsevier, Boston.

Itodo, A.U., Itodo, H.U, Utilizing D-R and Temkin isotherms with GCMS external standard technique in forecasting liquid phase herbicide sorption energies, *EJEAFChe*, Vol. 9(11), 1792-1802, 2010.

Juang, Ruey-Shin., Wu, Feng-Chin., Tseng, Ru-Ling., Adsorption Isotherms of Phenolic Compounds From Aqueous Solutions Onto Activated Carbon Fibers, *Journal of Chemical and Engineering Data*, Vol. 41, No. 3, 487-492, 1996.

Kirk-Othmer Encyclopedia of Chemical Technology: Wiley InterScience, 2010.

Lagergren, S., About the theory of so-called adsorption of soluble substances, *Kungliga Svenska Vetenskapsakademiens, Handlingar*, Vol. 24, No. 4, 1-39, 1898.

Lee, I.H., Kuan, Yu-Chung, Chern, Jia-Ming, Prediction of ion-exchange column breakthrough curves by constant-pattern wave approach, *Journal of Hazardous Materials*, Vol. 152, 241–249, 2008.

Mier, M.V., Callejas, R.L., Gehr, R., Cisneros, B.E.J., Alvarez, P.J.J., Heavy Metal Removal With Mexican Clinoptilolite: Multi-Component Ionic Exchange., *Wat. Res.* Vol. 35, No.2, pp. 373-378, 2001.

Mumford, K.A., Shallcross, D.C., Snape, I., Stevens, G.W., Application of a Temperature-Dependent Semiempirical Thermodynamic Ion-Exchange Model to a Multicomponent Natural Zeolite System, *Ind. Eng. Chem. Res.*, Vol. 47, 8347–8354, 2008.

Nagarale, R.K., Gohil, G.S., Shaki, V.K., Recent developments on ion-exchange membranes and electro-membrane processes, *Advances in Colloid and Interface Science*, Vol. 119, Issues 2–3, Pages 97–130, 2006.

Ostroski, I.C., Barros M.A.S.D., Silva, E.A., Dantas, J.H., Arroyo, P.A., Lima, O.C.M., A comparative study for the ion exchange of Fe(III) and Zn(II) on zeolite NaY, *Journal of Hazardous Materials*, Vol. 161, 1404–1412, 2009.

Ostroski, I.C., Dantas, J.H., Silva, E.A., Arroyo, P.A., Barros M.A.S.D., Competing Ion Exchange of Zn^{2+} and Fe^{3+} in NaY Zeolite: A comparative study for the ion exchange of Fe(III) and Zn(II) on zeolite NaY, *Adsorption Science & Technology*, Vol.30, No.4., 275-291, 2012.

Payne, K.B., Abdel-Fattah, T.M., Adsorption of divalent lead ions by zeolites and activated carbon: Effects of pH, temperature and ionic strength, *Journal of Environmental Science and Health Part A-Toxic/Hazardous Substances & Environmental Engineering*, Vol. A39, No.9., 2275-2291, 2004.

Pehlivan, E., Altun, T., Ion-exchange of Pb^{2+} , Cu^{2+} , Zn^{2+} , Cd^{2+} , and Ni^{2+} ions from aqueous solution by Lewatit CNP 80, *Journal of Hazardous Materials*, Vol. 140, 299–307, 2007.

Perry, R.T., Green, D.W., Perry's Chemical Engineering Handbook, 8th Edition, McGraw-Hill New York, 2008.

Rajoriya, R.K., Prasad, B., Mishra, I.M., Wasewar, K.L., Adsorption of benzaldehyde on granular activated carbon: kinetics, equilibrium, thermodynamic, *Chem. Biochem. Eng. Q.* Vol. 21 (3), 219-226, 2007.

Robinson, S.M., Arnold, W.D., Byers, C.H., Mass-transfer mechanisms for zeolite ion exchange in wastewater treatment, *AIChE Journal, Environment and Energy Engineering*, Vol. 40, No.12. 2045-2054, 1994.

Ruthven, D.M., Principles of Adsorption and Adsorption Processes, John Wiley and Sons, Inc., 1984.

Sheinford, C., Rebhun, M., Sheintuch, M. A Freundlich-type multicomponent isotherm, *Journal of Colloid and Interface Science*, Vol.79, No.1, 136-142, 1981.

Shahmohammadi-Kalalagh, S., Babazadeh, H., Nazemi, A.H., Manshour, M. Isotherm and Kinetic Studies on Adsorption of Pb, Zn and Cu by Kaolinite, *Caspian J. Env. Sci.*, Vol. 9 No.2, 243-255, 2011.

Shebil, S.B., Sungur, A.A., Ozdural, A.R., Fixed-bed ion exchange columns operating under non-equilibrium conditions: estimation of mass transfer properties via non-equilibrium modelling, *Reactive & Functional Polymers*, Vol. 67, 1540-1547, 2007.

Shehata, F.A., El-Kamash, A.M., El-Sorougy, M.R., Aly, H.F., Prediction of multicomponent ion-exchange equilibria for a ternary system from data of binary systems, *Separation Science and Technology*, Vol. 35(12), 1887-1900, 2000.

Sprynskyy, M., Buszewski, B., Terzyk, A.P., Namiéśnik, J., Study of the selection mechanism of heavy metal (Pb^{2+} , Cu^{2+} , Ni^{2+} , and Cd^{2+}) adsorption on clinoptilolite, *Journal of Colloid and Interface Science*, Vol. 304, 21–28, 2006.

Trgo, M., Perić, J., Medvidović, N.V., A comparative study of ion Exchange kinetics in zinc/lead – modified zeolite-clinoptilolite systems, *Journal of Hazardous Materials*, Vol. 136, 938-945, 2006.

Urano, K., Tachikawa, H., Process development for removal and recovery of phosphorus from wastewater by a new adsorbent. II. Adsorption rates and breakthrough curves, *Industrial and Engineering Chemistry Research*, Vol. 30(8):1897-1899, 1991.

Valverde, J.L., Lucas, A., Rodriguez, J.F., Comparison between Heterogeneous and Homogeneous Mass Action Models in the Prediction of Ternary Ion Exchange Equilibria, *Industrial and Engineering Chemistry Research*, Vol.38, 251-259, 1999.

Weber, W.J. and Morris, J.C., Kinetics of Adsorption on Carbon from Solution, *J. Sanit. Eng. Div. ASCE*, Vol. 89, 31-59, 1963.

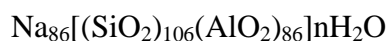
Yoon, Y.H., Nelson, J.H., Application of gas adsorption kinetics-II.A theoretical model for respirator cartridge service life and its practical applications, *American Industrial Hygiene Association Journal*, Vol. 45, Issue 8, pages 517-524, 1984.

Zagorodni, Andrei A., Ion Exchange Materials: Properties and Applications, Elsevier, London, 2007.

APPENDIX A

CALCULATION OF EXCHANGE CAPACITIES

The commercial zeolite NaX (13X) had the following chemical formula:



Atomic weights of the atoms in the zeolite content

$$\text{Na} = 22.9898 \text{ g/mol}$$

$$\text{Si} = 28.0855 \text{ g/mol}$$

$$\text{Al} = 26.9815 \text{ g/mol}$$

$$\text{O} = 15.9994 \text{ g/mol}$$

$$\text{H} = 1.0079 \text{ g/mol}$$

Molecular weight of the zeolite

$$= (86x\text{Na}) + (106x\text{Si}) + (86x\text{Al}) + (384x\text{O}) + nx(2x\text{H} + \text{O})$$

$$= (86x22.9898) + (106x28.0855) + (86x26.98154) + (384x15.9994) + nx(2x1.0079 + 15.9994)$$

$$= 13418.3678 + nx18.0512$$

TGA analysis was done in order to find out the water content of the zeolite. Moisture content of the zeolite was found as 22.035 wt % from TGA analysis (Figure A.1.). So

$$22.035 = \frac{n \times 18.0512}{13418.36784 + n \times 18.0512} \times 100$$

$$n = 210.09$$

Having obtained the value of n, the molecular weight of the zeolite calculated as:

$$\text{MW}_{\text{zeolite (hydrated)}} = 13418.36784 + 210.09 \times 18.0512 = 17210.75847 \text{ g/mol}$$

By taking 86 mol Na per formula weight,

$$\text{Exchange capacity} = \frac{86 \times 10^3 \text{ meq/mol}}{17210.75847 \text{ g/mol}} = 4.99687 \frac{\text{meq}}{\text{g}} \quad (\text{A. 1})$$

$$\text{MW}_{\text{zeolite (unhydrated)}} = 13418.36784 \text{ g/mol}$$

$$\text{Exchange capacity} = \frac{86 \times 10^3 \text{ meq/mol}}{13418.36784 \text{ g/mol}} = 6.409 \frac{\text{meq}}{\text{g}} \quad (\text{A. 3})$$

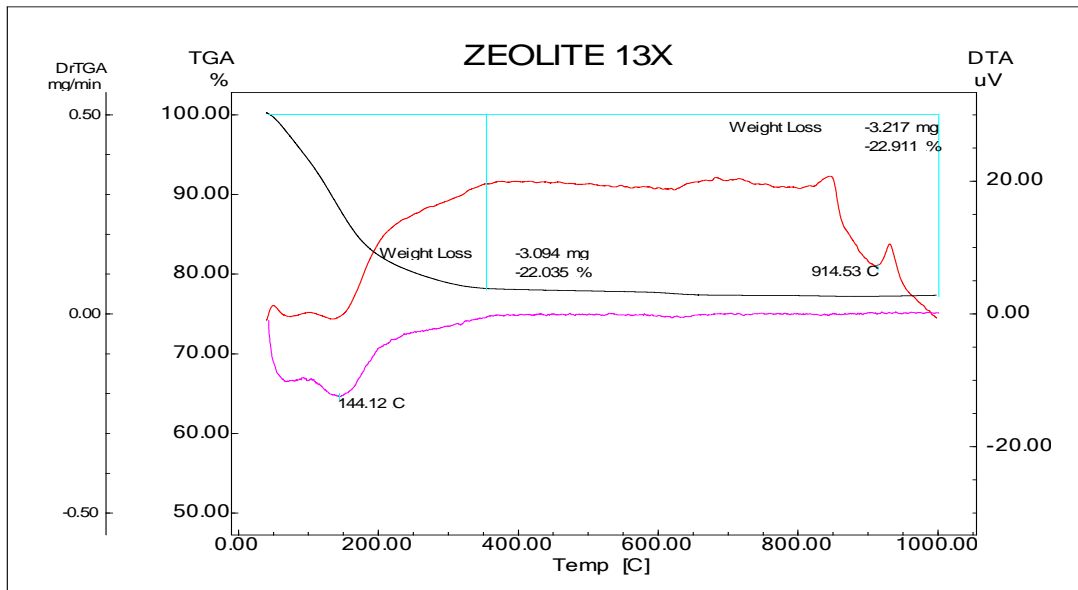


Figure A.1. TGA of commercial zeolite 13X beads.

APPENDIX B

MAXIMUM EXCHANGE LEVEL (MEL) DATA

Table B.1. Total exchange capacity results for Pb²⁺- NaX and Cd²⁺- NaX exchange on Zeolite13X beads at 0.1N total concentration

Sample Weight	Pb concentration at equilibrium (mg/L)	Cd concentration at equilibrium (mg/L)	Pb-Na Capacity (meq/g)	Cd-Na Capacity (meq/g)
0.2	7262.0	3618.6	7.5	8.9
0.4	6387.0	1691.2	4.8	8.7
0.6	3775.0	2611.0	5.3	4.5
0.8	928.0	227.6	5.7	6.0
0.8	19.3	1384.0	6.2	4.7
1.0	7.7	1645.8	5.0	3.5

Table B.2. Total exchange capacity results for Pb²⁺ - NaX and Cd²⁺ - NaX exchange on Zeolite13X beads at 0.05N total concentration

Sample Weight	Pb concentration at equilibrium (mg/L)	Cd concentration at equilibrium (mg/L)	Pb-Na Capacity (meq/g)	Cd-Na Capacity (meq/g)
0.2	1289.4	1540.4	9.4	5.6
0.4	915.5	723.2	5.1	4.6
0.6	48.1	225.4	4.1	3.8
0.8	13.5	58.9	3.1	3.1
0.8	17.3	68.3	3.1	3.1
1.0	5.8	9.2	2.5	2.5

Table B.3. Total exchange capacity results for Pb²⁺ - NaX, Cd²⁺ - NaX and Zn²⁺ - NaX exchange Zeolite13X beads at 0.05N total concentration and 0.8 g sample weight

Metal ions	Concentration at equilibrium (mg/L)	Cation exchange Capacity (meq/g)
Pb ²⁺	2.1	3.1
	9.5	3.1
Cd ²⁺	11.0	3.1
	5.0	3.1
Zn ²⁺	160.0	2.8
	136.0	2.9

APPENDIX C

SINGLE COMPONENT ION EXCHANGE ISOTHERM DATA

Table C.1. Pb²⁺- NaX binary exchange on zeolite 13X beads at 25 °C

Experiment No	Co (N)	Co (ppm)	C* (ppm)	Co-C* (ppm)	q*=V(Co-C*)/m (mg/g)
SI1	0.01	1036.0	0.0	1035.9	64.7
SI2	0.02	2072.0	0.3	2071.7	129.5
SI3	0.03	3108.0	0.7	3107.3	194.2
SI4	0.04	4144.0	0.7	4143.3	259.0
SI5	0.05	5180.0	15.0	5165.0	322.8
SI6	0.06	6216.0	29.5	6186.5	386.7
SI7	0.07	7252.0	85.0	7167.0	447.9
SI8	0.08	8288.0	459.5	7828.5	489.3
SI9	0.09	9324.0	613.0	8711.0	544.4
SI10	0.10	10360.0	813.7	9546.2	596.6

Table C.2. Cd²⁺ - NaX binary exchange on zeolite 13X beads at 25 °C

Experiment No	Co (N)	Co (ppm)	C* (ppm)	Co-C* (ppm)	q*=V(Co-C*)/m (mg/g)
SI11	0.01	562.0	0.1	561.9	35.1
SI12	0.02	1124.1	0.7	1123.4	70.2
SI13	0.03	1686.1	14.9	1671.2	104.4
SI14	0.04	2248.2	51.9	2196.2	137.3
SI15	0.05	2810.2	183.1	2627.1	164.2
SI16	0.06	3372.3	225.3	3147.0	196.7
SI17	0.07	3934.3	604.2	3330.1	208.1
SI18	0.08	4496.4	1070.0	3426.4	214.1
SI19	0.09	5058.4	1274.7	3783.7	236.5
SI20	0.10	5620.5	1807.2	3813.3	238.3

Table. C.3. Zn²⁺ - NaX binary exchange on zeolite 13X beads at 25 °C

Experiment No	Co (N)	Co (ppm)	C* (ppm)	Co-C* (ppm)	q*=V(Co-C*)/m (mg/g)
SI21	0.01	326.9	16.7	310.1	19.4
SI22	0.02	653.8	63.1	590.7	36.9
SI23	0.03	980.7	144.4	836.3	52.3
SI24	0.04	1307.6	255.0	1052.6	65.8
SI25	0.05	1634.5	642.3	992.2	62.0
SI26	0.06	1961.4	688.8	1272.6	79.5
SI27	0.07	2288.3	888.8	1399.5	87.5
SI28	0.08	2615.2	1183.6	1431.6	89.5
SI29	0.09	2942.1	1219.8	1722.3	107.6
SI30	0.10	3269.0	1441.1	1827.9	114.2

APPENDIX D

MULTI COMPONENT ION EXCHANGE ISOTHERM DATA

Table D.1. Pb²⁺ - Cd²⁺ - NaX ternary exchange on Zeolite 13X beads at 25 °C

Run No	Metal Ions	Co (N)	Co (ppm)	C* (ppm)	Co-C* (ppm)	q*=V(Co-C*)/m (mg/g)
MI1	Pb ²⁺	0.01	1036.0	10.0	1026.0	64.1
	Cd ²⁺	0.09	5058.4	1582.3	3476.1	217.3
MI2	Pb ²⁺	0.02	2072.0	35.3	2036.6	127.3
	Cd ²⁺	0.08	4496.4	1460.5	3035.9	189.7
MI3	Pb ²⁺	0.03	3108.0	59.5	3048.5	190.5
	Cd ²⁺	0.07	3934.3	1361.9	2572.4	160.8
MI4	Pb ²⁺	0.04	4144.0	90.2	4053.8	253.4
	Cd ²⁺	0.06	3372.3	1343.6	2028.7	126.8
MI5	Pb ²⁺	0.05	5180.0	145.2	5034.8	314.7
	Cd ²⁺	0.05	2810.2	1276.0	1534.2	95.9
MI6	Pb ²⁺	0.06	6216.0	508.3	5707.6	356.7
	Cd ²⁺	0.04	2248.2	857.1	1391.1	86.9
MI7	Pb ²⁺	0.07	7252.0	701.1	6550.9	409.4
	Cd ²⁺	0.03	1686.1	814.6	871.5	54.5
MI8	Pb ²⁺	0.08	8288.0	787.4	7500.6	468.8
	Cd ²⁺	0.02	1124.1	714.4	409.7	25.6
MI9	Pb ²⁺	0.09	9324.0	888.7	8435.3	527.2
	Cd ²⁺	0.01	562.0	395.7	166.3	10.4

Table D.1 (cont'd). Pb²⁺- Cd²⁺ - NaX ternary exchange on Zeolite 13X beads at 25 °C

MI10	Pb ²⁺	0.10	10360.0	1022.4	9337.6	583.6
	Cd ²⁺	0.00	0.00	0.00	0.00	0.00

Table D.2. Pb²⁺- Zn²⁺ - NaX ternary exchange on Zeolite 13X beads at 25 °C

Run No	Metal Ions	Co (N)	Co (ppm)	C* (ppm)	Co-C* (ppm)	q*=V(Co-C*)/m (mg/g)
MI11	Pb ²⁺	0.01	1036.0	6.3	1029.7	64.4
	Zn ²⁺	0.09	2942.1	1190.8	1751.3	109.5
MI12	Pb ²⁺	0.02	2072.0	20.6	2051.4	128.2
	Zn ²⁺	0.08	2615.2	1034.6	1580.6	98.8
MI13	Pb ²⁺	0.03	3108.0	55.6	3052.4	190.8
	Zn ²⁺	0.07	2288.3	1024.7	1263.6	79.0
MI14	Pb ²⁺	0.04	4144.0	56.2	4087.7	255.5
	Zn ²⁺	0.06	1961.4	879.7	1081.7	67.6
MI15	Pb ²⁺	0.05	5180.0	313.0	4867.0	304.2
	Zn ²⁺	0.05	1634.5	758.8	875.7	54.7
MI16	Pb ²⁺	0.06	6216.0	420.9	5795.1	362.2
	Zn ²⁺	0.04	1307.6	561.8	745.8	46.6
MI17	Pb ²⁺	0.07	7252.0	625.1	6626.9	414.2
	Zn ²⁺	0.03	980.7	457.6	523.1	32.7
MI18	Pb ²⁺	0.08	8288.0	653.2	7634.8	477.2
	Zn ²⁺	0.02	653.8	449.8	204.0	12.7
MI19	Pb ²⁺	0.09	9324.0	816.5	8507.5	531.7
	Zn ²⁺	0.01	326.9	204.9	122.0	7.6
MI20	Pb ²⁺	0.10	10360.0	852.8	9507.20	594.20
	Zn ²⁺	0.00	0.00	0.00	0.00	0.00

Table D.3. Zn²⁺ - Cd²⁺ - NaX ternary exchange on Zeolite 13X beads at 25 °C

Run No	Metal Ions	Co (N)	Co (ppm)	C* (ppm)	Co-C* (ppm)	q*=V(Co-C*)/m (mg/g)
MI21	Zn ²⁺	0.01	326.9	102.4	224.5	14.03
	Cd ²⁺	0.09	5058.4	1683.9	3374.5	210.9
MI22	Zn ²⁺	0.02	653.8	237.2	416.6	26.0
	Cd ²⁺	0.08	4496.4	1557.2	2939.2	183.7
MI23	Zn ²⁺	0.03	980.7	326.2	654.5	40.9
	Cd ²⁺	0.07	3934.4	1239.3	2695.0	168.4
MI24	Zn ²⁺	0.04	1307.6	492.4	815.2	50.9
	Cd ²⁺	0.06	3372.3	1110.6	2261.7	141.4
MI25	Zn ²⁺	0.05	1634.5	602.3	1032.2	64.5
	Cd ²⁺	0.05	2810.2	852.0	1958.2	122.4
MI26	Zn ²⁺	0.06	1961.4	700.8	1260.6	78.8
	Cd ²⁺	0.04	2248.2	641.5	1606.7	100.4
MI27	Zn ²⁺	0.07	2288.3	921.3	1367.0	85.4
	Cd ²⁺	0.03	1686.1	438.4	1247.7	78.0
MI28	Zn ²⁺	0.08	2615.2	962.3	1652.9	103.3
	Cd ²⁺	0.02	1124.1	247.9	876.2	54.8
MI29	Zn ²⁺	0.09	2942.1	1107.0	1835.1	114.7
	Cd ²⁺	0.01	562.0	92.1	469.9	29.4
MI30	Zn ²⁺	0.10	3269.0	1167.5	2101.5	131.3
	Cd ²⁺	0.00	0.00	0.00	0.00	0.00

Table D.4. Pb²⁺ - Zn²⁺ - Cd²⁺ - NaX quaternary exchange on Zeolite 13X beads.

Run No	Metal Ions	Co (N)	Co (ppm)	C* (ppm)	Co-C* (ppm)	q*=V(Co-C*)/m (mg/g)
MI31	Pb ²⁺	0.010	1036.0	35.8	1000.1	62.5
	Cd ²⁺	0.045	2529.2	730.9	1798.3	112.4
	Zn ²⁺	0.045	1471.0	642.0	829.0	51.8
MI32	Pb ²⁺	0.020	2072.0	67.8	2004.2	125.3
	Cd ²⁺	0.040	2248.2	617.4	1630.8	101.9
	Zn ²⁺	0.040	1307.6	595.1	712.5	44.5
MI33	Pb ²⁺	0.030	3108.0	128.9	2979.1	186.2
	Cd ²⁺	0.035	1967.2	595.7	1371.5	85.7
	Zn ²⁺	0.035	1144.1	555.	589.1	36.8
MI34	Pb ²⁺	0.040	4144.0	343.0	3801.0	237.6
	Cd ²⁺	0.030	1686.1	570.8	1115.3	69.7
	Zn ²⁺	0.030	980.7	535.8	444.9	27.8
MI35	Pb ²⁺	0.050	5180.0	376.9	4803.1	300.2
	Cd ²⁺	0.025	1405.1	537.4	867.7	54.2
	Zn ²⁺	0.025	817.2	514.4	302.8	18.9
MI36	Pb ²⁺	0.060	6216.0	509.6	5706.3	356.6
	Cd ²⁺	0.020	1124.1	514.7	609.4	38.1
	Zn ²⁺	0.020	653.8	424.7	229.1	14.3
MI37	Pb ²⁺	0.080	7252.0	888.5	6363.5	397.7
	Cd ²⁺	0.015	843.1	385.4	457.7	28.6
	Zn ²⁺	0.015	490.3	329.8	160.5	10.
MI38	Pb ²⁺	0.080	8288.0	1062.9	7225.1	451.6
	Cd ²⁺	0.010	562.0	217.8	344.2	21.5
	Zn ²⁺	0.010	326.9	191.6	135.2	8.4
MI39	Pb ²⁺	0.090	9324.0	1220.8	8103.1	506.4
	Cd ²⁺	0.005	281.0	128.5	152.5	9.5
	Zn ²⁺	0.005	163.4	111.4	52.0	3.2
MI40	Pb ²⁺	0.100	10360.0	1748.5	8611.5	538.2
	Cd ²⁺	0.000	0.00	0.00	0.00	0.00
	Zn ²⁺	0.000	0.00	0.00	0.00	0.00

APPENDIX E

ION EXCHANGE BATCH KINETICS DATA

Table E.1. Kinetics for Pb²⁺-NaX binary exchange on Zeolite 13X at 0.05N

Time (min)	C _t (ppm)	q _t =V(C _o -C)/m (mg/g)
5.0	5050.2	38.9
10.0	4890.6	85.0
15.0	4810.9	106.1
20.0	4699.1	135.2
30.0	4600.4	159.4
45.0	4588.1	159.1
60.0	4395.9	205.8
90.0	4284.1	229.6
120.0	4220.0	240.0
150.0	4109.1	261.0
180.0	3990.8	282.4
210.0	3933.2	288.3
500.0	3890.0	290.2
1000.0	3890.0	290.2
1620.0	3890.0	290.2

Table E.2. Kinetics for Cd²⁺-NaX binary exchange on Zeolite 13X beads at 0.05N

Time (min)	C _t (ppm)	q _t =V(C ₀ -C)/m (mg/g)
5.0	2222.5	7.8
10.0	2047.1	59.2
15.0	2033.6	61.8
20.0	1987.9	73.3
30.0	1920.6	90.2
45.0	1920.1	88.3
60.0	1827.7	110.5
90.0	1784.1	119.0
120.0	1740.0	127.1
150.0	1711.8	130.8
180.0	1695.9	131.2
210.0	1650.0	138.4
500.0	1572.0	152.2
1000.0	1572.0	152.2
1620.0	1572.3	152.1

Table E.3. Kinetics for Zn²⁺-NaX binary exchange on Zeolite 13X beads at 0.05N

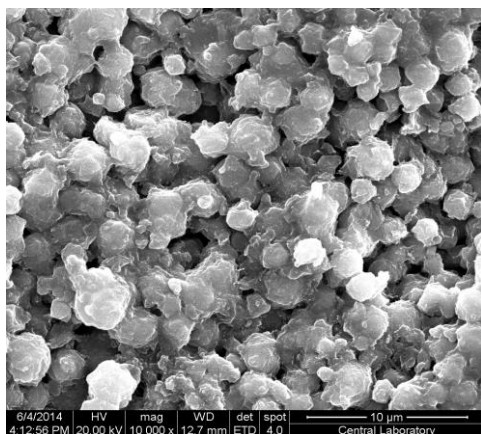
Time (min)	C _t (ppm)	q _t =V(C ₀ -C)/m (mg/g)
5.00	1230.5	23.1
10.00	1205.9	29.9
15.00	1134.6	49.7
20.00	1088.8	61.5
30.00	1088.2	60.3
45.00	1054.8	67.9
60.00	1044.2	69.1
90.00	1020.9	73.5
120.00	1019.4	72.0
150.0	1009.9	72.6
180.0	992.2	74.9
210.0	979.0	76.0
500.0	944.6	81.7
1000.0	944.6	81.7
1620.0	944.6	81.7

APPENDIX F

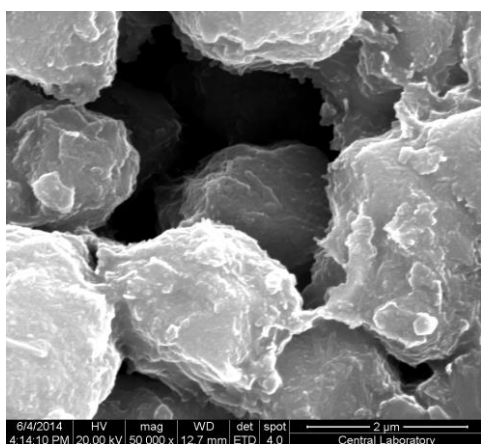
SEM and EDX RESULTS

1. Weight % Pb/Cd = 0.67

(Sample from Experiment Run No:MI2 of Table D.1)



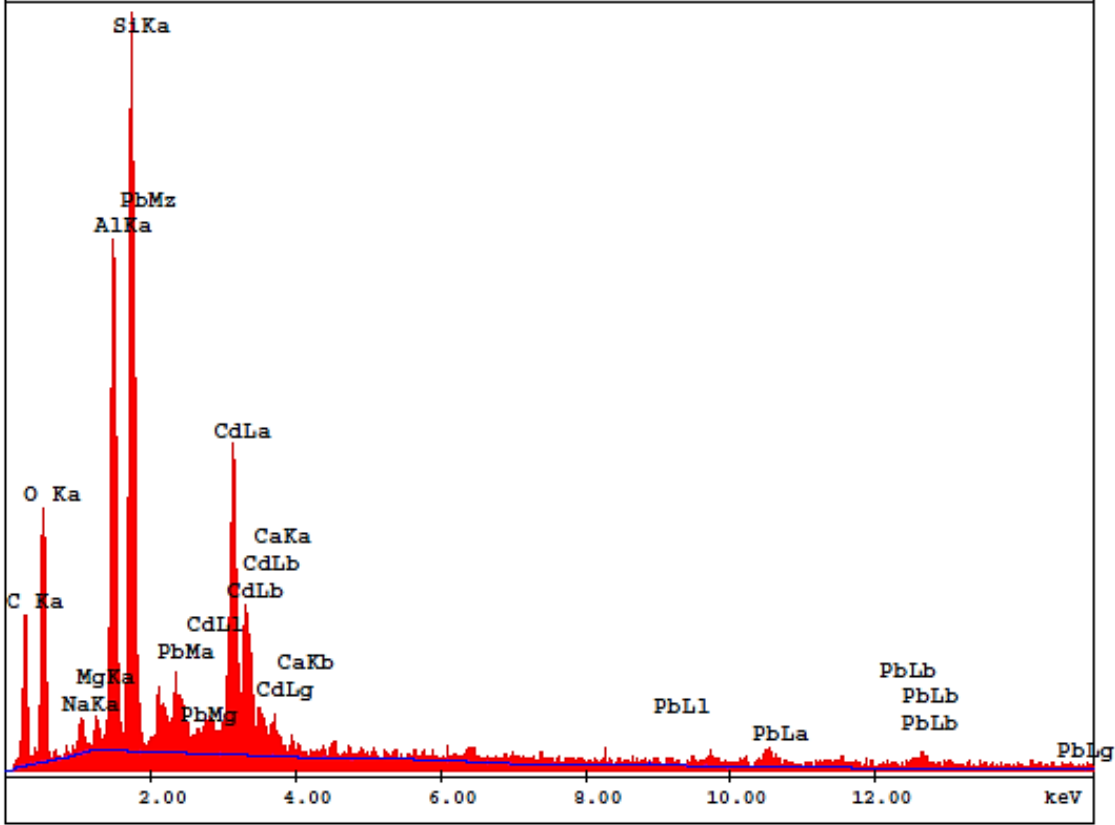
(a)



(b)

Figure F.1 (a) SEM Image of zeolite crystals in the Zeolite 13X beads (magnification: 10000x), (b) SEM Image of zeolite crystals in the Zeolite 13X beads (magnification: 50000x) for the Pb^{2+} - Cd^{2+} -NaX ternary ion exchange system.

c:\edax32\genesis\genspc.spc
 Label:
 kV:30.0 Tilt:0.0 Take-off:34.7 Det Type:SUTW+ Res:129 Amp.T:51.2
 FS : 803 Lsec : 17 4-Jun-2014 16:31:10



EDAX ZAF Quantification (Standardless)
 Element Normalized
 SEC Table : Default

Element	Wt %	At %	K-Ratio	Z	A	F
C K	30.88	50.20	0.0645	1.0584	0.1974	1.0002
O K	23.22	28.34	0.0358	1.0434	0.1476	1.0003
NaK	1.17	0.99	0.0029	0.9801	0.2556	1.0033
MgK	0.67	0.54	0.0024	1.0058	0.3506	1.0063
AlK	9.46	6.85	0.0439	0.9772	0.4709	1.0069
SiK	14.01	9.74	0.0698	1.0067	0.4936	1.0025
CdL	14.96	2.60	0.1177	0.7941	0.9907	1.0004
CaK	0.51	0.25	0.0039	0.9829	0.7670	1.0000
PbL	5.11	0.48	0.0390	0.7135	1.0689	1.0000
Total	100.00	100.00				

Figure F.2 EDX analysis of Pb²⁺-Cd²⁺-NaX ternary ion exchange system

2. Weight % Pb/Cd = 18.30

(Sample from Experiment Run No:MI8 of Table D.1)

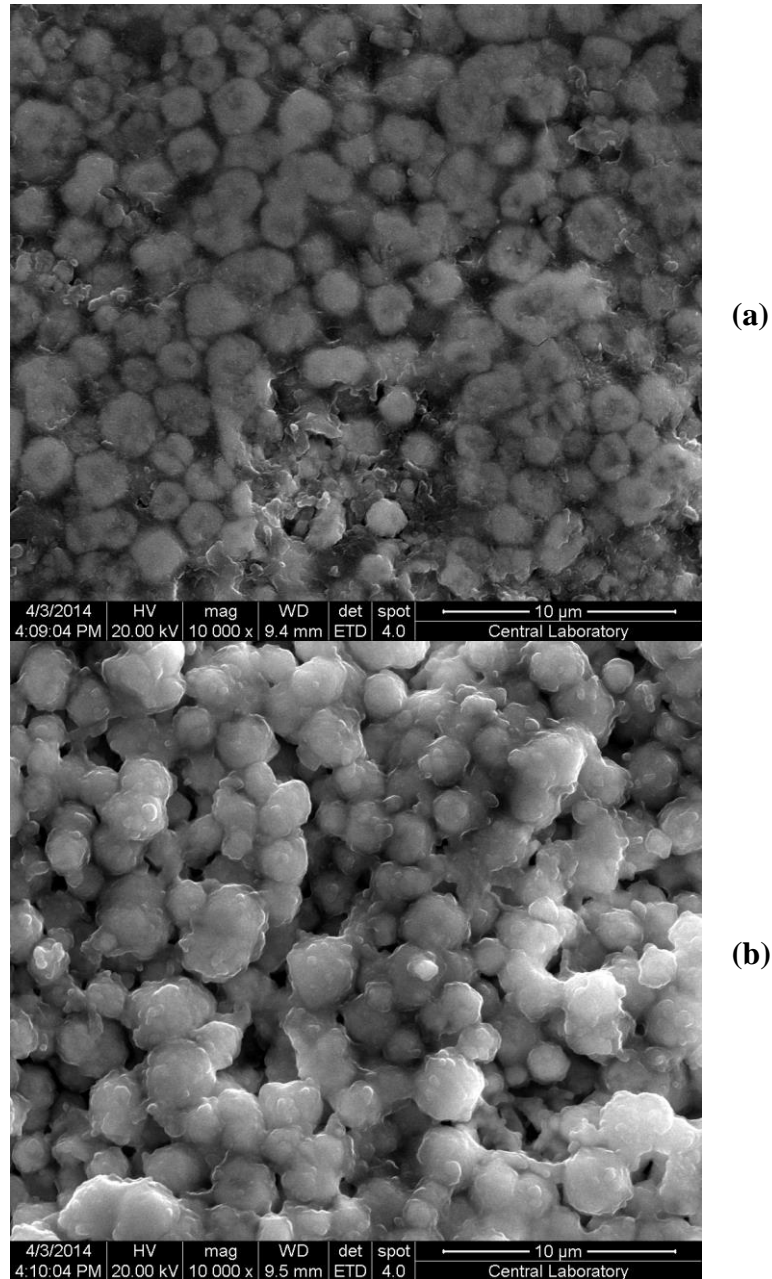
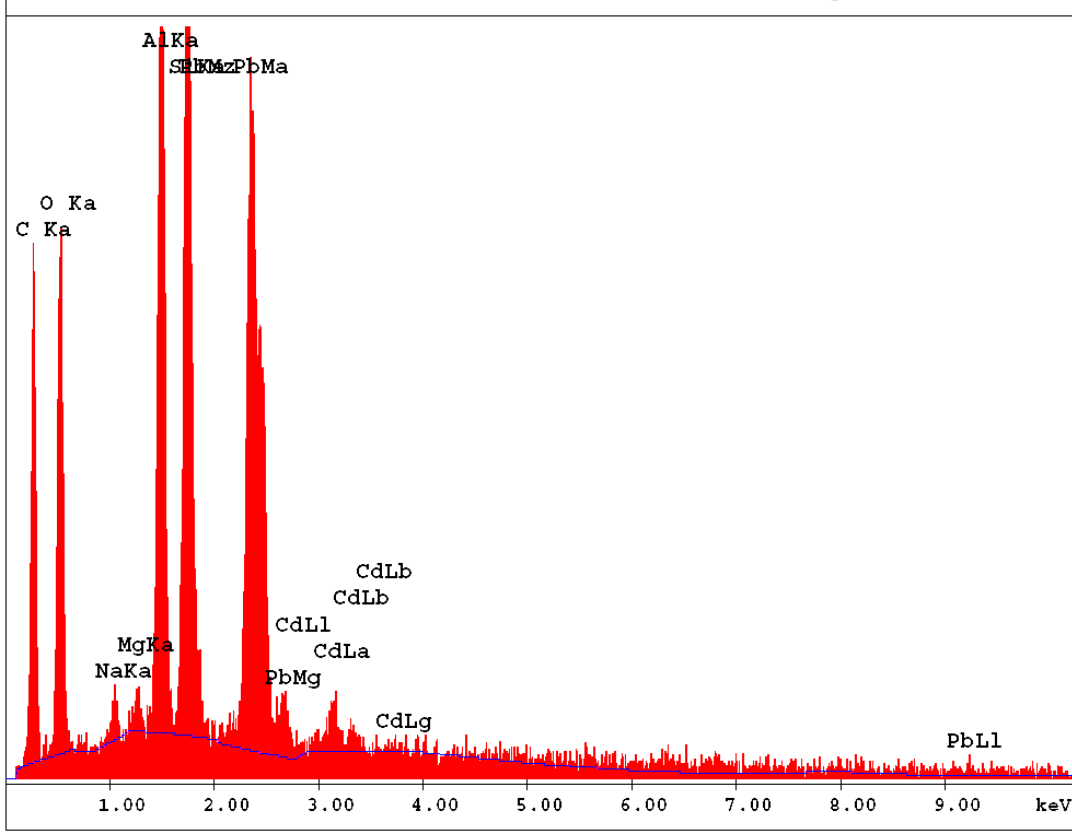


Figure F.3 (a) SEM Image of zeolite crystals in the Zeolite 13X beads (WD:9.4 mm),
(b) SEM Image of zeolite crystals in the Zeolite 13X beads (WD:9.5 mm)
for the Pb^{2+} - Cd^{2+} -NaX ternary ion exchange system.

```

c:\edax32\genesis\genspc.spc
Label:Chlorite (Nrm.%= 38.86, 20.96, 34.83, 1.14, 3.84, 0.28)
kV:20.0 Tilt:0.0 Take-off:34.5 Det Type:SUTW+ Res:128 Amp.T:102.4
FS : 376 Lsec : 18
3-Apr-2014 16:05:46

```



EDAX ZAF Quantification (Standardless)
Element Normalized
SEC Table : Default

Element	Wt %	At %	K-Ratio	Z	A	F
C K	34.02	60.63	0.0801	1.0945	0.2150	1.0001
O K	17.01	22.76	0.0334	1.0759	0.1825	1.0001
NaK	0.56	0.52	0.0021	1.0064	0.3700	1.0016
MgK	0.37	0.33	0.0019	1.0315	0.4959	1.0032
AlK	6.96	5.52	0.0435	1.0010	0.6222	1.0030
SiK	8.89	6.78	0.0615	1.0300	0.6715	1.0002
CdL	1.61	0.31	0.0111	0.8138	0.8435	1.0000
PbL	30.57	3.16	0.2101	0.6710	1.0244	1.0000
Total	100.00	100.00				

Figure F.4 EDX analysis of Pb²⁺-Cd²⁺-NaX ternary ion exchange system

3. Weight % Pb/Zn = 1.3

(Sample from Experiment Run No:MI12 of Table D.2)

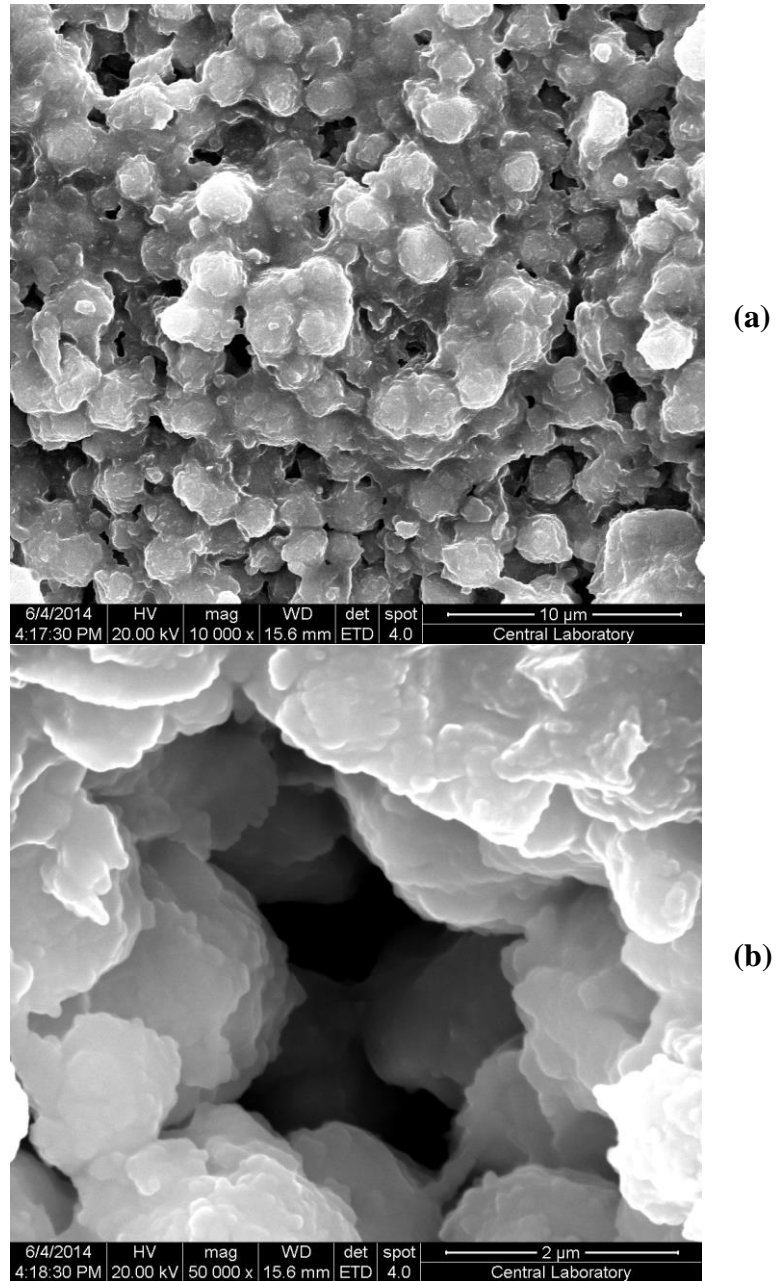


Figure F.5 (a) SEM Image of zeolite crystals in the Zeolite 13X beads (magnification: 10000x), (b) SEM Image of zeolite crystals in the Zeolite 13X beads (magnification: 50000x) for the Pb^{2+} - Zn^{2+} - NaX ternary ion exchange system.

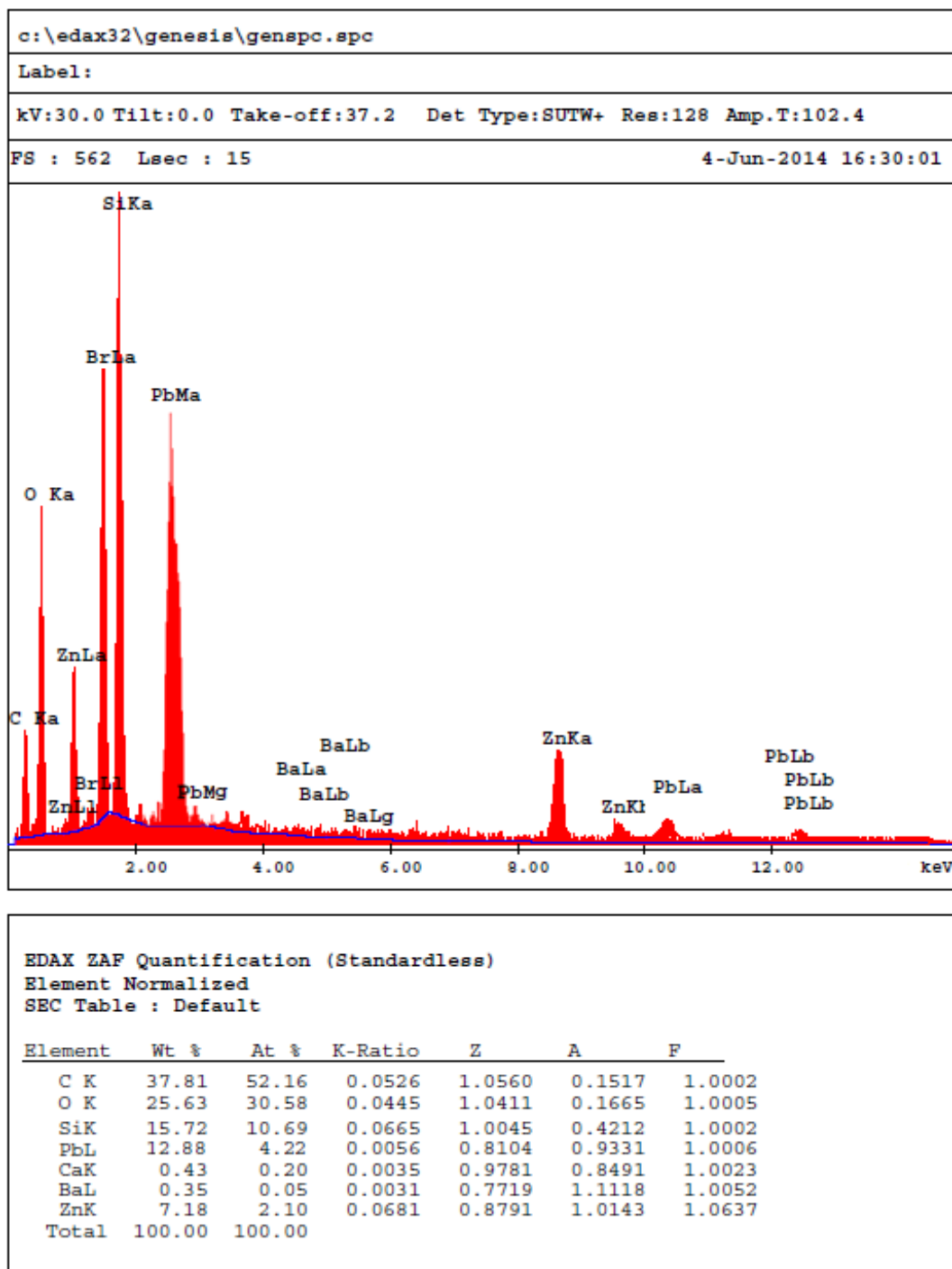


Figure F.6 EDX analysis of Pb²⁺-Zn²⁺-NaX ternary ion exchange system

4. Weight % Pb/Zn = 37.4

(Sample from Experiment Run No:MI18 of Table D.2)

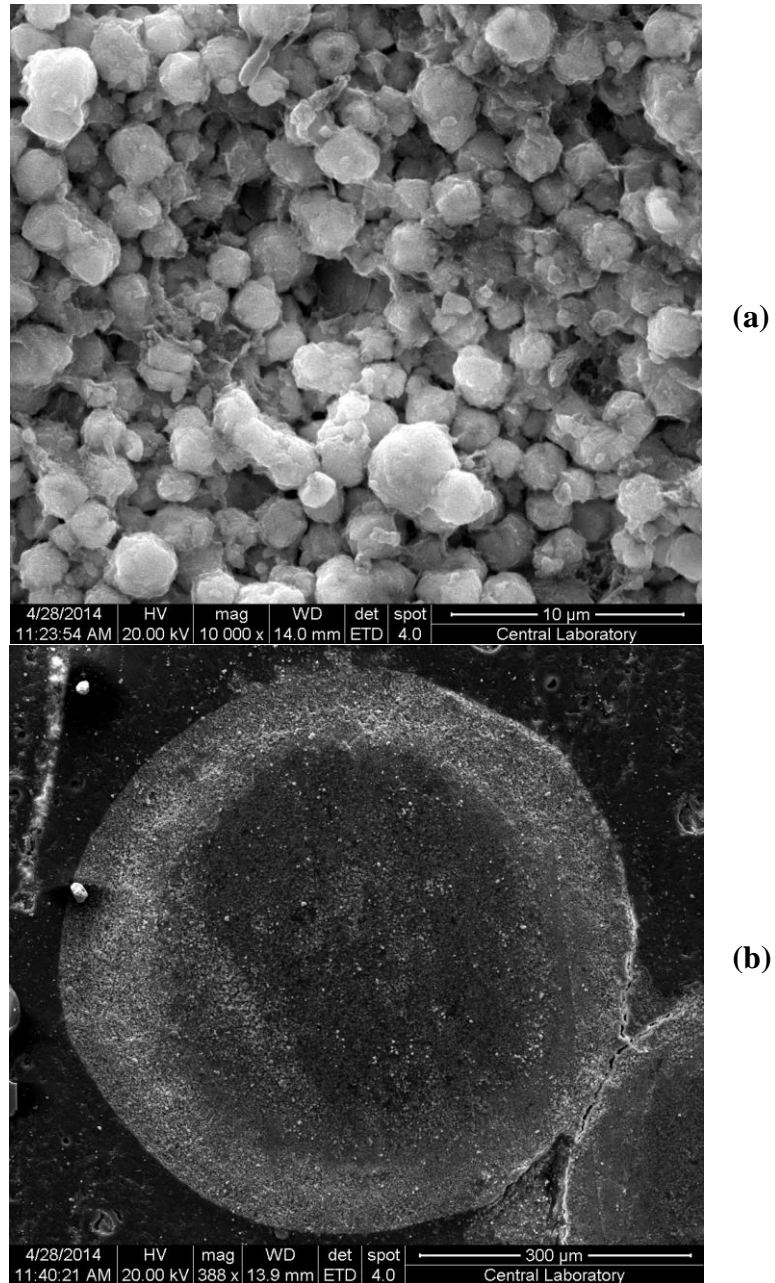
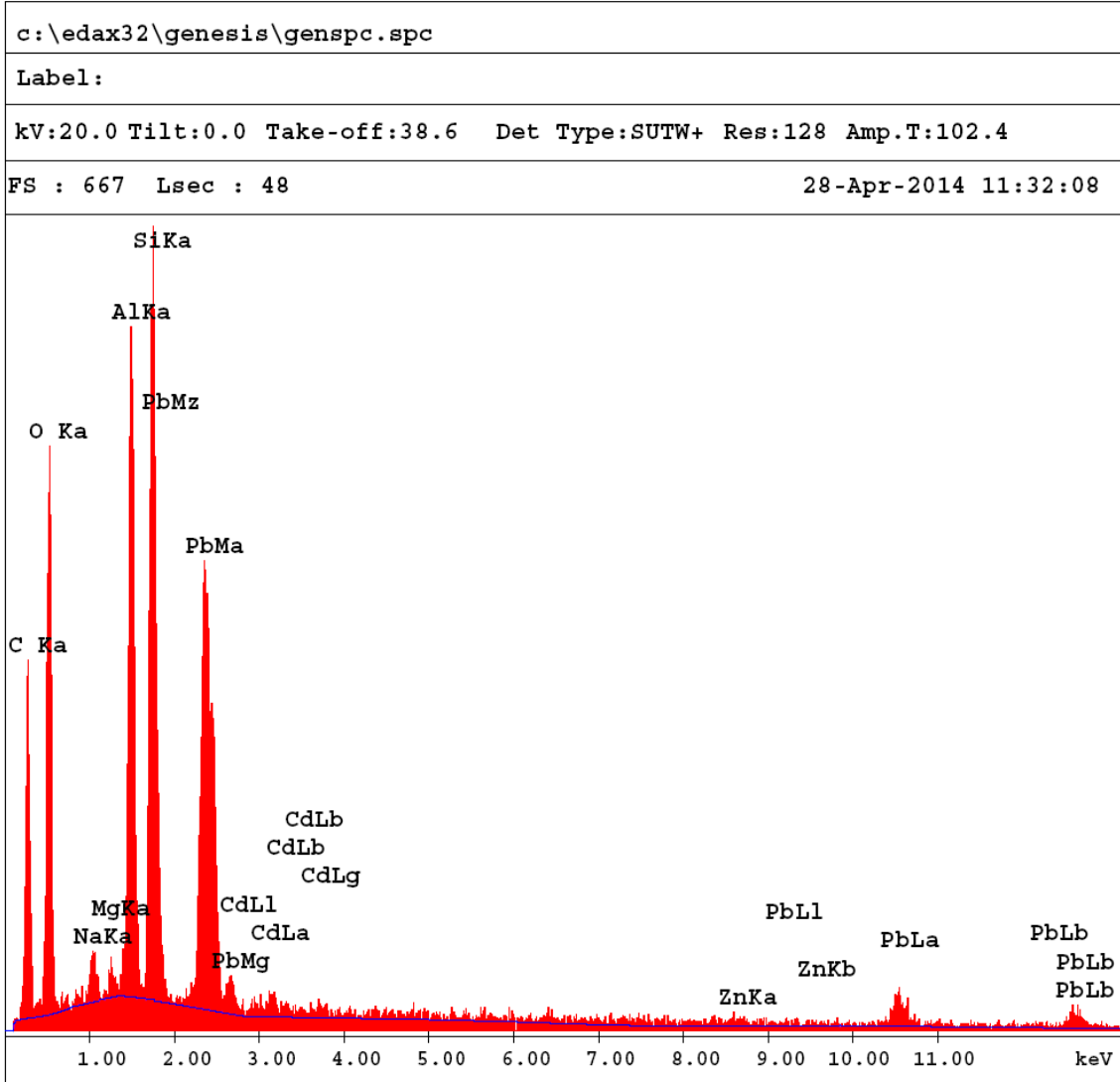


Figure F.7 (a) SEM Image of zeolite crystals in the Zeolite 13X beads, (b) cross-section of the Zeolite 13X bead for the Pb^{2+} - Zn^{2+} -NaX ternary ion exchange system



EDAX ZAF Quantification (Standardless)
 Element Normalized
 SEC Table : Default

Element	Wt %	At %	K-Ratio	Z	A	F
C K	30.13	54.23	0.0688	1.0926	0.2088	1.0002
O K	20.37	27.52	0.0442	1.0741	0.2019	1.0002
NaK	0.87	0.82	0.0034	1.0048	0.3871	1.0018
MgK	0.45	0.40	0.0024	1.0298	0.5099	1.0035
AlK	7.63	6.11	0.0486	0.9994	0.6354	1.0032
SiK	9.60	7.39	0.0672	1.0283	0.6806	1.0001
CdL	0.86	0.17	0.0060	0.8122	0.8582	1.0000
ZnK	0.98	0.33	0.0092	0.8984	0.9931	1.0504
PbL	29.10	3.04	0.1988	0.6684	1.0220	1.0000
Total	100.00	100.00				

Figure F.8 EDX analysis of Pb²⁺-Zn²⁺-NaX ternary ion exchange system.

5. Weight percentage Zn/Cd=0.14

(Sample from Experiment Run No:MI22 of Table D.3)

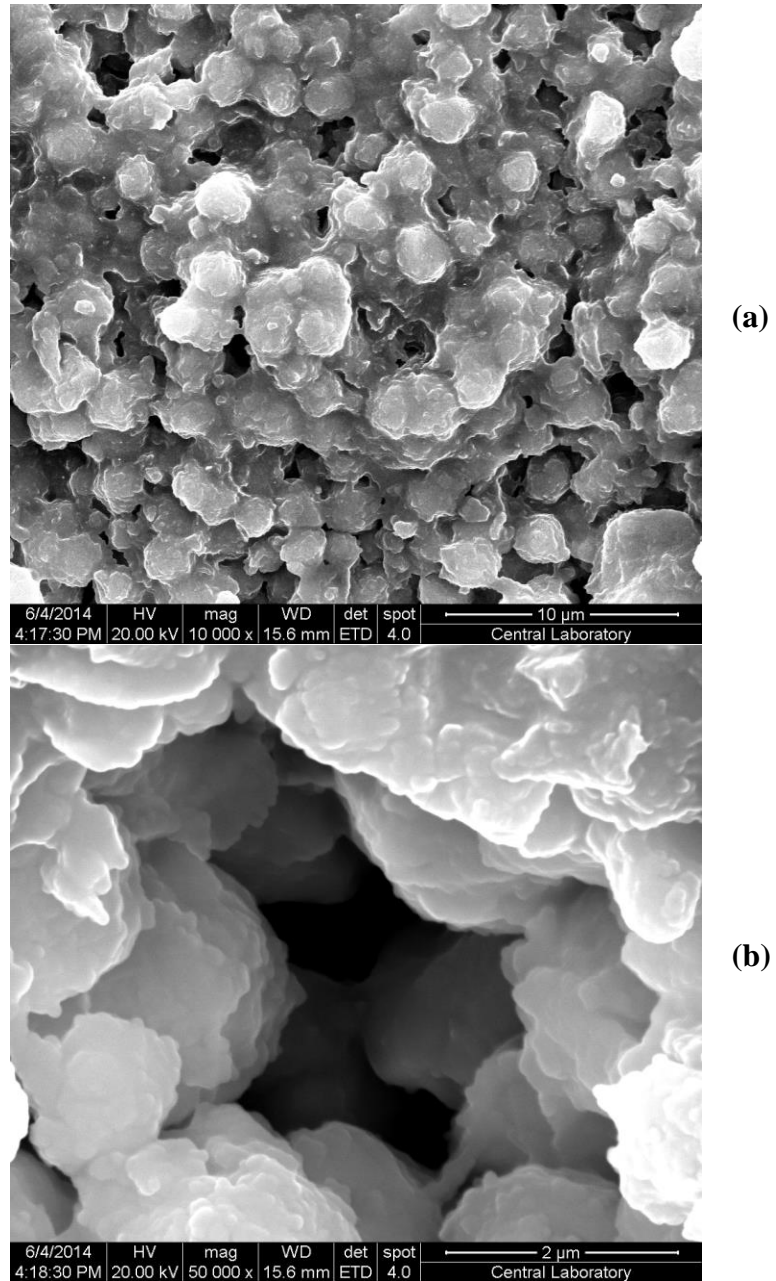


Figure F.9 (a) SEM Image of zeolite crystals in the Zeolite 13X beads (magnification: 10000x), (b) SEM Image of zeolite crystals in the Zeolite 13X beads (magnification: 50000x), for the Cd^{2+} - Zn^{2+} - NaX ternary ion exchange system.

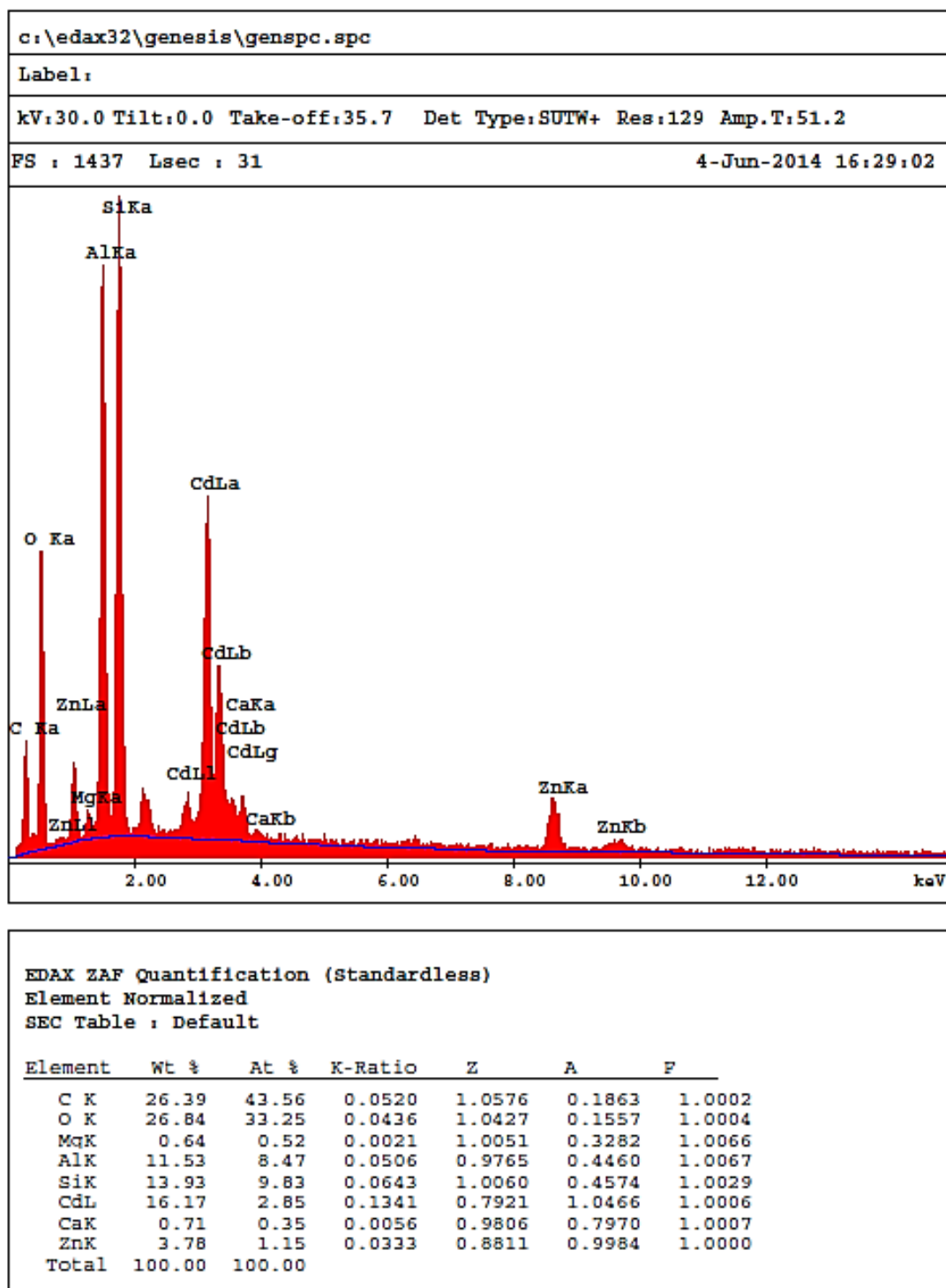


Figure F.10 EDX analysis of Cd²⁺-Zn²⁺-NaX ternary ion exchange system.

6. Weight percentage Zn/Cd=1.89

(Sample from Experiment Run No:MI18 of Table D.3)

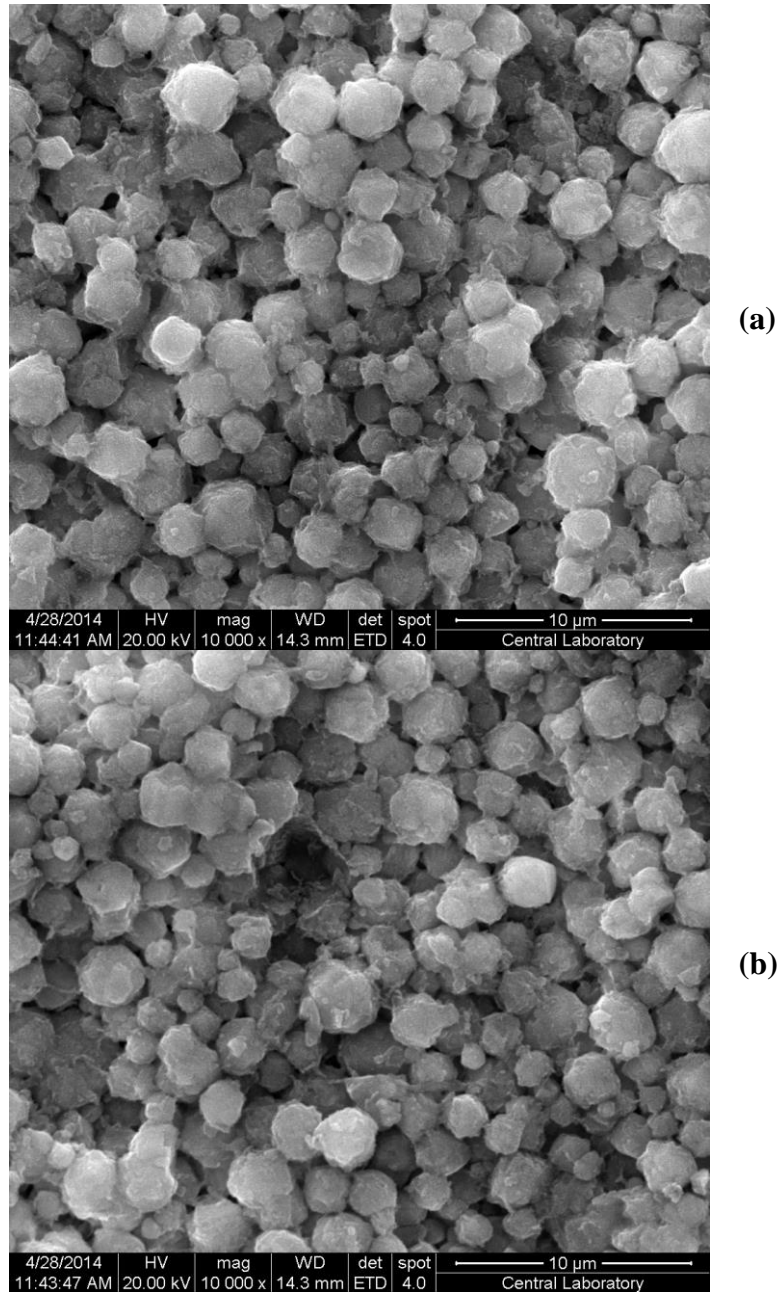
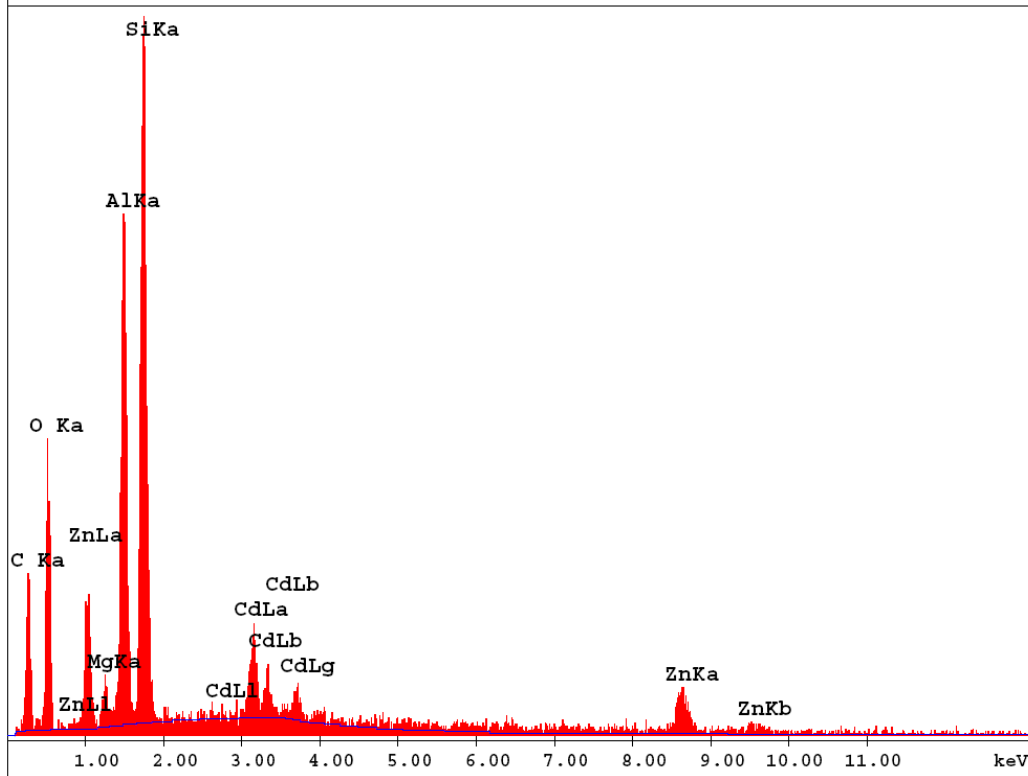


Figure F.11 (a) SEM Image of zeolite crystals in the Zeolite 13X beads, (b) SEM Image of zeolite crystals in the Zeolite 13X beads for the Cd^{2+} - Zn^{2+} - NaX ternary ion exchange system from another region.

```

c:\edax32\genesis\genspc.spc
Label:
kV:20.0 Tilt:0.0 Take-off:38.8 Det Type:SUTW+ Res:128 Amp.T:102.4
FS : 504 Lsec : 56 28-Apr-2014 11:46:39

```



EDAX ZAF Quantification (Standardless)
Element Normalized
SEC Table : Default

Element	Wt %	At %	K-Ratio	Z	A	F
C K	32.98	52.34	0.0594	1.0583	0.1702	1.0002
O K	18.49	22.03	0.0394	1.0405	0.2049	1.0005
MgK	1.07	0.84	0.0054	0.9982	0.4976	1.0060
AlK	11.82	8.35	0.0724	0.9688	0.6282	1.0061
SiK	17.78	12.07	0.1148	0.9971	0.6467	1.0009
CdL	6.84	1.16	0.0543	0.7823	1.0138	1.0000
ZnK	11.01	3.21	0.0943	0.8520	1.0047	1.0000
Total	100.00	100.00				

Figure F.12 EDX analysis of Cd²⁺-Zn²⁺-NaX ternary ion exchange system.

7. Weight % Pb/Cd= 1.23; Pb/Zn=2.81; Zn/Cd=0.44

(Sample from Experiment Run No:MI32 of Table D.4)

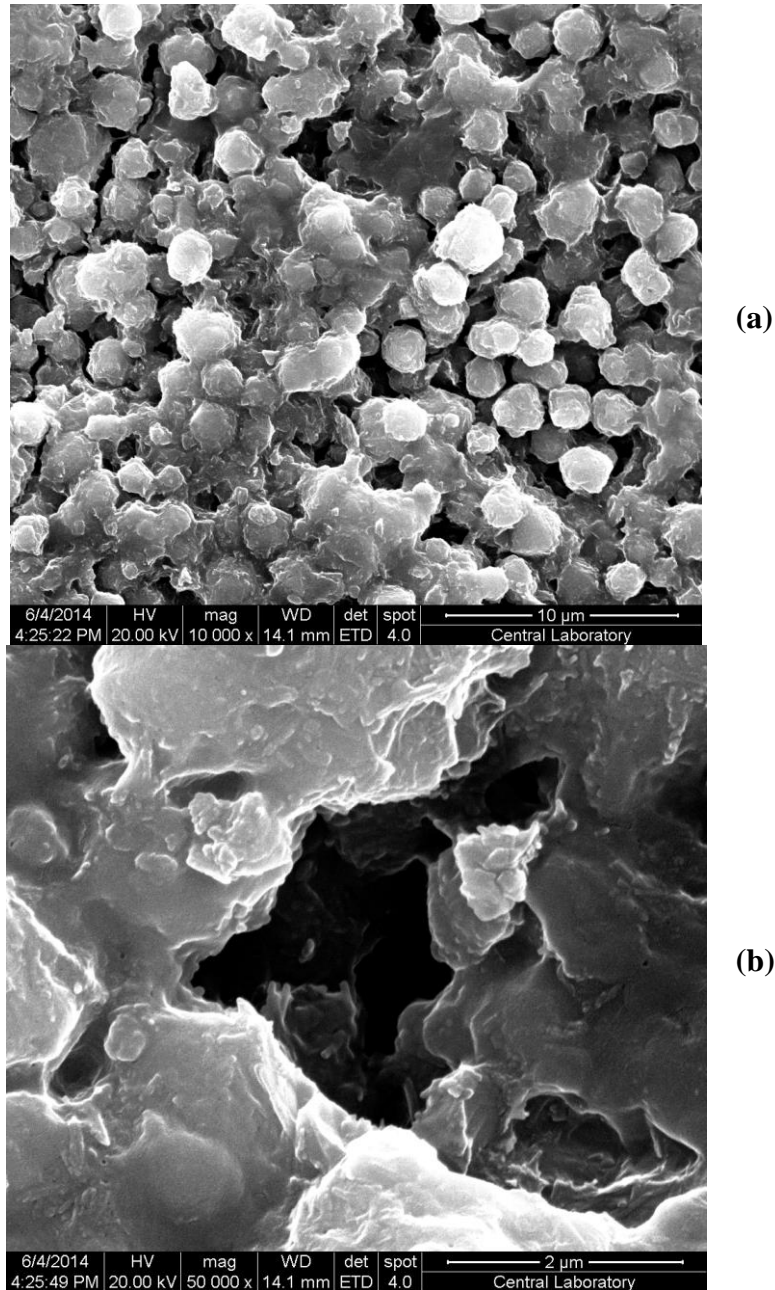


Figure F.13 (a) SEM Image of zeolite crystals in the Zeolite 13X beads (magnification: 10000x), (b) SEM Image of zeolite crystals in the Zeolite 13X beads (magnification: 50000x), for the Pb^{2+} - Cd^{2+} - Zn^{2+} -NaX quaternary ion exchange system.

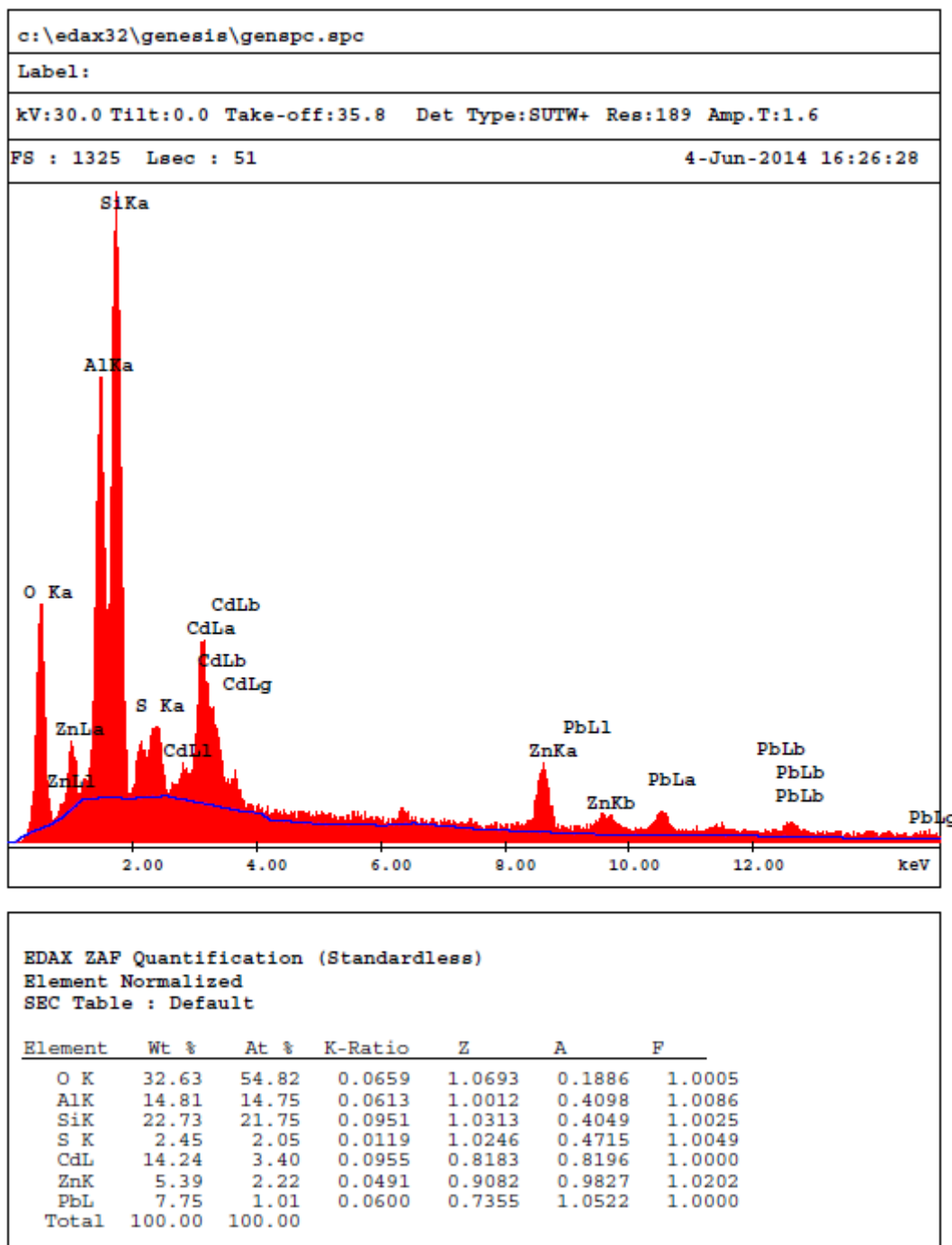


Figure F.14 EDX analysis of Pb^{2+} - Cd^{2+} - Zn^{2+} -NaX ternary ion exchange system.

8. Weight % Pb/Zn= 53.44; Pb/Cd=20.98; Zn/Cd=0.39
(Sample from Experiment Run No:MI38 of Table D.4)

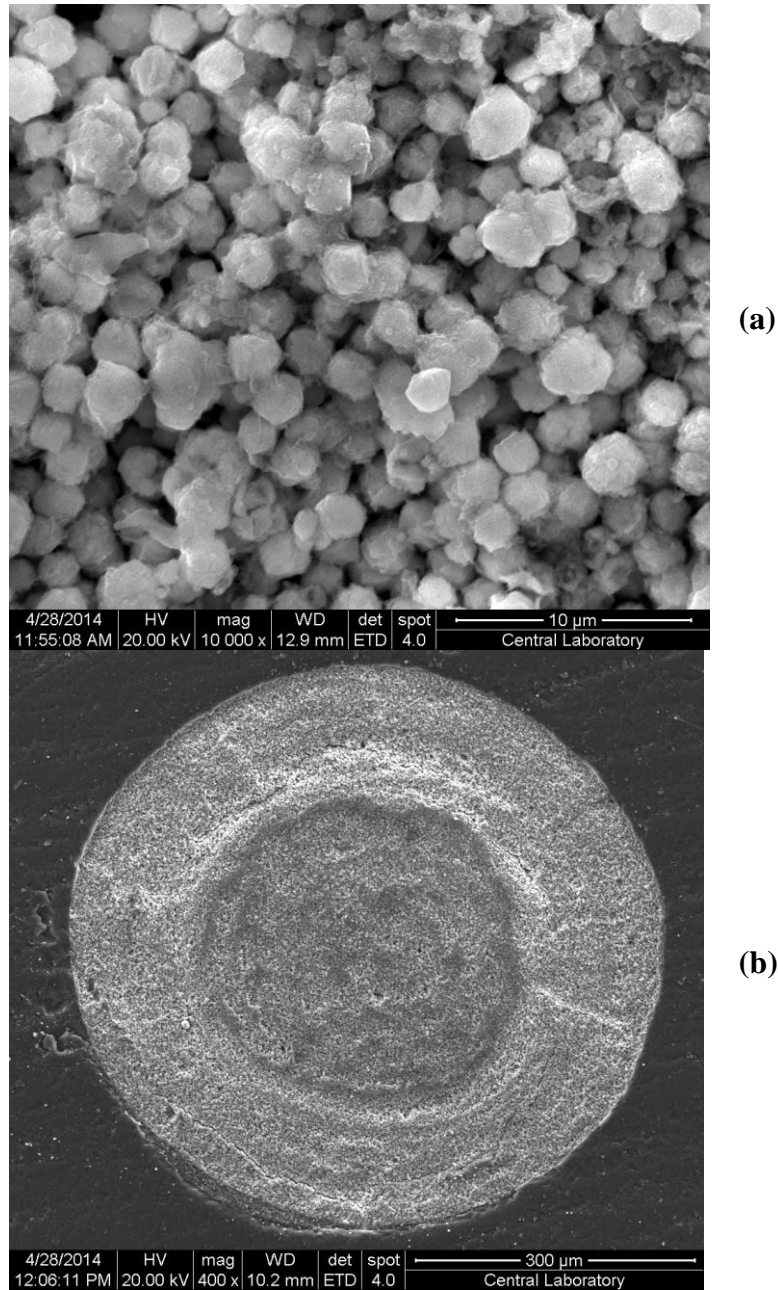
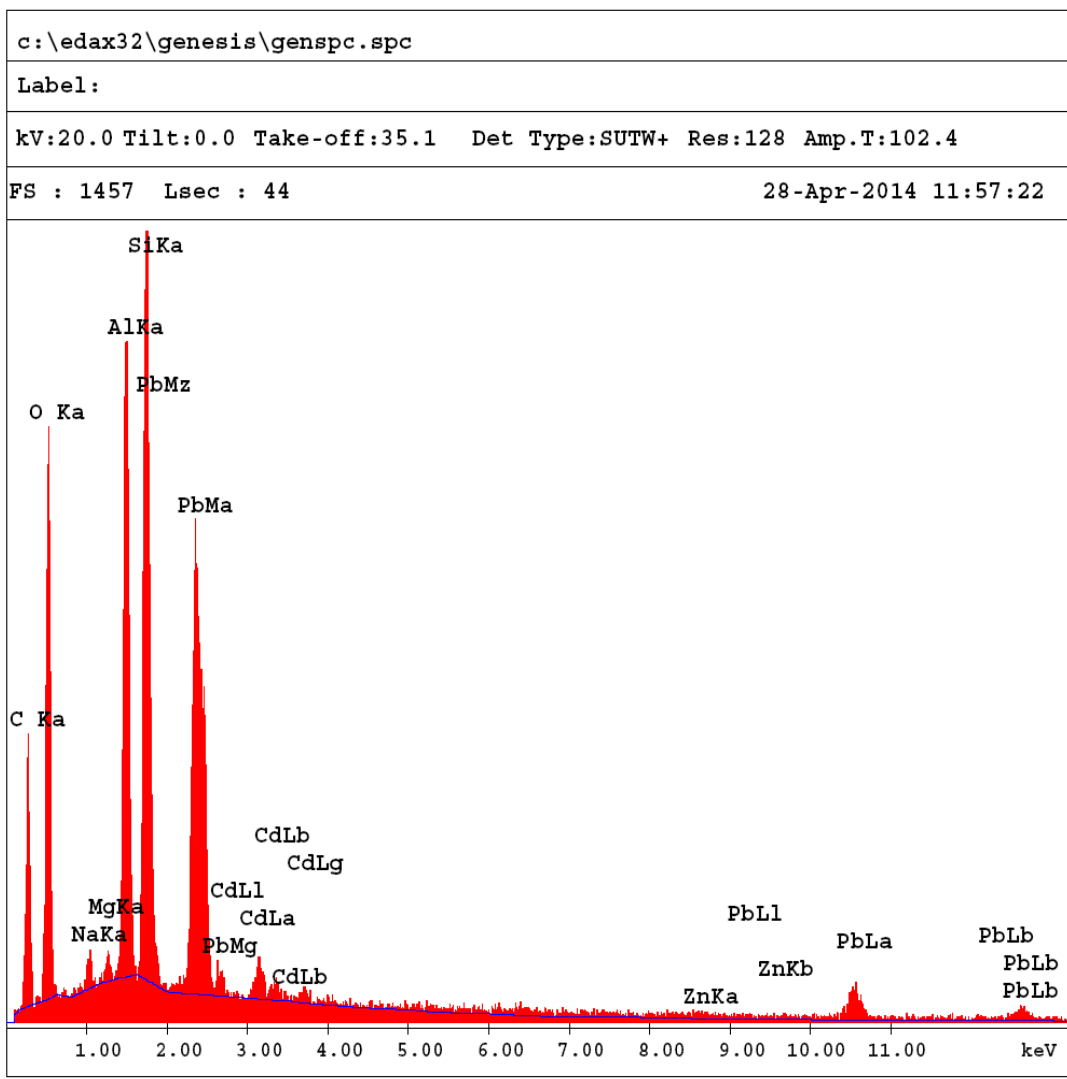


Figure F.15 (a) SEM Image of zeolite crystals in the Zeolite 13X beads, (b) cross-section of the Zeolite 13X bead for the Pb^{2+} - Cd^{2+} - Zn^{2+} - NaX quaternary ion exchange system



EDAX ZAF Quantification (Standardless)
 Element Normalized
 SEC Table : Default

Element	Wt %	At %	K-Ratio	Z	A	F
C K	26.22	49.40	0.0566	1.0989	0.1964	1.0002
O K	21.48	30.38	0.0457	1.0802	0.1970	1.0002
NaK	0.56	0.55	0.0021	1.0105	0.3613	1.0019
MgK	0.37	0.34	0.0018	1.0357	0.4833	1.0036
AlK	8.13	6.82	0.0500	1.0050	0.6101	1.0034
SiK	10.65	8.58	0.0719	1.0341	0.6533	1.0002
CdL	1.85	0.37	0.0127	0.8173	0.8378	1.0000
ZnK	0.84	0.29	0.0079	0.9050	0.9911	1.0479
PbL	29.91	3.27	0.2063	0.6740	1.0233	1.0000
Total	100.00	100.00				

Figure F.16 EDX analysis of Pb²⁺-Cd²⁺-Zn²⁺-NaX quaternary ion exchange system.

9. Pb/Cd dynamic exchange on Zeolite 13X

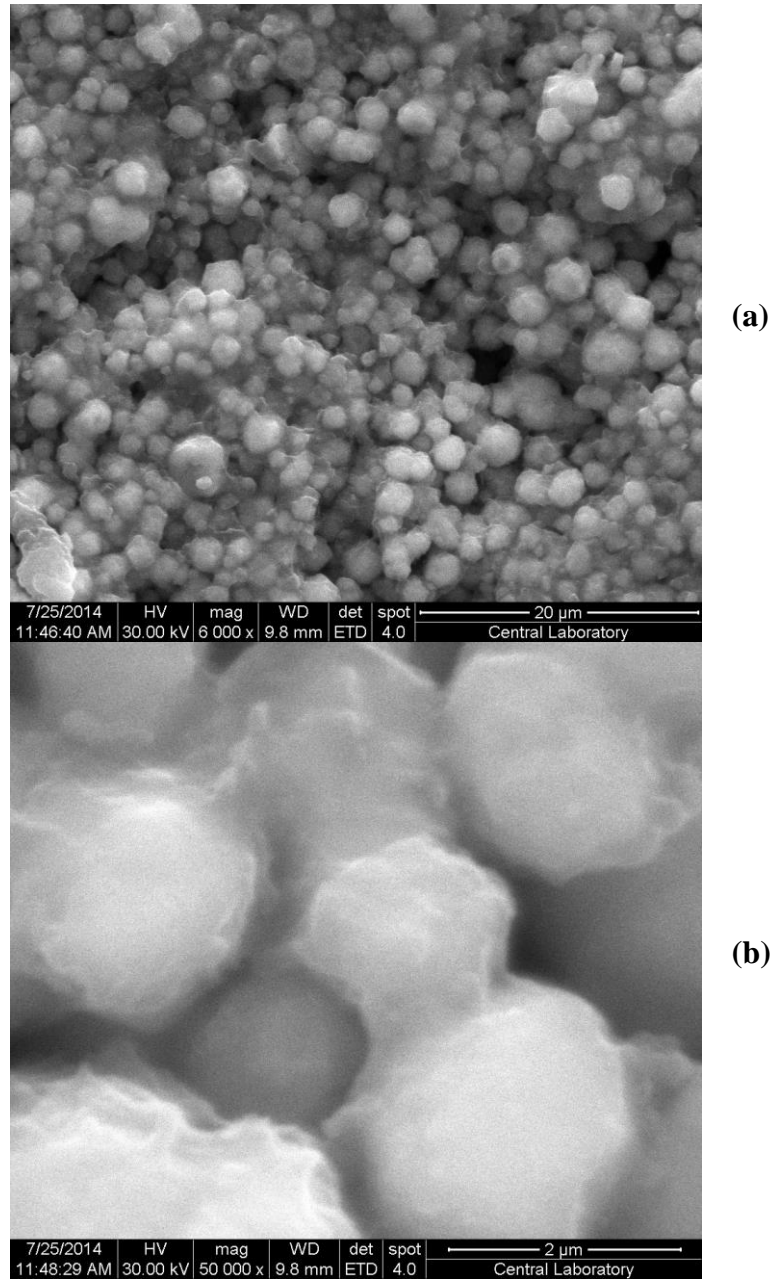


Figure F.17 (a) SEM Image of zeolite crystals in the Zeolite 13X beads (magnification: 6000x), (b) SEM Image of zeolite crystals in the Zeolite 13X beads (magnification: 50000x), for the Pb^{2+} - Cd^{2+} -NaX ternary dynamic ion exchange system.

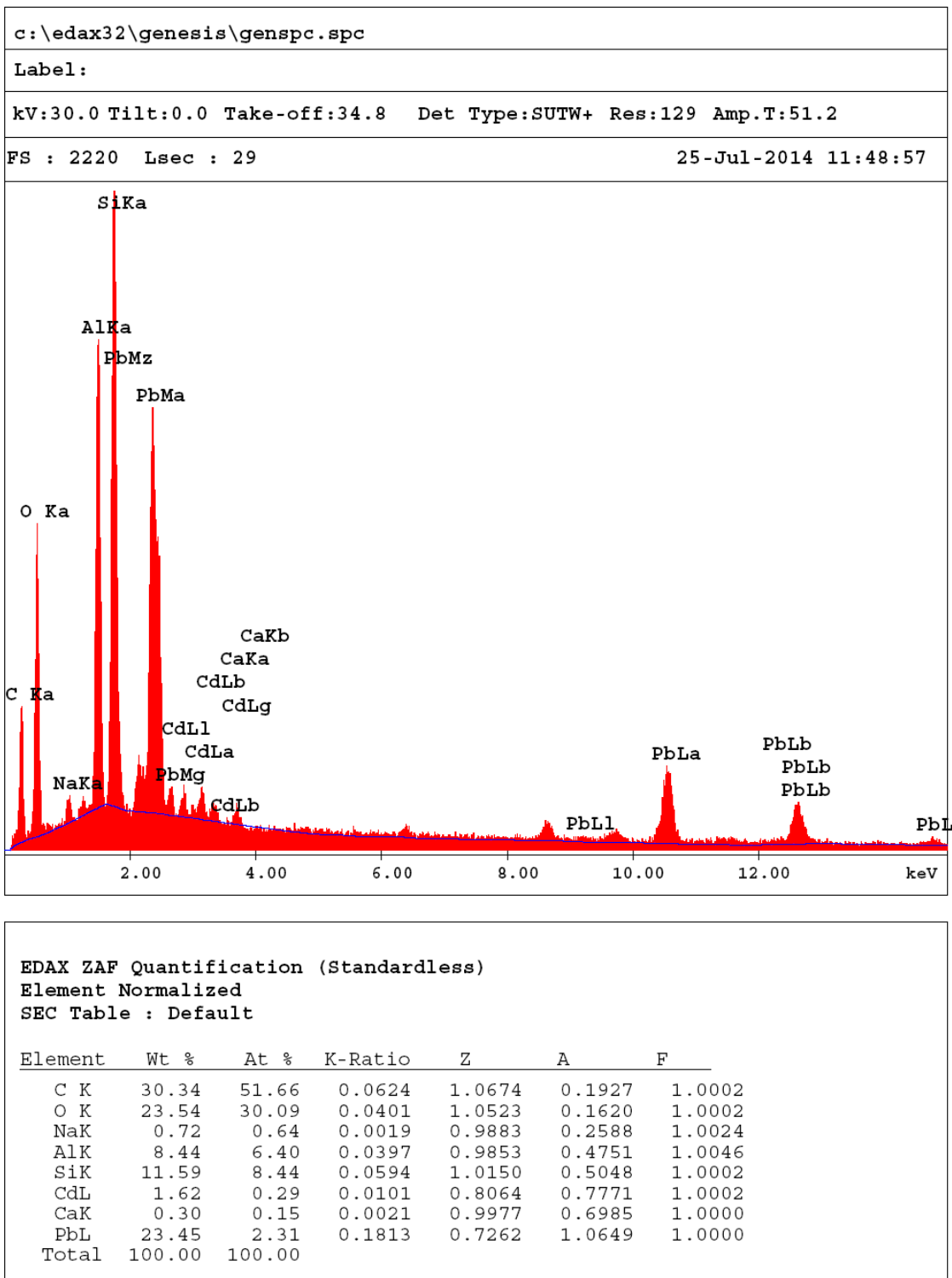


Figure F.18 EDX analysis of Pb^{2+} - Cd^{2+} - Zn^{2+} -NaX quaternary dynamic ion exchange system

APPENDIX G

DATA FOR BREAKTHROUGH CURVE

Table G.1. Pb²⁺-NaX binary ion exchange (particle size 25/30 Mesh and influent Pb²⁺ concentration 0.05 N, flow rate of 10 ml/min)

Sample No	V (ml)	time (min)	Pb ppm	Pb C/Co	Na ppm	Na C/Co
1	50	5	4.5	0.0	1500	0.9
2	100	10	4.2	0.0	1500	0.9
3	150	15	5.5	0.0	1500	0.9
4	200	20	11.1	0.0	1500	0.9
5	250	25	61.4	0.0	1500	0.9
6	300	30	159.3	0.0	1500	0.9
7	350	35	322.2	0.1	1400	0.9
8	400	40	486.2	0.1	1400	0.9
9	450	45	670.3	0.2	1300	0.8
10	500	50	900.0	0.2	1300	0.8
11	550	55	1000.0	0.3	1200	0.8
12	600	60	1200.0	0.3	1200	0.8
13	650	65	1350.0	0.4	1100	0.7
14	700	70	1400.0	0.4	1100	0.7
15	750	75	1500.0	0.4	1000	0.6
16	800	80	1616.7	0.4	1000	0.6
17	850	85	1700.0	0.5	900	0.6

Table G.1 (cont'd). Pb²⁺-NaX binary ion exchange (particle size 25/30 Mesh and influent Pb²⁺ concentration 0.05 N, flow rate of 10 ml/min) cont.

Sample No	V (ml)	time (min)	Pb ppm	Pb C/Co	Na ppm	Na C/Co
18	900	90	1888.2	0.5	800	0.5
19	950	95	1900.0	0.5	700	0.4
20	1000	100	2100.0	0.6	600	0.4
21	1050	105	2230.4	0.6	500	0.3
22	1100	110	2300.0	0.6	400	0.3
26	1300	130	2619.8	0.7	60	0.0
27	1350	135	2700.0	0.7	60	0.0
28	1400	140	2870.0	0.8	60	0.0
29	1450	145	2900.0	0.8	60	0.0
30	1500	150	3000.0	0.8	50	0.0
31	1550	155	3100.0	0.8	50	0.0
32	1600	160	3200.0	0.9	50	0.0
33	1650	165	3300.0	0.9	40	0.0
34	1700	170	3400.0	0.9	40	0.0
35	1750	175	3500.0	0.9	40	0.0
36	1800	180	3500.0	0.9	40	0.0
37	1850	185	3500.0	0.9	30	0.0
38	1900	190	3500.0	0.9	30	0.0
39	1950	195	3500.0	0.9	30	0.0
40	2000	200	3500.0	0.9	30	0.0

Table G.2. Cd²⁺-NaX binary ion exchange (particle size 25/30 Mesh and influent Cd²⁺ concentration 0.05 N, flow rate of 10 ml/min)

Sample No	V (ml)	time (min)	Cd ppm	Cd C/Co	Na ppm	Na C/Co
1	50	5	0.0	0.00	17200	1.00
2	100	10	51.6	0.02	14400	0.84
3	150	15	188.2	0.07	7600	0.44
4	200	20	449.6	0.16	5000	0.29
5	250	25	850.2	0.31	3200	0.19
6	300	30	1135.6	0.41	1600	0.09
7	350	35	1322.6	0.48	720	0.04
8	400	40	1486.4	0.53	560	0.03
9	450	45	1779.2	0.64	410	0.02
10	500	50	1912.2	0.69	340	0.02
11	550	55	1987.2	0.71	280	0.02
12	600	60	2006.0	0.72	250	0.01
13	650	65	2018.4	0.73	220	0.01
14	700	70	2120.0	0.76	200	0.01
15	750	75	2123.2	0.76	200	0.01
16	800	80	2185.8	0.79	180	0.01
17	850	85	2239.2	0.81	180	0.01
18	900	90	2290.8	0.82	170	0.01
19	950	95	2291.4	0.82	150	0.01
20	1000	100	2319.4	0.83	140	0.01
21	1050	105	2320.0	0.83	110	0.01
22	1100	110	2332.4	0.84	110	0.01
23	1150	115	2346.2	0.84	100	0.01
24	1200	120	2350.6	0.85	100	0.01

Table G.2 (cont'd). Cd²⁺-NaX binary ion exchange (particle size 25/30 Mesh and influent Cd²⁺ concentration 0.05 N, flow rate of 10 ml/min)

Sample No	V (ml)	time (min)	Cd ppm	Cd C/Co	Na ppm	Na C/Co
25	1250	125	2364.0	0.85	90	0.01
26	1300	130	2386.4	0.86	90	0.01
27	1350	135	2397.6	0.86	90	0.01
28	1400	140	2443.2	0.88	90	0.01
29	1450	145	2466.6	0.89	80	0.00
30	1500	150	2486.2	0.89	80	0.00
31	1550	155	2508.4	0.90	80	0.00
32	1600	160	2552.6	0.92	80	0.00
33	1650	165	2555.2	0.92	70	0.00
34	1700	170	2567.0	0.92	60	0.00
35	1750	175	2576.0	0.93	60	0.00
36	1800	180	2611.2	0.94	60	0.00
37	1850	185	2636.0	0.95	60	0.00
38	1900	190	2640.0	0.95	60	0.00
39	1950	195	2640.0	0.95	60	0.00
40	2000	200	2640.0	0.95	60	0.00

Table G.3. Zn²⁺-NaX binary ion exchange (particle size 25/30 Mesh and influent Zn²⁺ concentration 0.05 N, flow rate of 10 ml/min)

Sample No	V (ml)	time (min)	Zn ppm	Zn C/Co	Na ppm	Na C/Co
1	50	5	0.01	0.00	15200	1.00
2	100	10	4.84	0.00	12400	0.82
3	150	15	5.35	0.00	9000	0.59
4	200	20	100.0	0.05	5200	0.34
5	250	25	760.6	0.35	3000	0.20
6	300	30	879.2	0.41	880	0.06
7	350	35	1181.6	0.55	470	0.03
8	400	40	1455.0	0.67	350	0.02
9	450	45	1491.4	0.69	220	0.01
10	500	50	1534.4	0.71	150	0.01
11	550	55	1605.4	0.74	120	0.01
12	600	60	1676.4	0.77	100	0.01
13	650	65	1677.2	0.78	80	0.01
14	700	70	1716.0	0.79	80	0.01
15	750	75	1722.6	0.80	70	0.00
16	800	80	1730.2	0.80	60	0.00
17	850	85	1745.2	0.81	60	0.00
18	900	90	1752.4	0.81	50	0.00
19	950	95	1759.8	0.81	50	0.00
20	1000	100	1761.6	0.81	40	0.00
21	1050	105	1775.8	0.82	40	0.00
22	1100	110	1779.8	0.82	20	0.00
23	1150	115	1782.2	0.82	20	0.00
24	1200	120	1831.8	0.85	20	0.00

Table G.3 (cont'd). Zn²⁺-NaX binary ion exchange (particle size 25/30 Mesh and influent Zn²⁺ concentration 0.05 N, flow rate of 10 ml/min)

Sample No	V (ml)	time (min)	Zn ppm	Zn C/Co	Na ppm	Na C/Co
25	1250	125	1831.8	0.85	20	0.00
26	1300	130	1833.4	0.85	20	0.00
27	1350	135	1844.2	0.85	20	0.00
28	1400	140	1860.2	0.86	9	0.00
29	1450	145	1880.6	0.87	9	0.00
30	1500	150	1892.2	0.87	8	0.00
31	1550	155	1893.8	0.88	8	0.00
32	1600	160	1900.6	0.88	8	0.00
33	1650	165	1908.6	0.88	7	0.00
34	1700	170	1934.2	0.89	7	0.00
35	1750	175	1935.0	0.89	6	0.00
36	1800	180	1944.2	0.90	6	0.00
37	1850	185	2002.8	0.93	6	0.00
38	1900	190	2021.8	0.93	5	0.00
39	1950	195	2140.0	0.99	5	0.00
40	2000	195	2140.0	0.99	5	0.00

Table G.4. Pb²⁺-Cd²⁺-NaX ternary ion exchange (particle size 25/30 Mesh and influent total concentration of 0.05 N, flow rate of 10 ml/min).

Sample No	time (min)	Cd ppm	Cd C/Co	Na ppm	Na C/Co	Pb ppm	Pb C/Co
1	5	3.2	0.00	14000	1.00	11.9	0.00
2	10	4.4	0.00	11000	0.79	20.3	0.01
3	15	58.8	0.03	5600	0.40	30.1	0.01
4	20	218.5	0.12	4200	0.30	36.4	0.01
5	25	404.3	0.22	2600	0.19	117.9	0.04
6	30	696.8	0.39	1600	0.11	237.3	0.08
7	35	801.4	0.44	1500	0.11	388.1	0.12
8	40	1081.2	0.60	1300	0.09	727.0	0.23
9	45	1294.1	0.72	1200	0.09	973.3	0.31
10	50	1327.1	0.73	1100	0.08	1186.9	0.38
11	55	1390.2	0.77	1000	0.07	1380.8	0.44
12	60	1471.5	0.81	800	0.06	1433.1	0.46
13	65	1515.1	0.84	600	0.04	1463.7	0.47
14	70	1521.9	0.84	250	0.02	1546.6	0.49
15	75	1522.3	0.84	230	0.02	1575.9	0.50
16	80	1564.2	0.87	190	0.01	1629.5	0.52
17	85	1570.1	0.87	180	0.01	1700.0	0.54
18	90	1571.4	0.87	140	0.01	1753.7	0.56
19	95	1582.0	0.88	120	0.01	1761.5	0.56
20	100	1582.8	0.88	110	0.01	1791.4	0.57
21	105	1585.4	0.88	80	0.01	1809.0	0.58
22	110	1593.4	0.88	80	0.01	1828.5	0.58
23	115	1602.7	0.89	60	0.00	1836.1	0.59
24	120	1613.3	0.89	50	0.00	1940.6	0.62

Table G.4 (cont'd). Pb²⁺ - Cd²⁺ - NaX ternary ion exchange (particle size 25/30 Mesh and influent total concentration of 0.05 N, flow rate of 10 ml/min).

Sample No	time (min)	Cd ppm	Cd C/Co	Na ppm	Na C/Co	Pb ppm	Pb C/Co
25	125	1613.3	0.89	50	0.00	2015.3	0.64
26	130	1632.4	0.90	50	0.00	2029.9	0.65
27	135	1635.7	0.91	40	0.00	2075.0	0.66
28	140	1656.9	0.92	40	0.00	2154.2	0.69
29	145	1658.2	0.92	15	0.00	2179.5	0.69
30	150	1666.6	0.92	14	0.00	2264.7	0.72
31	155	1672.6	0.93	14	0.00	2416.6	0.77
32	160	1687.0	0.93	13	0.00	2458.0	0.78
33	165	1695.4	0.94	11	0.00	2513.2	0.80
34	170	1703.5	0.94	9	0.00	2513.2	0.80
35	175	1731.6	0.96	8	0.00	2537.8	0.81
36	180	1745.0	0.97	8	0.00	2746.8	0.88
37	185	1747.5	0.97	7	0.00	2791.5	0.89
38	190	1769.5	0.98	7	0.00	2896.0	0.92
39	195	1794.9	0.99	7	0.00	3000.0	0.96
40	195	1794.9	0.99	7	0.00	3000.0	0.96

Table G.5. Zn²⁺ - Cd²⁺ - NaX ternary ion exchange (particle size 25/30 Mesh and influent total concentration of 0.05 N, flow rate of 10 ml/min)

Sample No	time (min)	Cd ppm	Cd C/Co	Na ppm	Na C/Co	Zn ppm	Zn C/Co
1	5	0.22	0.00	2000	1.00	0.55	0.00
2	10	1.19	0.00	1900	0.95	1.13	0.00
3	15	11.48	0.01	1850	0.93	1.18	0.00
4	20	12.48	0.01	1800	0.90	29.25	0.04
5	25	35.91	0.04	1800	0.90	36.75	0.05
6	30	77.75	0.08	1750	0.88	66.69	0.10
7	35	125.81	0.13	1730	0.87	105.93	0.16
8	40	182.17	0.18	1700	0.85	141.43	0.21
9	45	226.43	0.23	1650	0.83	207.60	0.31
10	50	237.30	0.24	1640	0.82	233.70	0.34
11	55	297.20	0.30	1620	0.81	242.20	0.36
12	60	303.10	0.31	1600	0.80	269.30	0.40
13	65	337.00	0.34	1550	0.78	273.60	0.40
14	70	430.80	0.44	1500	0.75	353.70	0.52
15	75	465.40	0.47	1450	0.73	355.30	0.52
16	80	488.30	0.49	1430	0.72	366.50	0.54
17	85	537.60	0.54	1400	0.70	419.70	0.62
18	90	572.50	0.58	1300	0.65	432.20	0.64
19	95	599.50	0.61	1100	0.55	446.90	0.66
20	100	611.80	0.62	610	0.31	460.20	0.68
21	105	628.80	0.64	550	0.28	478.30	0.70
22	110	642.90	0.65	510	0.26	487.60	0.72
23	115	673.80	0.68	500	0.25	492.60	0.72
24	120	694.00	0.70	500	0.25	501.40	0.74

Table G.5 (cont'd). Zn²⁺ - Cd²⁺ - NaX ternary ion exchange (particle size 25/30 Mesh and influent total concentration of 0.05 N, flow rate of 10 ml/min)

Sample No	time (min)	Cd ppm	Cd C/Co	Na ppm	Na C/Co	Zn ppm	Zn C/Co
25	125	725.60	0.73	490	0.25	526.20	0.77
26	130	731.30	0.74	480	0.24	529.40	0.78
27	135	755.20	0.76	460	0.23	540.80	0.80
28	140	763.10	0.77	440	0.22	550.40	0.81
29	145	768.80	0.78	440	0.22	551.50	0.81
30	150	800.90	0.81	400	0.20	553.90	0.81
31	155	803.50	0.81	400	0.20	559.20	0.82
32	160	818.40	0.83	400	0.20	566.90	0.83
33	165	837.60	0.85	360	0.18	573.00	0.84
34	170	842.50	0.85	350	0.18	615.30	0.90
35	175	922.40	0.93	300	0.15	620.40	0.91
36	180	927.30	0.94	260	0.13	638.50	0.94
37	185	941.10	0.95	260	0.13	639.30	0.94
38	190	941.10	0.95	260	0.13	647.00	0.95
39	195	943.20	0.95	260	0.13	647.00	0.95
40	200	943.20	0.95	260	0.13	647.00	0.95

Table G.6. Zn²⁺ - Pb²⁺ - NaX ternary ion exchange (particle size 25/30 Mesh and influent total concentration of 0.05 N, flow rate of 10 ml/min)

Sample No	time (min)	Zn ppm	Zn C/Co	Na ppm	Na C/Co	Pb ppm	Pb C/Co
1	5	10.0	0.01	6600	1.00	0.9	0.00
2	10	20.0	0.02	5200	0.79	1.1	0.00
3	15	37.9	0.04	3800	0.58	2.2	0.00
4	20	42.9	0.05	3000	0.45	6.4	0.00
5	25	98.5	0.12	2500	0.38	13.3	0.01
6	30	135.0	0.16	2300	0.35	22.4	0.02
7	35	148.9	0.18	2100	0.32	33.1	0.02
8	40	177.9	0.21	2000	0.30	47.2	0.04
9	45	204.9	0.24	1500	0.23	69.4	0.05
10	50	374.1	0.44	710	0.11	113.5	0.09
11	55	444.8	0.53	650	0.10	157.5	0.12
12	60	518.8	0.61	640	0.10	203.8	0.15
13	65	583.1	0.69	620	0.09	258.3	0.19
14	70	587.9	0.69	610	0.09	301.6	0.23
15	75	609.9	0.72	600	0.09	375.5	0.28
16	80	637.8	0.75	590	0.09	446.4	0.34
17	85	672.6	0.79	570	0.09	480.0	0.36
18	90	678.2	0.80	570	0.09	514.4	0.39
19	95	682.3	0.81	530	0.08	569.6	0.43
20	100	708.3	0.84	530	0.08	627.0	0.47
21	105	712.8	0.84	470	0.07	659.9	0.50
22	110	719.2	0.85	420	0.06	689.0	0.52
23	115	720.6	0.85	390	0.06	777.9	0.59
24	120	725.4	0.86	370	0.06	831.6	0.63

Table G.6 (cont'd). Zn²⁺ - Pb²⁺ - NaX ternary ion exchange (particle size 25/30 Mesh and influent total concentration of 0.05 N, flow rate of 10 ml/min)

Sample No	time (min)	Zn ppm	Zn C/Co	Na ppm	Na C/Co	Pb ppm	Pb C/Co
25	125	728.1	0.86	360	0.05	863.0	0.65
26	130	735.6	0.87	360	0.05	913.7	0.69
27	135	752.2	0.89	330	0.05	950.3	0.72
28	140	753.3	0.89	320	0.05	957.8	0.72
29	145	773.9	0.91	310	0.05	1039.2	0.78
30	150	791.1	0.93	300	0.05	1039.9	0.78
31	155	791.1	0.93	300	0.05	1045.1	0.79
32	160	791.3	0.94	290	0.04	1097.4	0.83
33	165	794.0	0.94	280	0.04	1098.9	0.83
34	170	806.6	0.95	280	0.04	1176.5	0.89
35	175	809.0	0.96	230	0.03	1202.7	0.91
36	180	814.4	0.96	230	0.03	1207.9	0.91
37	185	816.2	0.96	230	0.03	1244.5	0.94
38	190	828.3	0.98	210	0.03	1327.3	1.00
39	195	828.8	0.98	210	0.03	1327.3	1.00
40	200	828.8	0.98	210	0.03	1327.3	1.00

Table G.7. Zn²⁺ - Pb²⁺ - Cd²⁺ - NaX quaternary ion exchange (particle size 25/30 Mesh and influent total concentration of 0.05 N, flow rate of 10 ml/min)

time (min)	Cd ppm	Cd C/Co	Na ppm	Na C/Co	Pb ppm	Pb C/Co	Zn ppm	Zn C/Co
5	20.5	0.02	12000	1.00	9.9	0.01	20.29	0.02
10	21.7	0.02	7000	0.58	12.4	0.01	23.13	0.03
15	54.2	0.06	4000	0.33	14.7	0.01	63.16	0.08
20	150.5	0.17	3100	0.26	26.6	0.02	147.84	0.18
25	253.6	0.28	2100	0.18	27.3	0.02	206.1	0.25
30	297.0	0.33	2100	0.18	36.9	0.03	343.5	0.41
35	366.9	0.40	1800	0.15	38.7	0.03	436.7	0.53
40	413.4	0.45	1000	0.08	39.2	0.03	446.4	0.54
45	511.1	0.56	900	0.08	94.9	0.07	502.9	0.61
50	559.5	0.61	900	0.08	209.5	0.16	505.8	0.61
55	615.3	0.67	800	0.07	271.5	0.21	560.6	0.68
60	653.8	0.72	800	0.07	330.3	0.25	572.8	0.69
65	668.9	0.73	480	0.04	352.3	0.27	591.6	0.71
70	669.5	0.73	440	0.04	423.7	0.33	594	0.72
75	735.4	0.81	440	0.04	499.4	0.38	615.7	0.74
80	744.9	0.82	390	0.03	546.0	0.42	617.1	0.74
85	756.3	0.83	380	0.03	568.0	0.44	622.1	0.75
90	784.2	0.86	360	0.03	601.0	0.46	626.7	0.76
95	785.8	0.86	350	0.03	640.2	0.49	627.9	0.76
100	788.7	0.87	330	0.03	683.4	0.53	630.2	0.76
105	797.2	0.87	310	0.03	706.9	0.54	635.7	0.77
110	804.7	0.88	310	0.03	761.1	0.59	643.5	0.78
115	807.9	0.89	300	0.03	765.8	0.59	654.5	0.79
120	808.7	0.89	270	0.02	808.0	0.62	665.0	0.80

Table G.7 (cont'd). Zn²⁺ - Pb²⁺ - Cd²⁺ - NaX quaternary ion exchange (particle size 25/30 Mesh and influent total concentration of 0.05 N, flow rate of 10 ml/min)

time (min)	Cd ppm	Cd C/Co	Na ppm	Na C/Co	Pb ppm	Pb C/Co	Zn ppm	Zn C/Co
125	821.4	0.90	270	0.02	828.5	0.64	679.2	0.82
130	825.4	0.91	250	0.02	839.5	0.65	705.9	0.85
135	827.3	0.91	250	0.02	886.6	0.68	707.3	0.85
140	828.1	0.91	240	0.02	965.1	0.74	716.3	0.86
145	832.6	0.91	230	0.02	980.7	0.75	720.3	0.87
150	837.1	0.92	220	0.02	1043.5	0.80	730.5	0.88
155	844.0	0.93	220	0.02	1051.4	0.81	730.8	0.88
160	845.9	0.93	210	0.02	1082.7	0.83	731.1	0.88
165	848.0	0.93	210	0.02	1137.7	0.88	732.5	0.88
170	851.2	0.93	210	0.02	1137.7	0.88	752.8	0.91
175	861.5	0.94	210	0.02	1161.2	0.89	759.2	0.91
180	863.4	0.95	200	0.02	1208.3	0.93	760.6	0.92
185	894.5	0.98	200	0.02	1286.7	0.99	769.5	0.93
190	902.7	0.99	180	0.02	1294.6	1.00	787.4	0.95
195	902.7	0.99	180	0.02	1294.6	1.00	787.4	0.95
200	902.7	0.99	180	0.02	1294.6	1.00	787.4	0.95

APPENDIX H

BET SPECIFIC SURFACE AREA DETERMINATION

The BET Method which is an expansion of the Langmuir theory to multilayer sorption can be written as,

$$\frac{1}{V \left[\left(\frac{P_0}{P} - 1 \right) \right]} = \frac{1}{V_m C_{BET}} + \frac{(C_{BET} - 1) P}{V C_{BET} P_0} \quad (\text{C. 1})$$

where V is the specific volume of nitrogen sorbed at a given relative pressure (P/P_0), V_m is monolayer capacity, that is the volume of gas adsorbed at standard temperature and pressure (STP, @ 273 K and 1 atm), and C_{BET} is the BET constant.

From the slope (s) and y-intercept (i) of Equation (C.1), the monolayer capacity V_m can be calculated.

$$V_m = \frac{1}{s + i} = \frac{(C_{BET} - 1)}{s * C_{BET}} \quad (\text{C. 2})$$

Once V_m is determined, the total surface area A_{BET} can be computed using Equation (C.3).

$$A_{BET} = \frac{V_m * N_A * A_{sample}}{M_V} \quad (\text{C. 3})$$

where N_A is Avogadro's number, A_{sample} is the molecular cross sectional area of the Zeolite 13X and equals 0.162 nm^2 for a sorbed nitrogen molecule (ISO 9277:2010(en)), and M_V is the molar volume and equals 22414 mL.

In order to calculate the surface area using the Equation (C.1), five data points are used ideally (Table H.1). From the BET Isotherm of Zeolite 13X (Figure H.2) monolayer capacity is calculated as $158.63 \text{ cm}^3/\text{g}$.

$$V_m = \frac{1}{s + i} = \frac{1}{0.0063 + (4 \times 10^{-6})} = 158.63$$

$$A_{BET} = \frac{158.63 \text{ (cm}^3/\text{g)} * 0.162 \times 10^{-18} \text{ (m}^2) * (6.02 \times 10^{23})}{22414 \text{ (cm}^3)}$$

$$A_{BET} = 690.20 \text{ (m}^2/\text{g)}$$

In the range of $0.025 \leq (P/P_0) \leq 0.3$ just a couple of complete layers take place and the BET isotherm is precise. When the relative pressures are excessively low only monolayer formation happens and the BET isotherm fails to explain sorption in light of the fact that in determining the isotherm it was expected that all the layers on the solid surface are equal. This is not so much the case when just a couple of particles have sorbed and inhomogeneities in the solid surface get to be more critical.

When relative pressures are higher than 0.5, BET isotherm fails to explain sorption because of the surface roughness and the open pores or cavities on the surface. This is particularly valid for highly porous materials with a couple of monolayers. The filling of the open pores can alter the effective surface area of the gas sorption.

BET method can be applied to microporous materials at relative pressure values lower than 0.1. The BET plots of microporous materials at this relative pressure range can cause negative intercept and thus negative C_{BET} values.

Table H.1 BET isotherm values

Adsorption			Desorption		
Data Points	P/P ₀ (STP)	V (cc/g)	Data Points	P/P ₀ (STP)	V (cc/g)
1	0.02561	156.4241	25	0.90130	180.6597
2	0.03176	156.9502	26	0.84459	173.6222
3	0.04150	157.5996	27	0.79910	170.6496
4	0.05183	158.1194	28	0.74015	169.3035
5	0.06201	158.5437	29	0.68894	168.5905
6	0.08632	159.3112	30	0.63909	167.8815
7	0.11156	159.9110	31	0.58899	167.2459
8	0.16095	160.8334	32	0.53872	166.6440
9	0.21122	161.5606	33	0.48879	166.0476
10	0.26134	162.2166	34	0.43951	165.1134
11	0.31098	162.8957	35	0.38852	164.5597
12	0.36123	163.5302	36	0.33861	163.9554
13	0.41145	164.0655	37	0.28852	163.4045
14	0.46140	164.5668	38	0.23855	162.7345
15	0.51132	165.0800	39	0.18873	162.0054
16	0.56122	165.6371	40	0.13864	161.2095
17	0.61110	166.2418	41	0.08935	160.0890
18	0.66113	166.8006	42	0.06383	159.2433
19	0.71104	167.4246	43	0.03941	158.0506
20	0.76036	168.2470	44	0.02916	157.3390
21	0.80895	169.6054	45	0.01936	156.3319
22	0.85557	172.0897	45	0.01179	155.0410
23	0.89834	176.8739	45	0.00847	154.1151
24	0.95260	190.4946			

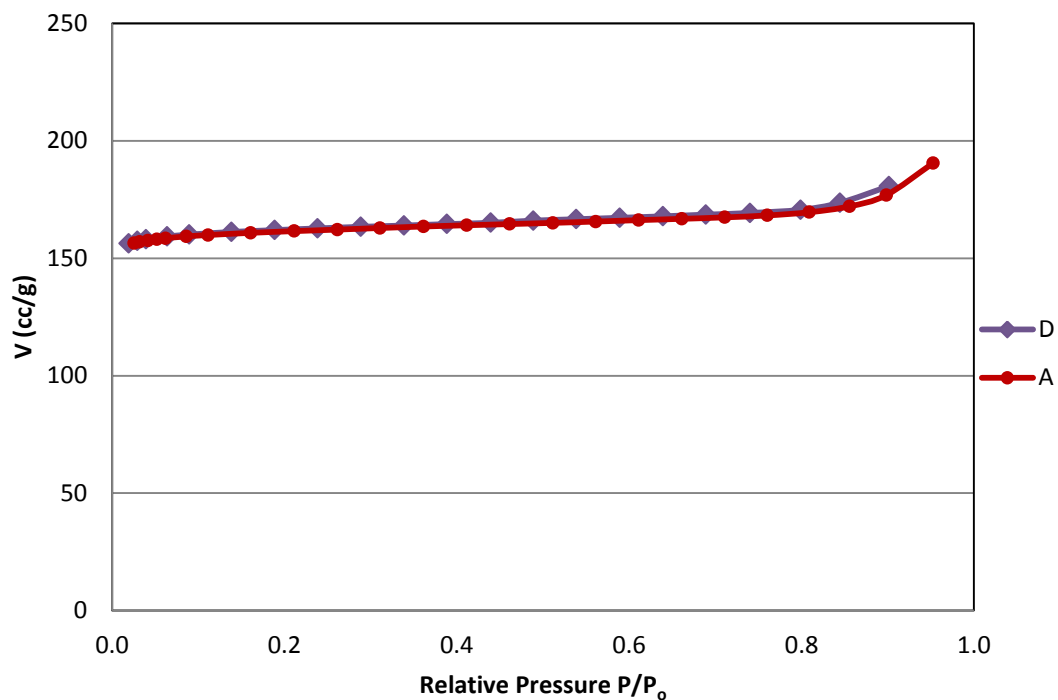


Figure H.1 BET Isotherm of Zeolite 13X

Table H.2 Multipoint BET values

Data Points	P/P_0	V (cc/g)	$1/[V(P_0/P)-1]$
1	0.02561	156.4241	0.000164
2	0.03176	156.9502	0.000202
3	0.04150	157.5996	0.000263
4	0.05183	158.1194	0.000328
5	0.06201	158.5437	0.000391

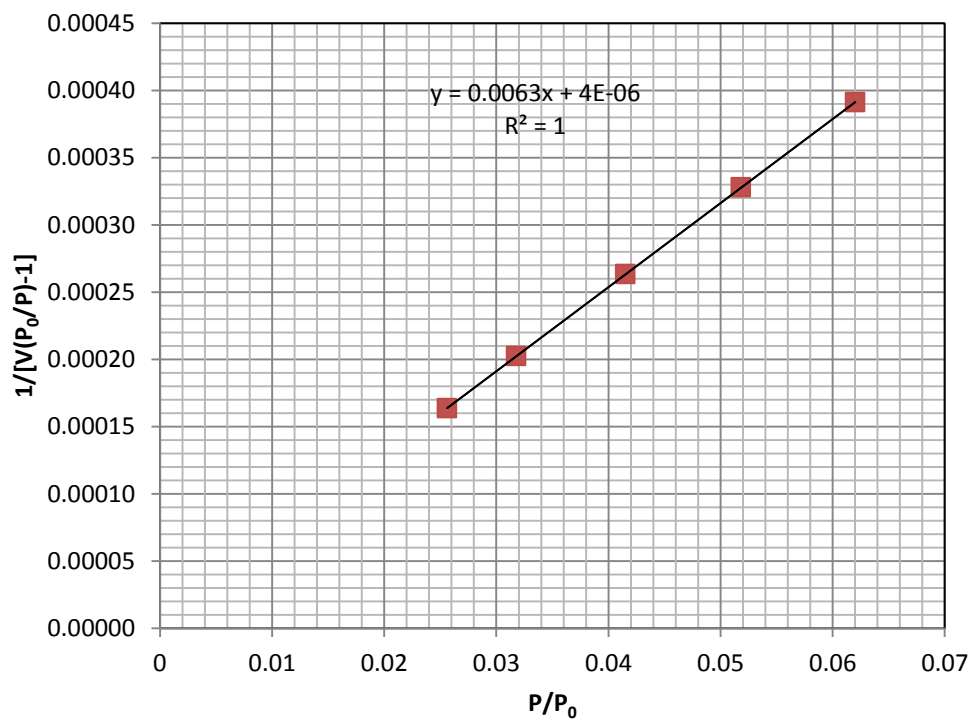


Figure H.2. Multipoint BET plot of Zeolite 13X

APPENDIX I

MATERIAL BALANCES

Material Balance on the Column:

[Rate of Mass transfer In] - [Rate of Mass transfer Out] = [Rate of Accumulation (pores+solid)]

$$A_s N|_z - A_s N|_{z+\Delta z} = \varepsilon_p A_s \Delta z \frac{\partial C}{\partial t} + \rho_b A_s \Delta z \frac{\partial q}{\partial t} \quad (\text{I. 1})$$

Dividing by $A_s \Delta z$ and taking limit as Δz

$$\begin{aligned} \lim_{\Delta z \rightarrow 0} \frac{N|_z - N|_{z+\Delta z}}{\Delta z} &= \varepsilon_p \frac{\partial C}{\partial t} + \rho_b \frac{\partial q}{\partial t} \\ - \frac{\partial N}{\partial z} &= \varepsilon_p \frac{\partial C}{\partial t} + \rho_b \frac{\partial q}{\partial t} \end{aligned} \quad (\text{I. 2})$$

N = convective mass transport + diffusion

$$N = -D_p \frac{\partial C}{\partial z} + uC \quad (\text{I. 3})$$

$$D_p \frac{\partial^2 C}{\partial z^2} + u \frac{\partial C}{\partial z} = \varepsilon_p \frac{\partial C}{\partial t} + \rho_b \frac{\partial q}{\partial t} \quad (\text{I. 4})$$

Material Balance on the Particle:

[Rate of Mass transfer In] - [Rate of Mass transfer Out] = [Rate of Accumulation (pores+solid)]

$$4\pi r^2 N|_r - 4\pi r^2 N|_{r+\Delta r} = \varepsilon_p 4\pi r^2 \Delta r \frac{\partial C}{\partial t} + \rho_s 4\pi r^2 \Delta r \frac{\partial q}{\partial t} \quad (\text{I. 5})$$

Dividing by $4\pi \Delta r$ and taking limit as Δr

$$\begin{aligned} \frac{1}{r^2} \lim_{\Delta r \rightarrow 0} \frac{r^2 N|_r - r^2 N|_{r+\Delta r}}{\Delta r} &= \varepsilon_p \frac{\partial C}{\partial t} + \rho_s \frac{\partial q}{\partial t} \\ -\frac{1}{r^2} \left[\frac{\partial(r^2 N)}{\partial r} \right] &= \varepsilon_p \frac{\partial C}{\partial t} + \rho_s \frac{\partial q}{\partial t} \end{aligned} \quad (I.6)$$

If pore diffusion is controlling then,

$$N = -D_p \frac{\partial C}{\partial r} \quad (I.7)$$

$$D_p \left[\frac{\partial^2 C}{\partial r^2} + \frac{2}{r} \frac{\partial C}{\partial r} \right] = \rho_b \frac{\partial q}{\partial t} \quad (I.8)$$

If solid diffusion is controlling then,

$$N = -D_s \rho_s \frac{\partial q}{\partial r} \quad (I.9)$$

$$D_s \left[\frac{\partial^2 q}{\partial r^2} + \frac{2}{r} \frac{\partial q}{\partial r} \right] = \frac{\partial q}{\partial t} \quad (I.10)$$

Accumulation term in the pores is eliminated assuming that the solute contained in the pores is negligible.

Fluid-film diffusion control:

$$D_s \left[\frac{\partial^2 q}{\partial r^2} + \frac{2}{r} \frac{\partial q}{\partial r} \right] = \frac{\partial q}{\partial t} = K_f (C - C_i) \quad (I.11)$$

When the solid diffusion is the controlling mechanism; the interface concentration C_i is equal to C_e equilibrium concentration.

APPENDIX J

CALCULATION OF MOLECULAR DIFFUSIVITY (D_m)

Nernst equation can be used to estimate the molecular diffusivities (D_m) of studied metal salt solutions.

$$D_m = \frac{R}{F} \times T \times \left(\frac{\lambda_+^o \times \lambda_-^o}{\lambda_+^o + \lambda_-^o} \right) \left(\frac{Z_+ + Z_-}{Z_+ \times Z_-} \right)$$

D_m = Molecular Diffusivity (cm^2/s)

R = Gas Constant, 8.3144621 J/(molK)

F = Faraday Constant, 96485 J per volt gram equivalent

T = Absolute Temperature (K)

λ_+^o, λ_-^o = limiting ionic conductances for cation and ion, mho/equivalent

Z_+, Z_- = Absolute ion valances for cation and anion

$$D_m = 8.931 \times 10^{-10} \times T \times \left(\frac{\lambda_+^o \times \lambda_-^o}{\lambda_+^o + \lambda_-^o} \right) \left(\frac{Z_+ + Z_-}{Z_+ \times Z_-} \right)$$

Limiting Equivalent Ionic Conductances at 25 °C were determined from Table 8.32 of Lange's Handbook of Chemistry (Dean, 1999).

$$\lambda_{Pb^{2+}}^o = 71.00 \text{ mho. cm}^2/\text{eq.}$$

$$\lambda_{Ca^{2+}}^o = 54.00 \text{ mho. cm}^2/\text{eq.}$$

$$\lambda_{Zn^{2+}}^o = 52.80 \text{ mho. cm}^2/\text{eq.}$$

$$\lambda_{Na^{2+}}^o = 50.11 \text{ mho. cm}^2/\text{eq.}$$

$$\lambda_{NO_3^-}^o = 71.42 \text{ mho. cm}^2/\text{eq.}$$

For the case of $NaNO_3$, where a neutralization reaction is occurring,

$$(D_m)_{NaNO_3} = (8.931 \times 10^{-10}) \times (298.15) \times \left(\frac{50.11 \times 71.42}{50.11 + 71.42} \right) \left(\frac{1 + 1}{1 \times 1} \right)$$

$$(D_m)_{NaNO_3} = 1.568 \times 10^{-5} \text{ (cm}^2/\text{s)}$$

For the case of $Pb(NO_3)_2$,

$$(D_m)_{Pb(NO_3)_2} = (8.931 \times 10^{-10}) \times (298.15) \times \left(\frac{71 \times 71.42}{71 + 71.42} \right) \left(\frac{2 + 1}{2 \times 1} \right)$$

$$(D_m)_{Pb(NO_3)_2} = 1.422 \times 10^{-5} \text{ (cm}^2/\text{s)}$$

Similarly for $Cd(NO_3)_2$ and $Zn(NO_3)_2$;

$$(D_m)_{Cd(NO_3)_2} = 1.228 \times 10^{-5} \text{ (cm}^2/\text{s)}$$

$$(D_m)_{Zn(NO_3)_2} = 1.213 \times 10^{-5} \text{ (cm}^2/\text{s)}$$

APPENDIX K

CALCULATION of the BREAKTHROUGH CAPACITY, TOTAL EXCHANGE CAPACITY and COLUMN EFFICIENCY from BREAKTHROUGH CURVES

Initial Pb^{+2} Concentration (C_o) : 0.05N (5180 ppm)

Temperature (T) : 25°C

pH: 5.5

Zeolite bed height in the column (h_T) = 5.8 cm

Diameter of the column (\emptyset) = 2.0 cm

Flow rate (Q) = 10 mL/min

50 mL of samples were taken every 5 min period of time. The experimental breakthrough curve (Figure 5.31) was obtained by plotting lead ion concentration versus time. The experimental breakthrough curve (Figure K.1) was obtained by plotting lead ion concentration versus volume of the solution collected.

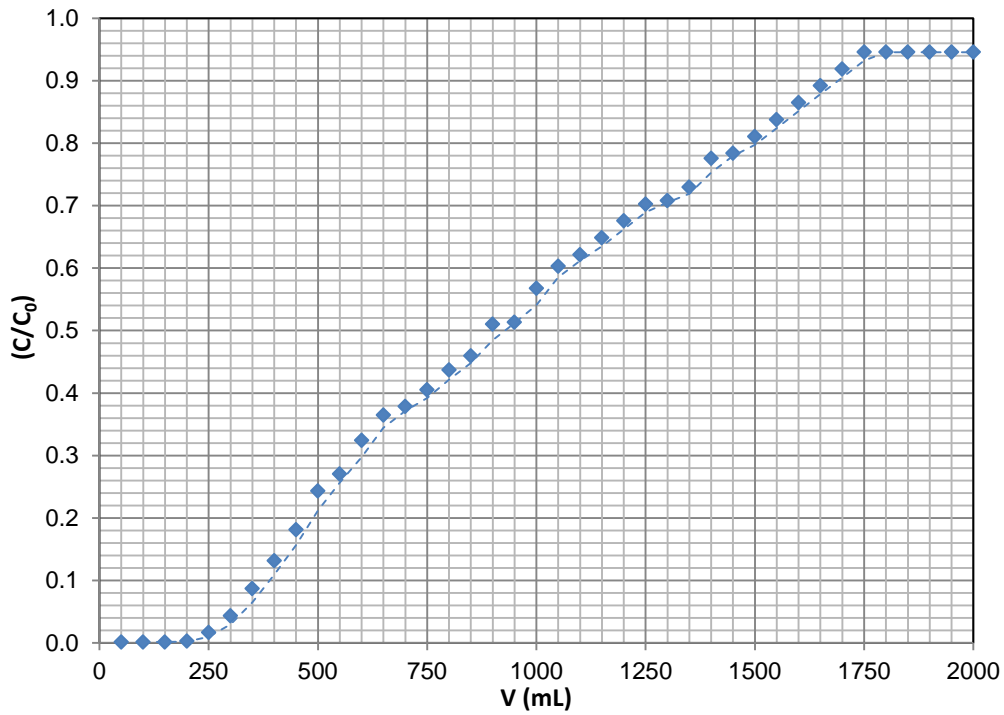


Figure K.1. Breakthrough curves- $C_{0,Pb} = 50 \text{ meq/L}$; $C_{0,Na} = 0 \text{ meq/L}$

The Breakthrough Capacity (Q_B)

Equation 2.69 can be re-written in the form:

$$Q_{br} = C_0 \int_0^{V_{br}} \left(1 - \frac{C}{C_0}\right) dV \quad (\text{K. 1})$$

Total area up to the breakthrough point is can be calculated as:

$$A_{br} = \int_0^{V_{br}} \left(1 - \frac{C}{C_0}\right) dV \quad (\text{K. 1})$$

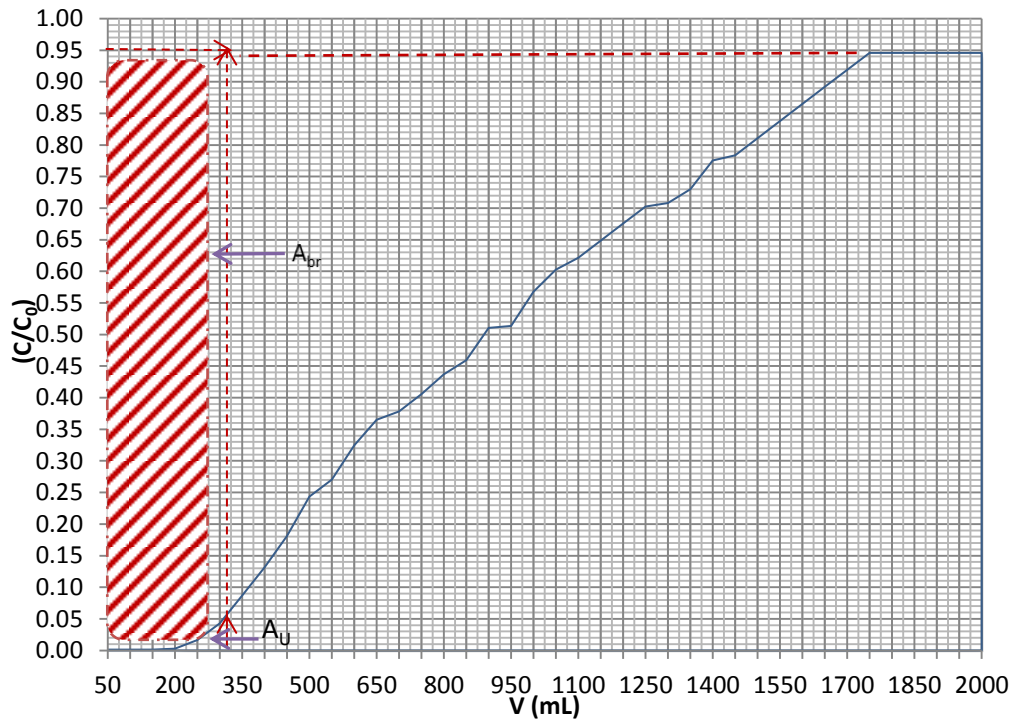


Figure K.2. Representation of area under the curve A_u and breakthrough area A_{br}

Simpson's Rule is used for the calculation of the area under the curve (A_u) until the breakthrough point:

$$A_u \cong \int_0^{V_{br}} f(x) dx \cong \frac{h}{3} \left[f(x_0) + 4 \sum_{\substack{i=1 \\ i=odd}}^{n-1} f(x_i) + 4 \sum_{\substack{i=2 \\ i=even}}^{n-2} f(x_i) + f(x_n) \right] \quad (\text{K. 2})$$

$f(x)$ indicates C/C_0 values, and h is given by:

$$h = \frac{V_n - V_0}{n}$$

A_{br} , is calculated as follows:

$$A_{br} = A_t - A_u.$$

where (A_t) is the total area until the breakthrough point

h , A_u and A_{br} is calculated as 50 mL, 2.8 and 307.1 respectively.

$$Q_{br} = \frac{307.1 \text{ (ml)} \times 0.05 \left(\frac{\text{meq}}{\text{ml}}\right)}{15 \text{ (g)}} = 1.02 \left(\frac{\text{meq}}{\text{g}}\right)$$

Similary, h , A_u (area under the curve) and A_T (total area) are calculated as 50 mL, 989.2 and 960.8 respectively. Then total exchange capacity and column efficiency can be calculated as follows:

$$\text{Total exchange capacity} = Q_T = \frac{960.8 \text{ (ml)} \times 0.05 \left(\frac{\text{meq}}{\text{ml}}\right)}{15 \text{ (g)}} = 3.2 \left(\frac{\text{meq}}{\text{g}}\right)$$

$$\text{Column Efficiency} = \eta_c = \frac{Q_{br}}{Q_T} = \frac{1.02}{3.2}$$

$$\text{Column Efficiency} = 32 \%$$

APPENDIX L

BREAKTHROUGH MODELS FOR Pb^{2+} -NaX EXCHANGE

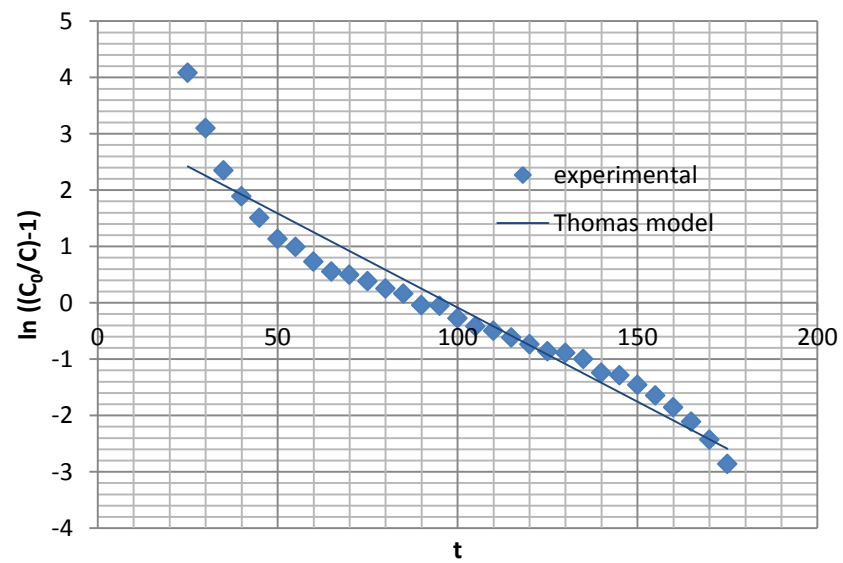


Figure L.1 Linearization of Thomas Model Pb^{2+} -NaX Exchange

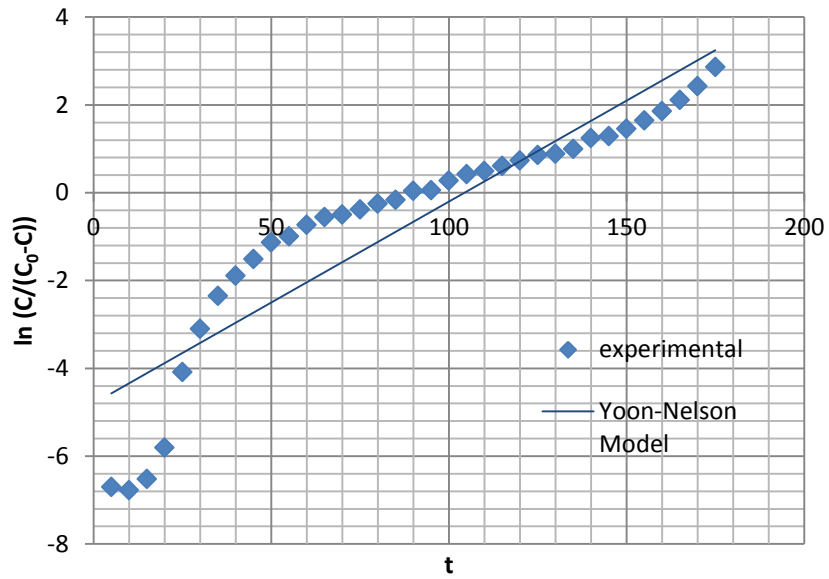


Figure L.2 Linearization of Yoon-Nelson Model Pb^{2+} -NaX Exchange

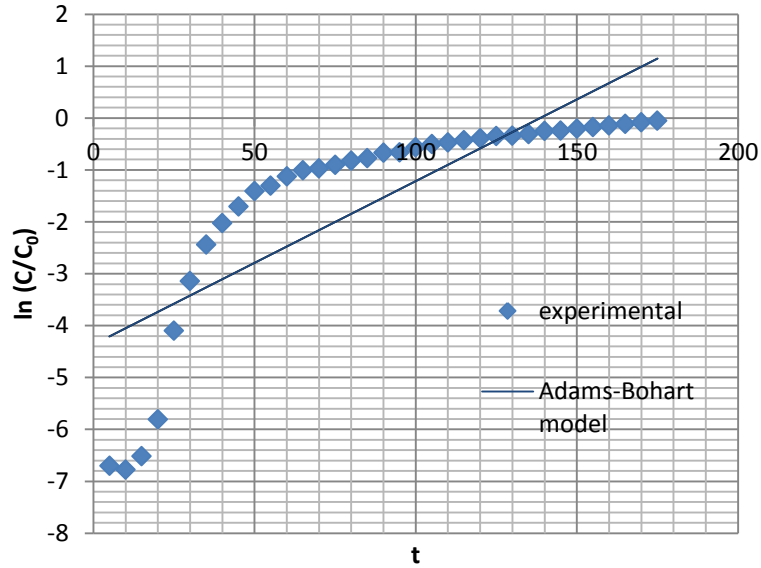


Figure L.3 Linearization of Adams-Bohart Model Pb^{2+} -NaX Exchange

APPENDIX M

BREAKTHROUGH MODELS FOR Cd²⁺-NaX EXCHANGE

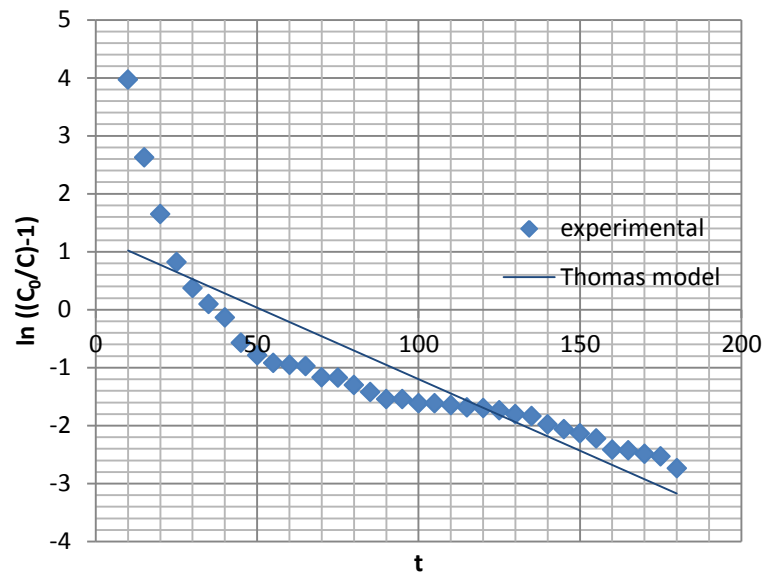


Figure M.1 Linearization of Thomas Model Cd²⁺-NaX Exchange

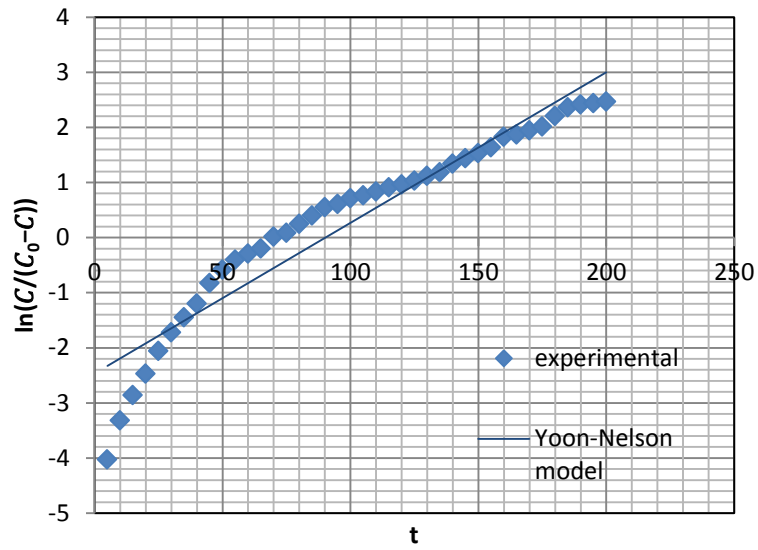


Figure M.2 Linearization of Yoon-Nelson Model Cd^{2+} -NaX Exchange

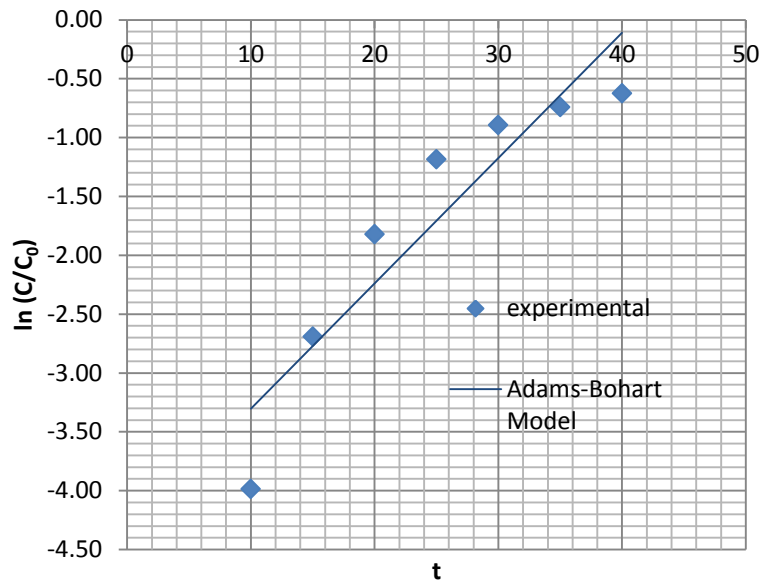


Figure M.3 Linearization of Adams-Bohart Model Cd^{2+} -NaX Exchange

APPENDIX N

BREAKTHROUGH MODELS FOR Zn²⁺-NaX EXCHANGE

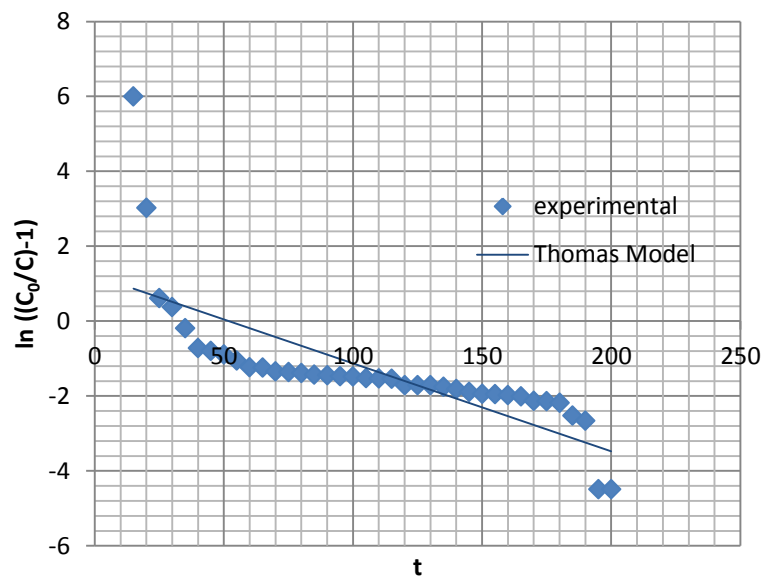


Figure N.1 Linearization of Thomas Model Zn²⁺-NaX Exchange

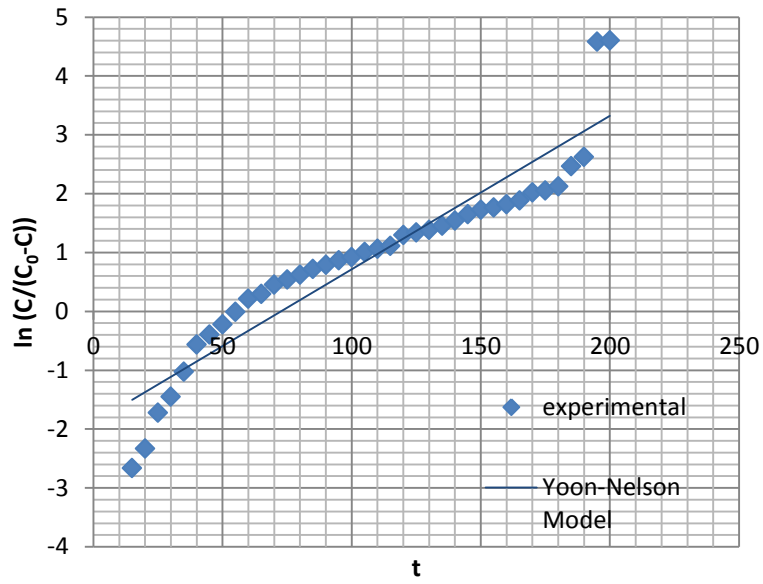


Figure N.2 Linearization of Yoon-Nelson Model Zn²⁺-NaX Exchange

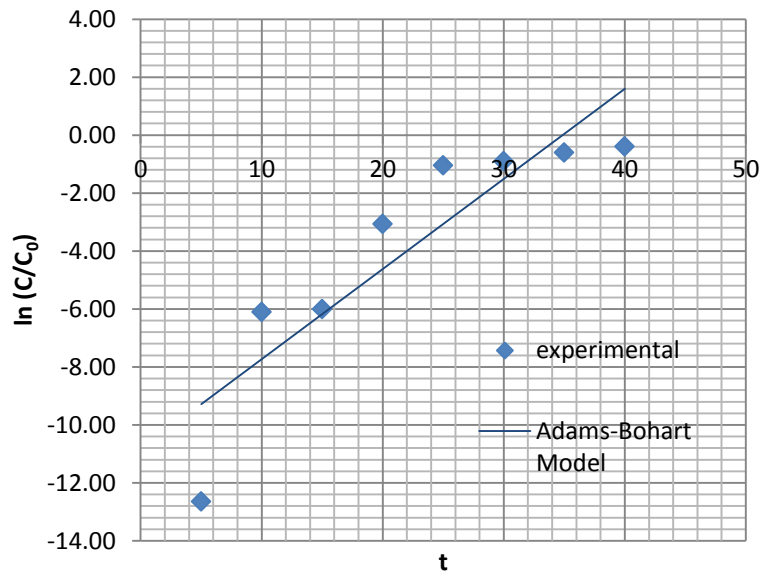


Figure N.3 Linearization of Adams-Bohart Model Zn²⁺-NaX Exchange

APPENDIX O

PRELIMINARY BREAKTHROUGH DATA

Table O.1. Pb²⁺-NaX binary ion exchange (concentration 0.1 N, flow rate of 15 ml/min)

Sample No	V (ml)	C (ppm) (8/12 mesh)	C (ppm) (20/25 mesh)	C (ppm) (25/30 mesh)
1	50	36.1	4.2	20.0
2	100	390.4	4.5	30.0
3	150	1170.4	97.0	34.0
4	200	2488.8	678.4	42.5
5	250	3133.0	1349.4	210.0
6	300	3421.0	2531.8	340.0
7	350	3889.2	3411.2	540.0
8	400	4879.4	4199.6	630.0
9	450	5473.6	5033.4	875.0
10	500	5815.8	5600.0	1235.4
11	550	6031.8	6252.4	1714.8
12	600	6319.8	6413.0	2544.6
13	650	6337.8	6549.4	3300.0
14	700	6516.4	6549.4	3800.0
15	750	6546.6	6595.0	4300.0
16	800	6592.0	6595.0	4800.0

Table O.1 (cont'd.) Pb²⁺-NaX binary ion exchange (concentration 0.1 N,
flow rate of 15 ml/min)

Sample No	V (ml)	C (ppm) (8/12 mesh)	C (ppm) (20/25 mesh)	C (ppm) (25/30 mesh)
17	850	6680.0	6898.2	5110.0
18	900	6788.0	6958.8	5300.0
19	950	6969.6	7019.4	5700.0
20	1000	7015.2	7019.4	5937.2
21	1050	7045.6	7034.6	6306.0
22	1100	7514.2	7201.4	6500.0
23	1150	7544.2	7322.6	6822.2
24	1200	7580.2	7656.2	7154.2
25	1250	7904.4	7732.0	7300.0
26	1300	7978.4	7807.8	7559.8
27	1350	7998.0	8035.2	7652.0
28	1400	8246.4	8035.2	7818.0
29	1450	8336.4	8202.0	8100.0
30	1500	8426.6	8262.6	8334.2
31	1550	8642.6	8338.4	8537.0
32	1600	8930.6	8414.2	8920.0
33	1650	9092.9	8570.0	9100.0
34	1700	9308.8	8750.0	9145.4
35	1750	9308.8	9152.0	9300.0
36	1800	9308.8	9152.0	9300.0
37	1850	9308.8	9152.0	9329.8
38	1900	9308.8	9263.2	9329.8
39	1950	9308.8	9263.2	9329.8
40	2000	9308.8	9263.2	9329.8

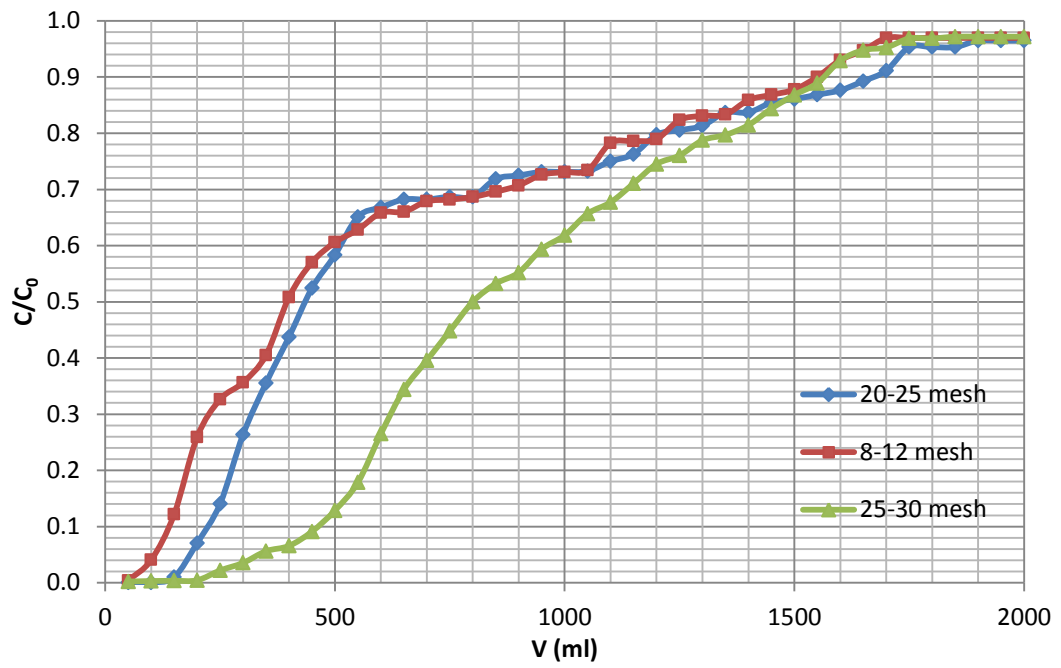


Figure O1. Breakthrough curves at different mesh sizes-($C_{0,Pb} = 50$ meq/L; $C_{0,Na} = 0$ meq/L ; concentration 0.1 N, flow rate of 15 ml/min)

Table O.2. Pb²⁺-NaX binary ion exchange (concentration 0.05 N, 25/30 mesh size)

Sample No	V (ml)	C ppm (10 ml/min)	C ppm (15 ml/min)	C ppm (20 ml/min)
1	50	0.9	51.8	54.20
2	100	5.2	103.6	414.40
3	150	7.5	518.0	673.40
4	200	10.4	621.6	1191.40
5	250	10.6	880.6	1502.20
6	300	20.7	1346.8	2072.00
7	350	103.6	1813.0	2434.60
8	400	207.2	2175.6	2590.00
9	450	310.8	2590.0	2797.20
10	500	621.6	2641.8	2900.80
11	550	880.6	2693.6	3315.20
12	600	1243.2	2745.4	3418.80
13	650	1398.6	2900.8	3470.60
14	700	1605.8	3108.0	3833.20
15	750	1761.2	3159.5	3936.80
16	800	1864.8	3211.6	4000.20
17	850	2020.2	3263.4	4195.80
18	900	2175.6	3315.2	4403.00
19	950	2279.2	3367.0	4454.80
20	1000	2434.6	3470.6	4506.60
21	1050	2693.6	3522.4	4510.20
22	1100	2952.6	3574.2	4520.00

Table O.2 (cont'd) Pb²⁺-NaX binary ion exchange (concentration 0.05 N,
25/30 mesh size)

Sample No	V (ml)	C ppm (10 ml/min)	C ppm (15 ml/min)	C ppm (20 ml/min)
23	1150	3108.0	3626.0	4558.40
24	1200	3211.6	3729.6	4560.00
25	1250	3522.4	3730.0	4610.20
26	1300	3781.4	3760.0	4620.00
27	1350	3885.0	3770.0	4630.00
28	1400	4195.8	3781.4	4713.80
29	1450	4299.4	3885.0	4765.60
30	1500	4558.4	3936.8	4817.40
31	1550	4662.2	4144.0	4869.20
32	1600	4817.4	4299.4	4940.00
33	1650	4921.5	4351.2	4940.00
34	1700	4921.5	4610.2	4940.00
35	1750	4921.5	4662.0	4940.00
36	1800	4921.5	4713.8	4940.00
37	1850	4921.5	4930.0	4940.00
38	1900	4921.5	4930.0	4940.00
39	1950	4921.5	4930.0	4940.00
40	2000	4921.5	4930.0	4940.00

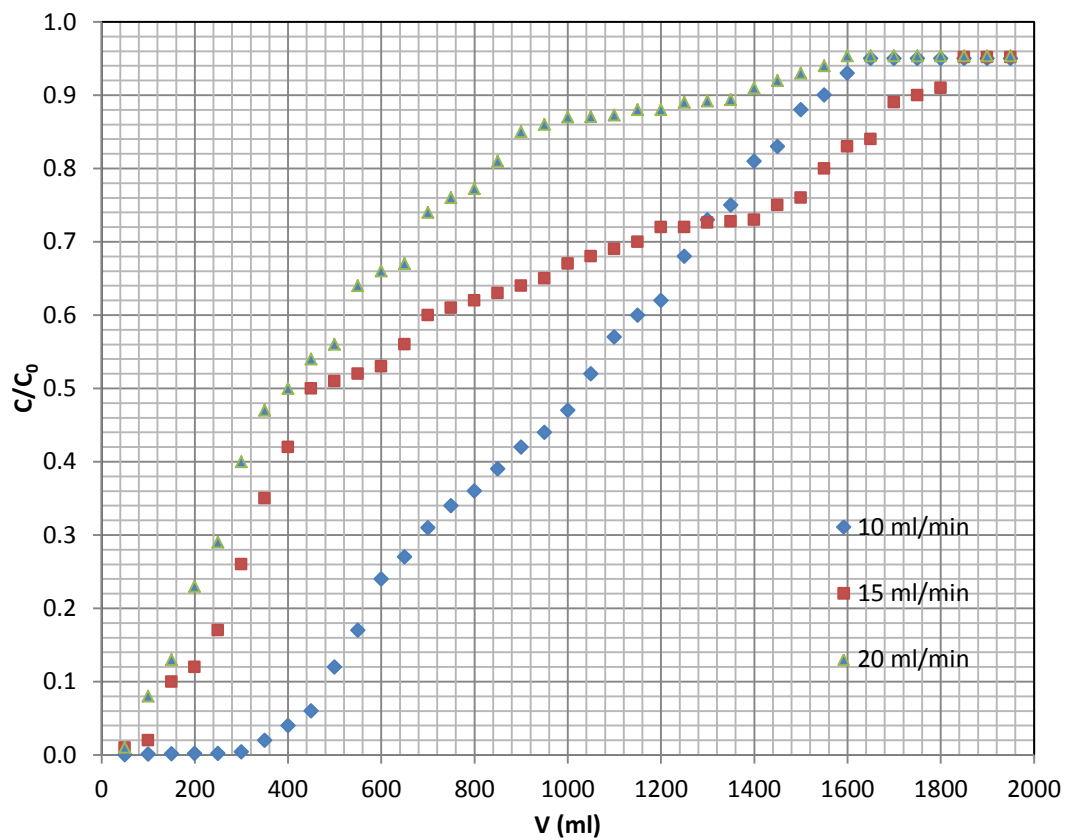


Figure O2. Breakthrough curves at different flow rates- ($C_{0,Pb}=50$ meq/L; $C_{0,Na}=0$ meq/L ; concentration 0.05 N, 25/30 mesh size)

APPENDIX P

EXPERIMENTAL COMPETITION COEFFICIENTS PRODUCT CALCULATION FOR THE SRS MULTICOMPONENT ISOTHERM MODEL

According to the Multicomponent SRS Isotherm Model the product of the competition coefficients a_{ij} must be equal to one

$$a_{12} \times a_{23} \times a_{31} = 1$$

Experimentally calculated competition coefficients for the metals (1= Pb^{2+} ; 2= Cd^{2+} ; 3= Zn^{2+}) were are given in Table 5.11 as follows:

$$a_{12} = 0.079$$

$$a_{23} = 1.80$$

$$a_{31} = 7.40$$

Experimental competition coefficients product values was

$$a_{12} \times a_{23} \times a_{31} = 0.079 \times 1.80 \times 7.40$$

$$a_{12} \times a_{23} \times a_{31} = 1.052$$

APPENDIX R

EFFICIENCY VALUES OF DIFFERENT COLUMNS

Table R.1. Efficiency values for different columns for Pb²⁺-NaX binary exchange (Mesh size: 20/25 (0.710-0.853 mm); Flow rate: 10 ml/min; packed height:5-6)

Inside Diameter (Ø) (cm)	Height (cm)	Breakthrough capacity (mg/g)	Total exchange capacity (mg/g)	Efficiency (μ)
1.0	20	0.29	4.00	0.07
2.0	20	1.07	2.60	0.41
3.2	20	0.39	1.68	0.23

CURRICULUM VITAE

PERSONAL INFORMATION

Surname, Name: Beşel Düzgün, Elif

Nationality: Turkish (TC)

Marital Status: Married

Email: ebesel@ssm.gov.tr

EDUCATION

Degree	Institution	Year of Graduation
M.S.	METU, Chemical Engineering	2003
B.S.	Anadolu University, Administration	2007
B.S.	Hacettepe University, Chemical Engineering	2001

PROFESSIONAL EXPERIENCE

Year	Place	Enrollment
2013-Present	SSM (Undersecretariat for Defence Industries) Department of R&D and Technology Management - Sensors	Engineer
2011 October-May	HAVELSAN & ASELSAN SSM Project Control Offices	Product Management
2008-2013	SSM (Undersecretariat for Defence Industries) Department of Naval Platforms -Amphibious Ship, Auxiliary Ship and Patrol Boats	Project Engineer

Year	Place	Enrollment
2004-2008	KARDEMİR Iron and Steel Works - Coke Plants	Operating Engineer
1999 July	TTK (General Directorate of the Turkish Hard Coal Enterprises)	Intern Engineer

PUBLICATIONS

1. Sixth National Chemical Engineering Congress, 7th-10th September 2004, UKMK-6 Ege University Department of Chemical Engineering Presentation Summary Book Presentation Topic “Usage of Triton X-114 ATPE method for the extraction of polyphenol Oxidases from *Agaricus bisporus*”.
2. Fifth (ESBES) European Symposium on Biochemical Engineering Science 8th – 11th September 2004 Stuttgart Germany. Poster Presentation Topic “Triton X-114 Based Aqueous Two-Phase Extraction Of Phenol Oxidases From *Agaricus Bisporus*.”
3. Twenty First National Chemistry Congress, 23th-27th August 2007, İnönü University Presentation Summary Book Presentation Topic “Tekstil Boyaları ve Bozunma Ürünlerinin Karakterizasyonu”

PARTICIPATION IN CONFERENCES

1. “Graphene and Related Technologies: from Laboratory to Industry - 2014” Workshop, October 13- 14, 2014, Cevahir Hotel Asia, Istanbul, Turkey.
2. “InterM2014 2nd International Multidisciplinary Microscopy and Microanalysis Congress & Exhibition” October 16-19, 2014, Liberty Hotels Lykia, Oludeniz, Turkey.

3. Microelectronics Technology, Circuits, and Systems for Space Applications Workshop, June 19-20, 2014 Sabancı University, İstanbul Turkey.
4. SID (The Society for Information Display) Display Week 2014 International Symposium, Seminar and Exhibition, June 1-6, 2014 San Diego Convention Center, California, United States.
5. SPIE (The International Society for Optics and Photonics) DSS (Defense and Security, Sensing Technology and Applications Symposium) 2014, May 5-9, 2014 Baltimore Convention Center, Baltimore, Maryland, United States
6. SID-ME (Mid-Europe) Chapter Spring Meeting 2014, April 7-8, 2014, Sakıp Sabancı Museum İstanbul, Turkey.
7. XXII. National Chemistry Congress, October 6-10, 2008 Eastern Mediterranean University, Magusa, Turkish Republic of Northern Cyprus.
8. IV. International Iron & Steel Congress, November 1-3, 2007 Karabük University, Turkey.
9. 15th Coal Congress of Turkey June 7-9, 2006, General Directorate of the Turkish Hard Coal Enterprises, Department of Occupational Health and Safety Management , Zonguldak, Turkey.

CERTIFICATES

2014	Entrepreneurship Certificate Program	METU GIMER
2013	Introduction to Systems Engineering	ATEGO
2013	Introduction to Materials Science	METU SEM
2001	Excellent Degree Diploma in English	TOMER Language Teaching Center

FOREIGN LANGUAGES

English, German

INTERESTS

Playing musical instruments (guitar and piano), playing sports (tennis, swimming, pilates, table tennis, kangoo jumps,), photography, reading, watching (ballet, theatre and opera)